Oxidation of phosphasalen complexes

Irene Mustieles Marín

NNT : 2017SACLX078

THESE DE DOCTORAT
DE
L'UNIVERSITE PARIS-SACLAY
PREPAREE A
"ECOLE POLYTECHNIQUE"

ECOLE DOCTORALE N° 571
2MIB | Sciences chimiques :
molécules, matériaux, instrumentation et biosystèmes

Spécialité de doctorat : Chimie

Par

Irene Mustieles Marín

Oxidation of phosphasalen complexes

Thèse présentée et soutenue à Palaiseau, le 26 octobre 2017 :

Composition du Jury :

Président : Dr. Yves Le Mest		
Mme Anxolabéhère-Mallart, Elodie	Directrice de Recherche à l'Université Paris Diderot	Examinatrice
M. Thomas, Fabrice	Professeur à l'Université Grenoble-Alpes	Examinateur
M. Le Mest, Yves	Directeur de Recherche à l'Université Bretagne Occidental	Rapporteur
Mme Sénéchal-David, Katell	Maitre de Conférences à l'Université de Paris-Sud	Rapporteur
Mme Auffrant, Audrey	Chargée de Recherche à l'Ecole Polytechnique	Directrice de thèse

Université Paris-Saclay
Espace Technologique / Immeuble Discovery
Route de l'Orme aux Merisiers RD 128 / 91190 Saint-Aubin, France

Oxidation of Phosphasalen Complexes

Irene Mustieles Marín

Chemistry

Ecole Polytechnique, Université Paris-Saclay

PhD thesis defended on:
October 2017

Financed by:

List of abbreviations

COE	Cyclooctene
CT	Charge Transfer
DABCO	1,4-diazabicyclo[2.2.2]octane
DCM	Dichloromethane
DFT	Density Functional Theory
EPR	Electronic Paramagnetic Resonance
Fc	Ferrocene
GC	Gas Chromatography
HOMO	Highest Occupied Molecular Orbital
HSAB	Hard Soft Acid Base
iPr	Isopropyl
KHMDS	Potassium bis(trimethylsilyl)amide
LMCT	Ligand Metal Charge Transfer
LUMO	Lowest Unoccupied Molecular Orbital
***m*-CP**	*meta*-chlorobenzoate
***m*-CPBA**	meta-chloroperoxybenzoic acid
Me	Methyl
NBO	Natural Bond Orbital
NBS	N-Bromosuccinimide
NMO	N-Methylmorpholine-N-Oxide
NMR	Nuclear Magnetic Resonance
OMe	Methoxy
ORTEP	Oak Ridge Thermal Ellipsoid Plot
Ph	Phenyl
ppm	Parts per million
PSalen	Phosphasalen
PSalophen	Phosphasalophen
Salen	N,N'-ethylenebis(salicylimine)
SCE	Saturated Calomel Electrode
SQUID	Superconducting Quantum Interference Device
SOMO	Singly Occupied Molecular Orbital
tBu	tert-butyl
THF	Tetrahydrofuran
TMS	Tetramethylsilane
$TMSN_3$	Trimethylsilyl azide
TS	Transition State
UV-Vis	Ultraviolet-Visible spectroscopy

Table of contents

Chapter 1: Introduction to phosphasalen ligands

1. Redox non-innocent ligands

1.1 Definition

Redox non-innocent ligands have been described as "ligands with more energetically accessible levels that allow redox reactions to change their charge state".[1] This concept of non-innocence was first introduced by Jorgensen in 1966[2] in order to account for the difficulties in assigning oxidation states to metals bearing certain ligands. Gray and co-workers determined that the oxidation state in square planar nickel and cobalt complexes featuring two dithiolene ligands (L^{2-}) were better described as Ni^{II} and Co^{II} complexes, despite the regular electron counting points to an oxidation state +IV for the metal centers.[3] Since these ligands do not necessarily possess a closed-shell configuration, it is important to make a difference between the *formal* and the *spectroscopic* oxidation state of a metal. The former arises from the ligand field theory and can be defined as "the charge left on the metal after all ligands have been removed in their normal, closed-shell configuration, that is with their electron pair".[4] However, this *formal* oxidation state can either match or not with the *spectroscopic* (or *physical*) oxidation state, which is the one obtained after measurements by various spectroscopic techniques.[5] This *spectroscopic* oxidation state better define the electronic configuration of the metal when featuring a redox-active ligand. The presence of redox non-innocent ligands may render the assignment of the oxidation state of the metal very difficult, and therefore a combination of spectroscopic, magnetic and computational studies must be used to give a response as accurate as possible.

Depending on the nature of the redox-active orbitals of the complex, ligand or metal-based, the redox process occurs on the ligand (redox non-innocent ligand) or on the metal (innocent ligand). In the latter case, *formal* and *spectroscopic* oxidation states match.

Aminophenol and phenylenediamine ligands are good examples of such redox non-innocence (Scheme 1).[6] Complexes displaying these ligands can undergo successive oxidations in which only the ligand is involved, and the metal center preserves its oxidation state.

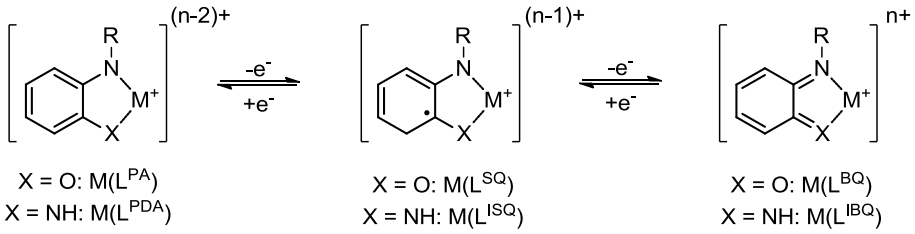

Scheme 1. Oxidation levels of the deprotonated aminophenol and phenylenediamine ligands and related nomenclature. [6]

Scheme 1 illustrates the oxidation levels of the deprotonated aminophenol and phenylenediamine ligands and the concomitant geometrical modifications experienced upon oxidation. These ligands can display three different oxidation levels: the initial dianionic forms L^{PA} and L^{PDA} (PA = phenolamine; PDA = phenyldiamine), a first oxidized form in which the ligands adopt a semiquinonate (L^{SQ}) and iminosemiquinonate pattern (L^{ISQ}), and a doubly oxidized form which exhibits a benzoquinone (L^{BQ}) and diiminobenzoquinone (L^{IBQ}) patterns.

1.2 Role of redox non-innocent ligands in catalysis

Catalysts are present in most industrial chemical reactions and allow the production of molecules and materials essentials for the society. Thus, the development of more efficient and selective catalysts remains an intense field of research.

Bas de Bruin and Volodymyr Lyaskovskyy highlighted in 2012 the importance of redox non-innocent ligands in catalysis,[7] which can either act as spectators or be involved in the catalytic cycle. They listed four different strategies that can be followed when utilizing these ligands.[7] The approaches proposed, as well as related illustrative examples, will be commented in this section.

They established four different strategies depending on the role played by these ligands during the catalytic reaction: I) The first one concerns the oxidation/reduction of the ligand in order to modify the electronic properties of the metal center (*e.g.* Lewis acidity). II) The second one implies the use of the ligand as an electron reservoir, since they can be successively oxidized or reduced, accepting or delivering electron density to the metal

center while this maintains its oxidation state, as illustrated Scheme 1. III) The third one corresponds to the participation of the ligand in bond breaking/forming reactions during the catalytic process; the ligand helps the metal in the substrate activation or formation of the product. IV) The last one arises in cases where the substrate itself can act as a redox non-innocent ligand, thus activation and modification of its properties can be performed. These four strategies can be classified in two different groups depending on the role played by the ligand: A) when the ligand is accepting or releasing electrons (strategies I and II), and B) when the ligand interferes in the cleavage or formation of chemical bonds (strategies III and IV).[7]

Strategy I concerns the modification of the electronic properties of the metal, usually achieved by modification of the substituents (electron-withdrawing or electron-donating groups) of the ligands, *via* redox changes of the non-innocent ligands. An illustrating example is the case of the cobaltocenium-rhodium complex depicted in Scheme 2.[8] This complex is used as a catalyst in hydrogenation reactions of olefines. The rate determining step in this reaction is the oxidative addition of a molecule of H_2, normally facilitated by electron-rich metals. The catalytic activity of complex **1**, bearing a redox-active metallocene motiv, can be enhanced by reducing the ligand (cobaltocene moiety) resulting in species **2**, which reacts sixteen times faster than **1**.[8]

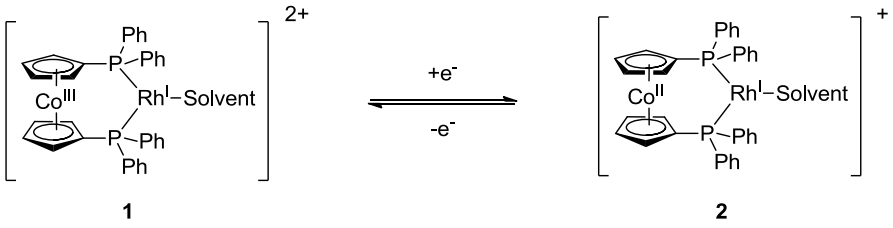

1 **2**

Scheme 2. Rhodium complexes studied by Wrighton and co-workers.[8]

Strategy II represents one of the most important applications of redox non-innocent ligands: their use as electron reservoirs.[7] Reductive activation or oxidative elimination are elemental two-electron transfer steps in homogenous catalysis, normally performed by complexes based on noble metals (Pd, Pt, Rh, etc). Thanks to the ability to store (or release) electrons of redox-active ligands, these can assist the metal during a catalytic reaction allowing non-noble transition metals (Fe, Co, Cu, etc.) to perform these transformations. Therefore, it is said that redox non-innocent ligands confer nobility to first-row transition metals. A good example for this strategy was illustrated by Chirik and co-workers in the study of the [2,2]cycloaddition reaction of dienes catalyzed by the iron(II) complex **3** (Scheme 3).[9]

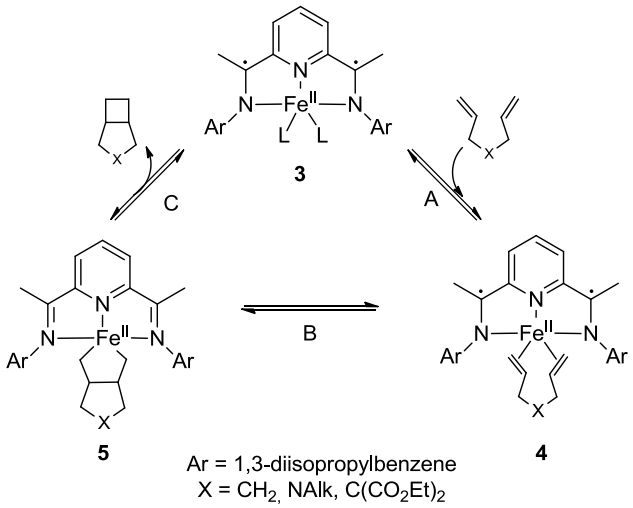

Scheme 3. Iron complex bearing a redox-active ligand acting as an electron reservoir.[9]

Complex **3** was established as a two-electron reduced bis(imino)pyridine Fe^{II} complex by computational spectroscopic and structural studies.[10] In presence of a diene this complex reacts to form the π-species **4** (Scheme 3, A). Complex **4** was found to be in equilibrium with complex **5** (Scheme 3, B), which has undergone the oxidative addition of the diene. This addition requires the transfer of two electrons from the complex to the substrate which have been delivered by the ligand. Hence, the ligand is present in its oxidized form in complex **5**, while the metal keeps its oxidation state +II. To complete the cycle, the substrate is released *via* a reductive elimination reaction and the ligand is doubly reduced, leading to the starting species **3** (Scheme 3, C). Over the whole catalytic reaction the ligand has acted as an electron reservoir allowing the metal to keep its oxidation state (+II).[8]

The cooperative substrate activation proposed as strategy III entails the participation of the ligand in the catalytic reaction, becoming an "actor" instead of being a "spectator", as in strategies I and II.[7] This is the case of redox-active ligands present in the metalloenzymes which mediate in the catalytic processes. An illustrating example is the Galactose Oxidase (GO), a copper-based enzyme which catalyzes the oxidation of D-galactose (primary alcohol) in D-galactohexodialdose (aldehyde) in presence of oxygen and has been largely investigated in recent years (Scheme 4).[11]

The inactive species of the active site of GO consists in a Cu^{II} complex bound to two histidine and two tyrosine residues and a molecule of water. This species is activated by the oxidation of one tyrosine residue from the basal plane and consequent formation of a Cu(II)-tyrosyl complex. After coordination of the substrate to the metal center, the oxidation occurs *via* a proton-coupled electron-transfer (PCET) reaction and release of the formed aldehyde leads to the reduced form of the enzyme (Cu^{I}).

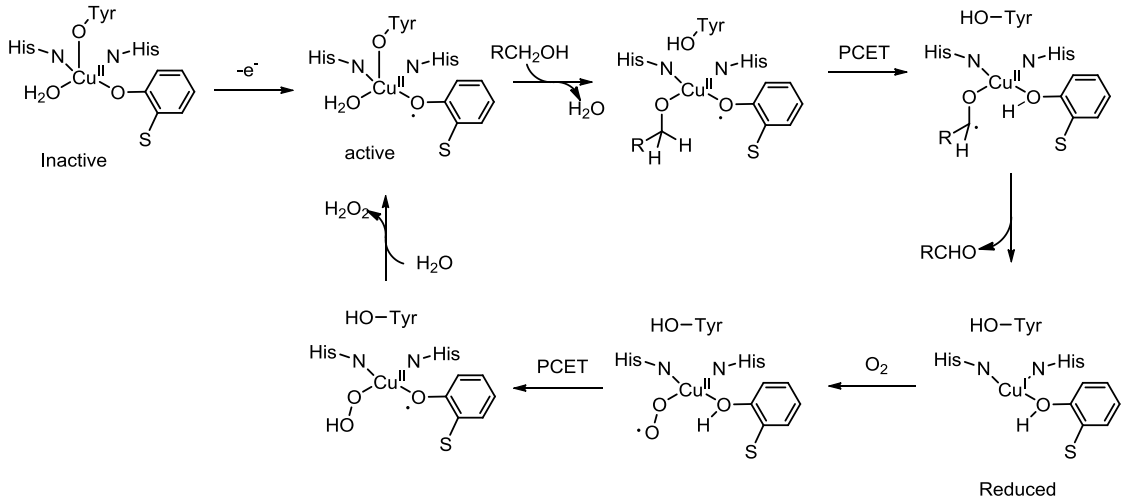

Scheme 4. Catalytic cycle of galactose oxidase enzyme.[7]

After reaction with dioxygen and a second proton-coupled electron-transfer reaction, the active site is recovered after the release of hydrogen peroxide. For this system, the redox-active role of the ligand is essential for the functioning of the catalytic system. The electronic structure of GO and the use of salen complexes as biomimetic models will be further discussed in section 2.2.2 of this chapter.

Another interesting example, where a redox-active ligand is exploited with another purpose than catalysis, was published by Wang and Stiefel in 2001.[12]

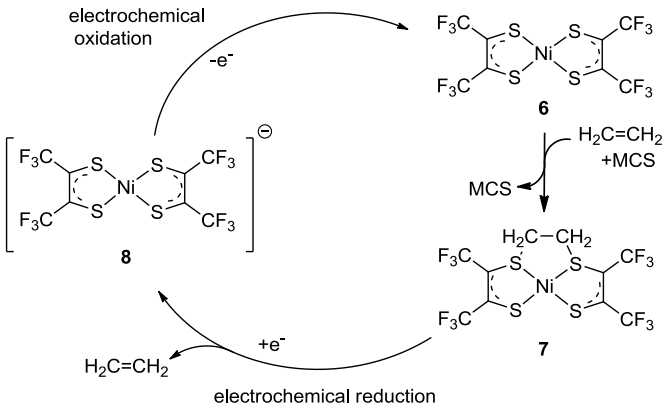

Scheme 5. Ethene purification by a dithiolene nickel complex. MCS = multicomponent stream.[12]

In this example mediation of a redox-active ligand allows the purification of light gases such as ethene. Neutral complex **6** reacts with ethene to form complex **7** (Scheme 5). The addition of ethene to the complex occurs through the sulfur ligand instead of the metal. The impurities commonly present in olefin streams such as hydrogen gas, carbon monoxide or acetylene, do not react with the complex, thus separating from the ethene.

The gas can be released from the complex by electrochemical reduction forming the anionic species **8**, which can be electrochemically oxidize to generate **6**.[12]

The last strategy (IV) arises from the use of the redox-active properties of the substrate itself.[7] Activation of the substrate by abstraction or donation of electron density, generates substrate-based radical species which possess a different reactivity and selectivity compared to their initial forms. Scheme 6 shows the example of the catalytic cycle of nitrene insertion into the C-H bond of the toluene.[13] The catalytic species is a non-heme complex of Fe^{II} (Scheme 6, **9**). The loss of one molecule of solvent yields **10**, and allows the coordination of an organic azide to form complex **11**. The loss of a molecule of N_2 generates a radical on the nitrene moiety. This reactive species abstracts a hydrogen from a toluene molecule leading to the formation of **13** and a benzyl radical which binds to the nitrogen and leaves the metal, recovering the catalyst **10** and releasing the insertion product.[13]

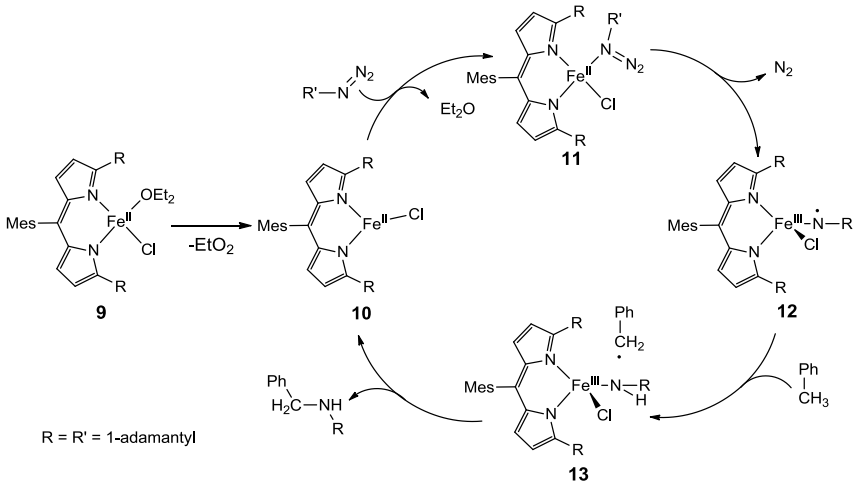

Scheme 6. Catalytic cycle of nitrene insertion in the C-H bond of toluene.[13]

The strategies presented in this section show how the use of redox non-innocent ligands can enhance the catalytic activity in various manners; their applications in catalysis have therefore opened new opportunities for chemists. However, they play also an important role in the chemistry of life.

1.3 Redox non-innocent ligands in bio-inorganic chemistry

Redox non-innocent ligands are found to participate as co-ligands in the active site of certain metallo-enzymes,[14] as well as substrates (O_2, NO, quinones).[15] The number of possible examples present in this area is very large and cannot be comprised in this

introduction. However, some illustrating examples will be briefly explained here in order to highlight the importance of these ligands in biological systems.

The non-innocent behavior of the O_2 molecule has been recognize due to its ability to bind under different oxidation states: dioxygen (O_2), which possesses a triplet ground state (S = 1), superoxide ($O_2^{\cdot-}$) as a doublet (S = 1/2), and peroxide (O_2^{2-}) which is diamagnetic (S = 0). Due to this redox variety, the coordination mode of the oxygen molecule in certain enzymes is still a topic of debate. This is case of the oxymyoglobin, the oxygenated form of myoglobin, a protein in charge of oxygen storage in muscle tissues. Since the determination of the X-ray structure of the oxymyoglobin in 1958,[16] different models concerning the coordination and oxidation state of the oxygen molecule have been proposed,[17] the most relevants by Pauling[17a] and Weiss[17e] (Scheme 7). The first one described the oxymyoglobin as a valence bond structure where the oxygen molecule is coordinated to the metal in an end-on way and both units are diamagnetic, as well as the whole molecule, in agreement with the spectroscopic data. However, Weiss proposed an electron transfer from the metal center to the oxygen molecule with consequent formation of a Fe^{III} center and a superoxide radical, which couple antiferromagnetically to lead to a diamagnetic molecule.[17e]

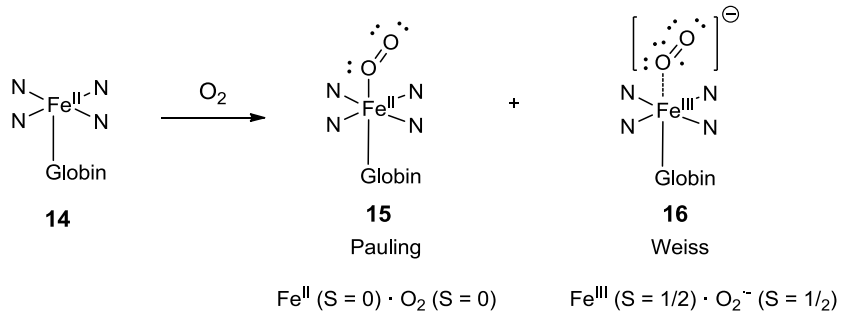

Scheme 7. Models for oxy-heme bindings. [17a,17e]

Both possibilities have been considered as valid, but recent theoretical investigations show a preference for the Weiss formulation, evidencing the non-innocent behavior of the oxygen molecule.[18]

Other redox active ligands widely present in nature are the quinones. These ligands participates in numerous biological systems[15,19] notably in respiration[20] and photosynthesis,[21] conferring them a high relevance. The design of redox-active ligands mimicking o-quinones or catechol systems has been comprehensively studied.[22] Phenyldithio, diamine and dioxolene ligands come up as the best candidates to mimic the electronic properties of these systems (Scheme 1).

Catechol dioxygenases are non-heme iron(III) enzymes which catalyzes intra-diol C-C bond cleavage reactions (Scheme 8).[23] The binding of catechol to the iron center (Scheme 8, **18**) and consequent electron transfer from the metal to the substrate generates the intermediate **19** where the substrate is activated and the iron center has been reduced to oxidation state +II. This intermediate is able to activate a dioxygen molecule (**20**) which inserts into the aromatic ring of the substrate (**21**) and promotes the bond cleavage.

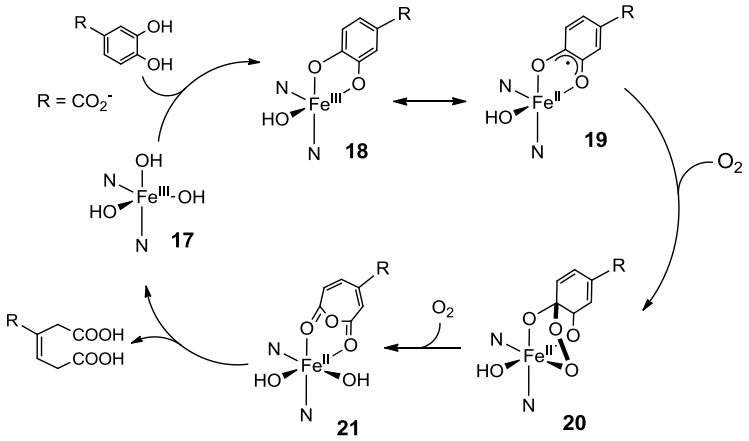

Scheme 8. Catalytic cycle of the protocatechuate 3,4-dioxygenase.[23]

Tetrapyrrolic macrocycles, such as porphyrins or corroles, are among the most important examples of redox-active ligands present in biological systems, able both to accept or donate electrons.[24] Porphyrins are dianionic ligands possessing four coordinating nitrogen atoms and a conjugated flat backbone (Por^{2-}). One-electron oxidation leads to the formation of the anionic radical $Por^{\cdot -}$, while one-electron reduction generates the trianionic form $Por^{\cdot 3-}$. One of the most well-known and studied examples of biological systems bearing porphyrin ligands is the cytochrome P-450. P-450 monoxygenases are heme-iron(II) enzymes which catalyze the oxidation of substrates *via* oxygen activation in a two-electron two-proton coupled reduction process (Equation 1).[25] One of the electronic structures proposed for the catalytic species involves an iron(IV)-oxo complex featuring one-electron oxidized phorphirinyl ligand ($Por^{\cdot -}$).[25c]

$$[Fe^{III}(Por^{2-})]^{+} + O_2 + 2e^{-} + 2H^{+} \rightarrow H_2O + [Fe^{IV}O(Por^{\cdot -})]^{\cdot +} \qquad \text{(Equation 1)}^{[25c]}$$

These examples give a general idea about the importance of redox non-innocent ligands in the field of catalysis for biological and industrial applications. The study and modification of the different mechanisms by which they work can allow us to control their reactivity, and thus to develop more selective and effective catalysts.

2. Salen ligands

The well-known salen ligands are very good example of redox non-innocent ligands and their properties have been largely investigated since their first synthesis.[26] Pfeiffer reported the synthesis of salen ligands (N,N′-Ethylenebis(salicylimine)) in 1933 by condensation of two salicylaldehydes with a diamine in mild conditions (Scheme 9).[27] Salen ligands contain two Schiff bases and two phenols that can act as coordinating groups, allowing the coordination of exogenous ligands in the axial positions.

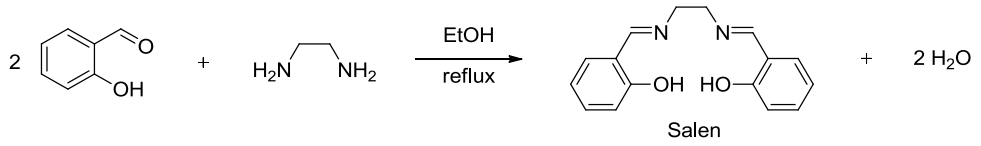

Scheme 9. Synthetic procedure for salen ligands.

Their convenient synthesis and the simplicity of the starting materials allow a large variety of structures for this ligand, *i.e.* a fine tuning of its electronic properties. The oxidation products of salen complexes lead in some cases to the formation of phenoxyl radical species, which has attracted the interest of numerous research groups.

2.1 Relevance of salen ligands in catalysis

Salen are NNOO moderate electron donor ligands. Their easy preparation allows the synthesis of a large number of ligands with wide structural and electronic diversity. The introduction of stereogenic centers is possible by introducing a chiral N,N linker. The conformation adopted by the complex and the different phenol substitutions can modulate the trajectory of the substrate approach and thus influence the diastereoselectivity. The presence of axial ligands also modifies the conformation of the complex. Theoretical calculations have shown that coordination of an axial donor ligand approaches the metal to the substrate in rate determining stereoselective processes.[26b]

Schiff-based complexes of early transition metals such as zirconium or titanium have been shown to be active in polymerization catalysis.[28] Recently the group of Wang has reported the use of a titanium(III) chloride salen complex as catalyst in the copolymerization of CO_2 and cyclohexene oxide.

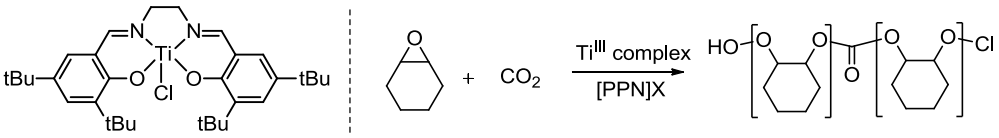

Scheme 10. [Ti(salen)Cl] complex (left) and copolymerization reaction (right).

Titanium salen complexes can also catalyze pinacol coupling of aromatic aldehydes following the protocol developed by Fürstner with the Ti^{IV} complex [Ti(salen)Cl_2].[29] Using a chiral linker, this coupling reaction can be made in an enantioselective manner with excellent enantiomeric yields (Scheme 11).[30]

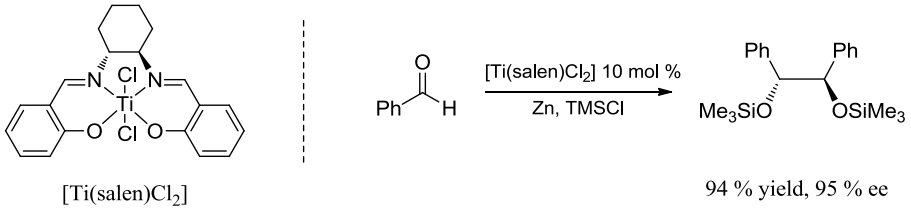

[Ti(salen)Cl_2]

Scheme 11. [Ti(salen)Cl_2] complex (left) and enantioselective pinacol coupling reaction (right). [30]

Iron salen complexes have been also investigated due to the similarity of salen ligands to porphyrins, which are widely present in biological systems. Fe(II)-salen complexes are unstable and get oxidized in presence of air and moisture, hindering their use in catalysis. However, Fe(III)-salen complexes prepared *in situ* promote the oxidation of sulfides in sulfoxides.[31] Dimeric chiral Fe(salen) μ-oxo species prepared by Nguyen are useful precursors for the formation of iron carbenes further used for the cyclopropanation of olefins (Scheme 12, left).[32] Complexes of ruthenium displaying chloride and nitrosyl groups in axial positions described by Katsuki, catalyze *cis* and *trans* epoxidation of olefins mediated by visible light (Scheme 12, right). Visible light irradiation promotes the dissociation of the nitrosyl ligand and thus the activation of the complex.[33]

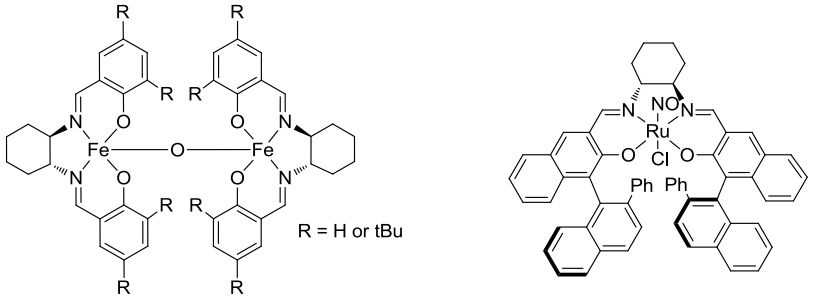

[Fe(salen)]$_2$ μ-oxo

22 **23**

Scheme 12. Fe(salen) μ-oxo species (left) and [Ru(NO)(Cl)] derivative (right). [32-33]

A stabilized ruthenium salen complex was synthesized by Nguyen using pyridine as axial ligands. This complex is a very efficient catalyst for the cyclopropanation of olefins (Scheme 13).[34]

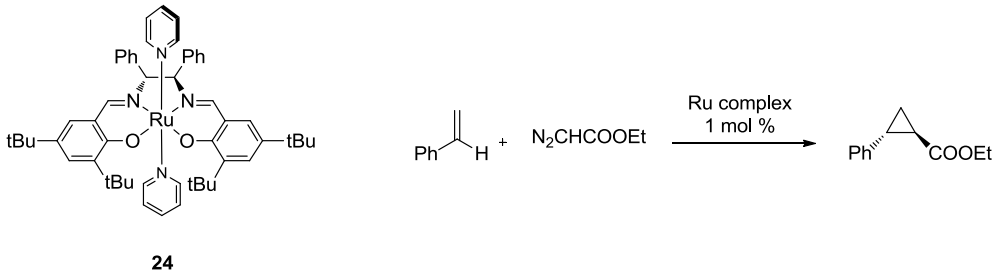

24

Scheme 13. [Ru(salen)$(py)_2$] complex (left) and diasteroselective cyclopropanation reaction.[34]

Cobalt salen complexes have been found to be active in various catalytic reactions. Co^{II} complexes displaying a square pyramidal geometry are able to bind O_2. Thus, [Co(salen)] has been used for the oxidation of phenols, indoles, flavonols and amines *via* coordination of the substrate to the metal center.[35] [Co(salen)] can be reduced to form Co^{I} species which are highly reactive and can activate small and inert molecules such as CO_2 *via* oxidative addition.[36]

Aluminum salen complexes are involved in the polymerization of propylene oxide, ethylene[37] and lactide.[38] Aluminum salen derivatives have been also useful in other reactions such as Meerwein-Ponndorf-Verley reductions,[39] Diels-Alder reactions or dipolar cycloadditions.[37]

Maybe one of the most known examples of salen-based catalysts is the Jacobsen's catalyst. In 1985 Kochi and co-workers reported the catalytic activity of manganese and chromium salen complexes in the epoxidation of alkenes by using PhIO as oxidant.[40] Some years later, Jacobsen and Katsuki independently reported the asymmetric epoxidation of alkenes using iodosylarenes as stoichiometric oxidants.

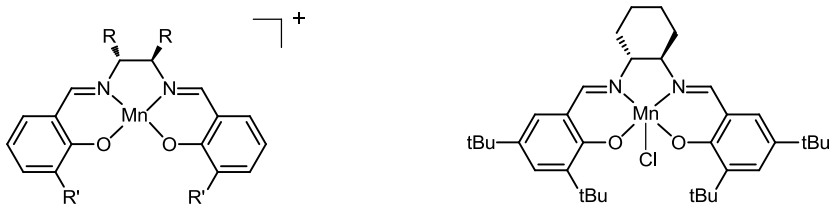

25 R = Ph, R' = H
26 R = Ph, R' = tBu

Jacobsen's catalyst

Scheme 14. First manganese salen complexes used in catalysis (left) and Jacobsen's catalyst (right).

First results obtained using complexes **25** and **26** (Scheme 14, left) included 1-8 mol % catalyst loadings and good-to-excellent enantiomeric yields (57-93 %) for the epoxidation of monosubstituted terminal, trisubstituted and *cis*-alkenes.[41] Some years later, Jacobsen introduced the used of bleach instead of iodosylarene as source of oxygen, making the reaction more operable.[42] The Jacobsen's catalyst displays *tert*-butyl substituents in the phenolate ring and a chiral diamine linker (Scheme 14, right), and was shown to catalyze the asymmetric epoxidation of a wide range of substrates such as *cis*-alkenes,[43] heterocyclic enamines,[44] or cinnamate esters.[45] The poor conversion of some substrates, such as terminal alkenes (styrene) was enhanced by using *m*-CPBA as oxidant. The Jacobsen's catalyst is utilized in industry and is commercially available.

2.2 Salen complexes as biomimetic models of galactose oxidase

Due to the electronic properties and the coordination environment of salen ligands, salen complexes have been used to build biomimetic models of Galactose Oxidase (GO) enzyme. Copper and, in another approach, nickel salen complexes have been proposed as mimics for the catalytic activity of GO. Before discussing the different complexes synthesized for this purpose, it is important to remind some aspects about the electronic configuration of copper and nickel centers, as well as that of the GO.

2.2.1 Electronic structure of Cu and Ni complexes displaying redox non-innocent ligands

Cu^{II} centers possess a $3d^9$ electronic configuration, thus leading to mononuclear paramagnetic complexes when featuring closed-shell ligands. They usually prefer octahedral geometries, but because of the important Jahn-Teller distortion present in these complexes,[46] square planar geometries are also very common. When bound to redox non-innocent ligands, the assignment of the oxidation state of the copper center becomes convoluted upon oxidation. Depending on the relative energy of both the metal and ligand orbitals (redox-active orbitals), the oxidation can take place either on the ligand or on the metal center. If the oxidation takes place on the metal center, a high-valent metal complex is generated (Scheme 15, left). Cu^{III} complexes possesses a $3d^8$ electronic configuration, and in square-planar environments this are diamagnetic (S = 0). It is the so-called "closed-shell singlet" configuration. On the other hand, if the frontier orbitals of the ligand possess higher energy than those of the metal, a ligand-centered oxidation occur leading to the formation of Cu(II)-radical species. In this case, where two unpaired electrons are present in the molecule, two configurations are possible.

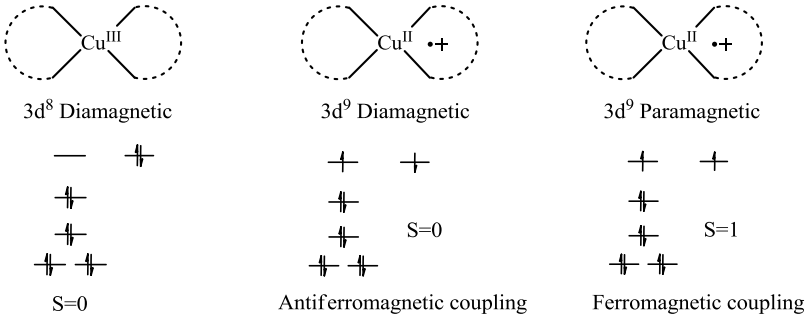

Scheme 15. Representation of the different electronic configurations for oxidized copper complexes in a square-planar environment.

If the unpaired spins couple antiferromagnetically, the total spin of the molecule is zero (S = 0), and the complex behaves as diamagnetic. This configuration is also called "open-shell singlet" configuration (Scheme 15, center). Contrarily, if these electrons couple ferromagnetically leading to a triplet state (S = 1), the molecule is paramagnetic (Scheme 15, right).

The similarity on the magnetic properties between the closed-shell and open-shell singlet configurations can lead to wrong or ambiguous oxidation state assignments. An illustrating example is found in the family of corrole complexes. Corroles are trianionic ligands and coordinated to Cu^{II} centers can give neutral complexes, so that in some cases these complexes have been described as Cu^{III} species.[47] This assumption led to the unfortunate formulation of Cu^{IV} species upon one-electron oxidation of the neutral corroles. However, structural[48] and computational studies[49] suggest an antiferromagnetically coupled radical complex as the best description for the ground state of neutral copper corroles. Nocera and co-workers illustrated this with the study of the electronic configuration of the one-electron oxidation and reduction products of a copper corrole (Scheme 16).[50]

The neutral species **21** displays a silent EPR spectrum and an "apparent" diamagnetic ^1H spectrum. When recording the NMR spectrum at different temperatures an important shift of certain signals was observed. This peculiar shift suggests a spin equilibrium between singlet and triplet species. Thanks to data obtained from VT-NMR and susceptibility measurements ,an open-shell ground state with a triplet state laying at 1236 ± 40 cm^{-1} was established.

The oxidized and reduced products both display EPR signals typical of Cu^{II} centers, demonstrating that both redox processes are ligand-based leading to closed-shell

configurations of the corrole macrocycle, this being tri-anionic in **21**$^{-}$ (Scheme 16, left) and mono-anionic in **21**$^{+}$ (Scheme 16, right).

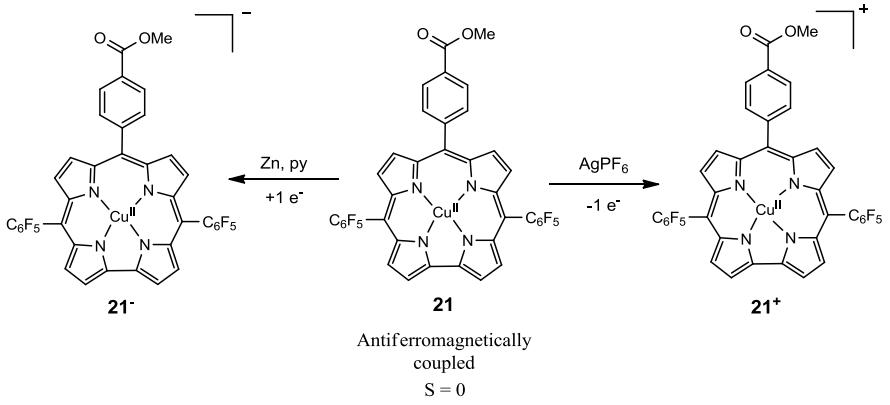

Scheme 16. Structures of the oxidized, neutral and reduced copper corrole investigated by Nocera and co-workers.[50]

The ferromagnetic or antiferromagnetic coupling between the metal center and the radical ligand seems to be governed by the geometry of the complex, which determines the overlap between the metal orbitals and the p orbitals of the π-system. For example, the semiquinone copper complexes presented in Scheme 17 present the same coordination environment but different electronic configurations.[51] The X-ray structure of [Cu(DBDE)]$^{+}$ (Scheme 17, left) shows a twist angle between the N-Cu-N and the O-Cu-O planes of 51°, while this angle was only of 14 ° for [Cu(TMCD)]$^{+}$ (Scheme 17, right). The ferromagnetic configuration is favored in planar complexes due to the orthogonality of the copper and semiquinone orbitals.[52] When the distortion from the planar geometry increases, the overlap between the basal copper orbitals and the semiquinone π system increases, favoring an antiferromagnetic coupling.[51]

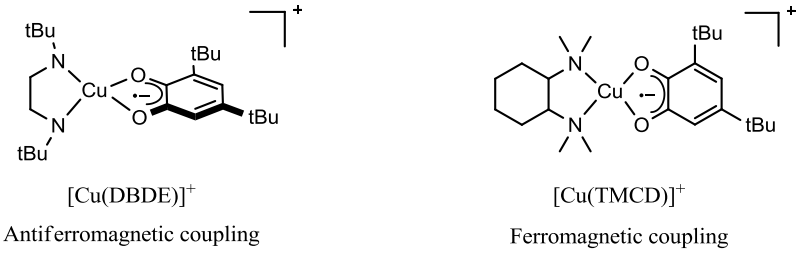

Scheme 17. Structures of semiquinone [Cu(DBDE)]$^{+}$ and [Cu(TMCD)]$^{+}$ complexes.[51]

Examples of Cu^{III} complexes displaying redox-non innocent ligands are rare in the literature.[52b] These complexes are usually stabilized in square planar geometries by the use of carboxylates,[53] thiolates,[54] or oxamates[55] as ligands.

Concerning the electronic structure of one-electron oxidized Ni complexes displaying redox non-innocent ligands, the assignment of the oxidation state of the metal becomes easier. Ni^{II} complexes possess a $3d^8$ configuration and are diamagnetic in a square planar environment. Upon oxidation, both high-valent metal (Ni^{III} $3d^7$, Scheme 18, left) and radical complexes ($Ni^{II}L^{+\cdot}$, Scheme 18, right) are paramagnetic (S = 1/2). Contrary to copper complexes, EPR techniques allow the assignment of the oxidation state of the metal relatively easy.

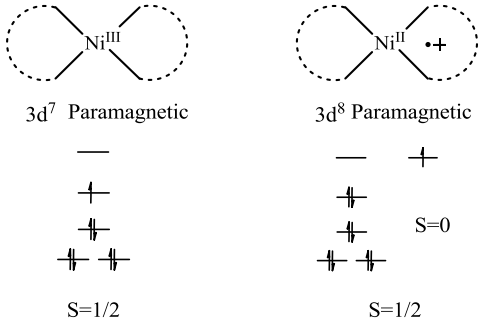

Scheme 18. Representation of the different electronic configurations for Ni oxidized complexes in a square-planar environment.

Few examples of Ni^{III} complexes exist in the literature. Octahedral environments favor the stabilization of these high-valent metal centers.[56] In a square planar geometry, these centers are stabilized by strong donating ligands such as amidates,[57] oxamidates,[58] and recently Mirica and co-workers reported the characterization of an organometallic Ni^{III} complex.[59]

Oxidized products of nickel salen complexes are usually characterized as Ni(II)-radical complexes. A valence tautomerism, where ligand radical species are favored at high temperatures and Ni^{III} species are stabilized at low temperatures, has been reported in some cases.[60] This was explained by the presence of exogenous ligands, whose coordination to the metal center was reinforced at low temperatures, favoring the stabilization of the Ni^{III} complex.[56,61] Another explanation related to the difference between the relaxation times of metal and organic radicals was proposed as well by J-L. Pierre and co-workers. Since the change on the EPR signal was observed at temperatures close to the melting point of the solvent, only the organic radical contribution, which relaxes slower than the metal, was observed in solution (high temperature), while the metal contribution, which relaxes faster, was observed for the frozen solutions (low temperature).[62]

2.2.2 Galactose oxidase enzyme

GO is an extracellular enzyme found in several fungal species[63] that belongs to the family of oxidoreductases. This copper enzyme catalyzes the two electron oxidation of primary alcohols to form the corresponding aldehydes with release of hydrogen peroxide. This two electron oxidation is effective thanks to the synergy between the copper center and a tyrosyl radical residue. The X-ray structure of GO, resolved in 1991,[64] shows that the copper center displays a square-based pyramidal coordination environment in the active site with two histidines, one tyrosine and an exogenous ligand (water or acetate molecule) in the equatorial positions, and another tyrosine residue occupying the apical position. The second coordination sphere is highly important in enzymes, therefore other structural factors have been shown to have an influence on the catalytic activity of the GO. A cysteine residue was found to be linked through a thioether bond to the carbon in *ortho* position to the oxygen in Tyr272. This binding reduces the flexibility of the tyrosine residue and is believed to lower the redox potential of the tyrosine, making its oxidation easier.[65] The catalytic cycle, already explained in section 1.2, is not discussed in this section.

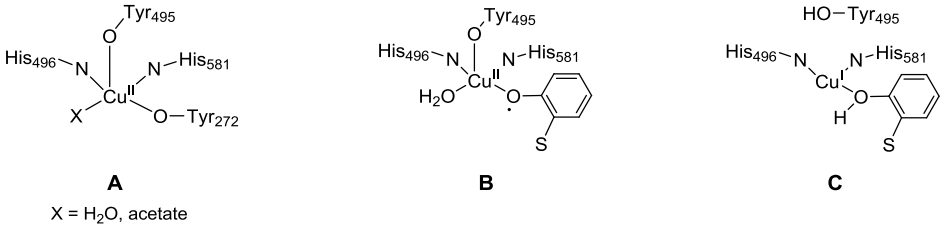

Scheme 19. Oxidation forms of the GO.[65a]

As mentioned above, the enzyme can be present in three different oxidation forms. In the inactive form (Scheme 19, **A**) all the amino acid residues bound to the Cu^{II} center are present in their closed-shell configuration. In the active form (Scheme 19, **B**), the Tyr272 has been oxidized and is bound to the Cu^{II} center as a tyrosyl radical. Finally, the reduced form (Scheme 19, **C**) consists in a Cu^{I} center bound to the protonated Tyr272 resulting from the release of the oxidized substrate.[65a]

These three species have been characterized by spectroscopic techniques and the active form (Scheme 19, B) turned out to possess a diamagnetic ground state due to a strong antiferromagnetic coupling between the unpaired electron of the copper center and the free radical of the tyrosyl moiety. From TD-DFT calculations the coupling constant has been calculated at 752 cm^{-1}.[66]

2.2.3 Examples

Several small molecules have been synthesized in an attempt to mimic the electronic and/or the geometrical properties of GO.[67] These ligands incorporate phenol groups bearing bulky substituents at the *ortho* and *para* positions which stabilize the formed radical and prevent dimerization through the phenoxyl ring.

In 1998, Stack and co-workers reported the electronic structure of four salen-type complexes, establishing the bases of the use of salen complexes as biomimetic models of the GO enzyme.[68] These complexes presented a salen-type ligand with disubstituted phenol rings (SPh, tBu, SiPr or Br) and a binaphtyl as bridging moiety. The X-ray structures of the neutral complexes displayed a non-square planar coordination geometry around the metal center.

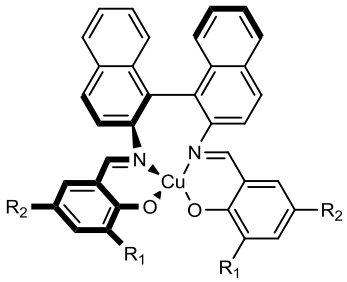

[Cu(II)BSP] R_1 = SPh, R_2 = tBu
[Cu(II)BSI] R_1 = SiPr, R_2 = tBu
[Cu(II)BDB] R_1 = R_2 = tBu
[Cu(II)BBR] R_1 = R_2 = Br

Scheme 20. Copper salen-type complexes reported by Stack and co-workers.[68]

The one-electron oxidation of these complexes occurs on the phenol moieties leading to the formation of EPR-silent species, in agreement with the electronic structure of the active form of GO (Scheme 19, B). These complexes demonstrated catalytic activity towards benzyl and allylic alcohols in presence of a small amount of base at 1 atm of O_2 and room temperature.

From these first examples, a wide variety of salen complexes have been studied in an attempt to establish new GO models, as well as tuning the oxidation locus; few of these examples will be discussed here.

One of the most relevant examples is the case of the salen complex [CuSal] (Scheme 21).[69] This complex presents tert-butyl substituents in the *ortho* and *para* positions of the phenol and a cyclohexyl linker. The importance of this complex does not reside on its catalytic activity, which was found to be rather low, but on its electronic structure. $[CuSal]^+$ was described as a Cu^{III} complex in the solid state thanks to X-ray diffraction, magnetic susceptibility, K-edge XAS, L-edge XAS and XPS measurements.[69] $[CuSal]^+SbF_6^-$ is the first example of a Cu^{III} complex featuring a salen ligand, while Cu^{III} centers are normally

stabilized in square planar environments by polyanionic or strong polarizable ligands.[55,70] Interestingly, this closed-shell configuration was reported to be involved in a temperature-dependent equilibrium with nearly isoenergetic triplet state radical species (S = 1, Scheme 21).[69]

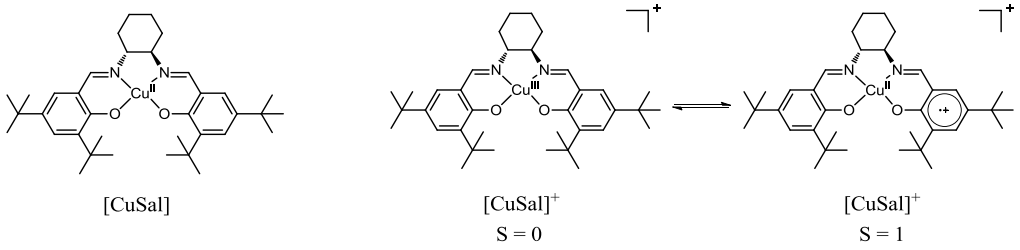

Scheme 21. [CuSal] complex (left) and spin equilibrium of $[CuSal]^+$ in solution.[69]

This equilibrium was established by variable temperature absorption spectroscopy, NMR and magnetic susceptibility measurements; the high-valent metal form being favored at low temperature. The presence of both species in solution was explained by a greater flexibility of the ligand in solution. The generated radical is coupling ferromagnetically with the electron of the copper, and displays an EPR-silent spectrum due to a large zero-field splitting. $[CuSal]^+$ displays weak catalytic activity in the oxidation of benzyl alcohol in which the rate determining step is the abstraction of the hydrogen atom from the α-position of the benzyl alcohol.[69]

Reduced salen derivatives, displaying amines instead of imines (labelled salan), have been studied as well (Scheme 22). Their copper complexes possess lower oxidation potentials due to the better σ-donation of the amine functions: $E^1_{1/2}$ = 0.08 and 0.11 V *vs.* Fc^+/Fc for $[CuSal^{red}]$ and $[CuSalen^{red}]$ respectively, while $E^1_{1/2}$ = 0.45 V for [CuSal].[71]

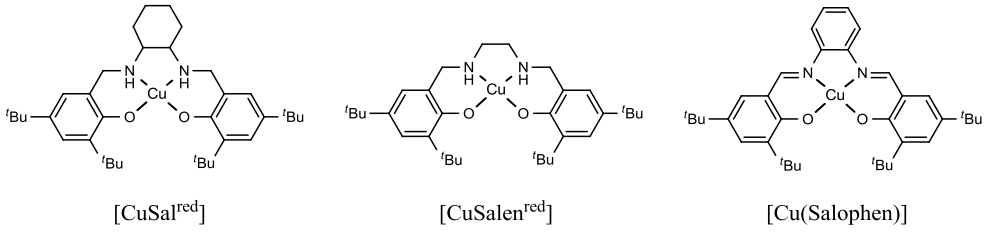

Scheme 22. $[CuSal^{red}]$ (left), $[CuSalen^{red}]$ (middle) and [Cu(Salophen)] (right) complexes.

The oxidized products of $[CuSal^{red}]$ and $[CuSalen^{red}]$ give temperature-invariant phenoxyl radical complexes which display silent EPR spectra[72] due to either an antiferromagnetic coupling between the spins, or a ferromagnetic coupling with a large zero-field splitting parameter. At low substrate concentrations $[CuSal^{red}]^+$ was found to catalyze the oxidation

of benzyl alcohol 12 times faster than $[CuSal]^+$ explained by disfavored axial substrate coordination to the Cu^{III} complex.[72] $[CuSalen^{red}]^+$ was shown to oxidize primary alcohols such as methanol, ethanol or *n*-butanol in their respective aldehydes in presence of catalytic amounts of base.

In order to increase the rigidity of the ligand, a phenyl ring was introduced in the ligand backbone as N,N linker. This does not modify only the geometry of the complex, but also the electronic properties because of conjugation of the phenolates and the aromatic linker *via* the imine functions. Despite the redox-active properties of the phenylene linker, oxidation of [Cu(Salophen)] leads also to the formation of Cu(II)-phenoxyl species. However, an equilibrium was established between the partially localized phenoxyl species in one side of the molecule and the fully delocalized structure present in solution and at room temperature.[73]

Due to their close electronic structure, nickel salen complexes have been also studied as biomimetic models of the Galactose Oxidase. The easier characterization of the one-electron oxidized products compared to the copper analogues, notably by EPR, helps for the better understanding of the electronic configuration of the oxidized products. Ni centers possess also a biological relevance as they are present in several enzymes.[74]

In most of the cases, similar electronic structures have been described for nickel and copper salen complexes when displaying the same ligand. For example, $[NiSal^{OMe}]^+$ and $[CuSal^{OMe}]^+$ complexes, which display methoxy substituents in the phenolate rings, were both characterized as phenoxyl radical complexes (Scheme 23). The X-ray structure of both oxidized species show a quinoid pattern of the phenoxyl ring.[75]

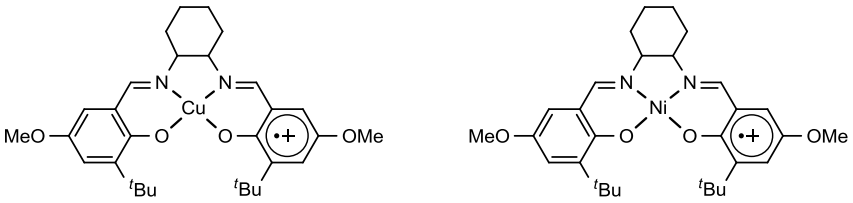

$[CuSal^{OMe}]^+$ $[NiSal^{OMe}]^+$

Scheme 23. $[NiSal^{OMe}]^+$ and $[CuSal^{OMe}]^+$ complexes.[75]

However, some differences have been found in the description of the nickel and copper oxidized species. While $[CuSal]^+$ was characterized as a Cu^{III} complex in the solid state, the radical form is favored in its nickel analogue, which remains a Ni(II)-radical complex from 5 to 295 K.[76] The EPR signal obtained at g_{iso} = 2.045, intermediate between those of

phenoxyl coordinated species and Ni^{III} complex (g_{av} = 2.13-2.17),[77] indicates a non-negligible contribution of the metal orbitals to the SOMO.

Another example of different electronic behavior was recently reported by Storr and co-workers.[78] A salen ligand displaying electron-withdrawing groups in the phenolate rings (CF_3) was shown to stabilize the high-valent metal form at low temperature for the copper derivative, while the nickel species are present in the radical form in the temperature range studied (Scheme 24).

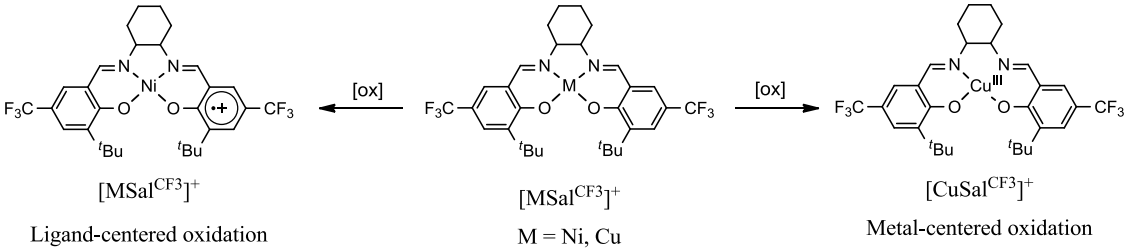

Scheme 24. Oxidized forms of [NiSal^{CF3}]$^+$ and [CuSal^{CF3}]$^+$.[78]

3. Phosphasalen ligands

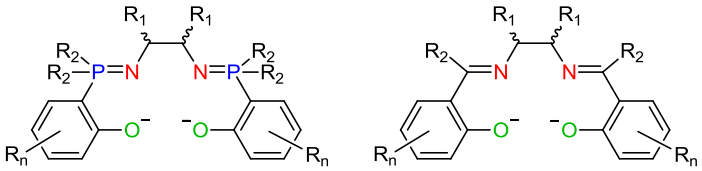

Scheme 25. Structures of phosphasalen and salen ligands.

Phosphasalen ligands have been developed in our laboratory and can be described as the phosphorus counterparts of the salen ligands.[79] Despite the different modifications introduced in the salen backbone, few examples including heteroatoms are present in the literature. Iminophosphorane functions possess completely different electronic and geometrical properties than imines. Therefore, this small variation in the salen structure entails a change of the electronic and geometric properties of the ligand, making them more electron-donating and more flexible. Their synthesis was first reported in 2011 together with the first coordination complexes.[80] Since then, phosphasalen ligands and their coordination chemistry have been developed, including their application in catalysis.[81]

3.1 The iminophosphorane function

Iminophosphorane functions often depicted with a double bond between a phosphorus and a nitrogen atom. They were first synthesized in 1919 by Jules Meyer and Herman Staudinger.[82] Iminophosphoranes are the conjugated bases of the aminophosphonium groups, where the nitrogen atom is protonated.

Scheme 26. Iminophosphorane and aminophosphonium functions.

3.1.1 Synthesis

The main methods concerning the synthesis of iminophosphorane functions are those developed by Staudinger (1919)[82] and Kirsanov (1950),[83] including the modification introduced by Horner and Oedinger (1959).[84]

The Staudinger reaction consists in the nucleophilic addition of an organic azide (R'-N_3) to a phosphine (PR_3) leading to the formation of the iminophosphorane function and releasing of nitrogen (Scheme 27).[82] Staudinger proposed the formation of a "nitrogen-rich compound", a phosphazide (R_3PN_3R'), during the reaction. Isotopic studies determined that the nitrogen atom incorporated to the phosphine corresponds to the N_γ.[86]

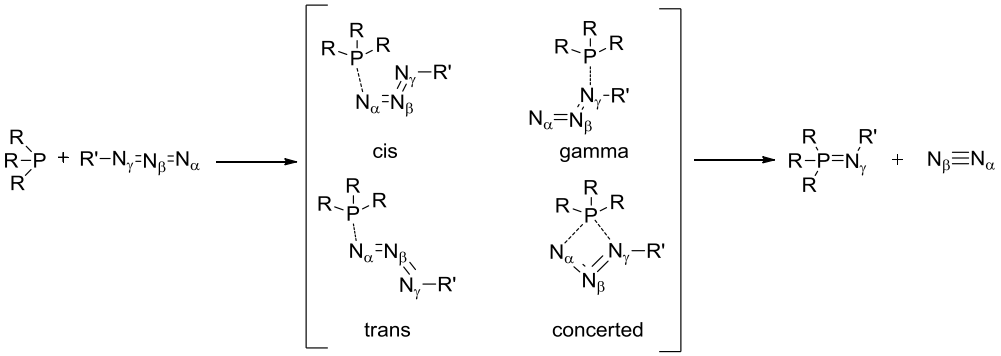

Scheme 27. Staudinger reaction and possible intermediates.[86]

Kinetic studies done by J.E. Leffler and R. D. Temple hypothesized that the formation of the iminophosphorane function occurs *via* a *cis* intermediate. Other possibilities, such a *trans* or gamma intermediates, or a concerted process were considered as well. Theoretical calculations done by the group of Wang using the reaction between PH_3 and NH_3 as model,

pointed to the *cis* intermediate as the most stable and possessing the lowest activation barrier.[86] One of the advantages of this reaction is the formation of N_2 as side product, which is easily removed of the reaction medium. Furthermore, the reaction can be applied to a wide range of phosphines. The only drawback of this reaction is the use of organic azides that can be explosive, the use of this method being unwise for large scale synthesis.

The second method derives from a reaction of PCl_5 with phenylsulfonamide described by Kirsanov in 1950.[83] During this reaction an aminophosphonium is formed which in presence of a Grignard reagent generates the corresponding iminophosphorane (Scheme 28).

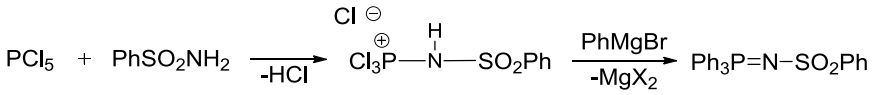

Scheme 28. Kirsanov reaction described in 1950.[83]

A modification of this reaction was done by Horner and Oedinger in 1959. They used an *in situ* generated bromophosphonium salt (Scheme 29, A), obtained by the bromination of a tertiary phosphine, instead of PCl_5. The nucleophilic substitution of the aromatic amine leads to the formation of the aminophosphonium salt (Scheme 29, B), which in presence of a tertiary sacrificial amine forms the iminophosphorane compound (Scheme 29, C).[84]

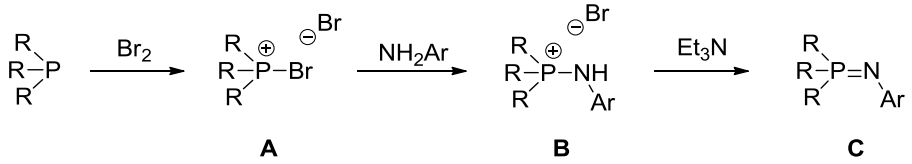

Scheme 29. Horner-Oedinger variation of Kirsanov reaction.[84]

In 1963, H. Zimmer applied this method using alkyl amines but the isolated product turned out to be the aminophosphonium salt.[88] The triethylamine was not strong enough to deprotonate the aminophosphonium and stronger bases, such as KHMDS, were necessary to form the iminophosphorane. This can be seen as an advantage since the ionic form is more stable towards humidity and air than iminophosphoranes. Thus, they can be stored under their stable aminophosphonium form and be generated *in situ* by using a strong base.

A great variety of amines can be used with this method, contrary to the Staudinger reaction which is limited by the hazards of the azides. The use of chiral amines is

especially interesting for applications in catalysis.[88] This reaction has been largely used in our laboratory, and is applied for the synthesis of phosphasalen ligands.[79]

3.1.2 Electronics and geometrical parameters

Iminophosphorane functions are usually described with a double bond between the nitrogen and phosphorus atoms (Scheme 30, B). However, due to the difference in the electronegativity of both atoms, the zwitterionic form, where the charges are separated, is valid as well (Scheme 30, A).

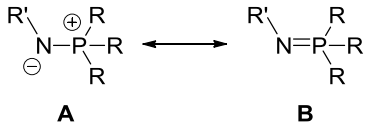

Scheme 30. Limiting resonant forms of the iminophosphorane function.

Based on literature data in the solid state, the average bond length for an iminophosphorane is 1.58 Å. This distance is intermediate between the average bond length of aminophosphines (1.71 Å) and that of iminophosphanes (1.55 Å),[89c] thus the double bond treatment of the iminophosphorane bond is acceptable.

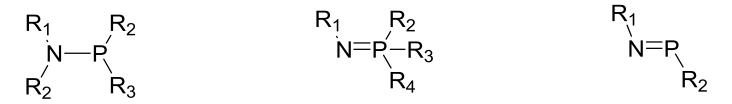

Scheme 31. Aminophosphine, iminophosphorane and iminophosphane structures and corresponding bond lengths averages.[89c]

Moreover, according to the Valence Shell Electron Pair Repulsion theory (VSEPR), the P-N-R angle in case of a double bond must be around 120 °, while this must be around 109 ° in case of a simple bond. In the solid state, an average of 123 ° has been found for iminophosphorane functions suggesting a strong double bond character in the solid state.[89c]

However, these experimental observations seem to be in contracdiction with *ab-initio* calculations concerning the rotation barrier of the P-N bond on the molecule $HN=PH_3$, which was found rather low, 2.1 kcal/mol, pointing to a simple character of the bond.

To get further information of this system, calculations of the molecule $HNPH_3$, as well as the imine ($HNCH_2$) and the ylure (H_2CPH_3) analogues have been performed using B3LYP

functional and 6-31+G* basis set. The following results have been published in the thesis of A. Buchard and T.P.A. Cao.[89]

NBO (Natural Bond Orbitals) analysis tends to localize the electrons for a given wave function, leading to a picture which is close to the Lewis structure. NBO analysis of $HNPH_3$ shows a localization of the lone pairs in the nitrogen atom, with a very small contribution of the phosphorus orbitals (Figure 1). The first pair (L1) is localized in a hybrid sp^x orbital (47 % s, 53 % p, occupancy 1.88), and the second one (L2) is localized in a pure p orbital (occupancy 1.75). These localized forms suggest that the zwitterionic form would better describe this bond. However, the occupancy in both orbitals is lower than 2 entailing a certain delocalization of the lone pairs in the phosphorus orbitals.

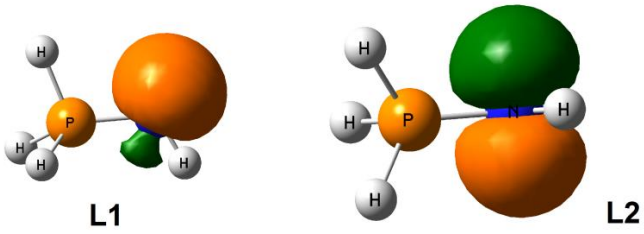

Figure 1. Lone pairs of the nitrogen for the molecule $HNPH_3$.[89]

Indeed, some electronic density is delocalized in the unoccupied σ*(P-H) antibonding orbitals, reinforcing the P-N bond. This interaction (delocalization) is named negative-hypercongugation, and is stabilizes the lone pair L1 by 17 kcal/mol and L2 by 33 kcal/mol (Figure 2 and Figure 3).[89]

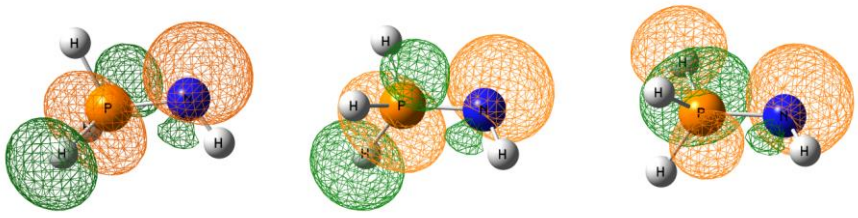

Figure 2. Stabilizing interactions between L1 and three σ*(P-H) antibonding orbitals.[89]

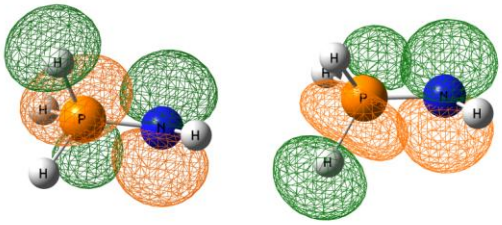

Figure 3. Stabilizing interactions between L2 and two σ*(P-H) antibonding orbitals.[89]

As said before, this analysis tends to localize the electrons and minimize delocalization, then these cannot be taken as the real molecular orbitals. It is necessary to check the orbitals obtained by DFT calculations.

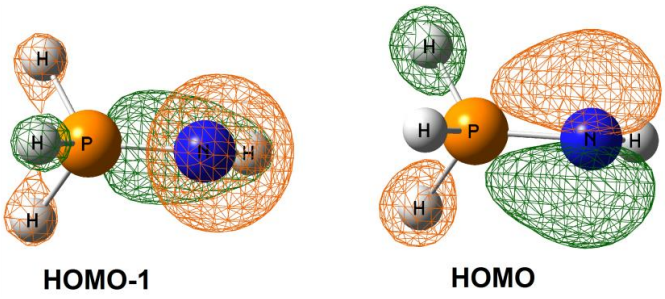

Figure 4. DFT calculated orbitals for $HNPH_3$. [89]

HOMO and HOMO-1 of the molecule $HNPH_3$ are depicted in Figure 4. The shape of these orbitals is not very different than that obtained for the localized pairs L1 and L2, discarding the possibility of a π-system for the P-N bond.

This is also supported by the Wiberg index obtained by NBO analysis, which estimates the bond order. Thus, the Wiberg index is 2.03 for the imine (H_2C=NH), while this is 1.34 for the iminophosphorane (HN=PH_3) and 1.37 for the ylure (H_3P-CH_2).[89]

From these analyses we can conclude that the P-N bond does not possess a double bond character and could be seen as a simple bond where a charge separation exists. However, the negative hyperconjugation between the lone pairs of the nitrogen and the phosphorus orbitals reinforces the P-N interaction. This will be determining on the reactivity of the iminophosphorane compounds.

Even though the P=N representation of bond is not strictly correct, it will be used in this manuscript as this is done in the literature.

3.1.3 Basicity and hydrolysis

Due to the presence of the localized lone pairs on the nitrogen, iminophosphoranes are strong bases. The first iminophosphorane base was synthesized by Schwesinger and co-workers in 1987 (Scheme 32) and is one of the strongest existing bases.[90] Since then, the design of iminophosphorane bases has been persecuted and a great variety of these superbases have been developed by Schwesinger and co-workers.[91] The basicity is increased by the introduction of electron-donating substituents. Some examples are present in Scheme 32.

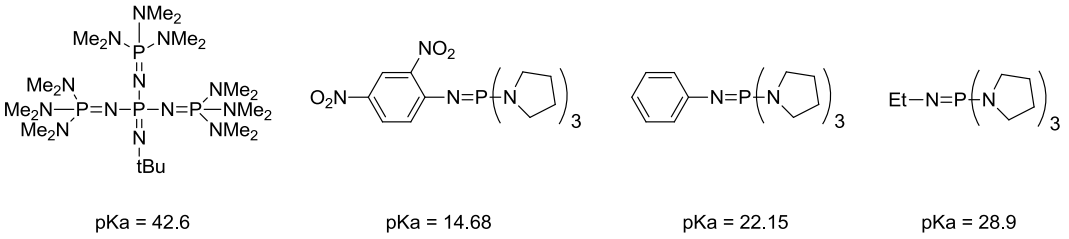

Scheme 32. Example of iminophosphorane bases.[90-91]

Because of the electrophilic character of the phosphorus, iminophosphorane functions usually decompose in water. It can be either by protonation of the nitrogen atoms in acid medium, or attack of hydroxides groups to the phosphorus in basic medium.

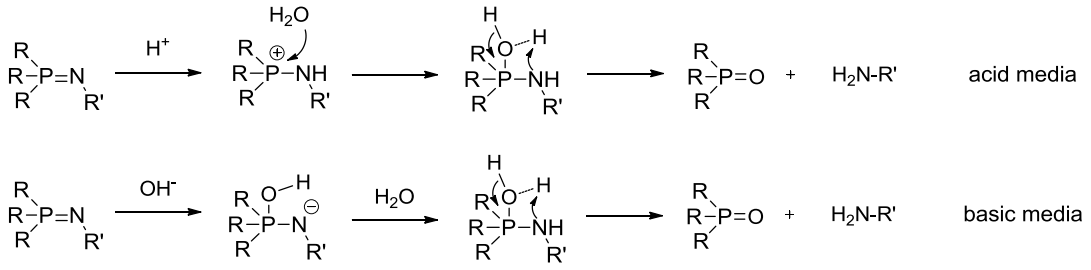

Scheme 33. Hydrolysis of the iminophosphorane function.

3.2 Electronic properties of phosphasalen ligands

Phosphasalen are dianionic ligands displaying two nitrogen and two charged oxygen coordinating atoms.

Due to the presence of two lone pairs in the nitrogen atoms iminophosphorane functions act as strong bases and their coordination properties differ markedly from those of imines. Iminophosphorane are strong σ and π donors. Because of the absence of a π-system in the P=N bond, there is not backbonding from the metal, contrary to imines which act as σ-donors and π-acceptors. The phosphorus atom does not participate in the coordination.

However, the phosphorus substituents create a steric hindrance in the second coordination sphere.

Iminophosphoranes are hard bases according to the HSAB theory,[92] thus they prefer to coordinate electron-poor metals, such as early transition metals or metals in high oxidation states.

Upon coordination, an elongation of the P=N bond occurs due to the shift of the electron density towards the metal leading to a weaker negative hyperconjugation. Consequently, a contraction of the P-R bonds must theoretically occur, because of the partial depopulation of the antibonding σ*(P-R) orbitals. This suggests that the zwitterionic form is reinforced upon coordination.

As in salen ligands, phenolate moieties are redox-active conferring them redox non-innocent properties. The electronics of the phenolate rings are easily modified by the substituents. Better electron-donating groups increase the electron density on the ring favoring its oxidation and stabilizing the generated radical.[93] On the other hand, electron-withdrawing groups decrease the energy of the phenolate orbitals, favoring a metal-centered oxidation.[78]

The phosphorus and nitrogen substituents determine the extent of the negative hyperconjugation, which influences the electronic properties and consequently, the coordination to the metal.

Because all of this, phosphasalen ligands are more electron-donating and more flexible than the salen analogues, and should favor the stabilization of high-valent metal complexes (discussed below).[79]

The tuning of the donating ability of iminophosphorane functions, as well as that of the phenolate rings, will be discussed in this manuscript.

3.3 Synthesis of phosphasalen ligands

The synthesis of phosphasalen ligands was first published in 2011[79,80] by the groups of P.Diaconescu and our group. The former followed the Staudinger reaction to synthesize the phosphorus analogues of salphen ligands, which include a ferrocene unit in the ligand backbone. In our case, we the Kirsanov reaction modified by Horner and Oedinger (see section 3.1.1).[84] Phosphasalen ligands are usually obtained as their aminophosphonium salt form. The retrosynthesis of the ligand is depicted in Scheme 34. A general synthetic

optimized procedure is here explained, a more detailed discussion concerning the synthesis of the different ligands used in this work will be found in each chapter.

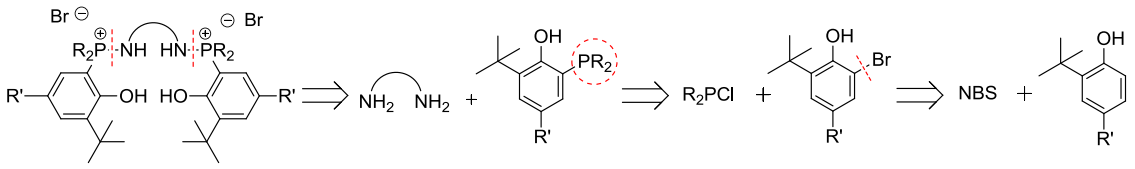

Scheme 34. Retrosynthesis of phosphasalen ligands.

Firstly, the phosphine is readily achieved from the corresponding phenol. The presence of a tert-butyl group in the *ortho* position provides a better solubility to the complex and avoids possible dimerization.

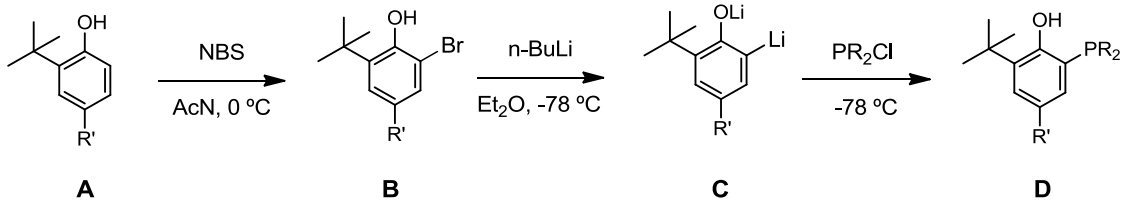

Scheme 35. General synthetic procedure for the phosphine starting materials.

The corresponding phenol is treated with N-bromosuccinimide to obtain the *ortho* brominated product **B** which reacts with two equivalents of n-BuLi to give the *ortho* lithiated product **C** which is then reduced with a chlorophosphine, leading to **D**. After aqueous work-up, the phosphines are obtained as powders in good yields.

Following the Horner-Oedinger modification of the Kirsanov reaction, the phosphine is brominated to obtain the phosphonium bromide intermediate **E** (Scheme 36). This intermediate reacts with the diamine bridge in presence of a non-nucleophilic base to form the desired product **F**, which is purified by precipitation.

The nature of the diamine linker and the solubility of the ammonium and aminophosphonium salts formed determine the choice of the sacrificial base. For example, tributylamine is used when the linker is ethylenediamine, while DABCO (1,4-Diazabicyclo[2.2.2]octane) is used when the ligand displays an aromatic linker.[89b]

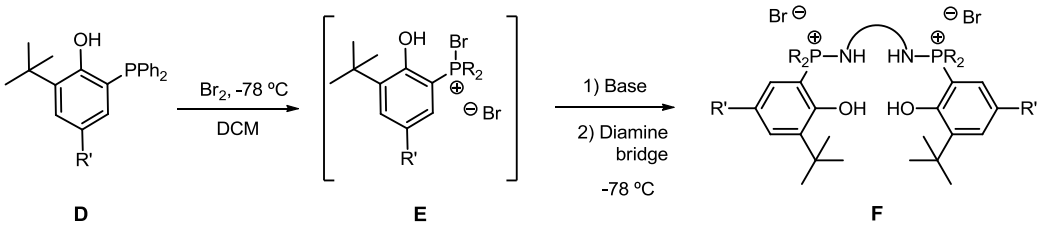

Scheme 36. General synthetic procedure for phosphasalen ligands.

Different variations can be introduced on these ligands by changing the phenolate substituents, the phosphorus substituents or the linker between the two nitrogens, allowing the creation of a great library of ligands.

Some already published phosphasalen ligands are shown in Scheme 37. These ligands were obtained as white powders in yields ranging from 69 to 78 %.[89b]

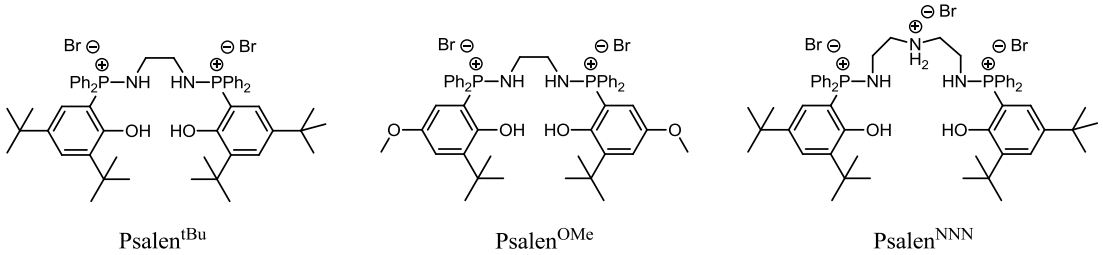

Scheme 37. Examples of phosphasalen ligands.[89b]

3.4 Previous work

3.4.1 First complexes

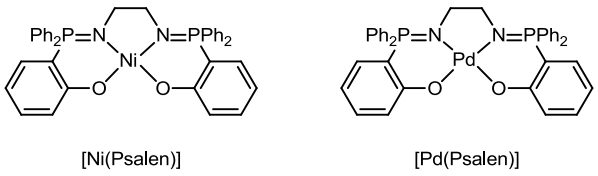

Scheme 38. [Ni(Psalen)] and [Pd(Psalen)] complexes.[79]

First coordination studies were made with nickel and palladium using unsubstituted ligands. These complexes were studied from a geometrical and theoretical point of view.[79] The X-ray structures of these complexes display nearly square planar geometries and the M-N and M-O bond lengths were longer in average compared to their salen counterparts. A significant difference with respect to the salen analogues was observed in the redox potentials of these complexes, which are more easily oxidable. This is due to the

presence of the better electron-donating iminophosphoranes instead of imines. These complexes were found to be essentially diamagnetic, but a small paramagnetic contribution was detected for the nickel derivative in solution (μ_{eff} = 1.40 μ_B). This was studied by DFT calculations which confirmed a small singlet-triplet energy gap, resulting in the presence of triplet species in solution.[79]

3.4.2 Catalytic applications

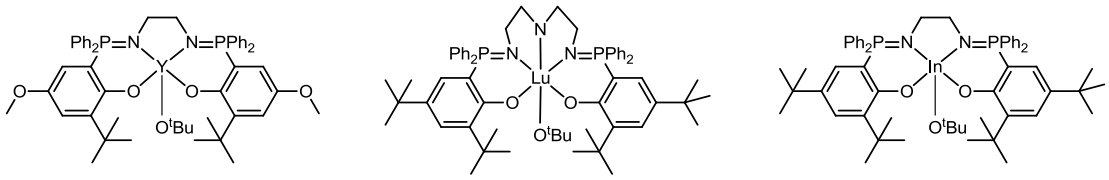

Scheme 39. Some of the phosphasalen complexes studied for rac-lactide polymerization.[81a]

A series of phosphasalen ligands differing by the amino-linker and the phenolate substituents were studied towards Ring Opening Polymerization (ROP) of lactide (LA).[81] ROP initiators are highly desirable because of the numerous of polylactid.[94] Yttrium, lutetium and indium phosphasalen complexes were found to be good initiators and exhibit high rates of ROP for *rac*-lactide, good selectivity and high stereo-control, even at low loadings. Depending on the ligand backbone and the metal, heteroselective or isoselective polymerization takes place. They present, in some cases, higher activity and rates than their salen analogues despite the reduced Lewis acidity of the metal which was explained by a more labil M-alkoxide bond allowing an easier migration and thus, a rapid propagation.[81b]

3.4.3 Ni^{III} phosphasalen complex

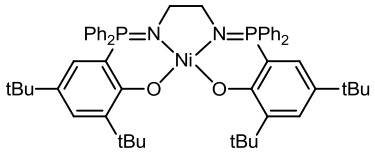

[Ni(Psalen^{tBu})]

Scheme 40. [Ni(Psalen^{tBu})] complex. [95]

In 2014 the synthesis and characterization of the [Ni(Psalen^{tBu})] complex and its one-electron oxidized species was reported (Scheme 40).[95] This complex displays *tert*-butyl substituents in the *ortho* and *para* positions of the phenolate rings, an ethylenediamine bridge and phenyl substituents on the phosphorus atoms.

[Ni(Psalen^{tBu})]$^{+}$SbF$_6^{-}$ turned out to be a high-valent Ni^{III} complex, stable in solution and in the solid state at room temperature. This was established by EPR spectroscopy, which shows for both solution and solid state samples a rhombic signal with g values typical for Ni^{III} centers.[95] Magnetic measurements confirmed this hypothesis for the solid state. This complex was characterized as well by X-ray diffraction and UV-visible spectroscopy.

This is the first example of a square planar Ni^{III} complex stabilized by a salen-type ligand at room temperature. This situation contrasts with those obtained for the salen analogues whose oxidation takes place on the ligand, leading to phenoxyl radical species.[76] Ni^{III} salen complexes have been only stabilized at low temperatures or using additional ligands generating an octahedral environment.[56,62]

4. Objectives

The objective of this work is to study the electronic structure of oxidized phosphasalen complexes in order to determine how the phosphorus atoms and the different substituents influence the oxidation locus. For this purpose, different phosphasalen ligands have been synthesized and their coordination to nickel and copper centers studied. This work has been divided according to the modifications of the ligand in three chapters.

The first chapter concerns the modifications introduced on the phenolate ring. The electronic properties of complexes featuring two different phosphasalen ligands are studied: Psalen^{tBu}, which displays tert-butyl substituents in the *para* positions of the phenolate rings, and Psalen^{OMe}, whose electron-donating ability is increased by the presence of methoxy groups in the *para* positions. A shift of the oxidation locus from the metal to the ligand is expected by this substitution.

In the second chapter we study the influence of the phosphorus groups. The aryl phosphorus substituents of the Psalen^{tBu} ligand have been substituted by alkyl groups. The electronic properties of the new ligand featuring isopropyl substituents, ^{iPr}Psalen, will be discussed in this chapter.

In the third chapter, the modification is introduced in the linker between the two nitrogens. Complexes featuring a phenylenediamine linker, Psalophen complexes, as well as some mono and di-substituted derivatives are studied in Chapter 4.

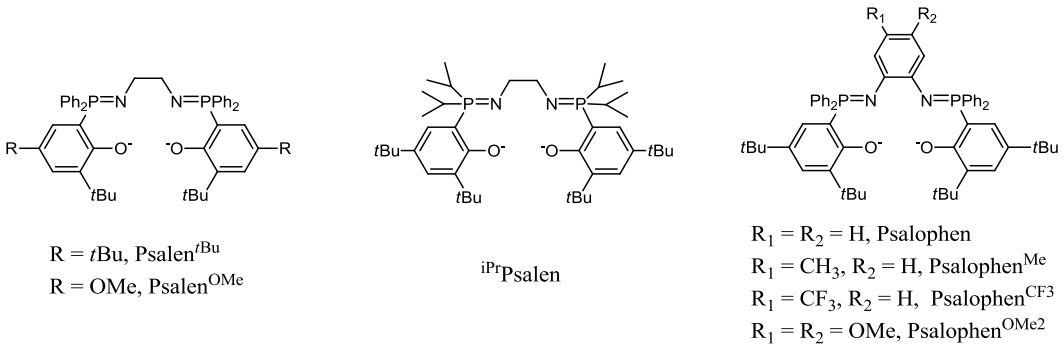

Scheme 41. Phosphasalen ligands studied in this work.

The generated complexes have been studied by cyclic voltammetry, X-ray diffraction, various spectroscopic techniques (EPR, NMR, UV-vis), magnetic measurements and theoretical calculations.

An additional study concerning the stabilization of manganese phosphasalen complexes in different oxidation states and their use in catalysis is present in Chapter 5.

5. References

[1] P. J. Chirik, K. Wieghardt, *Science* **2010**, *327*, 794-795.
[2] C. K. Jorgensen, *Coord. Chem. Rev.***1966**, *1*, 164-178.
[3] H. B. Gray, R. Williams, I. Bernal, E. Billig, *J. Am. Chem. Soc.* **1962**, *84*, 3596-3597.
[4] L. S. Hegedus, *Transition Metals in the Synthesis of Complex Organic Molecules*, University Science Books, Mill Valley, CA, **1994**.
[5] P. Chaudhuri, C. N. Verani, E. Bill, E. Bothe, T. Weyhermüller, K. Wieghardt, *J. Am. Chem. Soc.* **2001**, *123*, 2213-2223.
[6] a) A. Mederos, S. Domínguez, R. Hernández-Molina, J. n. Sanchiz, F. Brito, *Coord. Chem. Rev.***1999**, *193*, 913-939; b) H.-Y. Cheng, C.-C. Lin, B.-C. Tzeng, S.-M. Peng, *J. Chin. Chem. Soc.* **1994**, *41*, 775-781; c) D. Herebian, E. Bothe, F. Neese, T. Weyhermüller, K. Wieghardt, *J. Am. Chem. Soc.* **2003**, *125*, 9116-9128; d) D. Herebian, K. E. Wieghardt, F. Neese, *J. Am. Chem. Soc.* **2003**, *125*, 10997-11005.
[7] V. Lyaskovskyy, B. de Bruin, *ACS Catal.* **2012**, *2*, 270-279.
[8] I. M. Lorkovic, R. R. Duff, M. S. Wrighton, *J. Am. Chem. Soc.* **1995**, *117*, 3617-3618.
[9] M. W. Bouwkamp, A. C. Bowman, E. Lobkovsky, P. J. Chirik, *J. Am. Chem. Soc.* **2006**, *128*, 13340-13341.
[10] a) S. C. Bart, K. Chlopek, E. Bill, M. W. Bouwkamp, E. Lobkovsky, F. Neese, K. Wieghardt, P. J. Chirik, *J. Am. Chem. Soc.* **2006**, *128*, 13901-13912; b) B. de Bruin, E. Bill, E. Bothe, T. Weyhermüller, K. Wieghardt, *Inorg. Chem.* **2000**, *39*, 2936-2947.
[11] a) J. W. Whittaker, *Chem. Rev.* **2003**, *103*, 2347-2363; b) L. Que, W. B. Tolman, *Nature* **2008**, *455*, 333-340; c) J. W. Whittaker, *Arch. Biochem. Biophys.* **2005**, *433*, 227-239.
[12] K. Wang, E. I. Stiefel, *Science* **2001**, *291*, 106.
[13] E. R. King, E. T. Hennessy, T. A. Betley, *J. Am. Chem. Soc.* **2011**, *133*, 4917-4923.
[14] W. Kaim, B. Schwederski, *Coord. Chem. Rev.***2010**, *254*, 1580-1588.
[15] H. Nohl, W. Jordan, R. J. Youngman, *Advances in Free Radical Biology & Medicine* **1986**, *2*, 211-279.
[16] J. C. Kendrew, G. Bodo, H. M. Dintzis, R. G. Parrish, H. Wyckoff, D. C. Phillips, *Nature* **1958**, *181*, 662-666.
[17] a) L. Pauling, C. D. Coryell, *Proc. Natl. Acad. Sci. U.S.A.* **1936**, *22*, 210-216; b) J. E. Bennett, J. F. Gibson, D. J. E. Ingram, M. H. Thelma, G. A. Kerkut, K. A. Munday, *Physics in Medicine & Biology* **1957**, *1*, 309; c) J. P. Collman, R. R. Gagne, C. Reed, T. R. Halbert, G. Lang, W. T. Robinson, *J. Am. Chem. Soc.* **1975**, *97*, 1427-1439; d) J. P. Collman, R. R. Gagne, C. A. Reed, W. T. Robinson, G. A. Rodley, *Proc. Natl. Acad. Sci. U.S.A.* **1974**, *71*, 1326-1329; e) J. J. Weiss, *Nature* **1964**, *202*, 83-84.
[18] H. Chen, M. Ikeda-Saito, S. Shaik, *J. Am. Chem. Soc.* **2008**, *130*, 14778-14790.
[19] K. He, H. Nukada, T. Urakami, M. P. Murphy, *Biochem. Pharmcol.* **2003**, *65*, 67-74.
[20] a) E. R. Redfearn, J. Burgos, *Nature* **1966**, *209*, 711-713; b) M. A. Tocilescu, V. Zickermann, K. Zwicker, U. Brandt, *Biochim. Biophys. Acta (BBA) - Bioenergetics* **2010**, *1797*, 1883-1890.
[21] a) P. R. Pokkuluri, P. D. Laible, Y. L. Deng, T. N. Wong, D. K. Hanson, M. Schiffer, *Biochemistry* **2002**, *41*, 5998-6007; b) F. L. Crane, *Photosynth. Res.* **2010**, *103*, 195-209; c) J. Breton, C. Boullais, G. Berger, C. Mioskowski, E. Nabedryk, *Biochemistry* **1995**, *34*, 11606-11616.
[22] C. G. Pierpont, *Coord. Chem. Rev.***2001**, *216*, 99-125.
[23] M. Y. M. Pau, M. I. Davis, A. M. Orville, J. D. Lipscomb, E. I. Solomon, *J. Am. Chem. Soc.* **2007**, *129*, 1944-1958.
[24] D. C. Mauzerall, *Clin. Dermatol.***1998**, *16*, 195-201.
[25] a) C. M. Wilmot, *Science* **2007**, *316*, 379; b) C. Li, L. Zhang, C. Zhang, H. Hirao, W. Wu, S. Shaik, *Angew. Chem. Int. Ed.* **2007**, *46*, 8168-8170; c) N. Hessenauer-Ilicheva, A. Franke, D. Meyer, W.-D. Woggon, R. van Eldik, *Chem. Eur. J.* **2009**, *15*, 2941-2959.
[26] a) C. T. Lyons, T. D. P. Stack, *Coord. Chem. Rev.***2013**, *257*, 528-540; b) P. G. Cozzi, *Chem. Soc. Rev.* **2004**, *33*, 410-421; c) A. W. Kleij, *Eur. J. Inorg. Chem.* **2009**, *2009*, 193-205.
[27] P. Pfeiffer, E. Breith, E. Lübbe, T. Tsumaki, *Justus Liebigs Ann. Chem.* **1933**, *503*, 84-130.
[28] H. Makio, N. Kashiwa, T. Fujita, *Adv. Synth. Catal.* **2002**, *344*, 477-493.
[29] M. Bandini, P. G. Cozzi, S. Morganti, A. Umani-Ronchi, *Tetrahedron Lett.***1999**, *40*, 1997-2000.
[30] A. Chatterjee, T. H. Bennur, N. N. Joshi, *J. Org. Chem.* **2003**, *68*, 5668-5671.

[31] J. Legros, C. Bolm, *Angew. Chem. Int. Ed.* **2004**, *43*, 4225-4228.
[32] S. K. Edulji, S. T. Nguyen, *Organometallics* **2003**, *22*, 3374-3381.
[33] T. Uchida, R. Irie, T. Katsuki, *Tetrahedron* **2000**, *56*, 3501-3509.
[34] J. A. Miller, W. Jin, S. T. Nguyen, *Angew. Chem. Int. Ed.* **2002**, *41*, 2953-2956.
[35] C. L. Bailey, R. S. Drago, *Coord. Chem. Rev.***1987**, *79*, 321-332.
[36] S. Gambarotta, F. Arena, C. Floriani, A. Gaetani-Manfredotti, *J. Chem. Soc., Chem. Comm.* **1982**, 835-837.
[37] D. A. Atwood, M. J. Harvey, *Chem. Rev.* **2001**, *101*, 37-52.
[38] C. P. Radano, G. L. Baker, M. R. Smith, *J. Am. Chem. Soc.* **2000**, *122*, 1552-1553.
[39] T. Ooi, Y. Itagaki, T. Miura, K. Maruoka, *Tetrahedron Lett.***1999**, *40*, 2137-2138.
[40] E. G. Samsel, K. Srinivasan, J. K. Kochi, *J. Am. Chem. Soc.* **1985**, *107*, 7606-7617.
[41] a) W. Zhang, J. L. Loebach, S. R. Wilson, E. N. Jacobsen, *J. Am. Chem. Soc.* **1990**, *112*, 2801-2803; b) R. Irie, K. Noda, Y. Ito, N. Matsumoto, T. Katsuki, *Tetrahedron Lett.***1990**, *31*, 7345-7348.
[42] W. Zhang, E. N. Jacobsen, *J. Org. Chem.* **1991**, *56*, 2296-2298.
[43] a) N. H. Lee, A. R. Muci, E. N. Jacobsen, *Tetrahedron Lett.***1991**, *32*, 5055-5058; b) T. Kobayashi, K. Tanaka, J. Miwa, S. Katsumura, *Tetrahedron: Asymmetry* **2004**, *15*, 185-188.
[44] C. H. Sugisaki, P. J. Carroll, C. R. D. Correia, *Tetrahedron Lett.***1998**, *39*, 3413-3416.
[45] F. Aloui, B. B. Hassine, *Tetrahedron Lett.***2009**, *50*, 4321-4323.
[46] H. A. Jahn, E. Teller, *Proc. R. Soc. London, Se. A***1937**, *161*, 220.
[47] S. Will, J. Lex, E. Vogel, H. Schmickler, J.-P. Gisselbrecht, C. Haubtmann, M. Bernard, M. Gorss, *Angew. Chem. Int. Ed.* **1997**, *36*, 357-361.
[48] a) A. B. Alemayehu, E. Gonzalez, L. K. Hansen, A. Ghosh, *Inorg. Chem.* **2009**, *48*, 7794-7799; b) K. E. Thomas, J. Conradie, L. K. Hansen, A. Ghosh, *Eur. J. Inorg. Chem.* **2011**, *2011*, 1865-1870; c) K. E. Thomas, A. B. Alemayehu, J. Conradie, C. M. Beavers, A. Ghosh, *Acc. Chem. Res.* **2012**, *45*, 1203-1214.
[49] a) M. Bröring, F. Brégier, E. Cónsul Tejero, C. Hell, M. C. Holthausen, *Angew. Chem. Int. Ed.* **2007**, *46*, 445-448; b) A. Alemayehu, J. Conradie, A. Ghosh, *Eur. J. Inorg. Chem.* **2011**, *2011*, 1857-1864; c) K. Pierloot, H. Zhao, S. Vancoillie, *Inorg. Chem.* **2010**, *49*, 10316-10329.
[50] C. M. Lemon, M. Huynh, A. G. Maher, B. L. Anderson, E. D. Bloch, D. C. Powers, D. G. Nocera, *Angew. Chem. Int. Edit.* **2016**, *55*, 2176-2180.
[51] P. Verma, J. Weir, L. Mirica, T. D. P. Stack, *Inorg. Chem.* **2011**, *50*, 9816-9825.
[52] a) O. Kahn, R. Prins, J. Reedijk, J. S. Thompson, *Inorg. Chem.* **1987**, *26*, 3557-3561; b) A. Dei, D. Gatteschi, L. Pardi, U. Russo, *Inorg. Chem.* **1991**, *30*, 2589-2594.
[53] L. L. Diaddario, W. R. Robinson, D. W. Margerum, *Inorg. Chem.* **1983**, *22*, 1021-1025.
[54] J. Hanss, H.-J. Krüger, *Angew. Chem. Int. Ed.* **1996**, *35*, 2827-2830.
[55] B. Cervera, J. L. Sanz, M. J. Ibanez, G. Vila, F. Lloret, M. Julve, R. Ruiz, X. Ottenwaelder, A. Aukauloo, S. Poussereau, Y. Journaux, M. Carmen Munoz, *J. Chem. Soc., Dalton Trans.* **1998**, 781-790.
[56] O. Rotthaus, F. Thomas, O. Jarjayes, C. Philouze, E. Saint-Aman, J.-L. Pierre, *Chem. Eur. J.* **2006**, *12*, 6953-6962.
[57] a) T. J. Collins, T. R. Nichols, E. S. Uffelman, *J. Am. Chem. Soc.* **1991**, *113*, 4708-4709; b) C. L. Weeks, P. Turner, R. R. Fenton, P. A. Lay, *J. Chem. Soc., Dalton Trans.* **2002**, 931-940.
[58] a) X. Ottenwaelder, A. Aukauloo, Y. Journaux, R. Carrasco, J. Cano, B. Cervera, I. Castro, S. Curreli, M. C. Munoz, A. L. Rosello, B. Soto, R. Ruiz-Garcia, *Dalton Trans.* **2005**, 2516-2526; b) O. M. Kanderal, H. Kozlowski, A. Dobosz, J. Swiatek-Kozlowska, F. Meyer, I. O. Fritsky, *Dalton Trans.* **2005**, 1428-1437.
[59] B. Zheng, F. Tang, J. Luo, J. W. Schultz, N. P. Rath, L. M. Mirica, *J. Am. Chem. Soc.* **2014**, *136*, 6499-6504.
[60] Y. Shimazaki, F. Tani, K. Fukui, Y. Naruta, O. Yamauchi, *J. Am. Chem. Soc.* **2003**, *125*, 10512-10513.
[61] C. Freire, B. de Castro, *J. Chem. Soc., Dalton Trans.* **1998**, 1491-1498.
[62] O. Rotthaus, O. Jarjayes, F. Thomas, C. Philouze, C. Perez Del Valle, E. Saint-Aman, J.-L. Pierre, *Chem. Eur. J.* **2006**, *12*, 2293-2302.
[63] Z. B. Ögel, D. Brayford, M. J. McPherson, *Mycol. Res.***1994**, *98*, 474-480.
[64] a) N. Ito, S. E. V. Phillips, K. D. S. Yadav, P. F. Knowles, *J. Mol. Biol.***1994**, *238*, 704-814; b) N. Ito, S. E. V. Phillips, C. Stevens, Z. B. Ogel, M. J. McPherson, J. N. Keen, K. D. S. Yadav, P. F. Knowles, *Nature* **1991**, *350*, 87-90.

[65] a) J. W. Whittaker, *Adv. Protein Chem.* **2002**, *60*, 1-49; b) F. Wendt, M. Rolff, W. Thimm, C. Näther, F. Tuczek, *Z. Anorg. Allg. Chem.* **2013**, *639*, 2502-2509.
[66] D. Rokhsana, D. M. Dooley, R. K. Szilagyi, *J. Am. Chem. Soc.* **2006**, *128*, 15550-15551.
[67] a) R. C. Pratt, T. D. P. Stack, *J. Am. Chem. Soc.* **2003**, *125*, 8716-8717; b) F. Michel, F. Thomas, S. Hamman, C. Philouze, E. Saint-Aman, J.-L. Pierre, *Eur. J. Inorg. Chem.* **2006**, *2006*, 3684-3696; c) A. Sokolowski, H. Leutbecher, T. Weyhermüller, R. Schnepf, E. Bothe, E. Bill, P. Hildebrandt, K. Wieghardt, *J. Biol. Inorg. Chem.* **1997**, *2*, 444-453; d) R. C. Pratt, T. D. P. Stack, *Inorg. Chem.* **2005**, *44*, 2367-2375; e) J. A. Halfen, B. A. Jazdzewski, S. Mahapatra, L. M. Berreau, E. C. Wilkinson, L. Que, W. B. Tolman, *J. Am. Chem. Soc.* **1997**, *119*, 8217-8227.
[68] Y. D. Wang, J. L. DuBois, B. Hedman, K. O. Hodgson, T. D. P. Stack, *Science* **1998**, *279*, 537-540.
[69] T. Storr, P. Verma, R. C. Pratt, E. C. Wasinger, Y. Shimazaki, T. D. P. Stack, *J. Am. Chem. Soc.* **2008**, *130*, 15448-15459.
[70] a) H. Maeda, Y. Ishikawa, T. Matsuda, A. Osuka, H. Furuta, *J. Am. Chem. Soc.* **2003**, *125*, 11822-11823; b) G. Speier, V. Fulop, *J. Chem. Soc., Chem. Comm.* **1990**, 905-906.
[71] F. Thomas, *Eur. J. Inorg. Chem.* **2007**, *2007*, 2379-2404.
[72] F. Thomas, O. Jarjayes, C. Duboc, C. Philouze, E. Saint-Aman, J.-L. Pierre, *Dalton Trans.* **2004**, 2662-2669.
[73] K. Asami, A. Takashina, M. Kobayashi, S. Iwatsuki, T. Yajima, A. Kochem, M. van Gastel, F. Tani, T. Kohzuma, F. Thomas, Y. Shimazaki, *Dalton Trans.* **2014**, *43*, 2283-2293.
[74] a) R. K. Thauer, G. Diekert, P. Schönheit, *Trends Biochem. Sci.***1980**, *5*, 304-306; b) Y. Kung, C. L. Drennan, *Curr. Opin. Chem. Biol.* **2011**, *15*, 276-283.
[75] L. Chiang, A. Kochem, O. Jarjayes, T. J. Dunn, H. Vézin, M. Sakaguchi, T. Ogura, M. Orio, Y. Shimazaki, F. Thomas, T. Storr, *Chem. Eur. J.* **2012**, *18*, 14117-14127.
[76] T. Storr, E. C. Wasinger, R. C. Pratt, T. D. P. Stack, *Angew. Chem. Int. Edit.* **2007**, *46*, 5198-5201.
[77] Z. Xiao, B. O. Patrick, D. Dolphin, *Inorg. Chem.* **2003**, *42*, 8125-8127.
[78] L. Chiang, K. Herasymchuk, F. Thomas, T. Storr, *Inorg. Chem.* **2015**, *54*, 5970-5980.
[79] T. P. A. Cao, S. Labouille, A. Auffrant, Y. Jean, X. F. Le Goff, P. Le Floch, *Dalton Trans.* **2011**, *40*, 10029-10037.
[80] E. M. Broderick, P. S. Thuy-Boun, N. Guo, C. S. Vogel, J. T. Miller, K. Meyer, P. L. Diaconescu, *Inorg. Chem.* **2011**, 50, 2870-2877.
[81] a) T. P. A. Cao, A. Buchard, X. F. Le Goff, A. Auffrant, C. K. Williams, *Inorg. Chem.* **2012**, *51*, 2157-2169; b) C. Bakewell, T. P. A. Cao, N. Long, X. F. Le Goff, A. Auffrant, C. K. Williams, *J. Am. Chem. Soc.* **2012**, *134*, 20577-20580; c) D. Myers, A. J. P. White, C. M. Forsyth, M. Bown, C. K. Williams, *Angew. Chem. Int. Ed.* **2017**, *56*, 5277-5282; d) C. Bakewell, A. J. P. White, N. J. Long, C. K. Williams, *Angew. Chem. Int. Ed.* **2014**, *53*, 9226-9230.
[82] H. Staudinger, J. Meyer, *Helv. Chim. Acta* **1919**, *2*, 635-646.
[83] A. V. Kirsanov, *Isv Akad Nauk SSSR* **1950**, 426.
[84] L. Horner, H. Oedinger, *Justus Liebigs Ann. Chem.* **1959**, 627 (1), 142-162.
[85] H. Bock, M. Schnöller, *Angew. Chem. Int. Ed.* **1968**, *7*, 636-636.
[86] W. Q. Tian, Y. A. Wang, *J. Org. Chem.* **2004**, *69*, 4299-4308.
[87] P. J. Alonso, A. B. Arauzo, M. A. Garcia-Monforte, A. Martin, B. Menjon, C. Rillo, M. Tomas, *Chem. Eur. J.* **2009**, *15*, 11020-11030.
[88] H. Zimmer, G. Singh, *J. Org. Chem.* **1963**, *28*, 483-486.
[89] a) A. Buchard, *Chimie de coordination des iminophosphoranes et nouveaux systèmes catalytiques*, Ecole polytechnique, **2009**; b) T.-P.-A. Cao, *Coordination chemistry and catalysis with mixed ligands associating iminophosphorane to thiolate or phenolate*, Ecole Polytechnique, **2012**; c) T. Cheisson, *Synthèse et réactivité de complexes à ligand iminphosphorane: desmétaux de transition aux actinides*, Ecole Polytechnique, **2015**.
[90] A. Steiner, D. Stalke, *Angew. Chem. Int. Ed.* **1995**, *34*, 1752-1755.
[91] I. Kaljurand, T. Rodima, I. Leito, I. A. Koppel, R. Schwesinger, *J. Org. Chem.* **2000**, *65*, 6202-6208.
[92] a) R. G. Pearson, *J. Am. Chem. Soc.* **1963**, *85*, 3533-3539; b) R. G. Pearson, *J. Chem. Educ.***1968**, *45*, 581; c) R. G. Pearson, *J. Chem. Educ.***1968**, *45*, 643.
[93] M. Orio, O. Jarjayes, H. Kanso, C. Philouze, F. Neese, F. Thomas, *Angew. Chem. Int. Edit.* **2010**, *49*, 4989-4992.
[94] R. H. Platel, L. M. Hodgson, C. K. Williams, *Polym. Rev.* **2008**, *48*, 11-63.

[95] T. P. A. Cao, G. Nocton, L. Ricard, X. F. Le Goff, A. Auffrant, *Angew. Chem. Int. Ed.* **2014**, *53*, 1368-1372.

Chapter 2: Influence of the phenolate substituents in Ni and Cu phosphasalen complexes

1. Introduction

As it was presented in Chapter 1, this study concerning the oxidation of phosphasalen complexes started some years ago with the synthesis and characterization of a stable tetracoordinated Ni^{III} phosphasalen complex.[1] This was ascribed to the better electron donating properties of the phosphasalen ligands compared to their salen counterparts. To get further insight into the stereo-electronic effects of the ligands on the structure of the one-electron oxidized complexes we targeted the synthesis of the copper analogue derivative. The study of the electronic structure of copper salen-type complexes has become a hot topic since these complexes were established as biomimetic models of the metallo-enzyme Galactose Oxidase (see Chapter 1, section 2.2.2).[2] The control of the oxidation locus, *i.e.* electronic structure, in these complexes has been well pursued in those studies. Few examples of high-valent Cu^{III} salen complexes have been reported in the literature,[3] the most relevant being the one published by Stack and co-workers in 2008.[3a] $[CuSal]^+SbF_6^-$ complex (Scheme 42) was characterized as a Cu^{III} complex in the solid state using X-ray structure and magnetic measurements (among other characterizations). A different situation was found in solution where this Cu^{III} turned out to be in equilibrium with the triplet state corresponding to the ferromagnetic coupled radical cation complex. VT-NMR and UV-vis spectroscopies were crucial to draw this conclusion. Since $Psalen^{tBu}$ ligand has been demonstrated to be able to stabilize a Ni^{III} center, the stabilization of the analogue Cu^{III} complex seems to be likely.

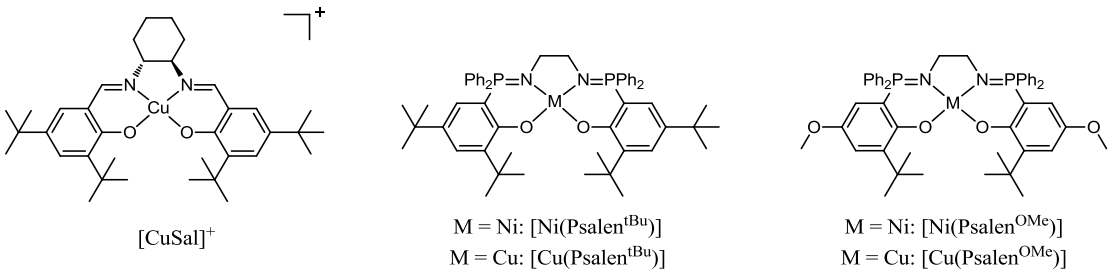

Scheme 42. Structure of $[CuSal]^+$ (left) and phosphasalen complexes studied.[3a]

To modulate the electronic properties of the ligand and to study the influence of the different substitutions on the electronic structure of the complexes, we first focused on the phenolate substituents. In order to favor the formation and stabilization of a radical ligand in the complex, methoxy substituents were introduced in the *para* positions of the phenolate rings (Scheme 42, right).

This strategy turned out to be very efficient in the case of salen complexes, where nickel and copper oxidized derivatives ($[CuSal^{OMe}]^+SbF_6^-$ and $[NiSal^{OMe}]^+SbF_6^-$) were isolated as phenoxyl radical complexes (Scheme 43).[4] In particular, the X-ray structure of $[CuSal^{OMe}]^+SbF_6^-$ derivative evidenced differences in the bond lengths in one of the phenolate rings which points to the localization of the radical on one side of the molecule. The phenoxyl ring presents a quinoid pattern as the C-O and the central C-C bonds shorten while the others lengthen (Scheme 43).[4-5] An interaction between this ring and the counter anion was also observed. The other aromatic ring only experiences slight variations and preserves its phenolate character.

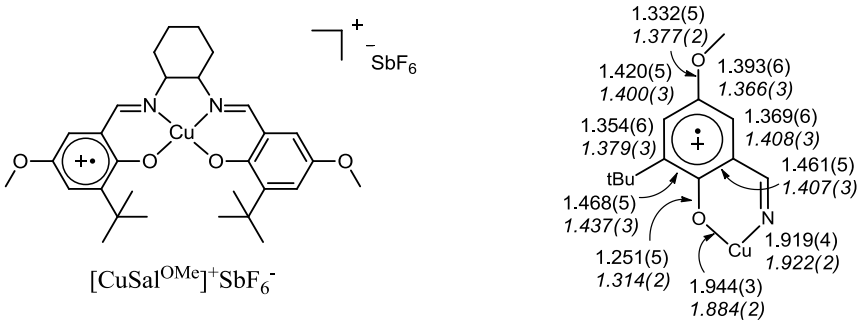

Scheme 43. Structure of $[CuSal^{OMe}]^+SbF_6^-$ and experimental bond distances for the phenoxyl ring (normal police) and the phenolate ring in $[CuSal^{OMe}]$ (italic). [4]

The EPR spectrum of $[CuSal^{OMe}]^+SbF_6^-$ turned out to be silent. This was explained by the presence of a triplet ground state whit a large zero-field splitting. This was supported by DFT calculations which predicted orthogonal metal and ligand molecular orbitals. [4]

The X-ray structure of [NiSal^{OMe}]$^{+}$SbF$_6^{-}$ indicates that the radical is localized in one part of the molecule, but the EPR measurements and DFT calculations pointed to a greater involvement of the metal orbitals in the SOMO, allowing radical delocalization.[4]

As explained in the introduction chapter, in the case of the copper complex, three different electronic configurations can be obtained upon oxidation, thus render the determination of the oxidation state of the metal ambiguous (see Chapter 1, section 2.2.1). For phosphasalen complexes, the electron-donating ability of the iminophosphorane functions may render the metal oxidation competitive with phenolate oxidation

For a better comparison and understanding of the influence of the methoxy groups, both Ni and Cu derivatives have been studied. Ni^{II} 3d^8 complexes being isoelectronic with Cu^{III} complexes can help in the characterization of the latter. Additionally, nickel oxidized complexes, featuring a sole unpaired electron, will be easier to characterize using EPR spectroscopy.

The synthesis and characterization of the neutral [Cu(Psalen^{tBu})], [Ni(Psalen^{OMe})] and [Cu(Psalen^{OMe})] complexes and their one-electron oxidized products, as well as the determination of the electronic structure, will be discussed in this chapter.

2. Synthesis of the ligand and neutral complexes

The ligands were obtained by oxidation of the corresponding phosphine with bromine at low temperature, leading to the formation of the phosphonium bromide intermediate. It was then trapped by adding of the ethylenediamine in presence of a non-nucleophilic amine, tributyl amine. After precipitation with THF the ligands were isolated as their bis-aminophosphonium salt, (H_4Psalen^{tBu})Br_2 and (H_4Psalen^{OMe})Br_2, as white powders in good yields.[6]

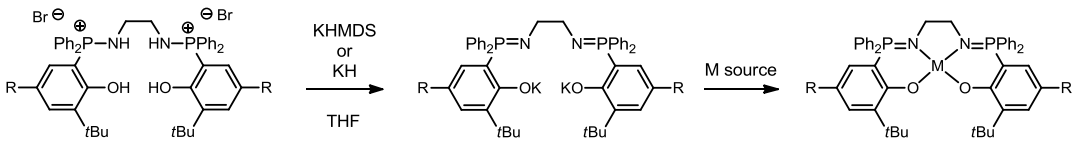

R = *t*Bu, δ_P = 40 ppm
R = OMe, δ_P = 42 ppm

R = *t*Bu, δ_P = 15.4 ppm
R = OMe, δ_P = 18.0 ppm

M = Ni, R = OMe, δ_P = 34.5 ppm, 85%
M = Cu, R = *t*Bu, ^{31}P silent, 66 %
M = Cu, R = OMe, ^{31}P silent, 82 %

Scheme 44: Complexation reaction and the corresponding ^{31}P chemical shifts in THF.

The complexation of the ligand takes place in two steps: first the deprotonation of the ligand is carried out in THF using either 4 equivalents of KHMDS or an excess of KH (Scheme 44). The reaction can be easily followed by ^{31}P NMR, the deprotonation is completed once the signal of the protonated ligand disappears, 40 ppm for $(H_4Psalen^{tBu})Br_2$ and 42 ppm for $(H_4Psalen^{OMe})Br_2$, and the one corresponding to the anion appears at 15.4 ppm for $Psalen^{tBu}$ and 18.0 ppm for $Psalen^{OMe}$. Then, removal of the insoluble potassium salts followed by addition of the metallic precursor, $[NiBr_2(DME)]$ or $CuBr_2$, induces a color change of the solution from pale yellow to purple and green, respectively. The complexation is finished for $[Ni(Psalen^{OMe})]$ once a sole singlet is present at 34.5 ppm in the $^{31}P\{^1H\}$ NMR spectrum. In the case of the copper complexes the total disappearance of the ligand signal indicates the end of the complexation (no signal corresponding to the copper neutral complexes was seen because of its paramagnetism. The solvent was evaporated from the mixtures and the residues dissolved in dichloromethane and centrifuged. The solutions were concentrated and a precipitate appeared by addition of petroleum ether. The solids were washed with more petroleum ether and dried under reduced pressure to lead $[Ni(Psalen^{OMe})]$ as purple solid in 85 % yield, and $[Cu(Psalen^{tBu})]$ and $[Cu(Psalen^{OMe})]$ as green solids in 66 and 82 % yield, respectively.

3. Characterization of neutral complexes $[Ni(Psalen^{OMe})]$, $[Cu(Psalen^{tBu})]$ and $[Cu(Psalen^{OMe})]$

3.1 NMR spectroscopy

$[Ni(Psalen^{OMe})]$, $[Cu(Psalen^{tBu})]$, and $[Cu(Psalen^{OMe})]$ complexes and their oxidized products were characterized by multinuclear NMR spectroscopy.

$[Ni(Psalen^{OMe})]$, being a $3d^8$ square planar complex, displays a diamagnetic ^1H NMR and a $^{31}P\{^1H\}$ resonance at 35.2 ppm in $CDCl_3$. All the signals observed were assigned: the phenyl phosphine protons are present between 7.5 and 8.5 ppm as multiplets, the phenolate protons are present at 6.88 ppm as a doublet ($^4J_{H,H}$ = 3.0 Hz), and at 5.68 ppm as a doublet of doublets ($^3J_{P,H}$ = 15.5 Hz, $^4J_{H,H}$ = 3.0 Hz).

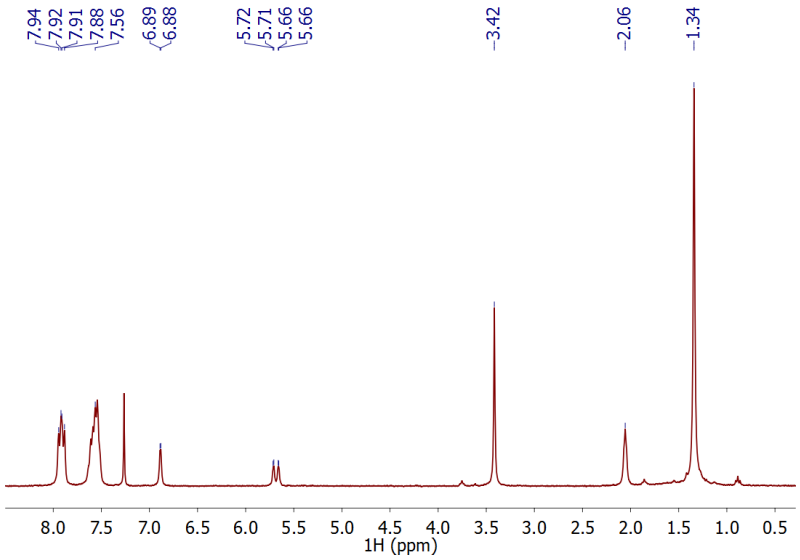

Figure 5. ^{1}H NMR spectrum of [Ni(Psalen^{OMe})] in $CDCl_3$ at room temperature.

The methoxy protons are seen at 3.42 ppm as a singlet, the ethylene bridge protons are observed at 2.06 as a triplet ($^{3}J_{H,H}$ = 3.8 Hz) and the tert-butyl protons at 1.34 ppm as a singlet.

The Cu^{II} complexes display paramagnetic ^{1}H NMR spectra with broad signals between 0 and 10 ppm where the protons could only be tentatively assigned by considering their relative areas (Figure 6 and Figure 7). Two different types of aromatic signals could be identified: the phenyl phosphine protons around 9 ppm and the phenolate protons around 7 ppm. The methoxy protons of [Cu(Psalen^{OMe})] are observed at 3.69 ppm while the tert-butyl group is observed at 1.50 ppm. The tert-butyl protons of [Cu(Psalen^{tBu})] are seen at 1.56 and 0.99 ppm. The ethylene bridge protons of both of them are present around 3.40 ppm. No phosphorus resonance was observed for these complexes.

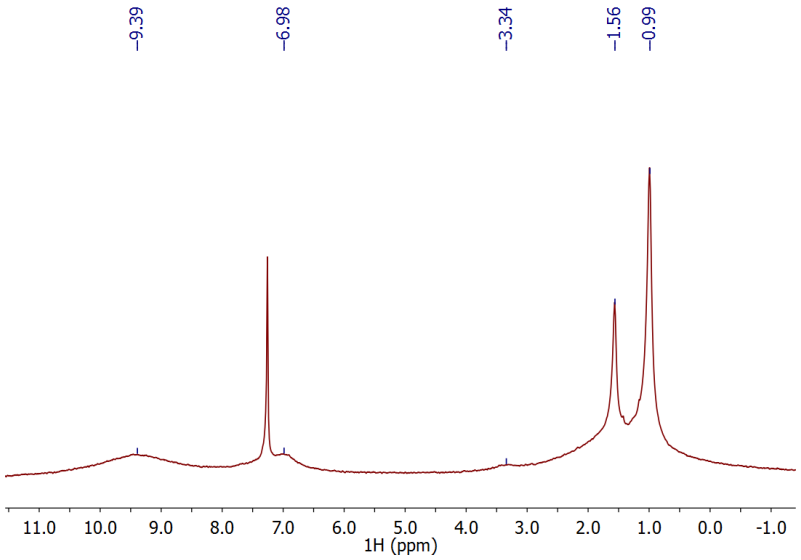

Figure 6. ^{1}H NMR spectrum of [Cu(Psalen^{tBu})] in $CDCl_3$ at room temperature.

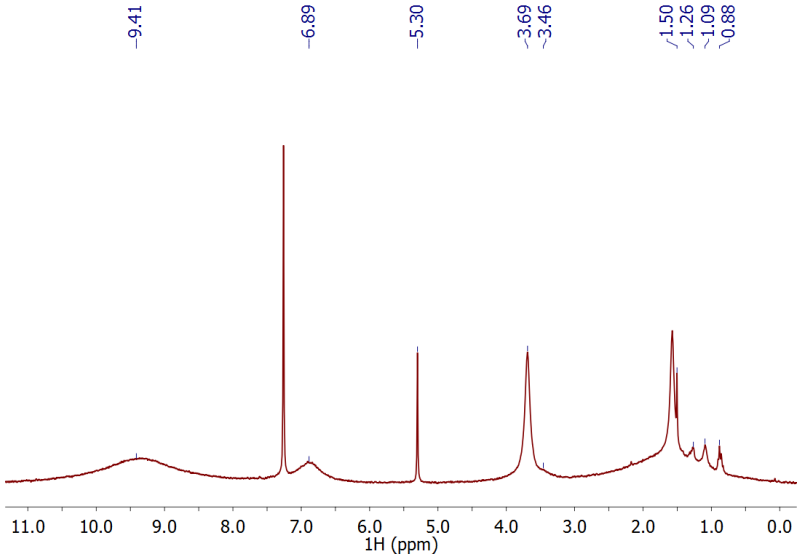

Figure 7. ^{1}H NMR spectrum of [Cu(Psalen^{OMe})] in $CDCl_3$ at room temperature. Signals at 5.30, 1.50, 1.26, 0.88 ppm correspond to dichloromethane, water and pentane.

3.2 EPR spectroscopy

To get further information into the electronic structure of [Cu(Psalen^{tBu})] and [Cu(Psalen^{OMe})] complexes, EPR studies were carried out at room temperature for dichloromethane solutions. Figure 8 and Figure 9 show the experimental spectra of [Cu(Psalen^{tBu})] and [Cu(Psalen^{OMe})] with their simulated spectra. Copper centers have a nuclear spin of 3/2 so the signal possesses a four-line split pattern. These spectra are in good agreement with a $3d^9$ Cu^{II} center in a rhombic environment. Even if the ligand

imposes a square planar geometry to the metal center its flexibility authorizes a strong distortion in solution which made us run the simulation under rhombic conditions. These spectra are very similar to those recorded by X.R. Bu for a series of bulky substituted copper salen complexes.[8]

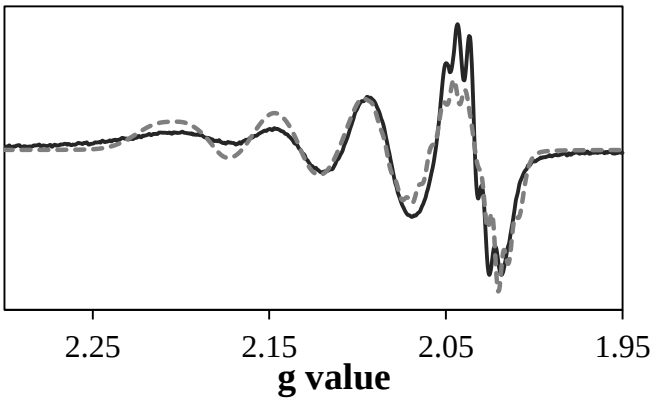

Figure 8. Comparison of experimental (black) and simulated (dashed grey) EPR spectra of a dichloromethane solution of [Cu(Psalen^{tBu})] at room temperature. Conditions: Frequency: 9.356 GHz; Power: 1.003 mW; modulation frequency: 100 kHz; amplitude: 0.2 mT.

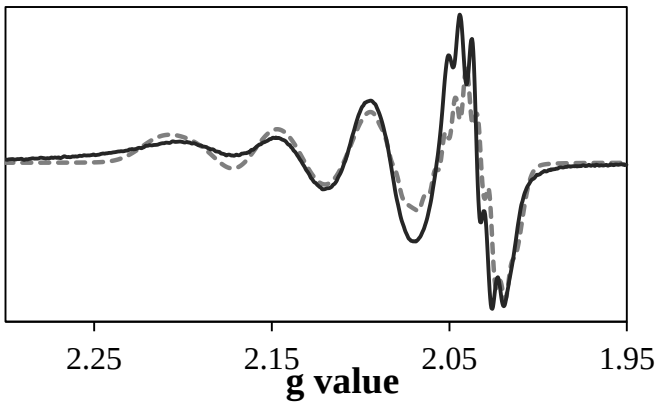

Figure 9. Comparison of experimental (black) and simulated (dashed grey) EPR spectra of a dichloromethane solution of [Cu(Psalen^{OMe})] at room temperature. Conditions: Frequency: 9.363 GHz; Power: 1.003 mW; modulation frequency: 100 kHz; amplitude: 0.2 mT.

The g values obtained from the simulation for both complexes are $g_1 = 2.124$, $g_2 = 2.107$, $g_3 = 2.051$. The hyperfine coupling constants obtained for the Cu atom are 251, 210 and 90 MHz for [Cu(Psalen^{tBu})] and 251, 210 and 75 MHz for [Cu(Psalen^{OMe})]. A superhyperfine coupling with the ^{14}N atoms is only seen in g_3 with a value of $A_N = 28$ MHz for both complexes. Similar couplings with N atoms have been also observed in other salen or corrole copper complexes.[9] All the parameters concerning the simulation of these spectra are summarized in Table 1.

		[Cu(Psalen^{tBu})]	[Cu(Psalen^{OMe})]
g values	g_1	2.124	2.122
	g_2	2.107	2.105
	g_3	2.051	2.051
|A| Cu (MHz)	x	251	251
	y	210	210
	z	90	75
|A| N_1 (MHz)	x	28	28
	y	28	28
	z	28	28
|A| N_2 (MHz)	x	28	28
	y	28	28
	z	28	28

Table 1. EPR simulation parameters for Cu^{II} complexes.

3.3 UV-visible spectroscopy

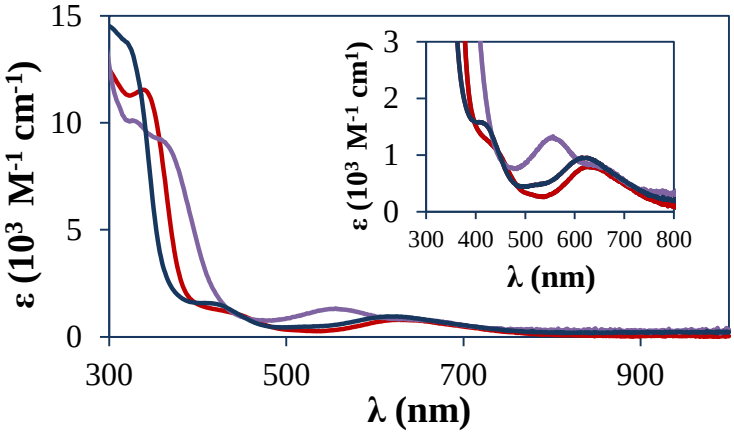

Figure 10. UV-vis spectra of [Ni(Psalen^{OMe})] (purple line), [Cu(Psalen^{tBu})] (blue line) and [Cu(Psalen^{OMe})] (red line) in CH_2Cl_2 at 298 K.

The absorption spectrum of [Ni(Psalen^{OMe})] exhibits two weak transitions centered at 664 nm (ε = 780 M^{-1} cm^{-1}) and 560 nm (ε = 1300 M^{-1} cm^{-1}) and an intense band at 370 nm (ε = 8800 M^{-1} cm^{-1}). The first two bands can be assigned to MLCT transitions as established for [Ni(Psalen^{tBu})].[1]

[Cu(Psalen^{tBu})] complex exhibits a weak d-d transition at 625 nm (ε = 960 M^{-1} cm^{-1}), characteristic of a Cu^{II} d^9 complex,[7] and an intense band at 310 nm (ε = 14000 M^{-1} cm^{-1}). This assignment was done according to the absorption spectrum observed for the analogous salen complex, [CuSal],[3a] which exhibits bands at 384 and 568 nm with similar intensities. In addition, another weak transition is observed for [Cu(Psalen^{tBu})] at 430 nm

(ε = 1400 M^{-1} cm^{-1}), which was tentatively assigned to a transfer involving the iminophosphorane functions.

[Cu(Psalen^{OMe})] displays an analogous absorption spectrum with a weak transition at 620 nm (ε = 800 M^{-1} cm^{-1}), also attributed to a d-d transition,[7] and an intense transition (CT) at 340 nm (ε = 11500 M^{-1} cm^{-1}). A weak transition is also observed at 440 nm (ε = 1000 M^{-1} cm^{-1}), may correspond to a transfer involving the iminophosphorane functions, as presumed for [Cu(Psalen^{tBu})].

3.4 X-Ray diffraction

Suitable crystals of [Ni(Psalen^{OMe})] for X-ray diffraction were obtained *via* petroleum ether diffusion into a saturated dichloromethae solution.

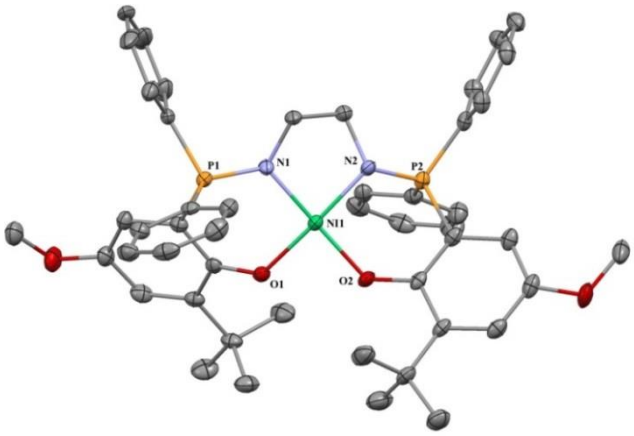

Figure 11. ORTEP of [Ni(Psalen^{OMe})] with thermal ellipsoids at 50 % probability. Hydrogen atoms have been omitted for clarity.

[Ni(Psalen^{OMe})] displays a distorted square planar geometry around the metal center (Figure 11). The plane defined by the two oxygens and the two nitrogens atoms (NOON plane) presents a torsion of 11.96 °, larger than the one found in [Ni(Psalen^{tBu})] (6.15 °). The metal center experiments a tetrahedral distortion where N1 and O2 are placed above the NOON plane, and N2 and O1 are below it, as observed in [Ni(Psalen^{tBu})]. Ni-O and Ni-N bond distances are similar to those in [Ni(Psalen^{tBu})] and shorter than in the salen analogues. P-N bonds distances are slightly shorter compared to [Ni(Psalen^{tBu})], 1.605 Å in average versus 1.619 Å.[1] Table 2 gathers selected bond lengths and angles for [Ni(Psalen^{tBu})], previously published, and for [Ni(Psalen^{OMe})].[1]

	[Ni(Psalen^{tBu})]	[Ni(Psalen^{OMe})]
Ni-O1	1.878(1)	1.880(2)
Ni-O2	1.878(1)	1.885(2)
Ni-N1	1.888(2)	1.877(2)
Ni-N2	1.888(2)	1.884(2)
P1-N1	1.619(2)	1.603(2)
P2-N2	1.619(2)	1.606(2)
Torsion angle[a]	6.15	11.96

Table 2. Selected bond distances (Å) and angles (°) for [Ni(Psalen^{tBu})] and [Ni(Psalen^{tBu})].[1] [a] Torsion of the NOON plane.

Green single crystals of [Cu(Psalen^{tBu})] and [Cu(Psalen^{OMe})] were obtained by evaporation of a $CDCl_3$ solution and *via* pentane diffusion into a saturated CH_2Cl_2 solution, respectively.

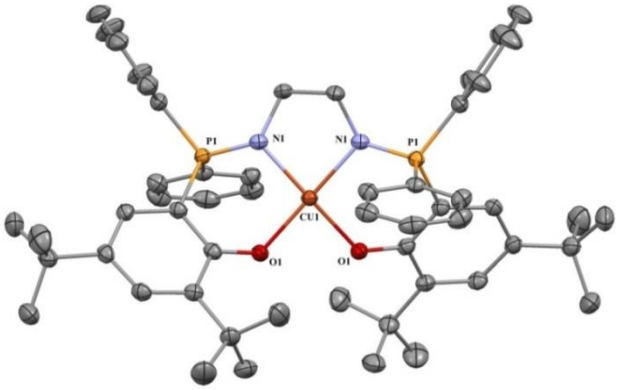

Figure 12. ORTEP of [Cu(Psalen^{tBu})] with thermal ellipsoids at 50 % probability. Hydrogen atoms have been omitted for clarity.

Both copper complexes display square planar geometries with comparable Cu-N and Cu-O bond distances (Figure 12 and Figure 13). Similar to the nickel complexes, they present a tetrahedral distortion which is more pronounced in the methoxy derivative.

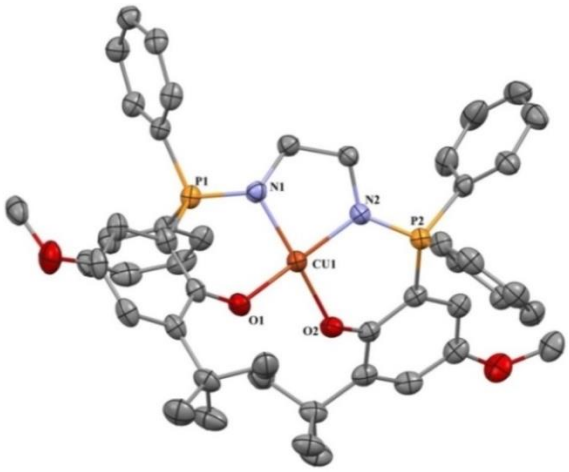

Figure 13. ORTEP of [Cu(Psalen^{OMe})] with thermal ellipsoids at 50 % probability. Hydrogen atoms have been omitted for clarity.

The torsion of the main NOON plane is 13.02 ° for [Cu(Psalen^{tBu})] and 19.40 ° for [Cu(Psalen^{OMe})]. For both complexes the Cu-O bond distances range between 1.917(2) and 1.922(2) Å, and Cu-N between 1.941(2) and 1.951(2) Å. These values are slightly higher than those observed in their corresponding salen analogues, probably due to the better flexibility of the phosphasalen ligand. The P-N bond lengths are also equivalent with values ranging between 1.593(2) and 1.603(2) Å, and are very similar to these observed for [Ni(Psalen^{OMe})].

	[Cu(Psalen^{tBu})]	[Cu(Psalen^{OMe})]
Cu-O1	1.917(2)	1.923(2)
Cu-O2	1.917(2)	1.919(2)
Cu-N1	1.951(2)	1.948(2)
Cu-N2	1.951(2)	1.941(2)
P1-N1	1.603(2)	1.597(2)
P2-N2	1.602(2)	1.593(2)
Torsion angle[a]	13.02	19.40

Table 3. Selected bond distances (Å) and angles (°) for [Cu(Psalen^{tBu})] and [Cu(Psalen^{OMe})]. [a] Torsion of the NOON plane.

3.5 Magnetic measurements

SQUID measurements were carried out for the neutral copper complexes [Cu(Psalen^{OMe})] and [Cu(Psalen^{tBu})]. Their magnetic temperature-dependent curves are shown in Figure 14Figure 15. Both complexes follow the Curie-Weiss law with a C constant of 0.429 cm^3 K mol^{-1} and a Weiss θ of 4.54 K for [Cu(Psalen^{tBu})], and a C constant of 0.411 cm^3 K mol^{-1} and a Weiss θ of 1.54 K, for [Cu(Psalen^{OMe})], in agreement with Cu^{II} 3d^9 centers. The magnetic moment calculated for both complexes at room temperature is 1.93 μ_B.

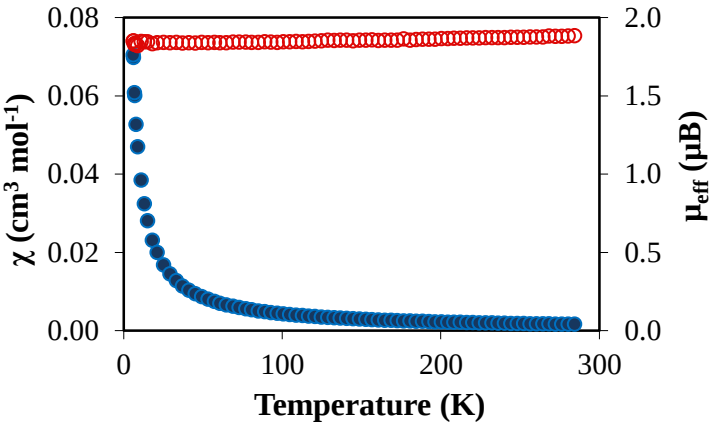

Figure 14. Plot of magnetic susceptibility (blue circles) and effective magnetic moment (red circles) *vs.* temperature for [Cu(Psalen^{tBu})].

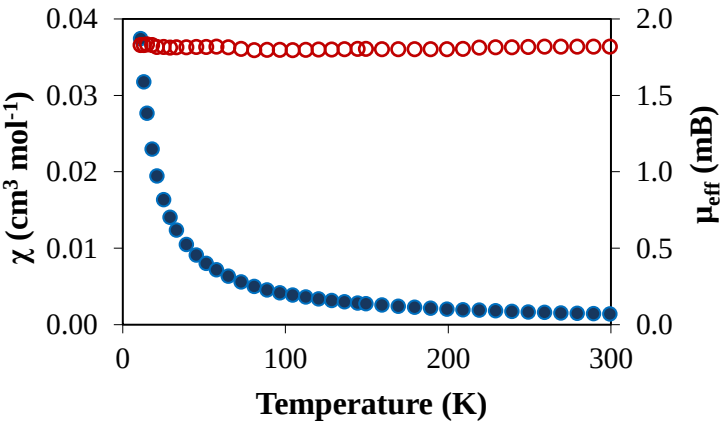

Figure 15. Plot of magnetic susceptibility (blue circles) and effective magnetic moment (red circles) *vs.* temperature for [Cu(Psalen^{OMe})].

3.6 Electrochemical studies

The electrochemical properties of the ligands and the complexes were studied by cyclic voltammetry in dichloromethane. All the redox potentials reported and discussed in this manuscript are expressed versus the Fc^+/Fc reference couple, which was used as internal reference.

3.6.1 Cyclic voltammetry of the ligands

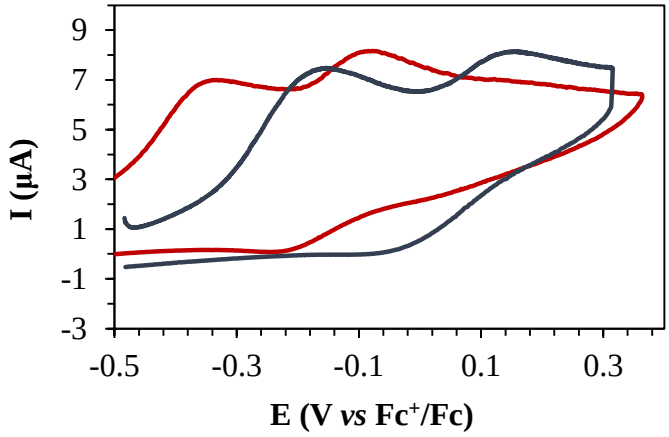

Figure 16. Cyclic voltammetry curves of the potassium salts of the ligands Psalen^{tBu} (blue) and Psalen^{OMe} (red) in CH_2Cl_2 (containing 0.12 M of $TBAPF_6$) at carbon electrode. The curve of Psalen^{OMe} has been normalized.

The voltammograms of the ligands Psalen^{OMe} and Psalen^{tBu}, depicted in Figure 16, show two irreversible oxidations for both ligands. These oxidations are attributed to the successive oxidation of both phenolate rings, and the low stability of the products formed may be the reason of this non-reversibility. For the Psalen^{tBu} ligand these oxidations take place at $E^1_{p,a}$ = -0.15 V and $E^2_{p,a}$ = 0.15 V, while they occur at $E^1_{p,a}$ = -0.33 V and $E^2_{p,a}$ = -0.07

V for the Psalen^{OMe} ligand. As expected, the introduction of the methoxy groups in the phenolate moieties facilitates the oxidation of the ligand. The difference between the first and the second oxidation is 0.30 and 0.26 V for Psalen^{tBu} and Psalen^{OMe}, respectively. This difference is similar for both adducts demonstrating that the methoxy substitution is not significantly changing the electronic structure of the oxidized products but only favoring the oxidations with respect to the Psalen^{tBu} ligand.

3.6.2 Cyclic voltammetry of the complexes

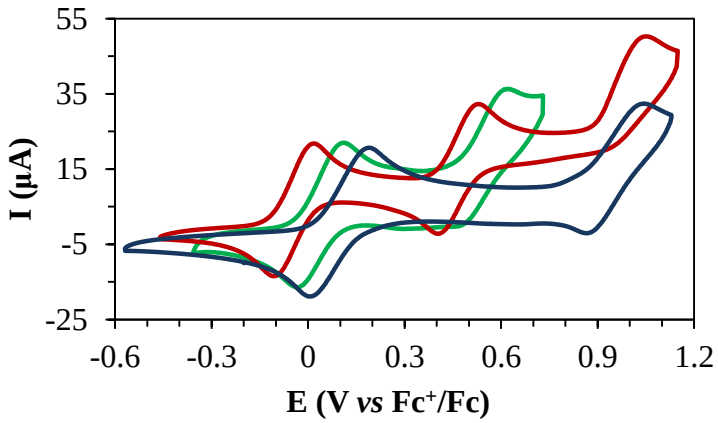

Figure 17. Cyclic voltammetry curves of [Cu(Psalen^{tBu})] (blue), [Cu(Psalen^{OMe})] (green) and [Ni(Psalen^{OMe})] (red). Conditions: 3 mM of complex in dichloromethane at 0.1 V/s. The intensity of the curve of [Cu(Psalen^{tBu})] has been normalized.

The cyclic voltammogram of [Ni(Psalen^{OMe})] displays two reversible oxidations at $E^1_{1/2}$ = -0.06 V and $E^2_{1/2}$ = 0.47 V, and an irreversible one at $E^3_{p,a}$ = 1.00 V (Figure 17). These waves may correspond to the oxidation of the metal center and both phenoxide rings and take place at lower potentials compared to [Ni(Psalen^{tBu})] complex, $E^1_{1/2}$ = 0.01 V, $E^2_{1/2}$ = 0.82 V and $E^3_{p,a}$ = 1.24 V,[1] evidencing again the influence of the methoxy groups on the oxidation process. The important point to note in these values is the difference between the first and the second oxidation: ΔE_{1-2} = 0.53 and 0.81 V for [Ni(Psalen^{OMe})] and [Ni(Psalen^{tBu})], respectively. This gap is related to the electronic structure of the mono-oxidized products and provides information of the species formed. If the generated radical is localized and no interaction exists with the second redox unit, the gap between the two oxidations would be small (around 0.036 V).[10] On the other hand, if the radical is delocalized in the rest of the molecule or in the metal center, this gap would become larger. For the salen derivative [Ni(salen^{tBu})], the two first oxidations differ by 0.46 V and were attributed to the oxidation of both phenolate rings.[10] For [Ni(Psalen^{OMe})], the gap is slightly larger (0.53 V) suggesting a greater contribution of the metal center in the magnetic orbitals of the mono-

oxidized product, while for [Ni(Psalen^{tBu})] this gap is larger (0.81 V) and the mono-oxidized product was established as a Ni^{III} complex.[1]

Compound	$E^1_{1/2}$	$E^2_{1/2}$	ΔE_{1-2}	E^3_{pa}
[Ni(Psalen^{tBu})]	0.01	0.82	0.81	1.24
[Ni(Psalen^{OMe})]	-0.06	0.47	0.53	1.00
[Cu(Psalen^{tBu})]	0.10	0.95	0.85	-
[Cu(Psalen^{OMe})]	0.04	0.54	0.50	-

Table 4. Redox potentials for nickel and copper complexes expressed in V versus Fc^+/Fc in CH_2Cl_2 (3 mM of complex, 0.12 M of $TBAPF_6$, scan rate 0.1 V/s).

Copper complexes display two reversible oxidations at $E^1_{1/2}$ = 0.04 and 0.10 V and $E^2_{1/2}$ = 0.54 and 0.95 V for [Cu(Psalen^{OMe})] and [Cu(Psalen^{tBu})], respectively. These waves may correspond to the oxidation of the metal center or the oxidation of both phenoxide rings. No wave corresponding to a third oxidation process was observed. The potentials obtained are slightly anodically shifted compared to the analogues nickel complexes. The methoxy derivative exhibits once more lower values compared to [Cu(Psalen^{tBu})]. The difference in the gap between the first and the second oxidation is again significant: ΔE_{1-2} is 0.85 V for the t-butyl derivative while only 0.50 V for the methoxy one, which may suggest a stronger metal character in the case of [Cu(Psalen^{tBu})]$^+$ and a greater ligand participation for [Cu(Psalen^{OMe})]$^+$.

The similar ΔE_{1-2} found in the two copper and nickel series suggests that the oxidized complexes present similar electronic structure when featuring the same ligand. The greater ΔE_{1-2} values obtained in the Psalen series compared to salen one, points to a larger involvement of the metal in the oxidation process. The redox potential values obtained for the Psalen complexes are lower than the salen ones,[3a,10] in agreement with the stronger electron-donating properties of the iminophosphorane functions.

4. Oxidation of neutral complexes

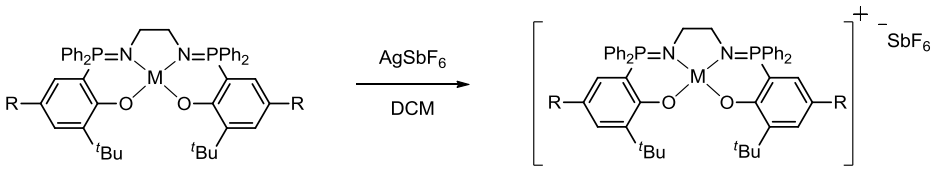

M = Ni, R = OMe, $[Ni(Psalen^{OMe})]^+SbF_6^-$, 82 %
M = Cu, R = tBu, $[Cu(Psalen^{tBu})]^+SbF_6^-$, 85 %
M = Cu, R = OMe, $[Cu(Psalen^{OMe})]^+SbF_6^-$, 84 %

Scheme 45. Chemical oxidation of $[M(Psalen^{tBu})]$ and $[M(Psalen^{OMe})]$ complexes, M = Cu, Ni.

$[Ni(Psalen^{OMe})]$, $[Cu(Psalen^{tBu})]$ and $[Cu(Psalen^{OMe})]$ were oxidized using one equivalent of $AgSbF_6$ in dichloromethane under inert conditions. Addition of the silver salt into a dichloromethane solution of $[Ni(Psalen^{OMe})]$ induces an immediate color change from blue to dark brown, while the solutions of $[Cu(Psalen^{tBu})]$ and $[Cu(Psalen^{OMe})]$ change from green to deep purple. The suspensions were filtered and the solutions concentrated. In the case of $[Cu(Psalen^{tBu})]$, dichloromethane was completely removed under reduced pressure and the residue dissolved in a small amount of diethyl ether. Addition of petroleum ether to the solutions induces the precipitation of the products. The powders were washed with petroleum ether and dried under vacuum to give $[Ni(Psalen^{OMe})]^+SbF_6^-$ as a brown solid in 82 % yield and $[Cu(Psalen^{tBu})]^+SbF_6^-$, and $[Cu(Psalen^{OMe})]^+SbF_6^-$ as purple solids in 85 and 84 % yield, respectively.

5. Characterization of the oxidized complexes

5.1 NMR spectroscopy

^1H NMR spectra of all four oxidized products turned out to be very informative. $[Ni(Psalen^{OMe})]^+$ showed at room temperature a ^1H NMR spectrum in CD_2Cl_2 similar to that observed for $[Ni(Psalen^{tBu})]^+$, with large signals between -3 and 35 ppm (Figure 18).

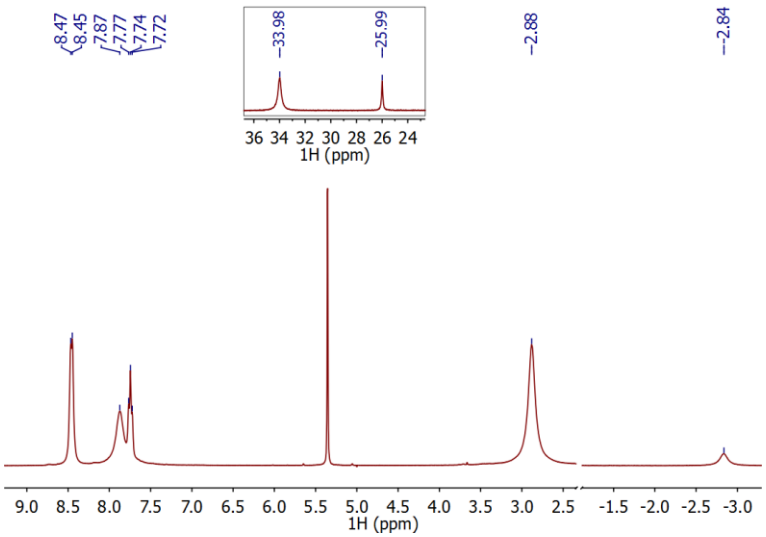

Figure 18. ^{1}H NMR spectrum of [Ni(Psalen^{OMe})]$^{+}$ at room temperature in CD_2Cl_2. Inset shows a zoom of the signals at low field.

Thanks to their integrated areas some signals could be assigned: the methoxy groups resonate at 33.98 ppm, the protons of the phenoxide ring correspond to the signals present at 25.99 and -2.84 ppm, and the t-butyl groups are shown at 2.88 ppm. The signals corresponding to the phenyl phosphine substituents appear between 7.5-8.5 ppm and do not experience a significant variation with respect to chemical shifts observed on the neutral complex. For [Ni(Psalen^{tBu})]$^{+}$ the phenoxide protons appear at 19.10 and 15.30 ppm, while the t-butyl substituents are observed at 8.31 and 3.17 ppm.[1] The difference between the chemical shifts observed for the paramagnetic oxidized complex and the diamagnetic neutral one, named paramagnetic isotropic shift ($\delta^{para} = \delta^{obs} - \delta^{dia}$), is larger in the case of the methoxy derivative. The δ^{para} of the phenoxide protons are 19.1 and 9.71 ppm in [Ni(Psalen^{OMe})]$^{+}$, while in [Ni(Psalen^{tBu})]$^{+}$ are 12.2 and 8.43 ppm.[1] The phenoxide substituents also experience larger δ^{para} in [Ni(Psalen^{OMe})]$^{+}$: 30.6 and 1.91 ppm for the methoxy and the t-butyl group, respectively, while in [Ni(Psalen^{tBu})]$^{+}$ are 1.14 and 1.81 ppm for the t-butyl substituents.[1] This reflects a difference in the electronic structure of these complexes which points to a larger contribution of the phenoxide ring in the SOMO for [Ni(Psalen^{OMe})]$^{+}$.

The ^{1}H NMR spectrum of [Ni(Psalen^{OMe})]$^{+}$ was recorded at different temperatures between 20 and -90 °C (Figure 19) and the variation of the chemical shifts were linear with the temperature, as expected for a paramagnetic compound following the Curie law (Figure 20).

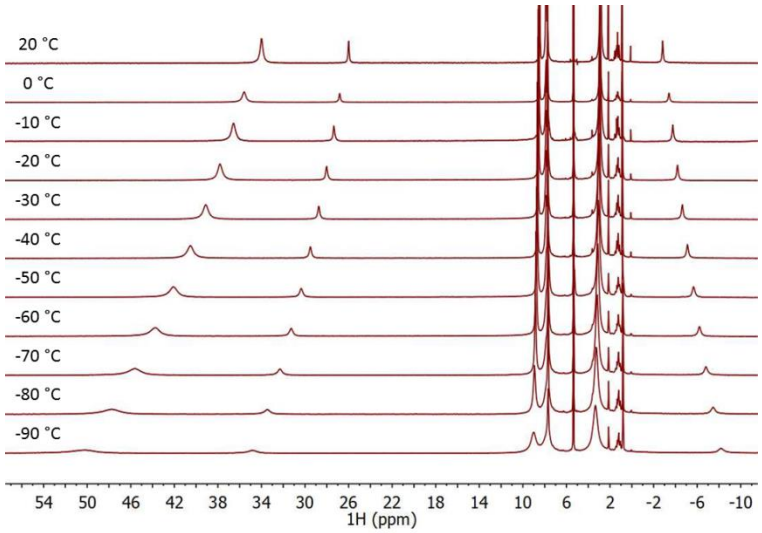

Figure 19. Variable temperature ^{1}H NMR spectra of $[Ni(Psalen^{OMe})]^{+}SbF_6^-$ in CD_2Cl_2.

The signals that experienced the largest variations were those present at very low and high fields: the resonance of the methoxy group shifts from 36.0 ppm at 20 °C to 52.0 ppm at -90 °C (Δδ = 16 ppm), one of the phenoxide protons shifts from 26 to 35 ppm (Δδ = 9 ppm), while the other shifts from -2 to -8 ppm (Δδ = 6 ppm). These shifts are larger than those found for $[Ni(Psalen^{tBu})]^{+}$ where the aromatic protons shifted by 12.2 and 8.43 ppm,[1] and suggest a greater participation of the phenoxide ring in the delocalization of the unpaired electron. The signals between 0 and 10 ppm do not experience strong variations. No phosphorus signal was detected over the temperature range studied.

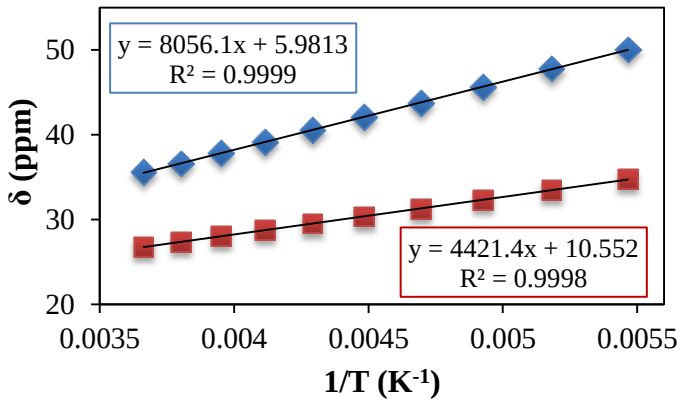

Figure 20. Plot of the chemical shifts of the phenoxide protons (red squares) and the methoxy protons (blue diamonds) with the inverse of the temperature, and corresponding linear fits.

Few ^{1}H NMR spectra have been reported for copper oxidized salen complexes since the formation of a radical ligand precludes the possibility of obtaining an informative spectrum. The ^{1}H NMR spectrum recorded for $[Cu(Psalen^{tBu})]^{+}$ in dichloromethane turned

out to be diamagnetic. It displays signals between 0 and 8 ppm, and a ^{31}P signal was observed at 41.70 ppm.

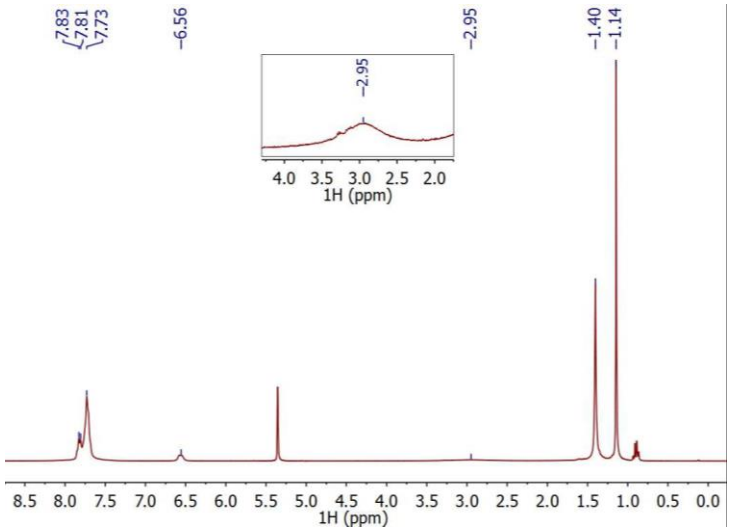

Figure 21. ^{1}H NMR spectrum of [Cu(Psalen^{tBu})]$^{+}$ at room temperature in CD_2Cl_2. Inset shows a zoom of the ethylene protons signal.

The signals can be easily assigned: the phenyl phosphine and one phenoxide protons resonate between 7.5-8.0 ppm, the other phenoxide proton at 6.56 ppm, the ethylene bridge protons are seen at 2.75 ppm as a very broad signal, and the t-butyl protons at 1.40 and 1.14 ppm.

To ensure the absence of paramagnetic species, this spectrum was also recorded between 20 and -90 °C (Figure 22) and no significant variation was noticed.

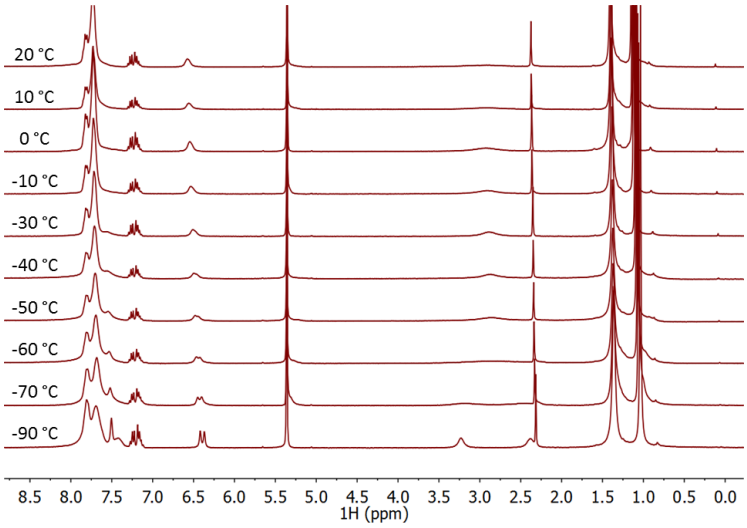

Figure 22. Variable temperature ^{1}H NMR spectra of [Cu(Psalen^{tBu})]$^{+}$ in CD_2Cl_2. Signals at 7.25 and 2.3 ppm correspond to toluene.

The most remarkable changes are the resolution of the signal at 6.56 ppm (which turns as a doublet), and the decoalescence of the signal of the ethylene bridge at 2.95 ppm, as a result of a more rigid structure at low temperature. The diamagnetic behavior is maintained in the temperature range studied, suggesting the presence of Cu^{III} species in solution.

$[Cu(Psalen^{OMe})]^+$ also displays an apparent ^1H diamagnetic spectrum in dichloromethane with signals between 0 and 8 ppm: the t-butyl substituents are present at 1.42 ppm, the methoxy protons at 4.55 ppm, one of the phenoxide protons at 5.65 ppm, and at 7.75 ppm the rest of the aromatic protons (Figure 23). This time, the ethylene protons are not observed, which may be caused by high fluxionality of the bridge at room temperature. An important difference from $[Cu(Psalen^{tBu})]^+$ is the absence of any signal in the ^{31}P NMR spectrum. Some resonances are also notably shifted with respect to their diamagnetic chemical shifts. Thus, the methoxy group resonates at 4.55 ppm while it is normally is seen around 3.5 ppm, and the phenoxide proton at 5.65 ppm which is up-field shifted.

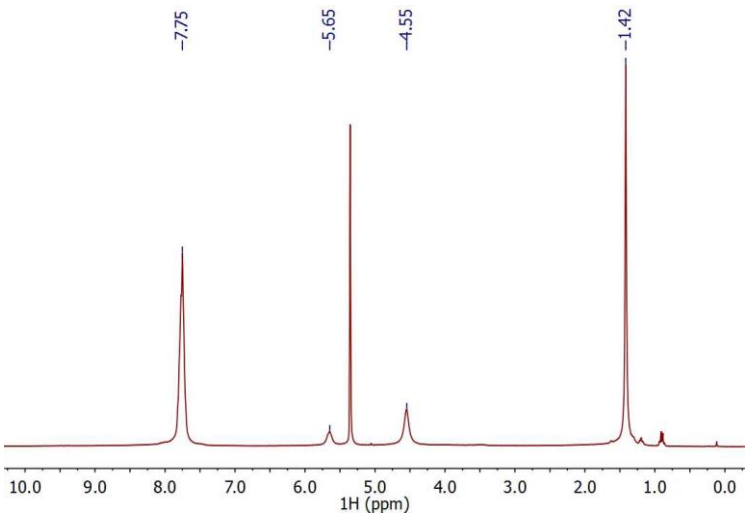

Figure 23. ^1H NMR spectrum of $[Cu(Psalen^{OMe})]^+$ at room temperature in CD_2Cl_2.

Assuming the formation of a Cu^{III} $3d^8$ complex, the difference between these values and those corresponding to the isoelectronic $3d^8$ $[Ni(Psalen^{OMe})]^+$ complex, the so-called isotropic shift δ^{iso}, is 2.23 ppm for the methoxy group, and 0.04 ppm if the aromatic proton is the one at the *ortho* position of the phosphorus atom, or 1.24 ppm if the aromatic proton is on the *para* position. For the t-butyl group the δ^{iso} is only 0.06 ppm.

To rule out the presence of paramagnetic species, the ^{31}P and ^1H spectra were recorded at different temperatures in THF-d^8, which allows studying a larger temperature range than dichloromethane. The stacked spectra are shown in Figure 24 and Figure 25. A ^{31}P signal

appears at 47.0 ppm when decreasing the temperature, at similar chemical shift to that of [Cu(Psalen^{tBu})]$^+$.

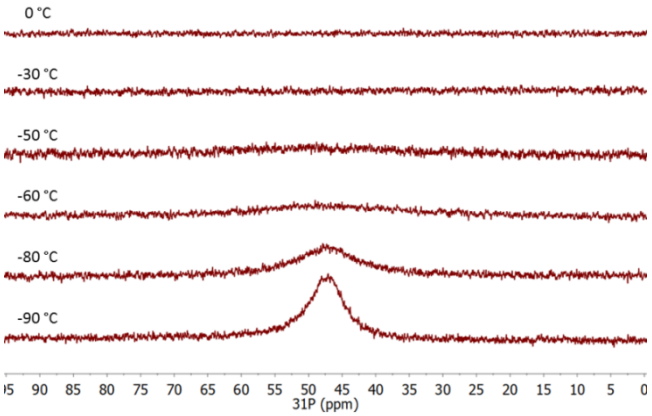

Figure 24. Variable temperature ^{31}P NMR spectra of [Cu(Psalen^{OMe})]$^+$ in thf-d_8.

Contrary to [Cu(Psalen^{tBu})]$^+$, an important shift of the signals mentioned above is observed: the methoxy protons shift from 6.64 ppm at 55 °C to 3.58 ppm at -90 °C, and the phenoxide proton from 4.65 ppm to 6.36 ppm. At -90 °C the isotropic shift of the methoxy group is only of 0.12 ppm. All the signals, except the one of the methoxy, become larger while decreasing the temperature, which could not be explained. The most important feature of this variation is the non-linear evolution of the chemical shifts with the temperature (Figure 26).

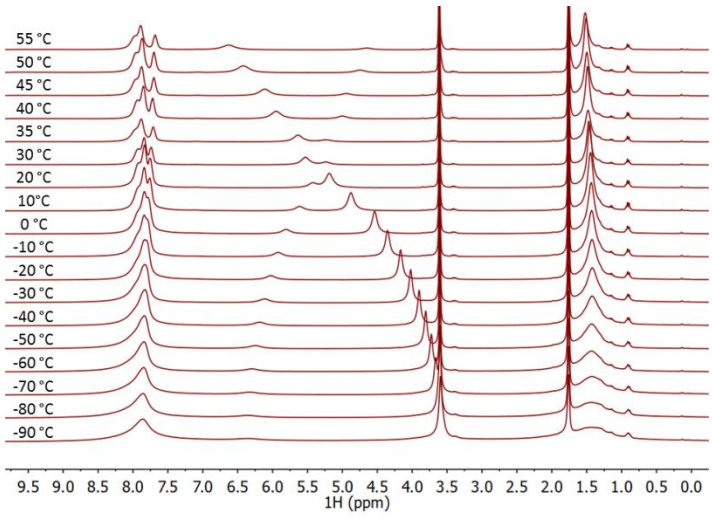

Figure 25. Variable temperature ^{1}H NMR spectra of [Cu(Psalen^{OMe})]$^+$ in THF-d_8.

5.1.1 Fit of the VT-NMR data of [Cu(Psalen^{OMe})]$^+$.

This particular behavior corresponds to a singlet ground state configuration with a triplet state which is partially populated at high temperatures. This behavior was also observed

by Nocera and co-workers in the study of copper corroles, where an antiferromagnetically coupled Cu^{II} radical complex was established as the ground state configuration (see Chapter 1, section 2.2.1).[9] To get further insight we used the equation proposed by Le Guennic *et al.*, which derives from the Fermi contact contribution of the paramagnetic isotropic shift, (Equation 2).[11] A fit of the chemical shift variations with this equation allows to calculate the energy gap between the triplet and the singlet state.[9]

$$\delta(\text{ppm}) = \delta_{\text{singlet}} + 10^6 \frac{g\beta_e}{g_N\beta_N} \frac{aS(S+1)}{kT} \left[3 + \exp\left(\frac{\Delta E_{S\text{-}T}}{RT}\right)\right]^{-1} \quad \text{(Equation 2)}$$

Where:

g, g_N = electronic and nuclear g-values respectively

β_e, β_N, = Bohr and nuclear magnetons respectively

a = isotropic hyperfine coupling constant

S = spin of the systems

k = Boltzmann constant

R = gas constant

This equation can be simplified to:

$$\delta(\text{ppm}) = A + 10^6 \frac{B}{T} \left[3 + \exp\left(\frac{C}{T}\right)\right]^{-1} \quad \text{(Equation 3)}$$

Where $A = \delta_{\text{singlet}}$, $B = \frac{g\beta_e}{g_N\beta_N} \frac{aS(S+1)}{kT}$, $C = \frac{\Delta E_{T\text{-}S}}{R}$.

A plot of the chemical shift variations of the phenoxide and the methoxy protons with the inverse of the temperature, and their corresponding fits, are shown in Figure 26.

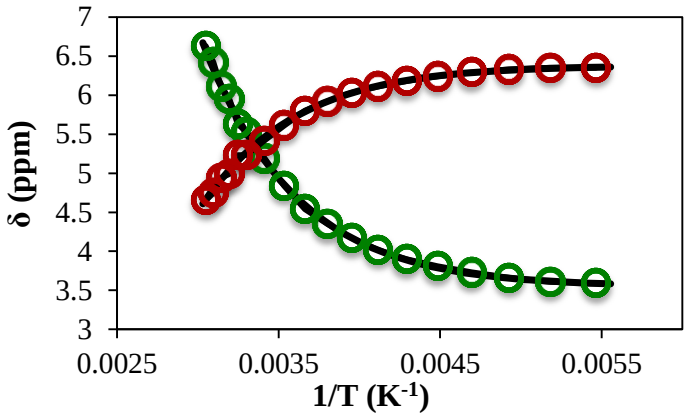

Figure 26. Plot of chemical shifts (δ) for the methoxy- protons (green circles) and the aromatic proton (red circles) *vs* 1/T for $[Cu(Psalen^{OMe})]^+$ (see Figure 25). Methoxy protons shift from 6.63 ppm at 55 °C to 3.59 ppm at -90 °C; the aromatic proton shifts from 4.65 ppm at 55 °C to 6.35 ppm at -90 °C and best fit of the data (see following).

From this fit we obtained the following parameters: $\delta^{singlet}$ = 3.55 ppm and a = -1.63 G for the methoxy group and $\delta^{singlet}$ = 6.38 ppm and a = 2.87 G for the aromatic proton. The energy difference between the two states $\Delta E_{T\text{-}S}$ is 16.99 kJ mol^{-1}, *i.e.*, 1420 cm^{-1} and 0.176 eV. This value is close to that reported by Nocera and co-workers,[9] and is indicative of a large energy gap between the singlet and the triplet state. Despite knowing the multiplicity of the ground state, the actual electronic configuration still needs to be determined since two possibilities agree with the singlet multiplicity: a high valent metal complex with a Cu^{III} $3d^8$ center or a Cu^{II} radical cation complex with a strong antiferromagnetic coupling between the two unpaired electrons. A clue concerning this question may be found in the difference between the calculated $\delta^{singlet}$ (obtained from Equation 2) for the methoxy and phenoxide protons and the corresponding δ^{dia} from the $[Ni(Psalen^{OMe})]^+$. This may indicate that another contribution influences $\delta^{singlet}$, pointing towards an antiferromagnetic coupled radical complex.

After these results, and even if the VT-NMR studies did not show significant changes in the chemical shifts for $[Cu(Psalen^{tBu})]^+$, we must also consider for this complex the possibility of an open-shell singlet ground state. A triplet state, lying at higher energy compared to $[Cu(Psalen^{OMe})]^+$, would not be populated enough to show significant NMR changes in temperature range studied.

5.2 EPR spectroscopy

The EPR spectrum of $[Ni(Psalen^{tBu})]^+$ obtained by T.P.A. Cao in a previous study is shown in Figure 27.[1] It exhibited a rhombic signal at low temperature that corresponds to a Ni^{III} center with g values of g_1 = 2.290, g_2 = 2.215 and g_3 = 2.061. No signal was observed at high temperatures due to the fast relaxation of the nickel center.

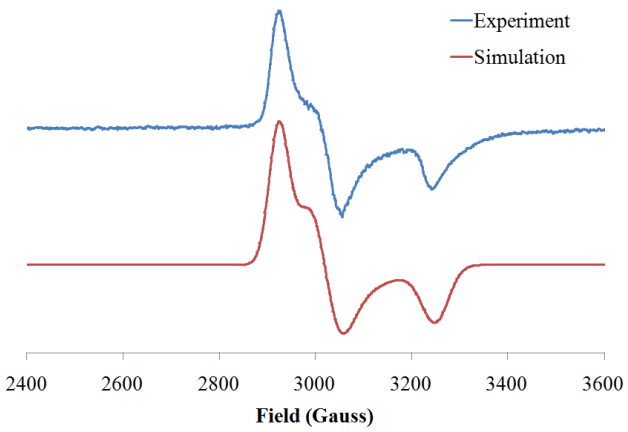

Figure 27. Experimental and simulated EPR spectrum of $[Ni(Psalen^{tBu})]^+$ in dichloromethane at 5K.[1]

To get more information about the electronic structure of [Ni(Psalen^{OMe})]$^+$, EPR studies were carried out at different temperatures for dichloromethane solutions and in the solid state. Contrary to what observed for [Ni(Psalen^{tBu})]$^+$, a complicated isotropic signal was present at room temperature at g_{iso} = 2.005, indicative of organic radical species.[12] This signal consists in a doublet split 9 or 10 times (some lines are superimposed) with a coupling constant of about 10 G (Figure 28, blue line). Assuming the presence of a phenoxyl radical, the simulation of this spectrum was made by taking in account the two protons of the phenoxyl ring and the 9 protons of the t-butyl group. The methoxy protons were not included in this simulation. This contrasts with the response observed in the VT-NMR where the chemical shift of these protons experiences an important variation with the temperature. The coupling constants obtained for the aromatic protons are A_H = 25.83 MHz and A_H = 2.01 MHz. The assignment of these coupling constants with the related aromatic protons was not possible. The superhyperfine coupling constant with the 9 t-butyl protons is a_H = 3.08 MHz. While decreasing the temperature, the resolution of this signal diminishes and at 140 K only a doublet is observed (Figure 28, orange line). This loss of resolution is caused by a broadening of the spectrum when the temperature is decreased, which is a typical feature of organic radicals.[12a] The signal continues to broaden until becoming a singlet at 10 K. On the other hand, at 80 K a new signal centered at g value 2.14 appears; this was assigned to a $3d^7$ Ni^{III} center. The spectrum at 10 K was registered under saturated conditions for the radical signal in order to obtain a better defined metallic signal, so spin quantification was not possible in this case. This spectrum was also simulated and the values obtained were g_{iso} = 2.005 for the organic radical, and g_1 = 2.216, g_2 = 2.136 and g_3 = 2.067 for the Ni^{III} signal (g_{av} = 2.14). A summary of all the parameters obtained by simulation is present in Table 5.

a)

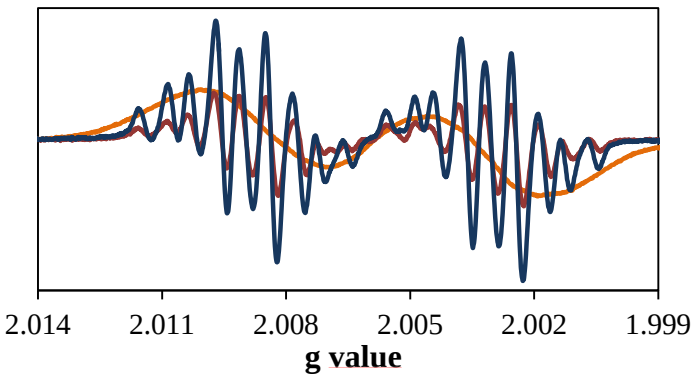

b)

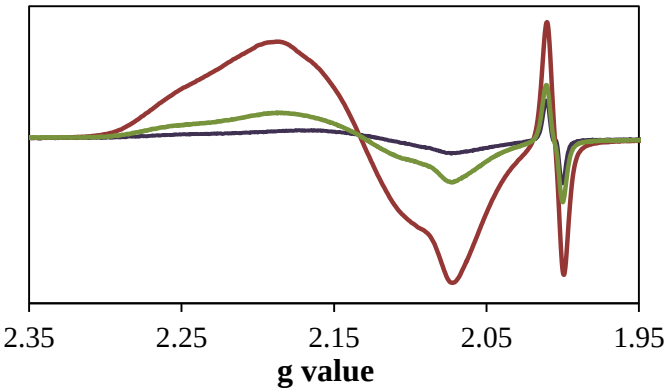

Figure 28. X-band EPR spectra of [Ni(Psalen^{OMe})]$^+$ in CH_2Cl_2 at (a) 220 K (blue line), 180 K (red line) and 140 K (orange line); (b) 10 K (red line), 40 K (green line) and 80 K (blue line).

In the case of [Ni(Psalen^{tBu})]$^+$ no organic radical signal was present at any temperature. The g_{av} value for [Ni(Psalen^{tBu})]$^+$ is 2.19,[1] slightly higher compared to the 2.14 obtained for the methoxy derivative, which implies a minored metal character of the SOMO in [Ni(Psalen^{OMe})]$^+$. The simulation of the spectrum recorded at 10 K is present in Figure 29

The presence of these two signals in the EPR spectrum is not usual for this kind of systems. For nickel salen-type complexes the radical species generated normally display signals with g values above 2.006, depending on the contribution of metal orbitals into the SOMO of the complex.[13] Equilibrium between the two oxidized forms, ligand radical and high valent metal complex, has also been observed in nickel salen derivatives due to a valence tautomerism, or associated to a phase transition in the solvent.[10,14] In some cases this equilibrium is due to the coordination of exogenous ligands, *e.g.* the solvent, which strongly binds to the metal at low temperatures stabilizing Ni^{III} octahedral species.[14] In our case, the observation of the two signals may be explained by either an incomplete equilibrium between the radical form and the metal-oxidized form close in energy, making both signals visible at low temperature, or a multiconfigurational ground state, where metal-based and ligand-based configurations coexist (which possesses the same multiplicity), and thus both signals were observed.

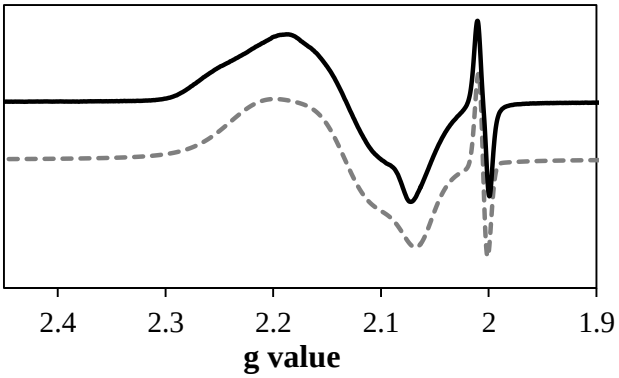

Figure 29. X-band EPR spectra of [Ni(Psalen^{OMe})]$^{+}$ in a dichloromethane solution at 10 K (solid line) and simulation (dashed line). Conditions: 9.383 GHz; Power: 0.1003 mW; modulation frequency: 100 kHz; amplitude: 0.2 mT.

		Ni center	radical	T
g values	g_1	2.2157	2.0052	10 K
	g_2	2.1362		
	g_3	2.0668		
g value			2.0058	290 K
|A| H (MHz)			25.8367	
|A| H (MHz)			2.00714	
|a| H(9) (MHz)			3.08318	

Table 5. EPR simulation parameters for the [Ni(Psalen^{OMe})]$^{+}$ at 10 and 290 K.

The EPR spectrum of [Ni(Psalen^{OMe})]$^{+}$$SbF_6^{-}$ was also recorded in the solid state. Figure 30 shows a rhombic signal centered at g = 2.14 which was assigned to a Ni^{III} center, however the organic radical signal was not observed. This difference in the electronic structure between the solid state and the solution was also observed by Stack and co-workers for the [CuSal]$^{+}$$SbF_6^{-}$ derivative.[3a] The g values obtained by simulation are g_1 = 2.2081, g_2 = 2.1406 and g_3 = 2.0680 (g_{av} = 2.14), very similar to those obtained for the frozen solution.

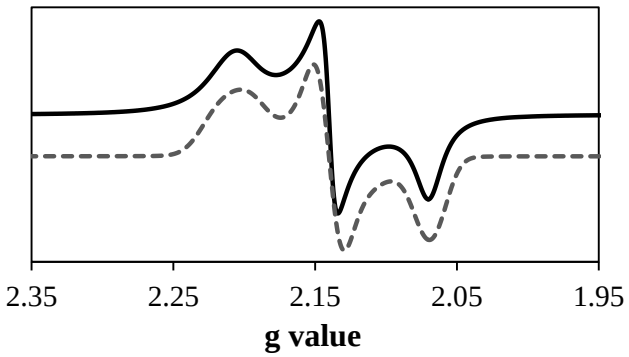

Figure 30. X-band EPR spectra of [Ni(Psalen^{OMe})]$^{+}$SbF$_6^{-}$ in the solid state at 20 K (solid line) and simulation (dashed line). Conditions: Frequency: 9.386 GHz; Power: 0.006 mW; modulation frequency: 100 kHz; amplitude: 0.6 mT.

The EPR spectra of both copper oxidized complexes were recorded from 77 K to room temperature and were silent throughout this temperature range. This is in agreement with the singlet ground states established by the NMR studies.

5.3 UV-vis spectroscopy

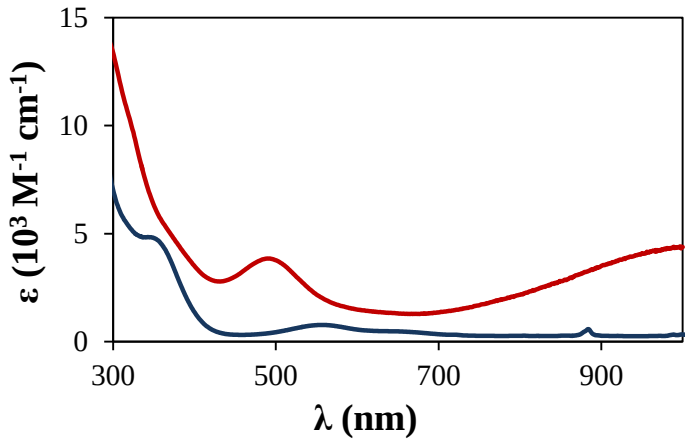

Figure 31. UV-vis spectra of [Ni(Psalen^{tBu})] (blue line) and [Ni(Psalen^{tBu})]$^{+}$ (red line) in CH_2Cl_2 at 298 K.

Figure 31 shows the UV-vis spectra obtained for [Ni(Psalen^{tBu})] and [Ni(Psalen^{tBu})]$^{+}$SbF$_6^{-}$, made by T.P.A. Cao.[1] The spectrum of the neutral complex is characterized by two weak transitions at 565 nm (ε = 770 M^{-1} cm^{-1}) and 630 nm (ε = 480 M^{-1} cm^{-1}) which were assigned to metal to ligand charge transfers (MLCT) typical from Ni^{II} square planar complexes.[15] A more intense transition was also observed at 350 nm (ε = 4800 M^{-1} cm^{-1}). The spectrum of the oxidized complex exhibits two intense transitions at 490 nm (ε =

3800 M^{-1} cm^{-1}) and above 1000 nm (ε = 4400 M^{-1} cm^{-1}) which were tentatively assigned to ligand to metal charge transfers thanks to the TD-DFT analysis.[1]

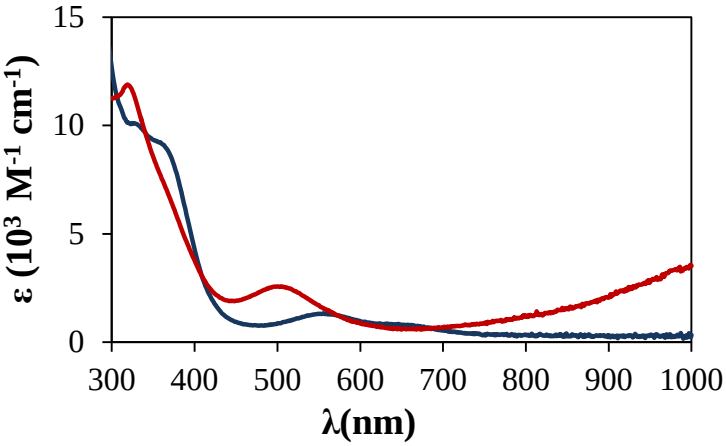

Figure 32. UV-vis spectra of [Ni($Psalen^{OMe}$)] (blue line) and [Ni($Psalen^{OMe}$)]$^+$ (red line) in CH_2Cl_2 at 298 K.

The spectra of [Ni($Psalen^{MeO}$)] and [Ni($Psalen^{OMe}$)]$^+$ are very similar to those of the t-butyl derivative (Figure 32). These weak transitions observed for [Ni($Psalen^{OMe}$)] are not present in the spectrum of the oxidized complex which exhibits a new transition at 510 nm (ε = 2500 M^{-1} cm^{-1}), and in the NIR region (ε = 3600 M^{-1} cm^{-1}). Both absorptions are less intense that the ones present in the spectrum of [Ni($Psalen^{tBu}$)]$^{+\cdot}$.[1]

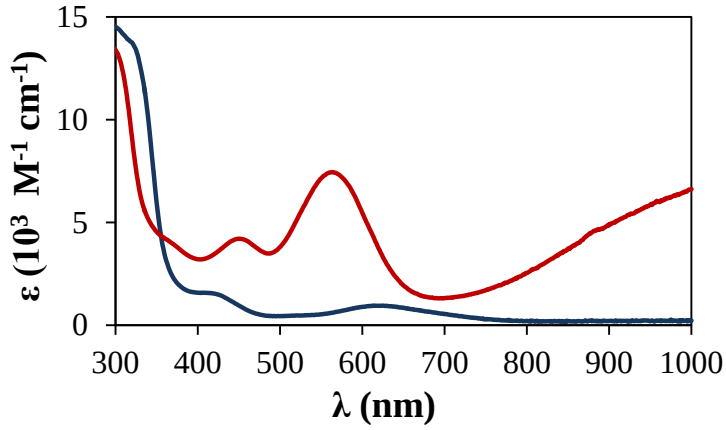

Figure 33. UV-vis spectra of [Cu($Psalen^{tBu}$)] (blue line) and [Cu($Psalen^{tBu}$)]$^+$ (red line) in CH_2Cl_2 at 298 K.

Oxidation of [Cu($Psalen^{tBu}$)] to[Cu($Psalen^{tBu}$)]$^+$ induces the apparition of two new bands: an intense absorption at 560 nm (ε = 7400 M^{-1} cm^{-1}) and another one in the NIR region (ε = 6600 M^{-1} cm^{-1}). The transition at 430 nm seems to be enhanced and shifted to 450 nm (ε = 4200 M^{-1} cm^{-1}).

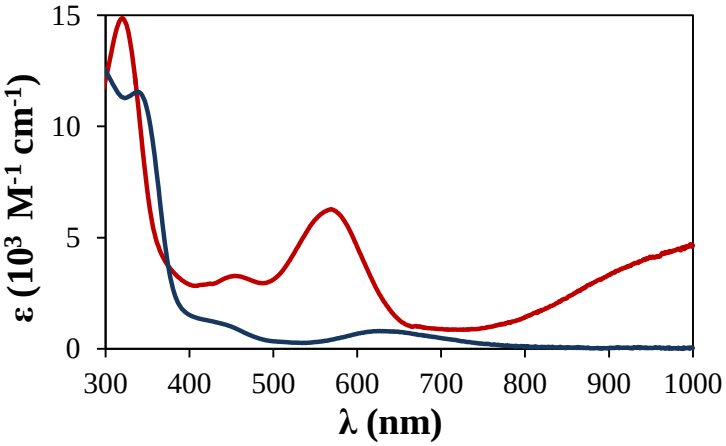

Figure 34. UV-vis spectra of [Cu(Psalen^{OMe})] (blue line) and [Cu(Psalen^{OMe})]$^{+}$ (red line) in CH_2Cl_2 at 298 K.

[Cu(Psalen^{OMe})]$^{+}SbF_6^{-}$ exhibits new bands centered at 570 nm (ε = 6300 M^{-1} cm^{-1}) and 320 nm (ε = 15000 M^{-1} cm^{-1}). A weaker band is also observed at 450 nm (ε = 3300 M^{-1} cm^{-1}) and a broad band in the NIR region (ε = 4600 M^{-1} cm^{-1}), less pronounced than that observed for [Cu(Psalen^{tBu})]$^{+}SbF_6^{-}$.

The recorded UV-vis spectra do not provide much pertinent information about the electronic structure of the complexes. The differences observed in the electrochemistry, NMR and EPR spectra when comparing the different copper and nickel complexes ([M(Psalen^{tBu})]$^{+}$ and [M(Psalen^{OMe})]$^{+}$) are not translated in the absorption spectra. Only slight differences in the intensity of the new bands were detected, these being more intense in the case of [M(Psalen^{tBu})]$^{+}$. Transitions present in the NIR region are normally attributed to ligand to ligand charge transfer (LLCT) or inter-valence charge transfer (IVCT) characteristic for fully delocalized systems,[16] which contrast with the description of a high-valent metal complex in the case of [Ni(Psalen^{tBu})]$^{+}$.

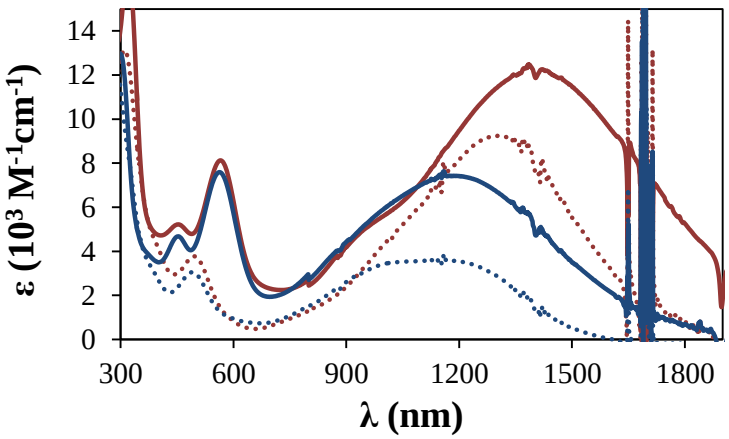

Figure 35. UV-NIR spectra of $[Ni(Psalen^{tBu})]^+$ (dashed red line), $[Ni(Psalen^{OMe})]^+$ (dashed blue line), $[Cu(Psalen^{tBu})]^+$ (solid blue line), and $[Cu(Psalen^{OMe})]^+$ (dashed blue line) in dichloromethane at room temperature.

The UV-NIR spectrum was recorded for the four oxidized complexes (Figure 35). They all show an intense broad band above 1000 nm. The intensity and position of this band change depending on the metal and the ligand. For $[Ni(Psalen^{tBu})]^+$ the band is centered at 1100 nm (ε = 3600 cm^{-1} M^{-1}) and present a $\Delta\nu_{1/2}$ = 550 nm. The band of $[Ni(Psalen^{OMe})]^+$ is red-shifted to 1300 nm and presents higher intensity (ε = 9200 cm^{-1} M^{-1}, $\Delta\nu_{1/2}$ = 520 nm). For $[Cu(Psalen^{tBu})]^+$ the band is centered at 1180 nm (ε = 7400 cm^{-1} M^{-1}, $\Delta\nu_{1/2}$ = 620 nm), while this band is red-shifted for to 1400 nm $[Cu(Psalen^{OMe})]^+$ and its intensity increases (ε = 7400 cm^{-1} M^{-1}, $\Delta\nu_{1/2}$ = 620 nm) as for $[Ni(Psalen^{OMe})]^+$.

For both nickel and copper complexes, the NIR band is more intense when featuring the $Psalen^{tBu}$. At the same time, the bands displayed by the nickel complexes possess higher intensity than the copper ones. Since many transitions can be included in the band observed, it is difficult to withdraw any conclusion about the electronic structure of the complexes. Notwithstanding, while the UV-vis spectra present very similar transitions for the series of nickel and copper complexes, the NIR spectra evidences the differences obtained by other characterization techniques.

5.4 X-ray diffraction

Table 6 gathers the geometrical data obtained for $[Ni(Psalen^{tBu})]$ and $[Ni(Psalen^{tBu})]^+SbF_6^-$ for the sake of comparison.

	[Ni(Psalen^{tBu})]	[Ni(Psalen^{tBu})]$^{+}$SbF$_6^{-}$	Δd
Ni-O1	1.878(1)	1.828(2)	-0.050
Ni-O2	1.878(1)	1.844(2)	-0.034
Ni-N1	1.888(2)	1.875(3)	-0.013
Ni-N2	1.888(2)	1.842(3)	-0.046
P1-N1	1.619(2)	1.639(3)	0.020
P2-N2	1.619(2)	1.650(3)	0.031
Torsion angle[a]	6.15	11.47	5.32

Table 6. Selected bond distances (Å) and angles (°) for [Ni(Psalen^{tBu})] and [Ni(Psalen^{tBu})]$^{+}$SbF$_6^{-}$.[1] [a] Torsion of the NOON plane.

Dark brown crystals of [Ni(Psalen^{OMe})]$^{+}$SbF$_6^{-}$ suitable X-ray diffraction were obtained by slow diffusion of petroleum ether into a saturated dichloromethane solution.

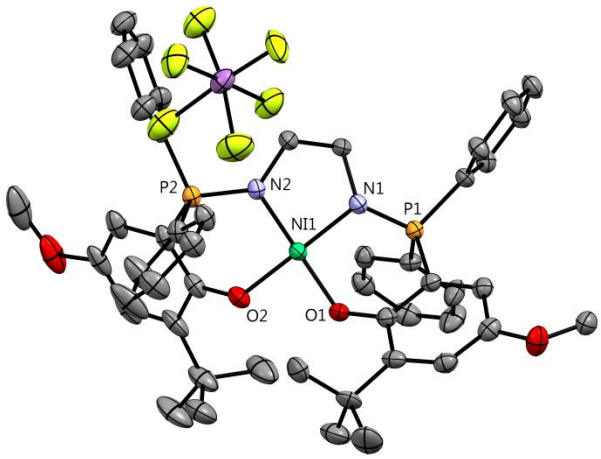

Figure 36. ORTEP of [Ni(Psalen^{OMe})]$^{+}$SbF$_6^{-}$ with thermal ellipsoids at 50 % probability. Hydrogen atoms have been omitted for clarity.

Upon oxidation, [Ni(Psalen^{OMe})]$^{+}$SbF$_6^{-}$ experiences a non-symmetric contraction of the coordination sphere: Ni-N bonds shorten by 0.003 and 0.043 Å and Ni-O by 0.051 and 0.021 Å (Figure 36). Due to this contraction, a long axis appears in [Ni(Psalen^{OMe})]$^{+}$SbF$_6^{-}$ along the N1-Ni-O2 segment. This feature was also observed for [Ni(Psalen^{tBu})]$^{+}$SbF$_6^{-}$ for which the Ni-N bonds shorten by 0.013 and 0.046 Å, and the Ni-O shorten by 0.050 and 0.034 Å.[1] As a consequence of the contraction of the Ni-N bonds, the P-N bonds lengthen by 0.024 and 0.026 Å, due to the shift of the electron density from the nitrogen towards the metal center.

The oxidation also affects the planarity of the complex. The distortion of the main plane increases to 16.02 °, again larger than in the tert-butyl analogue (11.47 °). The phenoxide rings, as well as the C-O bonds, do not experience significant variations, ruling out the possibility of a localized radical ligand.[4]

	[Ni(Psalen^{OMe})]	[Ni(Psalen^{OMe})]$^{+}$SbF$_6^{-}$	Δd
Ni-O1	1.880(2)	1.829(3)	-0.051
Ni-O2	1.885(2)	1.864(3)	-0.021
Ni-N1	1.877(2)	1.874(3)	-0.003
Ni-N2	1.884(2)	1.841(3)	-0.043
P1-N1	1.603(2)	1.627(3)	0.024
P2-N2	1.606(2)	1.632(3)	0.026
Torsion angle[a]	11.96	16.02	4.06

Table 7. Selected bond distances (Å) and angles (°) for [Ni(Psalen^{OMe})] and [Ni(Psalen^{OMe})]$^{+}$SbF$_6^{-}$. [a] Torsion of the NOON plane.

This is in contrast with the features observed for the salen analogue [Ni(Sal^{OMe})]$^{+}$SbF$_6^{-}$ for which a localized phenoxyl radical in one of the rings was evidenced.[4] In that complex, the whole coordination sphere does not experience a contraction but only the Ni-O bond associated to the non-oxidized phenolate ring shortens.

The contraction of the coordination sphere observed for [Ni(Psalen^{OMe})]$^{+}$SbF$_6^{-}$ indicates the oxidation of the metal. However, this contraction is smaller than that experienced by [Ni(Psalen^{tBu})]$^{+}$SbF$_6^{-}$, suggesting that the metal is involved in the oxidation process but in a lower extent than for [Ni(Psalen^{tBu})]$^{+}$SbF$_6^{-}$.

Dark purple crystals of [Cu(Psalen^{tBu})]$^{+}$SbF$_6^{-}$ and [Cu(Psalen^{OMe})]$^{+}$SbF$_6^{-}$ suitable X-ray diffraction were obtained after one week of storage of a saturated solution of toluene/CH_2Cl_2 at -40 °C.

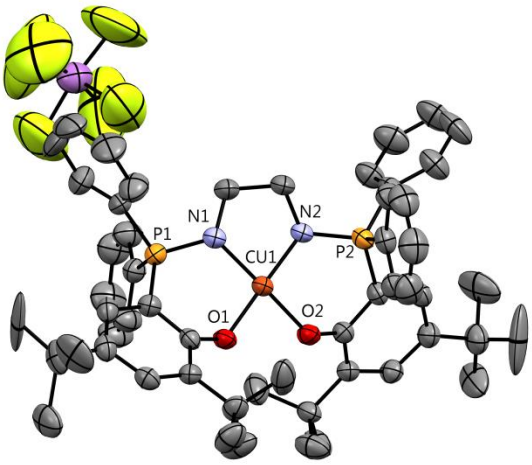

Figure 37. ORTEP of [Cu(Psalen^{tBu})]$^{+}$SbF$_6^{-}$ with thermal ellipsoids at 50 % probability. Hydrogen atoms have been omitted for clarity.

For both [Cu(Psalen^{tBu})]$^{+}$SbF$_6^{-}$ and [Cu(Psalen^{OMe})]$^{+}$SbF$_6^{-}$ complexes there is an important gain in planarity upon oxidation: the torsion angle of the main plane in [Cu(Psalen^{tBu})]$^{+}$SbF$_6^{-}$ is 1.01 °, and 1.87 ° for [Cu(Psalen^{OMe})]$^{+}$SbF$_6^{-}$ (Figure 37 and Figure

38, respectively). As [Cu(Psalen^{OMe})] presents a more distorted geometry, its gain in planarity upon oxidation is larger than for the tert-butyl derivative. [Cu(Psalen^{tBu})]$^{+}$SbF$_6^{-}$ experiences a large contraction of the coordination sphere: Cu-O bonds shorten by 0.062 Å and Cu-N by 0.056 Å. These variations are larger than those observed for [Ni(Psalen^{tBu})].[1] The P-N bonds lengthen by 0.049 Å in average. This important contraction and gain in planarity was also observed for the salen analogue [CuSal]$^{+}$SbF$_6^{-}$ which was characterized as a Cu^{III} complex in the solid state,[3a] so a metal-centered oxidation seems likely for [Cu(Psalen^{tBu})]$^{+}$SbF$_6^{-}$.

	[Cu(Psalen^{tBu})]	[Cu(Psalen^{tBu})]$^{+}$SbF$_6^{-}$	Δd
Cu-O1	1.917(2)	1.861(3)	-0.056
Cu-O2	1.917(2)	1.860(3)	-0.057
Cu-N1	1.951(2)	1.889(3)	-0.062
Cu-N2	1.951(2)	1.889(3)	-0.062
N1-P1	1.603(2)	1.644(4)	0.041
N2-P2	1.602(2)	1.657(4)	0.055
Torsion angle[a]	13.02	1.01	-12.01

Table 8. Selected bond distances (Å) and angles (°) for [Cu(Psalen^{tBu})] and [Cu(Psalen^{tBu})]$^{+}$SbF$_6^{-}$. [a] Torsion of the NOON plane.

For [Cu(Psalen^{OMe})]$^{+}$SbF$_6^{-}$, the contraction around the metal center is not symmetric: Cu-O bonds shorten by 0.028 Å while the Cu-N bonds shorten by 0.019 and 0.037 Å. The elongation of the P-N bonds is not symmetric with variations of 0.42 and 0.29 Å. The oxidation has no influence on the phenoxide rings, whose bonds do not experience significant changes. No interaction was observed between the SbF$_6^{-}$ anion and the aromatic rings, as observed in the [CuSal^{OMe}]$^{+}$SbF$_6^{-}$ analogue which was described as a phenoxyl radical cation complex.[4]

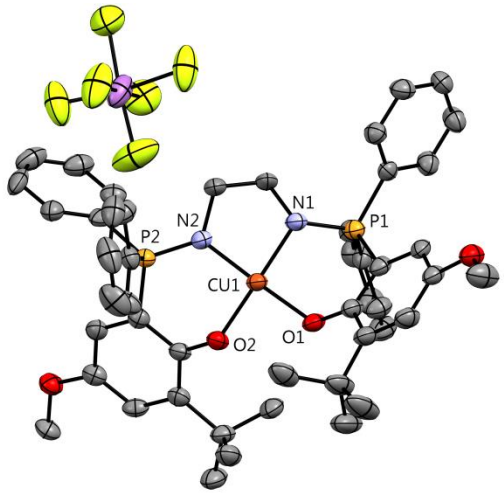

Figure 38. ORTEP of [Cu(Psalen^{OMe})]$^{+}$SbF$_6^{-}$ with thermal ellipsoids at 50 % probability. Hydrogen atoms have been omitted for clarity.

From the contraction observed in the coordination sphere of [Cu(Psalen^{OMe})]$^{+}$SbF$_6^{-}$, the metal seems to be involved in the oxidation process, but the presence of a fully delocalized radical ligand cannot be ruled out, as for [Ni(Psalen^{OMe})]$^{+}$SbF$_6^{-}$.

	[Cu(Psalen^{OMe})]	[Cu(Psalen^{OMe})]$^{+}$SbF$_6^{-}$	Δd
Cu-O1	1.923(2)	1.904(3)	-0.019
Cu-O2	1.919(2)	1.882(3)	-0.037
Cu-N1	1.948(2)	1.920(4)	-0.028
Cu-N2	1.941(2)	1.913(4)	-0.028
N1-P1	1.597(2)	1.639(4)	0.042
N2-P2	1.593(2)	1.621(4)	0.028
Torsion angle[a]	19.40	1.87	-17.53

Table 9. Selected bond distances (Å) and angles (°) [Cu(Psalen^{OMe})] and [Cu(Psalen^{OMe})]$^{+}$SbF$_6^{-}$. [a] Torsion of the NOON plane.

5.5 Magnetic measurements

[Ni(Psalen^{OMe})]$^{+}$SbF$_6^{-}$ displays a regular paramagnetic behavior, following the Curie-Weiss law, with a χT value of 0.427 cm^3 K mol^{-1} at room temperature (Figure 39). The g average value obtained from this data is 2.16, which is in good agreement with the value obtained from the EPR studies, 2.14. This value is lower than the one obtained for [Ni(Psalen^{tBu})]$^{+}$SbF$_6^{-}$ (2.22)[1] and indicates a diminished metal character of the orbitals involved in the delocalization of the radical. Data of this sample have been corrected with 2.6 % of ferromagnetic impurity.[17]

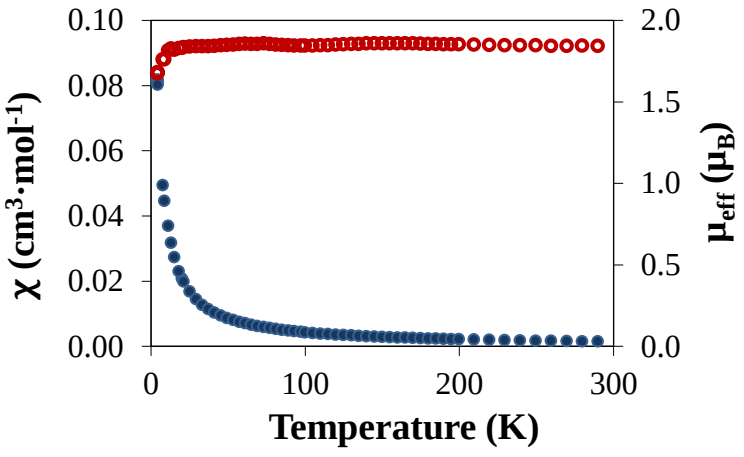

Figure 39. Plot of magnetic susceptibility (blue circles) and effective magnetic moment (red circles) *vs.* temperature for [Ni(Psalen^{OMe})]$^{+}$SbF$_6^{-}$.

The magnetic properties of the oxidized copper complexes were investigated using ground crystals. Both complexes display a very low magnetic response so the measurements were performed at higher magnetic fields than for the other complexes, 2 and 5 T. The χ *vs.* T

curves of [Cu(Psalen^{tBu})]$^{+}$SbF$_6^{-}$ and [Cu(Psalen^{OMe})]$^{+}$SbF$_6^{-}$ are represented in Figure 40. The data of both complexes have been corrected with 3 % of Cu^{II} impurity.[17]

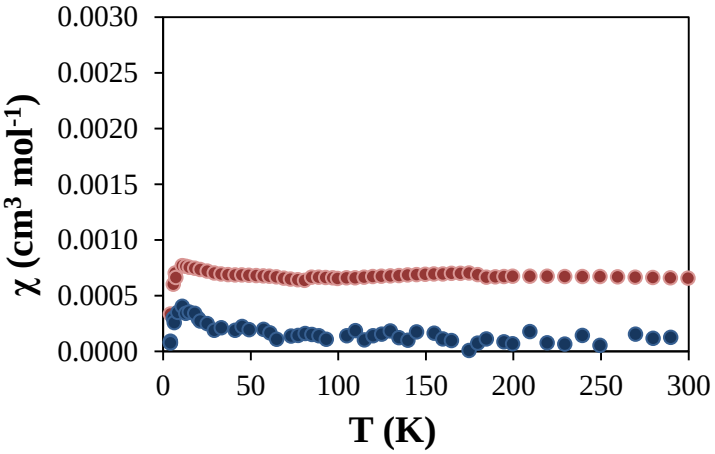

Figure 40. Plot of the magnetic susceptibilities *vs.* temperature of [Cu(Psalen^{tBu})]$^{+}$SbF$_6^{-}$ (blue circles) and [Cu(Psalen^{OMe})]$^{+}$SbF$_6^{-}$ (red circles).

[Cu(Psalen^{tBu})]$^{+}$SbF$_6^{-}$ and [Cu(Psalen^{OMe})]$^{+}$SbF$_6^{-}$ exhibit a Temperature Independent Paramagnetism (TIP)[18] behavior where the magnetic susceptibility χ is very low and constant through the temperature range studied. χ values are 0.00070(5) cm^3 mol^{-1} for [Cu(Psalen^{OMe})]$^{+}$SbF$_6^{-}$, and approximately 0.0001(1) cm^3 mol^{-1} for [Cu(Psalen^{tBu})]$^{+}$SbF$_6^{-}$. This magnetic behavior corresponds to a singlet ground state with a triplet excited state which is not populated, or in a very small extent (otherwise the χ values obtained would be higher and would follow the Curie law).[18] Therefore, the energy gap between the two states (-2J) is rather large (Scheme 46). This is in agreement with the results obtained from the VT-NMR studies of [Cu(Psalen^{OMe})]$^{+}$SbF$_6^{-}$ which established a singlet ground state and a triplet excited state separated by 1420 cm^{-1} (0.176 eV). The low χ value obtained for [Cu(Psalen^{tBu})]$^{+}$SbF$_6^{-}$ (seven times lower than [Cu(Psalen^{OMe})]$^{+}$SbF$_6^{-}$), and the absence of significant variation of the chemical shifts with the temperature, suggest that the energy gap between the singlet and triplet states is larger for [Cu(Psalen^{tBu})]$^{+}$SbF$_6^{-}$. However, the very low χ value obtained for [Cu(Psalen^{tBu})]$^{+}$SbF$_6^{-}$ has to be taken cautiously since the error is rather large.

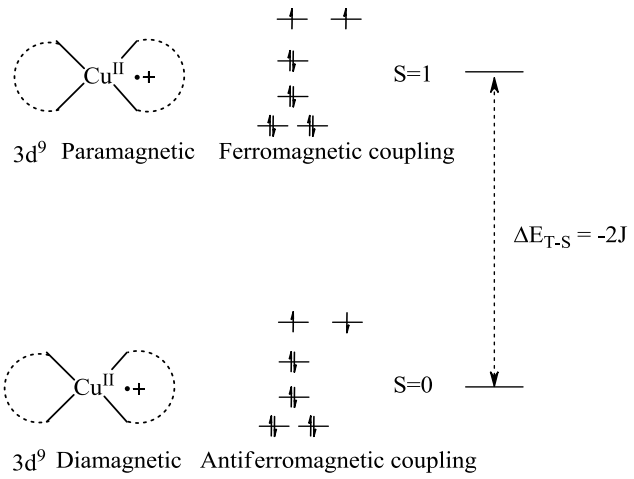

Scheme 46. Electronic configuration suggested by the magnetic measurements for [Cu(Psalen^{OMe})]$^{+}$.

6. Calculations

The electronic structure of the six complexes has been studied by computational theory methods by Dr. Carine Clavaguera. A first tentative of structure optimization was done with DFT calculations using the B3LYP and PBE functionals, but some of the bond distances and the planarity of the complexes were not well reproduced, especially for the oxidized complexes. Satisfactory results were obtained by using TPSSh-D3 functional and SVP as basis set. The geometrical changes obtained upon oxidation were in good agreement with the variations observed in the X-ray structures. Nevertheless the distortion observed in the neutral complexes could not be well reproduced. Table 10,Table 11 and Table 12 gather the experimental and calculated bond distances for the all six complexes.

	Exp.		**TPSSh-D3/SVP**		**Δ(II/III)**	
	[Ni(Psalen^{OMe})]	[NiPsalen^{OMe}]$^{+}$	[Ni(Psalen^{OMe})]	[NiPsalen^{OMe}]$^{+}$	Exp.	TPSSh-D3
O1-Ni	1.880	1.829	1.892	1.835	-0.051	-0.057
O2-Ni	1.885	1.864	1.896	1.879	-0.021	-0.017
N1-Ni	1.877	1.874	1.890	1.893	-0.003	0.003
N2-Ni	1.884	1.841	1.897	1.839	-0.043	-0.058
N1=P1	1.603	1.627	1.634	1.640	0.024	0.006
N2=P2	1.606	1.632	1.635	1.667	0.026	0.032
NOON	11.9	16.0	3.5	10.2	4.1	6.7

Table 10. Experimental and calculated bond distances for [Ni(Psalen^{OMe})] and [Ni(Psalen^{OMe})]$^{+}$ complexes and bond distance differences between the neutral and the oxidized species expressed in Å.

	Exp.		TPSSh-D3/SVP		Δ(II/III)	
	[Cu(Psalen^{tBu})]	[CuPsalen^{tBu}]$^{+}$	[Cu(Psalen^{tBu})]	[CuPsalen^{tBu}]$^{+}$	Exp.	TPSSh-D3
O1-Cu	1.914	1.861	1.989	1.937	-0.056	-0.052
O2-Cu	1.914	1.860	1.989	1.936	-0.057	-0.053
N1-Cu	1.951	1.889	1.956	1.907	-0.062	-0.049
N2-Cu	1.951	1.889	1.956	1.905	-0.062	-0.051
N1=P1	1.602	1.644	1.629	1.667	0.042	0.038
N2=P2	1.602	1.657	1.629	1.669	0.055	0.040
NOON	13.0	1.0	0.9	2.5	-12.0	1.6

Table 11. Experimental and calculated bond distances for [Cu(Psalen^{tBu})] and [Cu(Psalen^{tBu})]$^{+}$ complexesand bond distance differences between the neutral and the oxidized species expressed in Å.

	Exp.		TPSSh-D3/SVP		Δ(II/III)	
	[Cu(Psalen^{OMe})]	[CuPsalen^{OMe}]$^{+}$	[Cu(Psalen^{OMe})]	[CuPsalen^{OMe}]$^{+}$	Exp.	TPSSh-D3
O1-Cu	1.923	1.904	1.959	1.914	-0.019	-0.045
O2-Cu	1.919	1.882	1.952	1.914	-0.037	-0.038
N1-Cu	1.948	1.920	1.997	1.950	-0.028	-0.047
N2-Cu	1.941	1.913	1.987	1.949	-0.028	-0.038
N1=P1	1.598	1.639	1.627	1.659	0.042	0.032
N2=P2	1.595	1.621	1.628	1.660	0.028	0.032
NOON	19.4	1.9	1.0	2.7	-17.5	1.7

Table 12. Experimental and calculated bond distances for [Cu(Psalen^{OMe})] and [Cu(Psalen^{OMe})]$^{+}$ complexesand bond distance differences between the neutral and the oxidized species expressed in Å.

Molecular orbitals were calculated at the TPSSh-D3/ZORA/TZ2P level. For neutral complexes the calculated HOMOs are similar and have both metal and ligand contributions. The shape of these orbitals is similar despite the different substitution; a larger phenoxide contribution seems to be present in the methoxy derivatives due to the participation of the oxygen atoms (Figure 41). This delocalized structure is kept for all the three oxidized complexes. [Cu(Psalen^{tBu})]$^{+}$ and [Cu(Psalen^{OMe})]$^{+}$ display almost the same electronic structure, while a more important metal character is expected for [Cu(Psalen^{tBu})]$^{+}$. The characterization made for these complexes points to different electronic arrangements, contrary to what the DFT proposes.

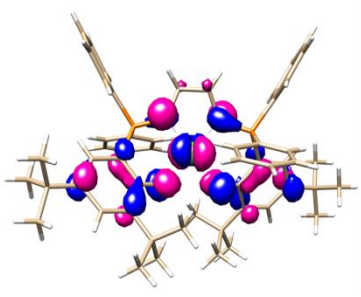

HOMO **[Ni(Psalen^{tBu})]**

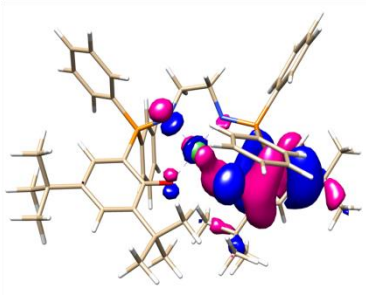

HOMO **[Ni(Psalen^{tBu})]$^{+}$**

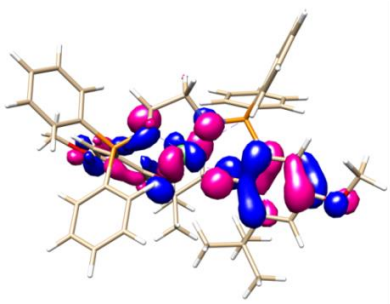

HOMO **[Ni(Psalen^{OMe})]**

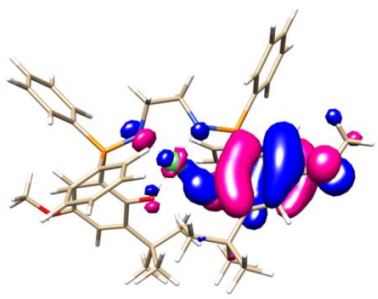

HOMO **[Ni(Psalen^{OMe})]$^{+}$**

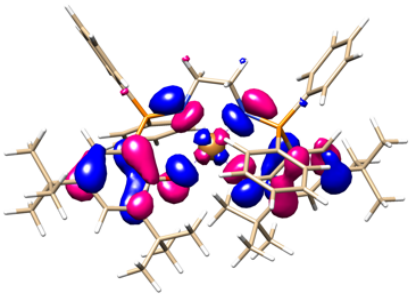

HOMO **[Cu(Psalen^{tBu})]**

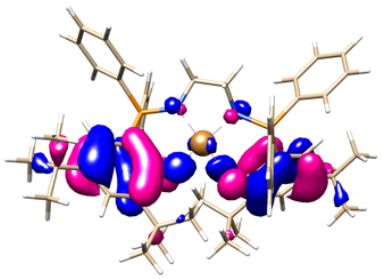

HOMO **[Cu(Psalen^{tBu})]$^{+}$**

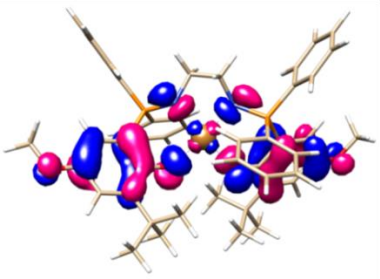

HOMO **[Cu(Psalen^{OMe})]**

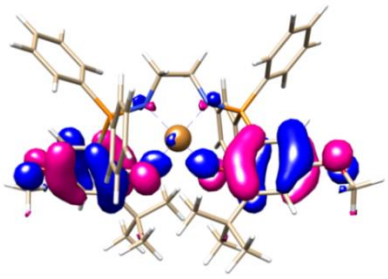

HOMO **[Cu(Psalen^{OMe})]$^{+}$**

Figure 41. Molecular orbital plots of neutral and oxidized complexes obtained by DFT.

DFT calculations cannot satisfactorily reproduce the electronic changes derived from the substitution of the *para* substituents. Therefore, to better understand the electronic structure of the oxidized complexes and in order to explain the multiple behaviors observed, Complete Active Space self-consistent field (CASSCF) calculations were performed by Dr. Carine Clavaguera. For these calculations the multiplicity and the number of electrons (N) and orbitals (M) must be specified: CASSCF(N,M).

The active space considered for $[Ni(Psalen^{OMe})]^+$ was (9,7) with a doublet as multiplicity (one unpaired electron), so 9 electrons to be placed in 7 orbitals. Three majority configurations were obtained: a main one which represents the 41 % of the ground state and corresponds to the unpaired electron delocalized in an orbital having both metal and ligand character. A second configuration representing an additional 11 % where the unpaired electron is located in a metal-type orbital; and a third one with a weight of 9 %, where the three electrons are placed in two mixed metal-ligand orbitals and one metal-type orbital. This evidences a multiconfigurational character of the ground state and a high delocalization of the unpaired electron on the ligand orbitals, which could explain the EPR spectrum observed. A scheme representing the different configurations obtained for the four complexes is shown in Chart 1.

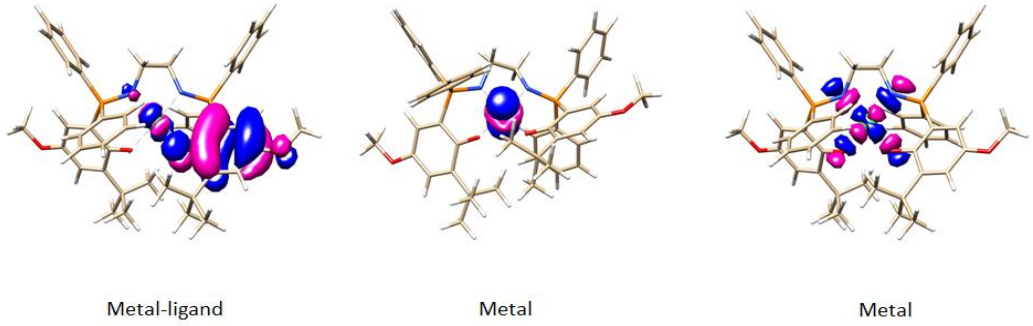

Figure 42. Active space molecular orbitals occupied by unpaired electrons associated to their "metal" or "ligand" character for $[Ni(Psalen^{OMe})]^+$.

The same calculations were performed with $[Ni(Psalen^{tBu})]^+$ and the main configuration (55 %) corresponds to the unpaired electron located in a metallic orbital. A second configuration representing a 12 % delocalizes the three valence electrons in two metal-type orbitals and one π-ligand orbital. The remaining 39 % in $[Ni(Psalen^{OMe})]^+$, and 33 % in $[Ni(Psalen^{tBu})]^+$, consists of several minor configurations. A plot of the calculated orbitals is present in Figure 42 and Figure 43.

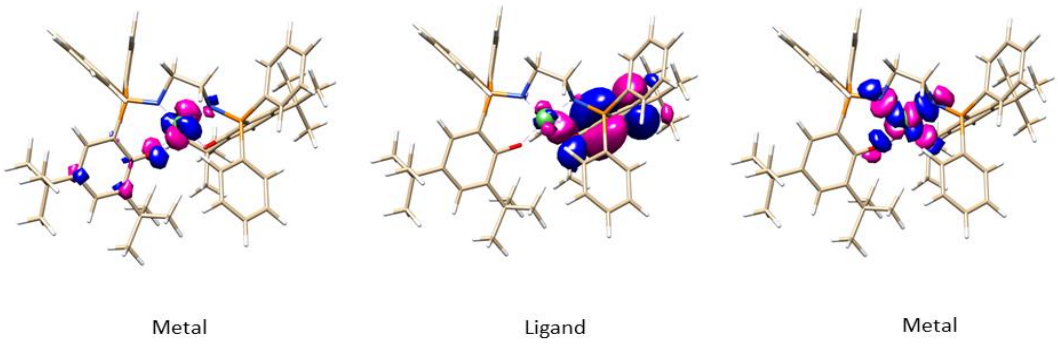

Figure 43. Active space molecular orbitals occupied by unpaired electrons associated to their "metal" or "ligand" character for [Ni(Psalen^{tBu})]$^{+}$.

Similar calculations were performed for both oxidized copper complexes considering an active space of CASSCF (8,6) and allowing both singlet and triplet multiplicities. The triplet state resulted to be higher in energy by 24.4 (2039.7 cm^{-1}) and 27.8 kJ/mol (2323.9 cm^{-1}) for [Cu(Psalen^{tBu})]$^{+}$ and [Cu(Psalen^{OMe})]$^{+}$, respectively.

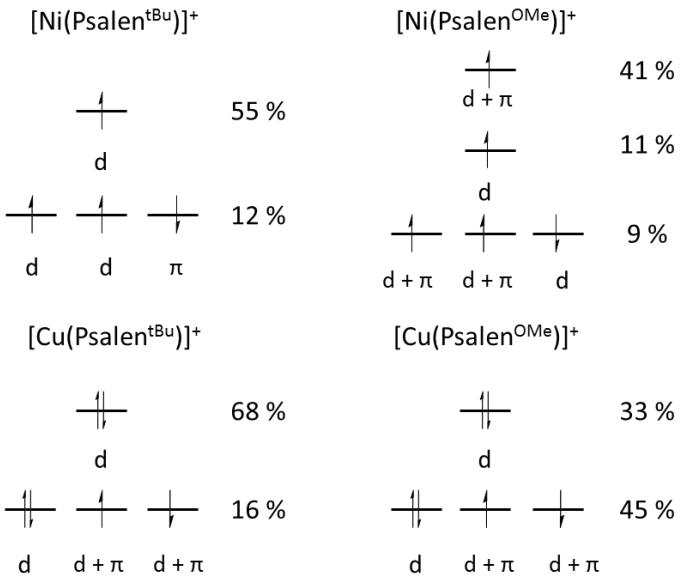

Chart 1. Electronic structure of [Ni(Psalen^{tBu})]$^{+}$SbF$_6^{-}$, [Ni(Psalen^{OMe})]$^{+}$SbF$_6^{-}$, [Cu(Psalen^{tBu})]$^{+}$SbF$_6^{-}$ and [Cu(Psalen^{OMe})]$^{+}$SbF$_6^{-}$ computed from CASSCF/TZVP state-average calculations.

As for the nickel complexes, the ground state of the copper complexes turned out to be multiconfigurational. For [Cu(Psalen^{tBu})]$^{+}$, the main configuration (68 %) corresponds to the closed-shell d^8 configuration, the second majority configuration (16 %) corresponds to two unpaired electrons located in two metal-ligand orbitals (Figure 44). The remaining 15 % is distributed among minor configurations. Thus, [Cu(Psalen^{tBu})]$^{+}$ is better described as Cu^{III} 3d^8 complex.

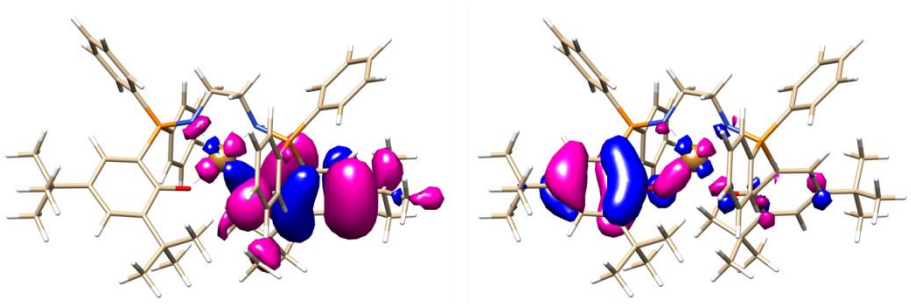

Figure 44. Active space molecular orbitals occupied by unpaired electrons with a "metal-ligand" character for [Cu(Psalen^{tBu})]$^{+}$.

For [Cu(Psalen^{OMe})]$^{+}$, the closed-shell d^{8} configuration represented only 33 % of the ground state. Two other configurations with a total weight of 45 % correspond to the two unpaired electrons located in two different metal-ligand orbitals (Figure 45), and the remaining 20 % is distributed among many other configurations. In this case, [Cu(Psalen^{OMe})]$^{+}$ is better described as a Cu(II) radical ligand complex in an open-shell configuration.

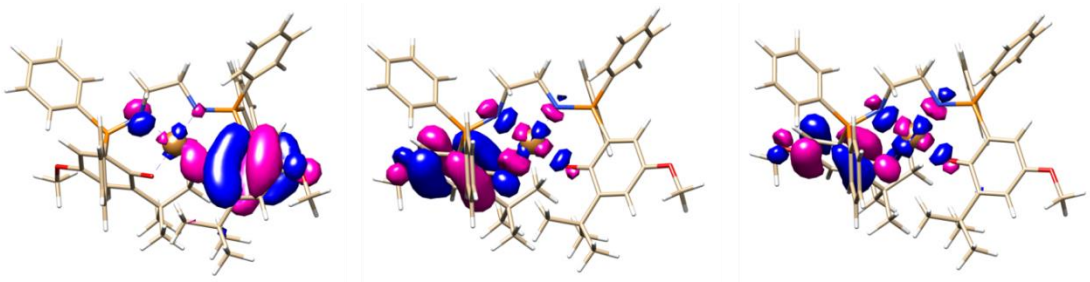

Figure 45. Active space molecular orbitals occupied by unpaired electrons with a "metal-ligand" character for [Cu(Psalen^{OMe})]$^{+}$.

7. Conclusion

[Cu(Psalen^{OMe})], [Cu(Psalen^{OMe})] and [Ni(Psalen^{OMe})] complexes and their one-electron oxidized products have been synthesized and characterized by cyclic voltammetry, X-ray diffraction, various spectroscopies (EPR, NMR, UV-vis) and magnetic measurements. An exhaustive study of the electronic structure of the oxidized complexes has been completed by DFT and CASSCF calculations. The latter points to the presence of multiconfigurational ground states for all of them, which explain the contradictions found in the characterizations of some complexes (*e.g.* [Cu(Psalen^{tBu})]$^{+}$).

The CV data seem to point towards similar electronic structure of nickel and copper oxidized complexes is similar when displaying the same ligand. The redox potentials obtained for this complexes show as well their facile oxidation compared to the salen analogues. The different characterizations, and especially the NMR studies, indicate that $[Cu(Psalen^{tBu})]^+$ is better described as a high-valent metal complex similarly to $[Ni(Psalen^{tBu})]^+$, and in agreement with the CASSCF calculations (68 % for the closed-shell configuration). It is therefore one of the few examples of Cu^{III} complexes bearing salen-type ligands. On the other hand, $Psalen^{OMe}$ ligand favors the formation of magnetic orbitals with more ligand character, as expected by better electron-donation of the methoxy substitution. $[Cu(Psalen^{OMe})]^+$ and $[Ni(Psalen^{OMe})]^+$ are better described as ligand radical complexes. From VT-NMR studies, a main open-shell singlet configuration can be established for $[Cu(Psalen^{OMe})]^+$, this electronic structure being reminiscent of that of the Galactose Oxidase.[19] The reactivity of these complexes towards the oxidation of primary alcohols is under investigation. $[Ni(Psalen^{OMe})]^+$ displays at low temperature an unusual EPR spectrum which shows both organic and Ni^{III} features. This can be explained by a multiconfigurational ground state, with both ligand radical and Ni^{III} d^7 configurations, which was confirmed by CASSCF calculations.

8. References

[1] T. P. A. Cao, G. Nocton, L. Ricard, X. F. Le Goff, A. Auffrant, *Angew. Chem. Int. Ed.* **2014**, *53*, 1368-1372.

[2] Y. D. Wang, J. L. DuBois, B. Hedman, K. O. Hodgson, T. D. P. Stack, *Science* **1998**, *279*, 537-540.

[3] a) T. Storr, P. Verma, R. C. Pratt, E. C. Wasinger, Y. Shimazaki, T. D. P. Stack, *J. Am. Chem. Soc.* **2008**, *130*, 15448-15459; b) L. Chiang, K. Herasymchuk, F. Thomas, T. Storr, *Inorg. Chem.* **2015**, *54*, 5970-5980.

[4] M. Orio, O. Jarjayes, H. Kanso, C. Philouze, F. Neese, F. Thomas, *Angew. Chem. Int. Edit.* **2010**, *49*, 4989-4992.

[5] P. Chaudhuri, C. N. Verani, E. Bill, E. Bothe, T. Weyhermüller, K. Wieghardt, *J. Am. Chem. Soc.* **2001**, *123*, 2213-2223.

[6] C. Bakewell, T. P. A. Cao, N. Long, X. F. Le Goff, A. Auffrant, C. K. Williams, *J. Am. Chem. Soc.* **2012**, *134*, 20577-20580.

[7] F. Thomas, O. Jarjayes, C. Duboc, C. Philouze, E. Saint-Aman, J.-L. Pierre, *Dalton Trans.* **2004**, 2662-2669.

[8] L. Dyers, S. Y. Que, D. VanDerveer, X. R. Bu, *Inorg. Chim. Acta* **2006**, *359*, 197-203.

[9] C. M. Lemon, M. Huynh, A. G. Maher, B. L. Anderson, E. D. Bloch, D. C. Powers, D. G. Nocera, *Angew. Chem. Int. Edit.* **2016**, *55*, 2176-2180.

[10] O. Rotthaus, F. Thomas, O. Jarjayes, C. Philouze, E. Saint-Aman, J.-L. Pierre, *Chem. Eur. J.* **2006**, *12*, 6953-6962.

[11] B. Le Guennic, T. Floyd, B. R. Galan, J. Autschbach, J. B. Keister, *Inorg. Chem.* **2009**, *48*, 5504-5511.

[12] a) P. Bertrand, *La spectroscopie de résonance paramagnétique électronique : fondements*, EDP sciences, Les Ulis, **2014**; b) Y. Shimazaki, T. Yajima, T. Shiraiwa, O. Yamauchi, *Inorg. Chim. Acta* **2009**, *362*, 2467-2474.

[13] F. Thomas, *Dalton Trans.* **2016**, *45*, 10866-10877.

[14] O. Rotthaus, O. Jarjayes, F. Thomas, C. Philouze, C. Perez Del Valle, E. Saint-Aman, J.-L. Pierre, *Chem. Eur. J.* **2006**, *12*, 2293-2302.

[15] T. Storr, E. C. Wasinger, R. C. Pratt, T. D. P. Stack, *Angew. Chem. Int. Edit.* **2007**, *46*, 5198-5201.

[16] Y. Shimazaki, T. D. P. Stack, T. Storr, *Inorg. Chem.* **2009**, *48*, 8383-8392.

[17] M. D. Walter, M. Schultz, R. A. Andersen, *New J. Chem.* **2006**, *30*, 238-246.

[18] J. H. Van Vleck, *The Theory of Electric and Magnetic Susceptibilities*, Oxford University Press, Oxford, **1932**.

[19] J. W. Whittaker, *Adv. Protein Chem.* **2002**, *60*, 1-49.

Chapter 3: Influence of the phosphorus substituents in Ni and Cu phosphasalen complexes

1. Introduction

In the previous chapter the study was focused on the influence of the phenolate substituents on the electronic structure of the oxidized phosphasalen complexes. In this chapter we will concentrate on the iminophosphorane functions, and more precisely on the phosphorus substituents. A significant change on the electronics and the steric hindrance of the ligand can be induced by the simple substitution of the aromatic groups by alkyl groups in the phosphorus atom. Alkyl substituents increase the basicity of the nitrogens due to a less efficient delocalization of the lone pairs of the nitrogen atoms in the P-C antibonding orbitals (lower negative hyperconjugation). Therefore, phosphasalen ligands incorporating dialkylphosphine groups are expected to be electron richer. To investigate how this influences the electronic structure of the oxidized complexes, we synthesized a new ligand analogous to Psalen$^{t\mathrm{Bu}}$ but featuring isopropyl ($^{i\mathrm{Pr}}$Psalen) instead of aryl groups in the phosphorus atoms (Scheme 47).

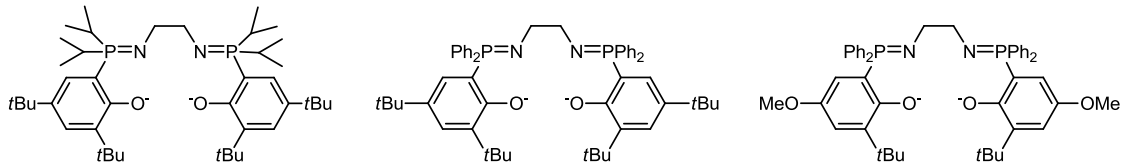

$^{i\mathrm{Pr}}$Psalen Psalen$^{t\mathrm{Bu}}$ Psalen$^{\mathrm{OMe}}$

Scheme 47. New phosphasalen ligand (left) and ligands studied in Chapter 2.

In salen chemistry, modifications of the electronic properties of the imine functions have been carried out by reducing them into amines. These are more electron-donating ligands which induce an increase of the electronic density on the metal (Scheme 48). These

ligands, named “salan”, displaying symmetric and asymmetric phenolate substitution have been studied by T. D. P. Stack.[1] Salan derivatives turned out to favor the oxidation of copper complexes with respect to their salen counterparts by ca. 350 mV, and the oxidized products were characterized as Cu(II)-phenoxyl and bis(phenoxyl) complexes.[1]

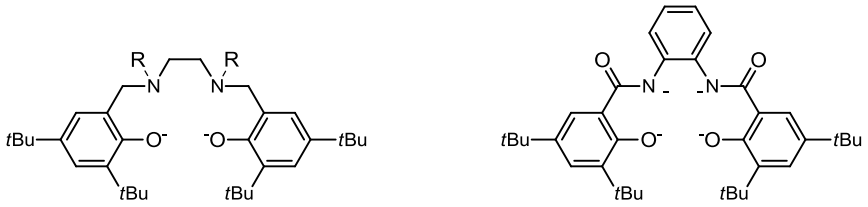

R = H, Salan
R = Me, Salan^{Me}

Bis-amidate ligand

Scheme 48. Ligands studied by Stack, Pierre and Thomas’ teams.[2]

Thomas and co-workers studied the oxidation of nickel complexes for which the amine of the salan bears a methyl group (Scheme 48, left).[2] This complex displayed a two-electron redox wave at 0.40 V *vs.* Fc^+/Fc couple corresponding to the oxidation of both phenolate rings. In that case, there is no interaction between the two redox units, so that the oxidation of one phenolate moiety does not influence the second one, and both occur at very similar potential. In contrast, when the ligand displays imine functions, the oxidation of the phenolate moieties takes place at higher potentials than for the salan derivatives, *via* two one-electron processes at 0.59 and 1.05 V *vs.* Fc^+/Fc, evidencing an electronic communication between the two redox units.[2] J-L. Pierre and co-workers also studied the replacement of one and two imine functions by amidate functions.[3] The electronic properties of these ligands are completely different from salen since the hybridization of the nitrogen atoms and the charge are different salen and salan ligands are di-anionic, while the mono-amidate ligands are tri-anionic, and the bis-amidate ligands are tetra-anionic (Scheme 48, right). The latter one is more similar to the phosphasalen ligand because of the presence of a lone pair on the nitrogen atom. Nickel complexes displaying bis-amidate ligands exhibit oxidations at lower potentials than those of salen: the first oxidation is favored by 0.84 V and the second by 0.50 V. Nevertheless, the introduction of amidate functions does not favor a metal-centered oxidation, but rather the formation of a phenoxyl radical partially delocalized in the nickel orbitals.[3]

Satisfactory results in the stabilization of high-valent metal species were obtained with the Psalen^{tBu} ligand (Chapter 2). The presence of isopropyl groups increases the electron-donating ability of the iminophosphorane functions, and is expected to promote a metal-centered oxidation to a larger extent than with Psalen^{tBu}.

As in Chapter 2, the electronic properties of this ligand have been investigated for both nickel and copper complexes, allowing a comparison with the previous studied ligands.

2. Synthesis of the ligand and neutral complexes

For this ligand, a new phosphine featuring isopropyl groups instead of aryl groups had to be synthesized. The synthesis followed the same procedure than described for the tert-butyl phosphine used in previous ligands (see Chapter 1, Section 3.3.3),[4] and occurs in two steps. The lithiation of the bromophenol with 2 equivalents of n-BuLi followed by the addition of chlorodiisopropyl phosphine at -78 °C led the corresponding phosphine as a white powder in 44 % yield after aqueous work-up. The diminished yield compared to diphenyl phosphine (90 %) derivative can be explained by the higher sensitivity of the alkyl phosphine.

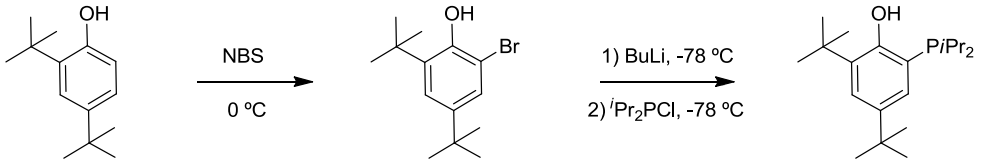

Scheme 49. Synthesis of the iPr-phosphine.

The ligand and the complexes were synthesized following a similar procedure used previously. The isopropyl phosphine was oxidized using bromine at -78 °C, and the mixture stirred at room temperature. The appearance of a singlet at 22.4 ppm in the $^{31}P\{^{1}H\}$ NMR indicates the formation of the phosphonium bromide intermediate (Scheme 50). The solution was cooled down again to -78 °C and tributyl amine was added followed by ethylenediamine. The mixture was warmed up and a white solid precipitated from the light pink solution. The $^{31}P\{^{1}H\}$ NMR displayed a large singlet at 66.7 ppm corresponding to the desired proligand while the presence of other minor signals resulting from the formation of side products. The mixture was stirred overnight at room temperature and centrifuged to remove insoluble salts. An emulsion was formed on top of the centrifugation tube which was recovered with the liquid phase. Addition of THF allows precipitating the ligand which was isolated by centrifugation. The solid was washed with more THF until the supernatant solution contained no phosphorylated compouds. The ligand was obtained as a white powder in its bis-aminophosphonium salt form ($H_4{}^{iPr}$Psalen)Br_2 in 80 % yield.

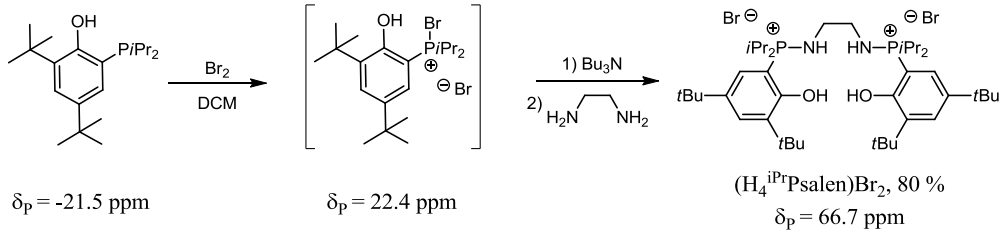

Scheme 50. Synthesis of the $(H_4^{iPr}Psalen)Br_2$ ligand and corresponding ^{31}P chemical shifts in dichloromethane.

The complexation takes place in two steps: the deprotonation of $(H_4^{iPr}Psalen)Br_2$ was achieved with either KH or KHMDS, followed by the addition of the metallic precursor, namely $CuBr_2$ or $[NiBr_2(DME)]$, to generate $[Cu(^{iPr}Psalen)]$ and $[Ni(^{iPr}Psalen)]$, respectively (Scheme 51).

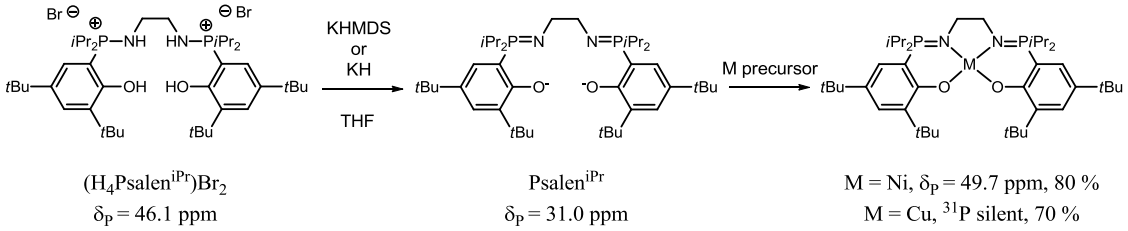

Scheme 51. Synthesis of the different complexes and their related ^{31}P NMR signals in THF.

The obtained complexes are more soluble in pentane and diethyl ether than $[M(Psalen^{tBu})]$ and $[M(Psalen^{OMe})]$, so their precipitation from the dichloromethane solution using these solvents failed. The complexes were obtained and purified by addition of methanol to concentrated dichloromethane solutions, or by washing the residue obtained from evaporation with diethyl ether. $[Cu(^{iPr}Psalen)]$ was isolated as a green powder in 70 % yield, and $[Ni(^{iPr}Psalen)]$ as a purple powder in 80 % yield.

3. Characterization of neutral complexes $[Ni(^{iPr}Psalen)]$ and $[Cu(^{iPr}Psalen)]$

3.1 NMR spectroscopy

$[Ni(^{iPr}Psalen)]$ was characterized by multinuclear NMR. The $^{31}P\{^1H\}$ signal appears at 49.3 ppm in $CDCl_3$.

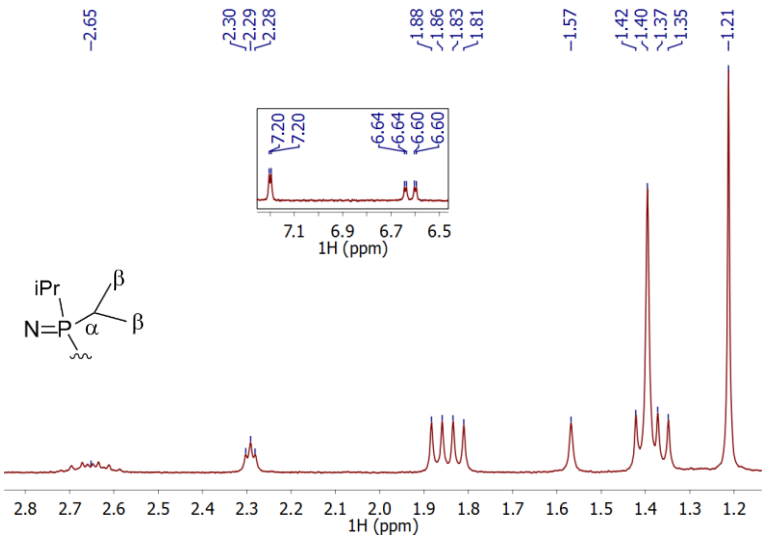

Figure 46. ^{1}H NMR spectrum of [Ni(^{iPr}Psalen)] at room temperature in CD_2Cl_2. Inset shows a zoom of the aromatic region. The signal at 1.55 ppm corresponds to water from the methanol used for precipitation.

Figure 46 shows the ^{1}H NMR spectrum of [Ni(^{iPr}Psalen)]. The signals were assigned and coupling patterns resolved thanks to the $^{1}H\{^{31}P\}$ NMR. The phenolate protons in the *para* position of the phosphorus atom are present at 7.20 ppm as a doublet ($^{4}J_{H,H}$ = 2.5 Hz) due to the coupling with the protons *ortho* to the phosphorus, which are present at 6.65 ppm as a doublet of doublets ($^{3}J_{P,H}$ = 12.4 Hz, $^{4}J_{H,H}$ = 2.5 Hz). The α protons of the isopropyl group display at a doublet of septet pattern 2.65 ppm due to the coupling with the six β protons of the isopropyl group and the phosphorus atom ($^{3}J_{H,H}$ = 7.3 Hz, $^{2}J_{P,H}$ = 10.9 Hz). The protons of the ethylene bridge are seen at 2.29 ppm as a triplet due to the coupling with the phosphorus atom ($^{3}J_{P,H}$ = 14.6 Hz) and the protons of the same ethylene bridge ($^{3}J_{H,H}$ = 7.3 Hz). The β protons of the isopropyl group are present at 1.85 ppm and 1.39 ppm as a doublet of doublets due to the coupling with the α protons of the isopropyl group and the phosphorus atom ($^{3}J_{H,H}$ = 7.3 Hz, $^{3}J_{P,H}$ = 14.6 Hz). Finally, the t-butyl substituents at 1.40 ppm and 1.21 ppm as two singlets.

For [Cu(^{iPr}Psalen)] the formation of the complex was considered completed once no signal was observed in the $^{31}P\{^{1}H\}$ NMR spectrum. The ^{1}H NMR spectrum does not provide much information about the structure of the complex (Figure 47). Large signals are present at 10.81, 3.89, 1.88, 1.63 and 1.15 ppm. Only the signals at 10.81 and 1.15 ppm were tentatively assigned to the phenolate protons and one or two t-butyl substituents, respectively. The other signals may correspond to the ethylene bridge and the isopropyl protons. The signal present at 3.89 ppm, being as intense as the others but broader, might correspond to one of the t-butyl substituents.

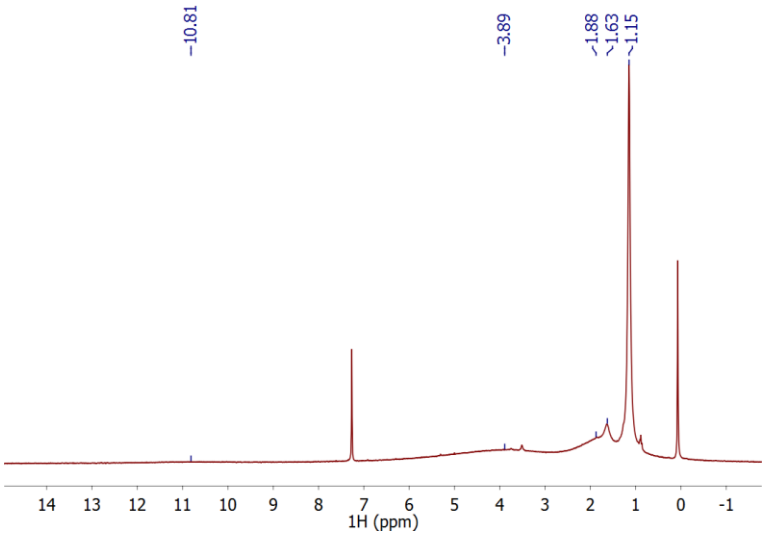

Figure 47. ^{1}H NMR of [Cu(^{iPr}Psalen)] in CD_2Cl_2 at 20 °C. The signal around 0 ppm corresponds to silicon grease.

3.2 EPR spectroscopy

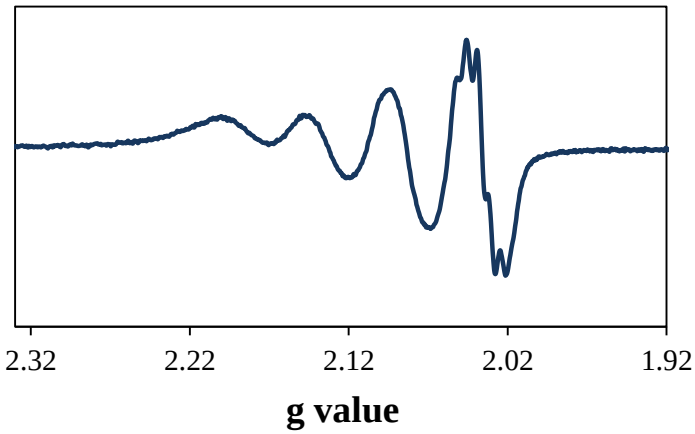

Figure 48. X-band EPR spectrum of [Cu(^{iPr}Psalen)] in dichloromethane at 290 K. Conditions: Frequency: 9.626 GHz; Power: 0.25 mW; modulation frequency: 100 kHz; amplitude: 0.2 mT.

The EPR spectrum of [Cu(^{iPr}Psalen)] at room temperature is characterized by a rhombic signal centered at g = 2.12 which displays a four-line pattern typical of a Cu^{II} center (I = 3/2). A superhyperfine coupling is also present in g_3 and corresponds to the coupling with the two ^{14}N atoms (I = ½). Since this spectrum is very similar to those obtained for copper Psalen^{tBu} and Psalen^{OMe} derivatives, same simulation parameters were considered for [Cu(^{iPr}Psalen)]. Thus, g_1 = 2.122, g_2 = 2.105, g_3 = 2.051, and hyperfine coupling constants of A_{Cu} = 250, 210 and 75 MHz, and superhyperfine constants of A_N = 28, 28, 28 MHz for g_1, g_2 and g_3, respectively. The similarity of this spectrum to those of the previous studied

phosphasalen complexes suggests that the introduction of the isopropyl substituents does not have an important influence on the coordination sphere of the copper center.

3.3 UV-visible spectroscopy

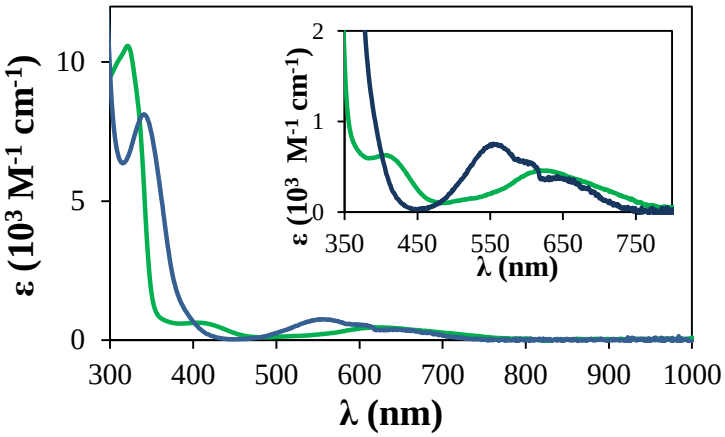

Figure 49. UV-vis spectra of [Ni(^{iPr}Psalen)] (blue line) and [Cu(^{iPr}Psalen)] (green line) in dichloromethane.

The UV-vis spectrum of [Ni(^{iPr}Psalen)] shows three different transitions: an intense band at 340 nm (ε = 8100 M^{-1} cm^{-1}), and two weak transitions at 555 nm (ε = 750 M^{-1} cm^{-1}) and at 645 nm (ε = 380 M^{-1} cm^{-1}). The two latter transitions were also observed for [Ni(Psalen^{OMe})] and [Ni(Psalen^{tBu})] and were attributed to metal to ligand charge transfers (MLCT).[5] The transition at 340 nm is similar to that observed for [Ni(Psalen^{tBu})] (350 nm) but blue-shifted with respect to the one observed for [Ni(Psalen^{OMe})] (370 nm).

The UV-vis spectrum of [Cu(^{iPr}Psalen)] in dichloromethane shows three different absorptions bands: a weak one around 620 nm (ε = 450 M^{-1} cm^{-1}), that can be attributed to a d-d transition, as in the previous cases;[6] another one at 410 nm (ε = 620 M^{-1} cm^{-1}), which is not present in salen derivatives and may be a transfer related to the iminophosphorane functions; and a third one at 320 nm (ε = 10500 M^{-1} cm^{-1}) which may account for a charge transfer.

3.4 X-ray diffraction

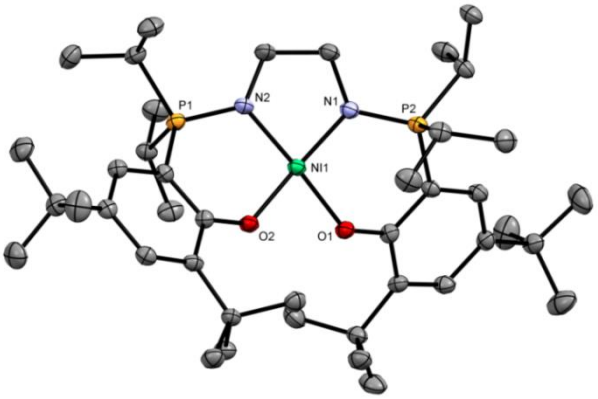

Figure 50. ORTEP of [Ni(^{iPr}Psalen)] with thermal ellipsoids at 50 % probability. Hydrogen atoms have been omitted for clarity.

Purple crystals of [Ni(^{iPr}Psalen)] suitable for X-ray diffraction were obtained by slow diffusion of methanol into a concentrated dichloromethane solution.

[Ni(^{iPr}Psalen)] complex displays a nearly square planar geometry around the nickel center. Coordination bond lengths are similar to those found for [Ni(Psalen^{tBu})] and [Ni(Psalen^{OMe})]: Ni-O bonds measure 1.880(3) and 1.887(2) Å, and Ni-N 1.906(2) and 1.892(2) Å. The torsion angle of the NOON main plane is 8.91 °, intermediate between that of [Ni(Psalen^{tBu})] (6.15 °) and [Ni(Psalen^{OMe})] (11.96 °) complexes. As observed with these complexes, the nickel center displays a tetrahedral distortion from the square planar geometry, where N1 and O2 are present above of the NOON plane while N2 and O1 lay below. P-N bond distances are not fully symmetrical, 1.633(2) and 1.620(2) Å, but are equivalent to those of [Ni(Psalen^{tBu})]. Experimental bond distances and torsion angles are present in Table 13.

	[Ni(^{iPr}Psalen)]	**[Cu(^{iPr}Psalen)]**
M-O1	1.880(2)	1.933(1)
M-O2	1.887(2)	1.917(1)
M-N1	1.906(2)	1.958(1)
M-N2	1.892(2)	1.959(1)
P1-N1	1.633(2)	1.603(2)
P2-N2	1.620(2)	1.601(2)
Torsion angle[a]	8.91	9.44

Table 13. Selected bond distances (Å) and angles (°) for [Ni(^{iPr}Psalen)] and [Cu(^{iPr}Psalen)]. [a] Torsion of the NOON plane.

Green/purple crystals of [Cu(^{iPr}Psalen)] were obtained from a dichloromethane/pentane solution stored in the fridge.

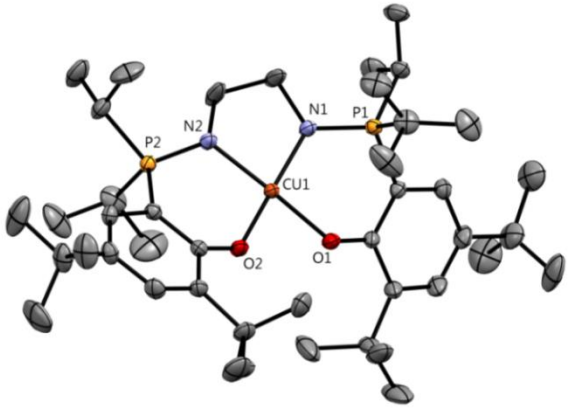

Figure 51. ORTEP of [Cu(^{iPr}Psalen)] with thermal ellipsoids at 50 % probability. Hydrogen atoms have been omitted for clarity.

[Cu(^{iPr}Psalen)] complex also displays a distorted square planar geometry where the Cu-O and Cu-N bond distances are very similar to those of [Cu(Psalen^{tBu})] and [Cu(Psalen^{OMe})] complexes. The isopropyl substitution has no consequence on the P-N bond lengths neither, which are also in the range measured for [Cu(Psalen^{tBu})] and [Cu(Psalen^{OMe})], 1.603(2) and 1.601(2) Å. The only difference between these structures is the distortion from the square planar geometry. [Cu(^{iPr}Psalen)] presents a torsion angle of the main plane of 9.44 °, significantly lower than those observed for [Cu(Psalen^{tBu})] (13.02 °) and [Cu(Psalen^{OMe})] (19.40 °). It is difficult to determine the origin of this difference; it may be due to the difference in steric hindrance between phenyl and isopropyl substituents, or simply related to cell packing parameters (presence of solvent, short contact interactions …).

3.5 Electrochemical studies

The electrochemical properties of these complexes were studied by cyclic voltammetry in dichloromethane solutions. All the potentials are expressed versus the Fc^+/Fc reference couple, which was used as internal reference.

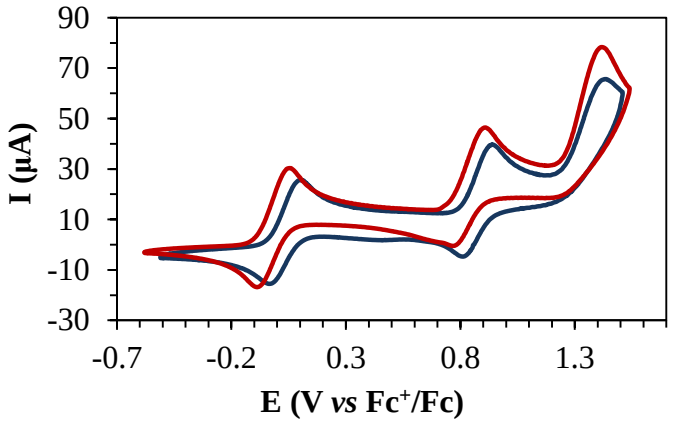

Figure 52. Cyclic voltammograms of [Cu(^{iPr}Psalen)] (blue line) and [Ni(^{iPr}Psalen)] (red line).

[Ni(^{iPr}Psalen)] displays two reversible oxidations at $E^1_{1/2}$ = -0.02 V and $E^2_{1/2}$ = 0.83 V, and an irreversible process at $E^3_{p,a}$ = 1.42 V (Figure 52, red line). The first oxidation occurs at an intermediate potential between that of [Ni(Psalen^{OMe})] ($E^1_{1/2}$ = -0.06 V), and that of [Ni(Psalen^{tBu})] ($E^1_{1/2}$ = 0.01 V). This is due to the better electron-donating properties of the iminophosphorane featuring alkyl substituents. The second oxidation of [Ni(^{iPr}Psalen)] is anodically shifted compared to [Ni(Psalen^{OMe})]. The difference between the first and the second oxidation, ΔE_{1-2} = 0.85 V, is very large in this case and similar to the value obtained for [Ni(Psalen^{tBu})] (ΔE_{1-2} = 0.81 V). As explained in the previous chapter, a large gap between the two oxidations points to a great involvement of the metal in the oxidation process, in this case, the formation of a SOMO with a main metallic character. If we assume a metal-centered oxidation for the first redox process, the second and third oxidation may correspond to an oxidation of the ligand, *i.e.*, the phenolate rings.

Compound	$E^1_{1/2}$	$E^2_{1/2}$	ΔE_{1-2}	$E^3_{p,a}$
[Ni(^{iPr}Psalen)]	-0.02	0.83	0.81	1.42
[Ni(Psalen^{tBu})]	0.01	0.82	0.81	1.24
[Ni(Psalen^{OMe})]	-0.06	0.47	0.53	1.00
[Cu(^{iPr}Psalen)]	0.03	0.84	0.81	1.42
[Cu(Psalen^{tBu})]	0.10	0.95	0.85	-
[Cu(Psalen^{OMe})]	0.04	0.54	0.50	-

Table 14. Redox potentials for copper and nickel phosphasalen complexes, expressed in V *vs* Fc^+/Fc.

As observed it the Psalen^{tBu} and Psalen^{OMe} series, the cyclic voltammogram of [Cu(^{iPr}Psalen)] is analogous to that of the nickel derivative, suggesting a similar electronic structure of the oxidized species (Figure 52, blue line). A first reversible oxidation is present at $E^1_{1/2}$ = 0.03 V, similar to that of [Cu(Psalen^{OMe})] ($E^1_{1/2}$ = 0.04 V) and lower than that found for [Cu(Psalen^{tBu})] ($E^1_{1/2}$ = 0.10 V). The second redox process takes place at $E^2_{1/2}$

= 0.84 V, showing also a large gap between the two oxidations of $\Delta E_{1\text{-}2}$ = 0.81 V, suggesting a metal-centered oxidation also for [Cu(^{iPr}Psalen)]. A third irreversible oxidation, which was not observed for [Cu(Psalen^{tBu})] and [Cu(Psalen^{OMe})], is also present at $E^3_{p,a}$ = 1.42 V, and may also correspond to a second oxidation of the ligand. Table 14 includes all the redox potentials obtained for the three series of phosphasalen complexes.

4. Oxidation of neutral complexes

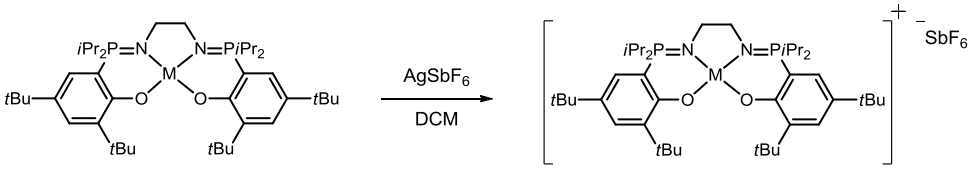

M = Ni, [Ni(^{iPr}Psalen)]$^+$SbF$_6^-$, 86 %
M = Cu, [Cu(^{iPr}Psalen)]$^+$SbF$_6^-$, 83 %

Scheme 52. Chemical oxidation of [Ni(^{iPr}Psalen)] and [Cu(^{iPr}Psalen)] complexes.

As in the case of [M(Psalen^{tBu})] and [M(Psalen^{OMe})], [M(^{iPr}Psalen)] complexes could be readily oxidized using silver salts in dichloromethane solutions. Addition of $AgSbF_6$ to a solution of the neutral complexes, induces an immediate color change from purple to dark brown in the case of [Ni(^{iPr}Psalen)]$^+$, and from green to deep purple for [Cu(^{iPr}Psalen)]$^+$. The solution of [Ni(^{iPr}Psalen)]$^+$ was evaporated and the residue dissolved in the minimum amount of THF. A dark solid was precipitated by addition of petroleum ether. The solution of [Cu(^{iPr}Psalen)]$^+$ was concentrated and a purple precipitate was obtained by addition of petroleum ether. The powders were washed with petroleum ether and dried under vacuum to yield [Ni(^{iPr}Psalen)]$^+$SbF$_6^-$ (86 %), and [Cu(^{iPr}Psalen)]$^+$SbF$_6^-$ (83 %).

5. Characterization of the oxidized complexes

5.1 NMR spectroscopy

The ^{1}H NMR spectrum of [Ni(^{iPr}Psalen)]$^+$ at room temperature evidences the paramagnetic nature of the complex (Figure 53). It displays broad signals between 2 and 21 ppm, as observed for [Ni(Psalen^{tBu})]$^+$ and [Ni(Psalen^{OMe})]$^+$ (see Chapter 2, section 5.1). These signals were tentatively assigned thanks to their integrated areas: signals at 2.27 and 3.96 ppm correspond to the t-butyl groups; at 4.76 and 4.37 ppm the β protons of the isopropyl

groups; and at 20.65 and 14.50 ppm the resonances of the aromatic protons. The signals for the ethylene bridge and the α protons of the isopropyl substituents were not observed. These signals may be too broad to emerge from the baseline or they could be superimposed with other signals such as those at 4.76 and 4.37 ppm, where a shoulder is observed at 4.59 ppm between the two signals. The paramagnetic isotropic shift for these signals ($\delta^{para} = \delta^{obs} - \delta^{dia}$) is 0.87 and 2.75 ppm for the t-butyl groups, 2.98 and 2.92 ppm for the β protons, and 14.02 and 7.3 ppm for the aromatic protons. These δ^{para} are slightly higher than those measured for [Ni(Psalen^{tBu})]$^+$: 1.14 and 1.81 ppm for the t-butyl protons, and 11.89 and 9.18 ppm for the aromatic protons, while the phenyl phosphine protons do not experience a significant variation. In [Ni(^{iPr}Psalen)]$^+$ the t-butyl and the phosphine protons experience larger δ^{para} compared to [Ni(Psalen^{tBu})]$^+$.

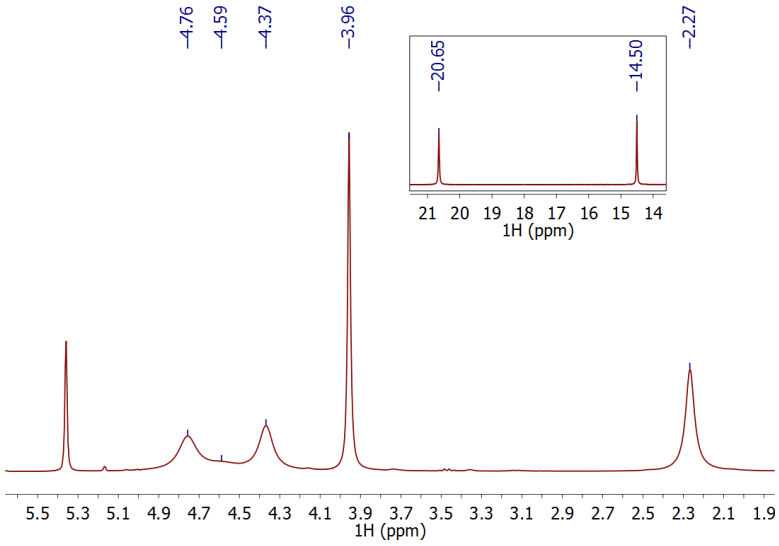

Figure 53. ^{1}H NMR spectrum of [Ni(^{iPr}Psalen)]$^+$ in CD_2Cl_2 at 20 °C. Inset shows a zoom of the low field signals.

An important difference between this spectrum and that obtained for [Ni(Psalen^{OMe})]$^+$ is the shift experienced by the phosphorus substituents. In [Ni(Psalen^{OMe})]$^+$, the chemical shifts of the phenyl phosphine substituents do not change much from those observed for the neutral complex. However, for [Ni(^{iPr}Psalen)]$^+$ the isopropyl protons shift by about 3 ppm with respect to the neutral complex, suggesting that the iminophosphorane functions may be involved in the delocalization of the generated electronic hole.

When considering the evolution of the chemical shifts of [Ni(^{iPr}Psalen)]$^+$ with temperature, all the signals in the oxidized complex, except the t-butyl resonance at 2.27 ppm, experienced an important temperature-dependent shift (Figure 54). This variation is

linear with the temperature as expected for paramagnetic compounds following the Curie law (Figure 55).

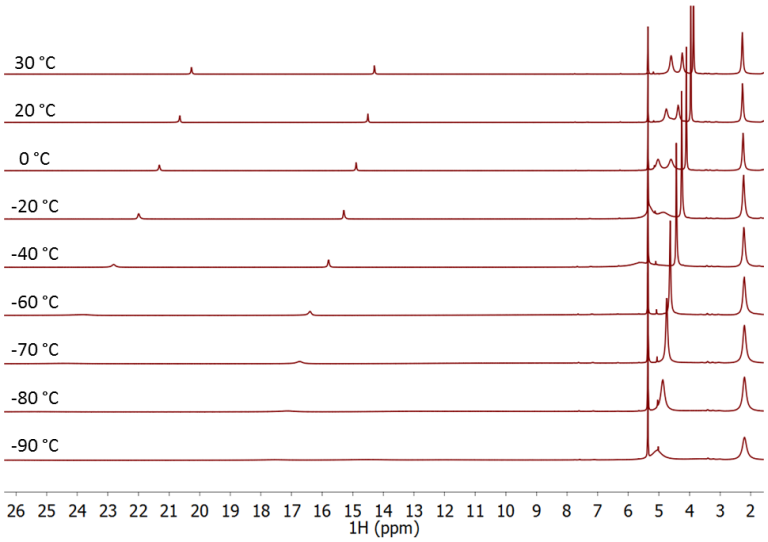

Figure 54. ^{1}H NMR spectra of [Ni(^{iPr}Psalen)]$^{+}$ in CD_2Cl_2 registered at different temperatures.

The largest variations were observed for the aromatic protons which shift from 14.29 ppm at 30 °C to 17.52 ppm at -90 °C (Δδ = 3.23 ppm), and from 20.27 ppm to 26.11 ppm (Δδ = 5.84 ppm). The t-butyl protons observed at 3.96 ppm at room temperature shift only by 1.09 ppm. These variations are rather small compared to those observed for [Ni(Psalen^{OMe})]$^{+}$ and [Ni(Psalen^{tBu})]$^{+}$ for which the aromatic signals shifted by 9 and 6 ppm for the former, and 12.2 and 8.43 ppm for the latter, suggesting a weaker participation of the aromatic cycle in the delocalization of the radical.

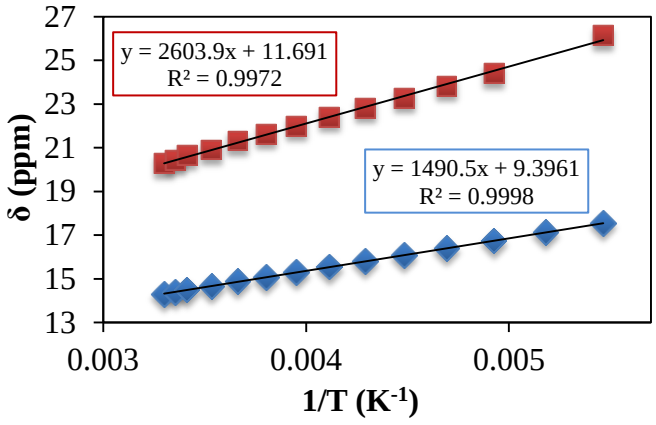

Figure 55. Plot of the chemical shifts of the phenoxide protons with the inverse of the temperature for compound [Ni(^{iPr}Psalen)]$^{+}$.

Most of the signals broaden until almost disappearing at -90 °C, while new signals appear at -19.66 and -2.29 ppm, and may correspond to the protons not observed at room

temperature: the ethylene bridge protons or the α protons of the isopropyl group (Figure 56).

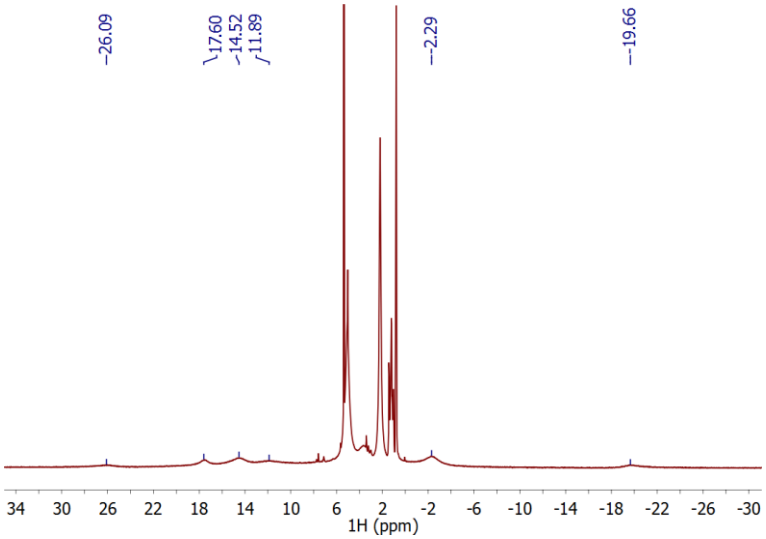

Figure 56. ^{1}H NMR spectrum of [Ni(^{iPr}Psalen)]$^{+}$ in CD_2Cl_2 at -90 °C.

The effective magnetic moment of [Ni(^{iPr}Psalen)]$^{+}$ was measured in solution using the Evans' method[7] throughout the temperature range studied and it was found almost constant with an average value of 1.90 μ_B, which corresponds to a g value of 2.19. This value is higher than the spin-only value (1.73 μ_B) evidencing a metallic contribution to the SOMO, so that a partial oxidation of the metal. [8]

The $^{31}P\{^{1}H\}$ NMR spectrum of [Cu(^{iPr}Psalen)]$^{+}$ shows a sharp signal at 65.38 ppm. The ^{1}H NMR spectrum of [Cu(^{iPr}Psalen)]$^{+}$ changes a lot when compared to the neutral one.

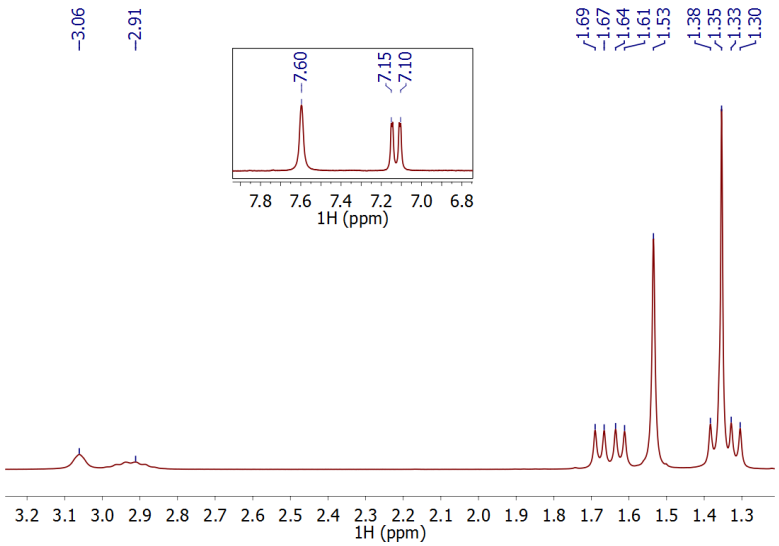

Figure 57. ^{1}H NMR of [Cu(^{iPr}Psalen)]$^{+}$ in CD_2Cl_2 at 20 °C. Inset shows a zoom of the aromatic region.

This spectrum is nicely defined suggesting a metal-centered oxidation leading to a diamagnetic Cu^{III} $3d^8$ complex. Figure 57 shows the ^1H NMR of $[Cu(^{iPr}Psalen)]^+$ where all the signals were assigned: the protons of the phenolate ring at 7.60 and 7.13 ppm, the latter couples with the phosphorus atom and the proton in *meta* position ($^3J_{P,H}$ = 12.0 Hz, $^4J_{H,H}$ = 2.0 Hz); at 3.06 ppm the ethylene bridge protons as a large singlet; the α protons of the isopropyl group at 2.92 ppm which displays a doublet of septet pattern due to the coupling with the phosphorus atom (whose coupling constant could not be determined) and the six β protons of the isopropyl group ($^3J_{H,H}$ = 7.2 Hz); at 1.65 and 1.34 ppm the β protons which are present in two set of signals as a doublet of doublets due the coupling with the α protons of the isopropyl group ($^3J_{H,H}$ = 7.2 Hz) and the phosphorus atom ($^3J_{P,H}$ = 16.4 Hz); and at 1.53 and 1.35 ppm the t-butyl groups as two singlets. The β protons, while being chemically equivalent, appear as two different signals. This may be due to the relative positions of each isopropyl group on the same phosphorus atom with respect to the center of the molecule. In the X-ray structure of $[Cu(^{iPr}Psalen)]^+$ (vide infra) one of the isopropyl groups is pointing towards the outside of the molecule while the other remains on the plane of the molecule. This may influence the resonance of these protons leading to their differentiation into two signals.

When comparing this spectrum with the one obtained for $[Ni(^{iPr}Psalen)]$ (also a $3d^8$ complex), the shift of certain signals is noticed. The signal corresponding to the ethylene bridge is down-field shifted in $[Cu(^{iPr}Psalen)]^+$ (3.06 ppm) compared to $[Ni(^{iPr}Psalen)]$ (2.29 ppm). One of the t-butyl protons is as well down-field shifted: 1.35 ppm in $[Cu(^{iPr}Psalen)]^+$, while 1.53 ppm in $[Ni(^{iPr}Psalen)]$. Contrarily, one of the signals corresponding to the β protons is up-field shifted for $[Cu(^{iPr}Psalen)]^+$ (1.65 ppm) compared to $[Ni(^{iPr}Psalen)]$ (1.85 ppm). This suggests a change in the electronics of these groups in $[Cu(^{iPr}Psalen)]^+$.

An apparent diamagnetic spectrum at room temperature does not ensure the presence of a Cu^{III} $3d^8$ configuration as observed for $[Cu(Psalen^{OMe})]^+$, which was found to be an antiferromagnetically coupled Cu^{II} radical complex. Thus, ^{31}P and ^1H spectra were recorded at different temperatures (Figure 58).

The ^1H NMR spectrum of $[Cu(^{iPr}Psalen)]^+$ in dichloromethane solution was studied in the -90 to 30 °C temperature range and no significant change was observed (Figure 58). The signals shift by a maximum of 0.20 ppm, which is rather small compared to what usually observed for paramagnetic complexes. The main change concerns the signals corresponding to the bridge and the α protons of the isopropyl group. Ethylene protons

appear as two broad singlets at 3.33 and 2.52 ppm at -90 °C due to the rigid structure at low temperature (Figure 58, green stars), as observed for [Cu(Psalen^{tBu})]$^+$. The α isopropyl protons seem to split also into two broad singlets at 2.94 and 2.82 ppm, which is explained by more difficult rotation around the P-C bond (Figure 58, red stars). The aromatic protons shift only by 0.13 ppm. A remarkable feature of these spectra is the better definition of the signal at 7.60 ppm, displaying a sharper shape at low temperatures. The same feature was observed in the VT-NMR spectra of [Cu(Psalen^{OMe})]$^+$ for the methoxy protons, without apparent explanation. The ^{31}P resonance does not experience a significant variation along this temperature range.

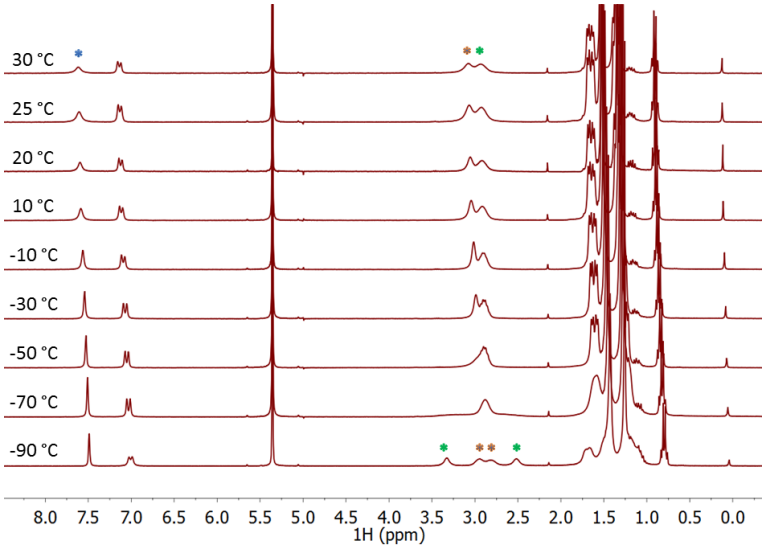

Figure 58. ^{1}H NMR spectra of [Cu(^{iPr}Psalen)]$^+$ in CD_2Cl_2 registered at different temperatures.

Assuming the formation of a Cu^{III} 3d^8 complex, the chemical shifts observed differ slightly from those of the isoelectronic complex [Ni(^{iPr}Psalen)] (discussed above). Comparing both species in the same solvent, we find that [Cu(^{iPr}Psalen)]$^+$ displays isotropic shifts (δ^{iso}) at room temperature ranging from 0.08 to 0.75 ppm, the one corresponding to the ethylene protons being the largest one, and that of the t-butyl protons the smallest one.

The effective magnetic moment (μ_{eff}) of the complex was measured at room temperature using the Evans' method[7] and a value of 0.66 μ_B was obtained, which corresponds to 0.2 unpaired electrons. This implies a certain paramagnetic nature of the complex that was not expected from the NMR spectra obtained. Three different explanations can be proposed: an equilibrium with the triplet form may exist in solution, if the d_{x2-y2} orbital is energetically accessible; the presence of a small amount of Cu^{II} radical ligand species leading to a valence tautomerism or multiconfigurational ground state, which could explain the isotropic shifts observed and the change on the shape of the aromatic signal

with the temperature; or an error in the measurement since this method is not very accurate.

5.2 EPR spectroscopy

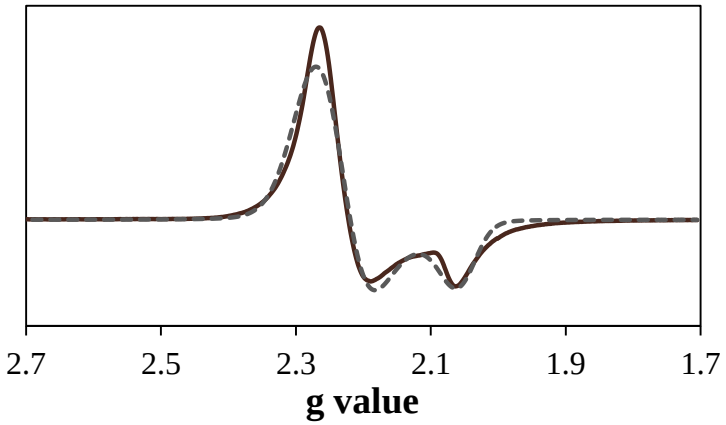

Figure 59. X-band EPR spectrum of [Ni(^{iPr}Psalen)]$^+$ in dichloromethane at 10 K. Conditions: Frequency: 9.634 GHz; Power: 2.00 mW; modulation frequency: 100 kHz; amplitude: 0.4 mT.

At 10 K the solution EPR spectrum (Figure 59) of [Ni(^{iPr}Psalen)]$^+$ is characterized by an axial signal centered at g = 2.19 with spin S =1/2, characteristic for a Ni^{III} center in a square planar geometry.[9] This signal disappears when increasing the temperature to 100 K and no other signal is observed above this temperature. The symmetry of the signal contrasts with the one obtained for [Ni(Psalen^{OMe})]$^+$ and [Ni(Psalen^{tBu})]$^+$, both having a rhombic symmetry. From the simulation we obtained the following parameters: $g_\perp$ = 2.249 and $g_\parallel$ = 2.061. The obtained g_{av} = 2.19 is the same as for [Ni(Psalen^{tBu})]$^+$ but larger than [Ni(Psalen^{OMe})]$^+$ (g_{av} = 2.14), suggesting that the SOMO of the complex possesses similar metal character as [Ni(Psalen^{tBu})]$^+$, *i.e.*, a mainly Ni^{III} configuration. The g_{av} obtained by EPR corresponds to the one obtained by the Evans' method. Contrary to [Ni(Psalen^{tBu})]$^+$, the axial symmetry of the signal indicates that the distortion from the square planar geometry is not significant in solution, hereby $g_x = g_y \gg g_z$. This is contradictory since both complexes display similar structural parameters as observed in the X-ray structures (see section5.5.4); notably the torsion of the main plane is 11.90 ° for [Ni(^{iPr}Psalen)]$^+$ and 11.47 ° for [Ni(Psalen^{tBu})]$^+$. Therefore, a different flexibility of the complexes in solution is likely. [Ni(^{iPr}Psalen)]$^+$ presenting less bulky substituents on the phosphorus atom might adopt a more planar structure than [Ni(Psalen^{tBu})]$^+$, because of a stereo-electronic repulsion between the phenyl substituents.

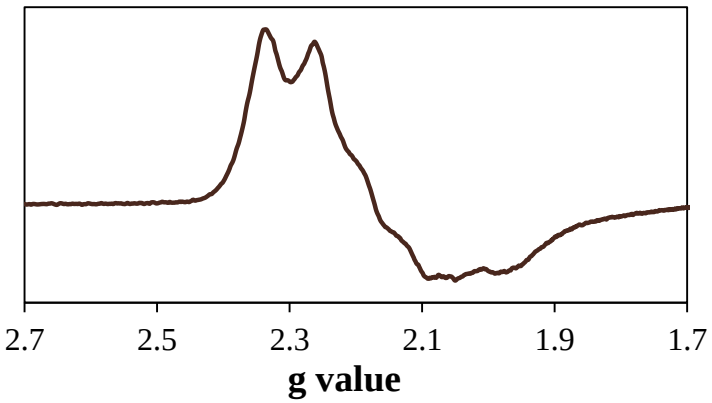

Figure 60. X-band EPR spectrum of [Ni(^{iPr}Psalen)]$^{+}$SbF$_6^{-}$ in the solid state at 10 K. Conditions: Frequency: 9.637 GHz; Power: 0.63 mW; modulation frequency: 100 kHz; amplitude: 0.4 mT.

Figure 60 shows the EPR spectrum for a solid sample recorded at 10 K. It displays a rhombic signal centered at g = 2.13, very different from the one obtained for the dichloromethane solution. The geometry of the observed signal is this time in agreement with the distortion from planarity seen in the X-ray structure. No hyperfine couplings with the ^{14}N or ^{31}P atoms were observed. The g values drawn from the experimental spectrum are g_1 = 2.34, g_2 = 2.18, g_3 = 1.98 (g_{av} = 2.17), very similar to those found for [Ni(Psalen^{tBu})]$^{+}$SbF$_6^{-}$ in the solid state, g_1 = 2.327, g_2 = 2.174, g_3 = 1.988. This is not surprising since both display similar structural parameters (discussed below).

Both EPR spectra in solution and in the solid state point to the formation of a high-valent Ni^{III} species upon oxidation.

The EPR spectrum of [Cu(^{iPr}Psalen)]$^{+}$SbF$_6^{-}$ was silent at both 10 and 150 K suggesting a diamagnetic compound.

5.3 UV-visible spectroscopy

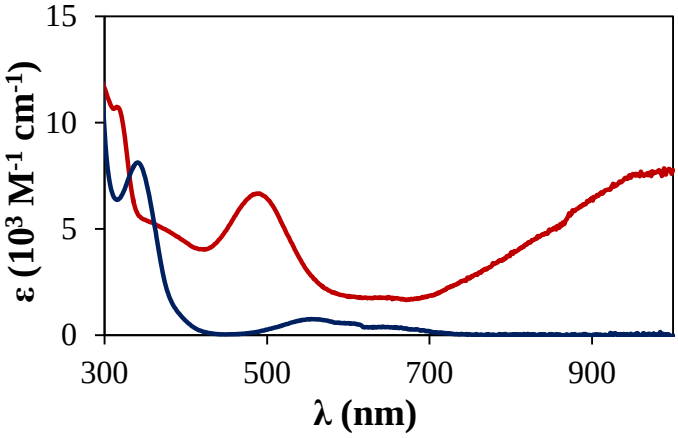

Figure 61. UV-vis spectra of [Ni(^{iPr}Psalen)] (blue line)and [Ni(^{iPr}Psalen)]$^{+}$ (red line)in dichloromethane.

The absorption spectrum of [Ni(^{iPr}Psalen)] changes significantly upon oxidation. [Ni(^{iPr}Psalen)]$^{+}$ displays intense bands at 490 nm (ε = 6700 M^{-1} cm^{-1}) and around 1000 nm (ε = 7600 M^{-1} cm^{-1}, Figure 61, red line). A shoulder is also observed at 362 nm (ε = 5000 M^{-1} cm^{-1}). This spectrum is very similar to those recorded for the other nickel phosphasalen derivatives. The intensity of the bands at 490 and 1000 nm is close to that measured for [Ni(Psalen^{tBu})], with ε ≥ 5000 M^{-1} cm^{-1}, larger than that of the methoxy derivative where ε ≤ 3600 M^{-1} cm^{-1}.

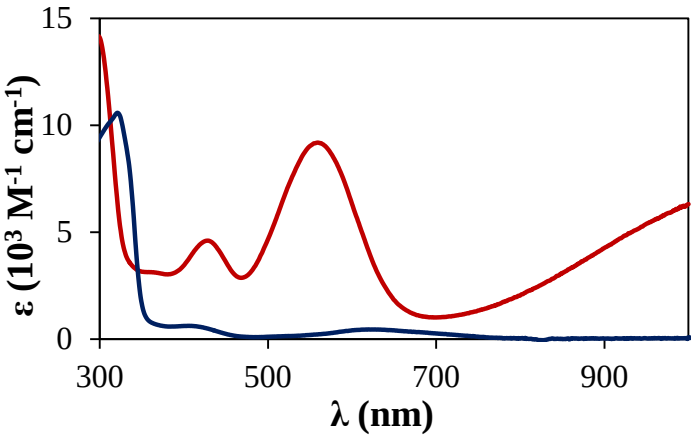

Figure 62. UV-vis spectra of [Cu(^{iPr}Psalen)] (blue line) and [Cu(^{iPr}Psalen)]$^{+}$ (red line) in dichloromethane.

The spectrum of [Cu(^{iPr}Psalen)]$^{+}$ (Figure 62, red line) exhibits two intense bands at 555 nm (ε = 9200 cm^{-1} M^{-1}) and at 425 nm (ε = 4600 cm^{-1} M^{-1}). An intense band also appears in the NIR region (ε = 6300 cm^{-1} M^{-1}). This spectrum was also registered in THF and no

change was observed suggesting no significant interaction between the complex and the solvent.

These spectra are very similar to those of Psalen^{tBu} and Psalen^{OMe} derivatives, suggesting similar electronic structure.

5.4 X-ray diffraction

Dark crystals of [Ni(^{iPr}Psalen)]$^{+}$$SbF_6^-$ suitable for X-ray diffraction were obtained by slow diffusion of petroleum ether into a concentrated dichloromethane solution (Figure 63).

In [Ni(^{iPr}Psalen)]$^{+}$$SbF_6^-$ the torsion of the main plane increased from 8.91 ° to 11.90 ° upon oxidation. This value is similar than that found for [Ni(Psalen^{OMe})]$^{+}$$SbF_6^-$ and [Ni(Psalen^{tBu})]$^{+}$$SbF_6^-$ which experienced a torsion of the main plane of 11.96 and 11.47 °, respectively. Upon oxidation there is a contraction of the coordination sphere where the Ni-O bond shortened by 0.018 and 0.050 Å, and the Ni-N lengths by 0.061 and 0.028 Å.

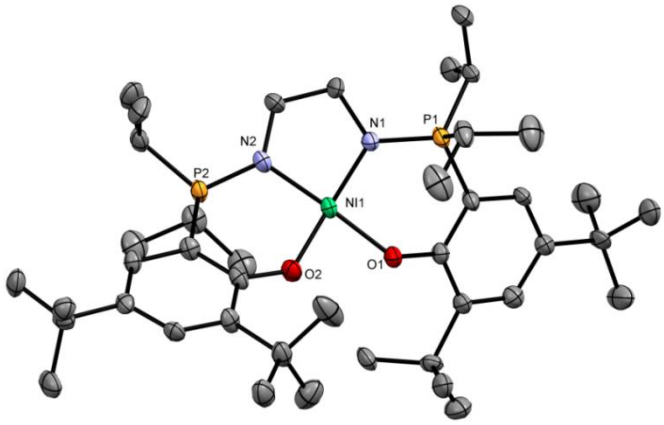

Figure 63. ORTEP of [Ni(^{iPr}Psalen)]$^{+}$$SbF_6^-$ with thermal ellipsoids at 50 % probability. Hydrogen atoms and a molecule of SbF_6^- have been omitted for clarity.

This non-symmetrical contraction, being more pronounced for Ni-O2 and Ni-N1, leads to the formation of a long axis along the N2-Ni-O1 segment. This feature was also found in the case of [Ni(Psalen^{OMe})]$^{+}$$SbF_6^-$ and [Ni(Psalen^{tBu})]$^{+}$$SbF_6^-$ complexes. As a consequence of the shift of the electronic density from the N towards the metal, the P-N bonds are elongated by 0.12 and 0.14 Å. This variation is smaller than that observed for other phosphasalen analogues studied. The bond distances in the phenoxide rings do not experience important variations upon oxidation, ruling out the possibility of a localized phenoxyl radical.[10]

The variations observed upon oxidation, being similar to those found for [Ni(Psalen^{tBu})]$^{+}$SbF$_6^{-}$, point to a metal-centered oxidation.

	[Ni(^{iPr}Psalen)]	[Ni(^{iPr}Psalen)]$^{+}$SbF$_6^{-}$	Δ
Ni-O1	1.880(2)	1.862(4)	-0.018
Ni-O2	1.887(2)	1.837(4)	-0.050
Ni-N1	1.906(2)	1.845(5)	-0.061
Ni-N2	1.892(2)	1.864(5)	-0.028
P1-N1	1.633(2)	1.645(5)	0.012
P2-N2	1.620(2)	1.634(5)	0.014
Torsion angle[a]	8.91	11.90	2.99

Table 15. Selected bond distances (Å) and angles (°) for [Ni(^{iPr}Psalen)] and [Ni(^{iPr}Psalen)]$^{+}$SbF$_6^{-}$. [a] Torsion of the NOON plane.

Deep purple crystals of [Cu(^{iPr}Psalen)]$^{+}$SbF$_6^{-}$ suitable for X-ray diffraction were obtained from a concentrated benzene solution.

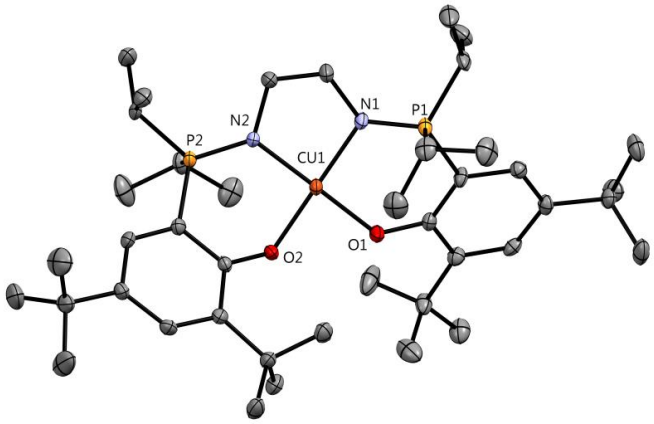

Figure 64. ORTEP of [Cu(^{iPr}Psalen)]$^{+}$SbF$_6^{-}$ with thermal ellipsoids at 50 % probability. Hydrogen atoms and a molecule of SbF$_6^{-}$ have been omitted for clarity.

Upon oxidation [Cu(^{iPr}Psalen)]$^{+}$SbF$_6^{-}$ experiences an important contraction around the metal center: Cu-N bonds shorten by 0.058 and 0.068 Å, while the Cu-O bonds shorten by 0.071 and 0.036 Å. This contraction is more important than that experienced by [Cu(Psalen^{tBu})]$^{+}$SbF$_6^{-}$ (Δd = 0.050-0.060 Å) and evidences the oxidation of the metal center. This structure turns out not to be as planar as [Cu(Psalen^{tBu})]$^{+}$SbF$_6^{-}$ and [Cu(Psalen^{OMe})]$^{+}$SbF$_6^{-}$, and presents a small torsion of the NOON plane, 2.20 °. Due to the better donation of the nitrogen lone pairs towards the metal, the P-N are elongated by 0.039 and 0.048 Å.

	[Cu(^{iPr}Psalen)]	[Cu(^{iPr}Psalen)]$^{+}$SbF$_6^{-}$	Δ
Cu-O1	1.933(1)	1.862(2)	-0.071
Cu-O2	1.917(1)	1.881(2)	-0.036
Cu-N1	1.958(1)	1.900(3)	-0.058
Cu-N2	1.959(1)	1.891(3)	-0.068
P1-N1	1.603(2)	1.642(5)	0.039
P2-N2	1.601(2)	1.649(5)	0.048
Torsion angle[a]	9.44	2.20	-7.24

Table 16. Selected bond distances (Å) and angles (°) for [Cu(^{iPr}Psalen)] and [Cu(^{iPr}Psalen)]$^{+}$SbF$_6^{-}$. [a] Torsion of the NOON plane.

5.5 Magnetic measurements

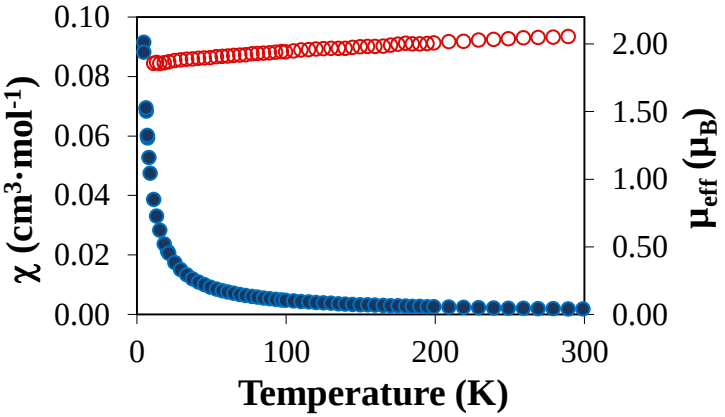

Figure 65. Plot of magnetic susceptibility (blue circles) and effective magnetic moment (red circles) *vs.* temperature for [Ni(^{iPr}Psalen)]$^{+}$SbF$_6^{-}$.

The magnetic properties of [Ni(^{iPr}Psalen)]$^{+}$SbF$_6^{-}$ were also studied in the solid state using a SQUID magnetometer. The complex follows the Curie law as expected for a paramagnetic compound. The χT value measured at 300 K is 0.537 cm^3 K mol^{-1} and the average magnetic moment is 1.95 μ_B. The calculated g_{iso} value is 2.25, higher than the one found for [Ni(Psalen^{tBu})]$^{+}$SbF$_6^{-}$, g_{iso} = 2.22. The metal contribution is higher compared to the methoxy derivative which exhibited a g_{iso} = 2.16. The higher g_{iso} value obtained for [Ni(^{iPr}Psalen)]$^{+}$SbF$_6^{-}$ indicates a SOMO with a stronger metal character, *i.e.*, the Ni^{III} 3d^7 must be the predominant configuration and is present in a higher extent than in [Ni(Psalen^{OMe})]$^{+}$SbF$_6^{-}$ and [Ni(Psalen^{tBu})]$^{+}$SbF$_6^{-}$ species.

6. Conclusion

[Ni(^{iPr}Psalen)] and [Cu(^{iPr}Psalen)] and their one-electron oxidized products were characterized using different spectroscopies in addition of cyclic voltammetry, X-ray

diffraction and magnetic measurements. The introduction of alkyl substituents on the phosphorus atom increases the electron-donating abilities of the iminophosphorane function, favoring a metal-centered oxidation in both copper and nickel complexes. EPR and magnetic measurements suggest that $[Ni(^{iPr}Psalen)]^{+}SbF_6^{-}$ possesses an electronic structure similar to that of $[Ni(Psalen^{tBu})]^{+}SbF_6^{-}$ in solution and in the solid state, but presenting a larger metal-character of the SOMO. The diamagnetic ^{1}H NMR spectrum and the X-ray structure of $[Cu(Psalen^{iPr})]^{+}$ are in agreement with the formation of a square planar Cu^{III} $3d^8$ complex in solution and in the solid state. SQUID measurements on crystals could not be conducted because of the higher solubility of this complex, precluding obtaining a reasonable amount of single crystals. The oxidized products of $[Ni(^{iPr}Psalen)]$ and $[Cu(^{iPr}Psalen)]$ can be described as high-valent Ni^{III} and Cu^{III} complexes. Thus, phosphasalen ligands belong to the few examples of salen-type systems able to stabilize these high-valent metal centers. The study of $[M(^{iPr}Psalen)]$ and $[M(^{iPr}Psalen)]^{+}SbF_6^{-}$ complexes remains incomplete since multi-referential calculations must be performed leading to a detailed description of the electronic structure.

This ligand has been proven to be more electron-donating than $Psalen^{tBu}$ and less redox-active than $Psalen^{OMe}$. The stabilization of other high-valent metal centers, such as iron or manganese, should be investigated.

7. References

[1] R. C. Pratt, C. T. Lyons, E. C. Wasinger, T. D. P. Stack, *J. Am. Chem. Soc.* **2012**, *134*, 7367-7377.

[2] O. Rotthaus, F. Thomas, O. Jarjayes, C. Philouze, E. Saint-Aman, J.-L. Pierre, *Chem. Eur. J.* **2006**, *12*, 6953-6962.

[3] O. Rotthaus, O. Jarjayes, F. Thomas, C. Philouze, C. Perez Del Valle, E. Saint-Aman, J.-L. Pierre, *Chem. Eur. J.* **2006**, *12*, 2293-2302.

[4] T. P. A. Cao, S. Labouille, A. Auffrant, Y. Jean, X. F. Le Goff, P. Le Floch, *Dalton Trans.* **2011**, *40*, 10029-10037.

[5] T. P. A. Cao, G. Nocton, L. Ricard, X. F. Le Goff, A. Auffrant, *Angew. Chem. Int. Ed.* **2014**, *53*, 1368-1372.

[6] T. Storr, P. Verma, R. C. Pratt, E. C. Wasinger, Y. Shimazaki, T. D. P. Stack, *J. Am. Chem. Soc.* **2008**, *130*, 15448-15459.

[7] J. L. Deutsch, S. M. Poling, *J.Chem. Ed.* **1969**, *46*, 167-168.

[8] a) Y. Shimazaki, T. Yajima, T. Shiraiwa, O. Yamauchi, *Inorganica Chim. Acta* **2009**, *362*, 2467-2474; b) P. Bertrand, *La spectroscopie de résonance paramagnétique électronique : fondements*, EDP sciences, Les Ulis, **2014**.

[9] a) Z. Xiao, B. O. Patrick, D. Dolphin, *Inorg. Chem.* **2003**, *42*, 8125-8127; b) D. Pinho, P. Gomes, C. Freire, B. de Castro, *Eur. J. Inorg. Chem.* **2001**, *2001*, 1483-1493.

[10] M. Orio, O. Jarjayes, H. Kanso, C. Philouze, F. Neese, F. Thomas, *Angew. Chem.-Int. Edit.* **2010**, *49*, 4989-4992.

Chapter 4: Influence of the N,N-linker in Ni and Cu phosphasalophen complexes

I. Introduction

The last chapters focused on the influence of the phenolate and phosphorus substituents on the electronic structure of nickel and copper complexes. In this chapter, we focus on the nature of the linker between the two iminophosphorane moieties; the ethylene linker of the Psalen^{tBu} ligand was substituted by a phenylene linker, leading to the phosphasalophen ligand (Psalophen). This substitution has an impact not only on the electronics of the ligand but also on the geometrical properties, since it confers a greater rigidity to the ligand backbone. Additionally, the phenylene bridge is a redox-active unit allowing larger delocalization on the ligand.

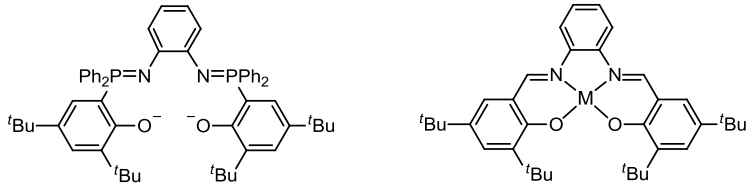

Psalophen

M = Ni, [Ni(salophen)]
M = Cu, [Cu(salophen)]

Scheme 53. Psalophen ligand (left) and nickel and copper salophen complexes (right).[1]

In salen chemistry, ligands featuring phenylene linkers, known as salophen ligands, have been widely investigated.[2] For salophen complexes, different electronic structures were described upon oxidation depending on the substituents present on the aromatic rings: a phenoxyl radical complex if the oxidation occurs on the phenoxide ring (Scheme 54, left), an *o*-diaminobenzene radical if the oxidation of the central ring is favored (Scheme 54, right), or a fully delocalized radical ligand complex.[2a,3]

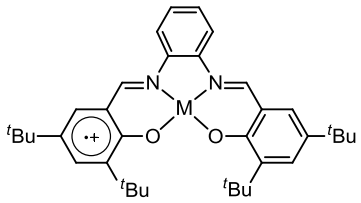

phenoxyl radical

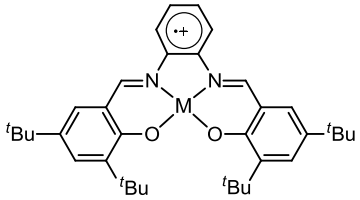

o-diaminobenzene radical

Scheme 54. Structures of phenoxyl and *o*-diaminobenzene radicals.

The synthesis and characterization of oxidized copper and nickel salophen complexes (Scheme 53) have been reported by the groups of J-L. Pierre and F. Thomas.[4] [Ni(salophen)] possesses oxidation potentials at $E^1_{1/2}$ = 0.58 V and $E^2_{1/2}$ = 0.80 V, higher values than those found for the alkyl-linked derivative [NiSal] ($E^1_{1/2}$ = 0.33 V and $E^2_{1/2}$ = 0.73 V). The gap between the first and the second oxidation is significantly different for both complexes, 0.22 V for [Ni(salophen)] while it is 0.40 V for [NiSal], which was attributed to a higher contribution of the metal orbitals in the electronic structure of the latter. The EPR spectrum of [Ni(salophen)] shows an isotropic signal at g_{iso} = 2.034 at room temperature which was assigned to phenoxyl species being slightly delocalized in metal orbitals. When decreasing the temperature below the melting point of the solvent, in this case dichloromethane, a rhombic signal was observed characterized by g_1 = 2.075, g_2 = 2.016 and g_3 = 1.991. [Ni(salophen)] was therefore described as a delocalized phenoxyl radical with a small contribution of the metal to the SOMO (6.6 %). However, the X-ray structure of $[Ni(salophen)]^+SbF_6^-$,[4b] recently resolved, does not show any changes in the bond lengths of the central ring, ruling out the possibility of an oxidation centered on the bridge. The coordination sphere, essentially symmetric, contracts slightly upon oxidation. A quinoid pattern, less pronounced than in other salen phenoxyl complexes, was observed in one of the phenoxide rings. Finally, $[Ni(salophen)]^+$ was described as a border line class II/III mixed-valence complex, according to the Robin and Day classification.[5]

[Cu(salophen)] present similar redox potentials to its nickel analogue, $E^1_{1/2}$ = 0.56 V and $E^2_{1/2}$ = 0.73 V. [2b] The EPR spectra of the oxidized complex turned out to be silent at both 100 and 4 K. This is consistent with a triplet state (S = 1) resulting from a ferromagnetic coupling between the electron of the copper center and that of the radical. $[Cu(salophen)]^+$ was described in solution as a fully delocalized radical ligand complex.[2b] However, the X-ray structure evidenced a localized radical complex in one side of the molecule.[2b]

The electronics of the central ring can be easily modified by the introduction of electron-withdrawing or electron-donating substituents, leading to either electron-richer or poorer

linkers. This influences the delocalization of the generated radical. Thus, nickel and copper salophen complexes featuring two methoxy substituents on the central ring ([M(Salophen^{OMe2})]) have been studied by Y. Shimazaki, F. Thomas, and M. Orio et coll. (Scheme 55, left).[3a,4a]

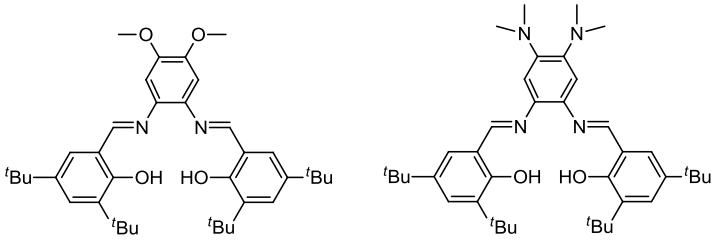

Scheme 55. Salophen^{OMe2} (left) and Salophen^{NMe2} (right) ligands.[3a,6]

Electrochemical, spectroscopic and theoretical studies of [Ni(Salophen^{OMe2})]$^+$ point to the formation of a phenoxyl radical cation upon oxidation; nevertheless the metal orbitals contribute slightly into the delocalization of the radical (6.8 %).[3a] Its EPR spectrum showed a rhombic signal with a g_{av} value of 2.029, intermediate between a phenoxyl radical (~2.005)[7] and a Ni^{III} species (~2.13-2.17).[8] For [Ni(Salophen^{OMe2})] only two reversible oxidation waves were observed in the cyclic voltammograms at $E^1_{1/2}$ = 0.45 V and $E^2_{1/2}$ = 0.69 V *vs.* Fc^+/Fc.[3a] Contrarily to [Ni(Salophen^{OMe2})]$^+$, the characterization of [Cu(Salophen^{OMe2})]$^+$ points towards the formation of the radical cation on the diaminobenzene ring.[4a] The redox potentials, $E^1_{1/2}$ = 0.41 V and $E^2_{1/2}$ = 0.70 V *vs.* Fc^+/Fc, are similar to those found for the nickel analogue. The X-ray structure of the oxidized product was informative about the oxidation locus. The coordination sphere does not experience important changes upon oxidation, while the C-O and C-N bonds of the phenylene ring shorten upon oxidation. The central ring displays a pattern similar to that found for the iminobenzosemiquinonate radicals described by Wieghardt *et al*. (Scheme 56).[10]

The dimethylamino salophen derivatives ([M(Salophen^{NMe2})]) were also investigated (Scheme 56).[6] In this case, [Ni(Salophen^{NMe2})]$^+$ was described as a diaminobenzene radical thanks to the nitrogen signature observed in the EPR spectrum, which shows a signal at g_{iso} = 2.004. The dicationic species were also studied and the second oxidation was found to take place also on the central ring which acquires a diiminoquinone pattern (Scheme 56). The redox potentials of [Ni(Salophen^{NMe2})], $E^1_{1/2}$ = 0.12 V and $E^2_{1/2}$ = 0.24 V *vs.* Fc^+/Fc, are significantly lower than those of [Ni(Salophen^{OMe2})].[6] This difference

accounts not only for the difference in the electron-donating ability of the two functional groups, but also for the shift of the oxidation locus from the phenolate to the diaminobenzene ring. A third redox process was observed for [Ni(Salophen^{NMe2})] occurring at $E^3_{1/2}$ = 0.97 V related to the oxidation of one phenolate ring.[6]

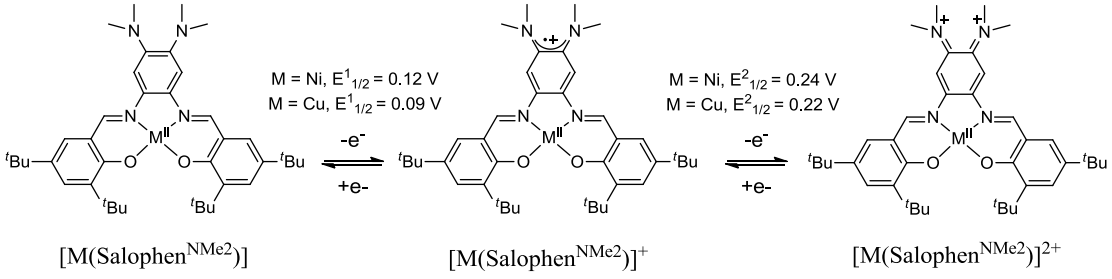

Scheme 56. Oxidation processes for [Ni(Salophen^{NMe2})] and [Cu(Salophen^{NMe2})] and related potentials in V *vs* Fc^+/Fc.[6,9]

The oxidized product [Cu(Salophen^{NMe2})]$^+$ was characterized as a bis(dimethylamino)-phenylene radical, similarly to [Ni(Salophen^{NMe2})]$^+$, where the unpaired electron is coupled ferromagnetically (S = 1) with the electron of the copper.[9] The redox processes for [Cu(Salophen^{NMe2})] occur at $E^1_{1/2}$ = 0.09 V and $E^2_{1/2}$ = 0.22 V *vs.* Fc^+/Fc, similar to those obtained for the nickel analogue. The second oxidation also concerns the central ring, leading to a closed-shell diiminoquinone ligand bound to a Cu^{II} center in [Cu(Salophen^{NMe2})]$^{2+}$.[9]

In our case, to further investigate the influence of the phenylene bridge in the electronics of the oxidized complexes, different mono and di-substituted phosphasalophen ligands were synthesized. In order to increase the electronic density in the phenylenediamine ring, to promote its oxidation, a new ligand was synthesized where a methyl group was introduced in the central ring, Psalophen^{Me} (Scheme 57, left). This substitution induces as well a higher steric hindrance and may avoid possible dimerization through the phenylene linker. On the other hand, in order to disfavor the oxidation of the central ring and increase the contribution of the metal orbitals, a new ligand was synthesized featuring a trifluoromethane group as electron-withdrawing group, Psalophen^{CF3} (Scheme 57, middle). A fourth phosphasalophen ligand was synthesized displaying two methoxy groups in the positions 4 and 5 of the diaminobenzene ring, Psalophen^{OMe2} (Scheme 57, right).

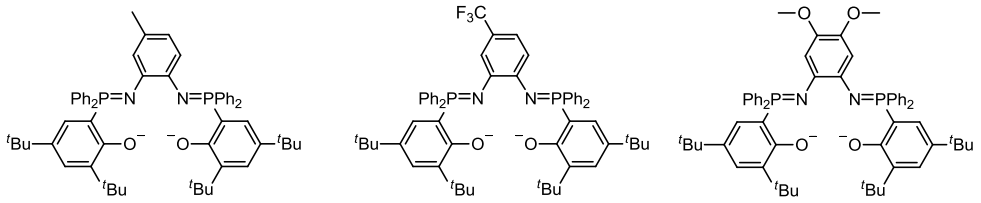

Scheme 57. Ligands studied in this chapter.

Nickel and copper neutral complexes and their oxidation products were synthesized and characterized. Three different products can be obtained upon oxidation depending on the oxidation locus: a phenoxyl M(II)-radical complex, a diaminobenzene M(II)-radical complex or, less likely, a high-valent M(III) complex. In the case of nickel, the three possible configurations are paramagnetic. For the copper derivative different spin states are possible, depending on the electronic coupling, leading to either triplet or singlet states. A representation of the possible mono-oxidized products is present in Scheme 58.

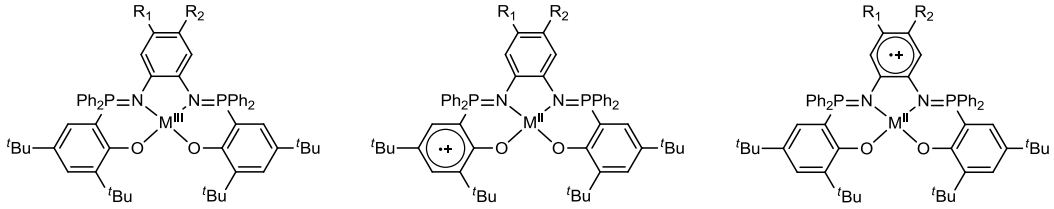

Scheme 58. Possible electronic configurations of the mono-oxidized products of [M(Psalophen^{X})] (M = Ni, Cu).

II. Psalophen complexes

1. Synthesis of the ligand and neutral complexes

Psalophen ligand was prepared as the other phosphasalen ligands shown in this manuscript. The only difference with the procedure described for the alkyl-linked phosphasalen ligands is the use of 1,4-diazabicyclo[2.2.2]octane (DABCO) instead of tributylamine for the trapping of the generated equivalent acid. Tributyl ammonium salts are soluble in THF as well as the desired product (H_4Psalophen)Br_2, but those of DABCO are not, so once the product is formed this can be separated from the DABCO salts by filtration of the THF solution.

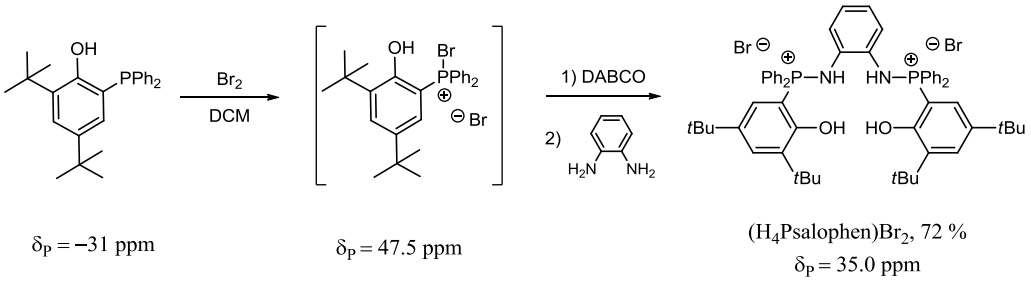

Scheme 59. Synthetic procedure of $(H_4Psalophen)Br_2$ and corresponding ^{31}P chemical shifts in dichloromethane.

The formation of the ligand is indicated by the presence of a signal at 35 ppm in the ^{31}P NMR spectrum and was obtained as a pale pink solid in its bis-aminophosphosnium salt form $(H_4Psalophen)Br_2$ in 72 % yield.

[Ni(Psalophen)] and [Cu(Psalophen)] complexes were obtained following the procedure shown in Scheme 60. The aminophosphonium salt $H_4Psalophen$ was dissolved in THF and deprotonated with KHMDS. The deprotonation is evidenced by the disappearance of the signal of $H_4Psalophen$ and the presence of a signal at 10.5 ppm corresponding to $K_2Psalophen$.

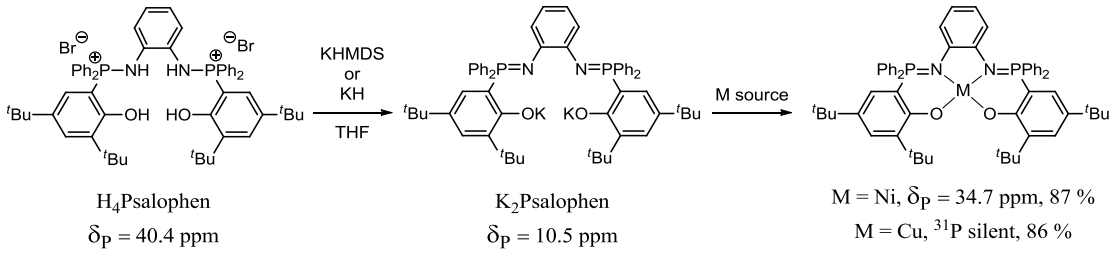

Scheme 60. Synthesis of the complexes and the related ^{31}P NMR signals in THF.

The solution was centrifuged to remove insoluble salts and the metal precursors, $CuBr_2$ or $[NiBr_2(DME)]$, were added. The solution changes from orange to blue when [Ni(Psalophen)] is formed, and a broad singlet is observed at 34.7 ppm in the $^{31}P\{^1H\}$ NMR spectrum, while the signal of the ligand disappears. In the case of [Cu(Psalophen)] the solutions turns to green, and no signal was observed when the signal of the ligand disappears, indicating the formation of a Cu^{II} paramagnetic species. To isolate the complexes, the solvent was evaporated and the residues dissolved in dichloromethane and centrifuged. The solutions were concentrated and addition of petroleum ether led to the precipitation of a solid. The powders were washed with petroleum ether and dried under vacuum to yield [Ni(Psalophen)] and [Cu(Psalophen)] as pale blue and green powders in 87 and 86 % yield, respectively. Both products, specially [Cu(Psalophen)], are slightly

soluble in petroleum ether so a loss of product occurs during the washing step. Both complexes were analyzed by elemental analysis and mass spectrometry giving satisfactory results.

2. Characterization of neutral complexes [Ni(Psalophen)] and [Cu(Psalophen)]

2.1 NMR spectroscopy

Both [Ni(Psalophen)] and [Cu(Psalophen)] were studied by NMR spectroscopy. [Ni(Psalophen)] complex shows a diamagnetic ^{1}H NMR spectrum and a ^{31}P resonance around 23.0 ppm in $CDCl_3$.

The ^{1}H NMR spectrum of [Ni(Psalophen)] (Figure 66) is similar to those of the nickel phosphasalen complexes previously discussed, but differing by the presence of the phenyl diamine signals instead of the ethylene diamine ones.

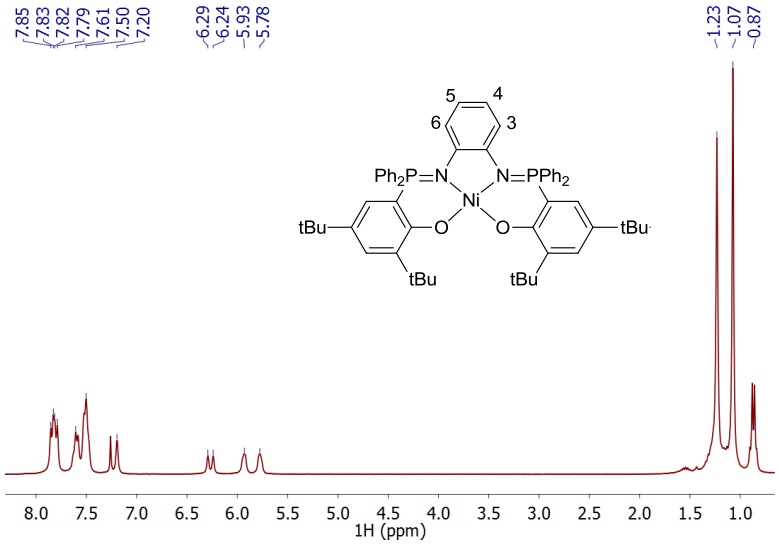

Figure 66. ^{1}H NMR spectrum of [Ni(Psalophen)] in $CDCl_3$. The signal at 0.87 ppm corresponds to pentane.

The phenyl phosphine protons are present between 7.0 and 8.0 ppm as multiplets, the phenolate protons in *para* position with respect to the phosphorous atom are observed at 7.12 ppm as a doublet ($^{4}J_{H,H}$ = 2.0 Hz), while the other phenolate protons are present at 6.20 ppm as a doublet of doublets due to the coupling with the phosphorous atom, and the other phenolate proton ($^{3}J_{P,H}$ = 15.6 Hz, $^{4}J_{H,H}$ = 2.0 Hz). The phenylene bridge protons in

positions 4 and 5 appear at 5.86 ppm as a doublet of doublets ($^{3}J_{H,H}$ = 5.9 Hz, $^{4}J_{H,H}$ = 3.6 Hz), and the phenylene bridge protons in positions 3 and 6 appear at 5.78 ppm as a non-resolved multiplet due to coupling with the phosphorus atom and the other phenylene protons. The tert-butyl protons are present at 1.16 and 1.00 ppm as singlets.

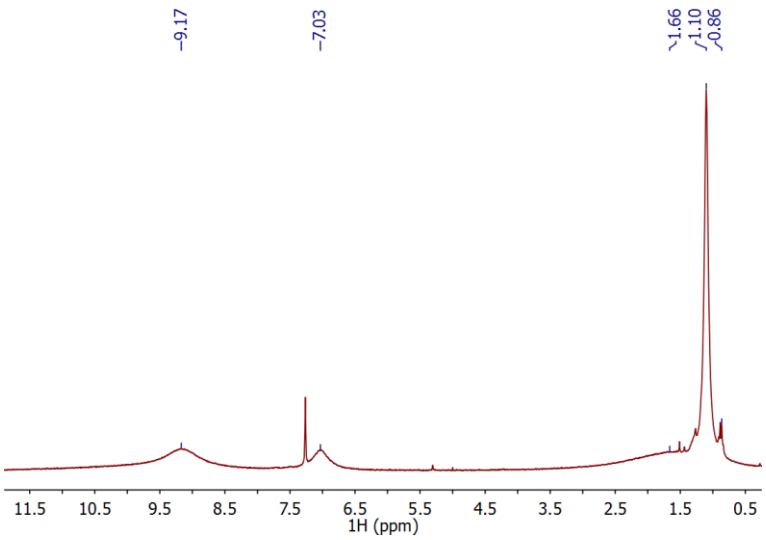

Figure 67. ^{1}H NMR spectrum of [Cu(Psalophen)] in $CDCl_3$ at 20 ° C. The signal present at 0.86 ppm corresponds to pentane.

[Cu(Psalophen)] displays a paramagnetic ^{1}H NMR spectrum with no ^{31}P signal as expected for a Cu^{II} $3d^{9}$ complex. The ^{1}H NMR spectrum (Figure 67) is similar to those observed for other copper phosphasalen complexes. Broad signals were observed between 0 and 11 ppm and were tentatively assigned as previously: the phenyl phosphine substituents at 9.17 ppm, the protons of the phenolate and the phenylene ring at 7.03 ppm, and the *t*-butyl groups at 1.66 ppm, as a very broad signal, and at 1.08 ppm.

2.2 EPR spectroscopy

The EPR spectrum of [Cu(Psalophen)] at room temperature is very similar to those obtained for the copper phosphasalen complexes already studied. It displays a rhombic signal with a four line pattern due to the hyperfine coupling with the Cu center (I = 3/2).

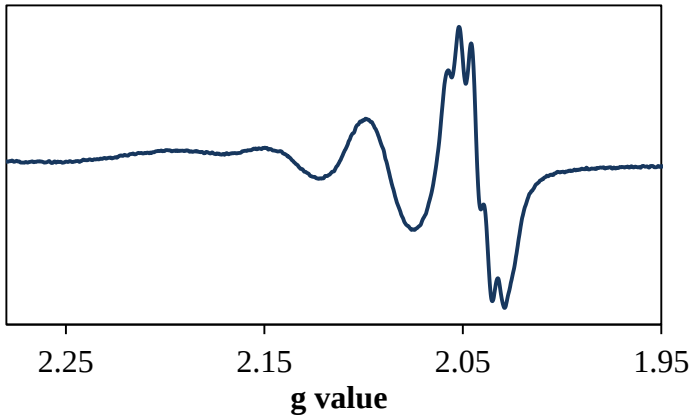

Figure 68. X-band EPR spectrum of [Cu(Psalophen)] in dichloromethane at 297 K. Conditions: Frequency: 9.847 GHz; amplitude: 0.3 mT.

A superhyperfine coupling is only observed on g_3. Since this spectrum and those obtained for the alkyl phosphasalen analogues are superimposable, we can assume that they possess the same g values and coupling constants. Thus, the EPR parameters are g_1 = 2.122, g_3 = 2.105 and g_3 = 2.051 and $|A|_{Cu}$ = 251, 210 and 75 MHz, and superhyperfine constants of $|A|_N$ = 28, 28 and 28 MHz for g_1, g_2 and g_3, respectively. The similarity with the spectra of the other alkyl phosphasalen complexes indicates that the electronics of the copper center does not change much with the introduction of the phenylene ring.

2.3 UV-vis spectroscopy

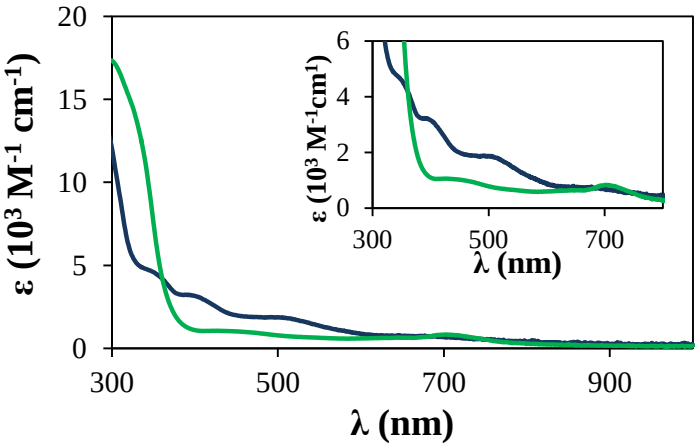

Figure 69. UV-vis spectra of [Cu(Psalophen)] (green line) and [Ni(Psalophen)] (blue line) in dichloromethane.

The UV-visible spectrum of [Ni(Psalophen)] (Figure 69, blue line) shows bands at 705 nm (ε = 800 M^{-1} cm^{-1}), 510 nm (ε = 1900 M^{-1} cm^{-1}), 380 nm (ε = 3200 M^{-1} cm^{-1}), and 350 nm (ε = 4700 M^{-1} cm^{-1}). More transitions appear compared to [Ni(Psalen^{OMe})], which shows a

transition at 560 nm (ε = 1300 M^{-1} cm^{-1}) and an intense band at 370 nm (ε = 8800 M^{-1} cm^{-1}). Assuming that the bands at 510 and 380 nm in [Ni(Psalophen)] are analogous to those observed at 560 and 370 nm in [Ni(Psalen^{OMe})], two additional bands are observed for the phenyl derivative at 705 and 350 nm, and may be related to transitions involving the phenylene bridge.

[Cu(Psalophen)] exhibits weak transitions at 440 nm (ε = 1000 M^{-1} cm^{-1}), 640 nm (ε = 630 M^{-1} cm^{-1}) and 700 nm (ε = 840 M^{-1} cm^{-1}) and an intense broad band which starts to appear at 390 nm and reaches high absorptions with ε = 17300 M^{-1} cm^{-1} at 300 nm. This spectrum is similar to that observed for the alkyl bridged derivatives, which display a broad band around 620 nm, attributed to a d-d transition, and a band around 430 nm, assigned to a transfer involving the iminophosphorane functions.

2.4 X-ray diffraction

Blue crystals of [Ni(Psalophen)] suitable for X-ray diffraction were obtained by slow diffusion of pentane into a concentrated dichloromethane solution.

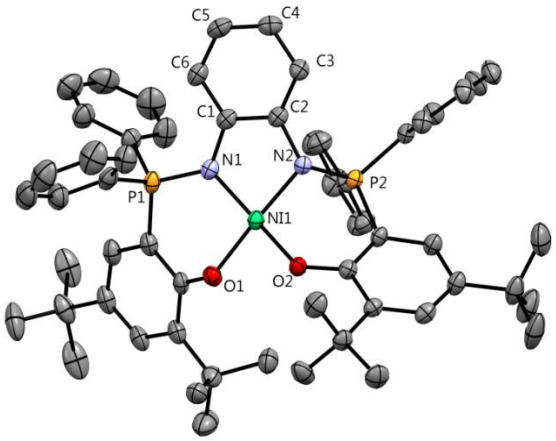

Figure 70. ORTEP of [Ni(Psalophen)] with thermal ellipsoids at 50 % probability. Hydrogen atoms and a molecule of pentane have been omitted for clarity.

[Ni(Psalophen)] displays a distorted square planar geometry around the metal center. Despite the planarity imposed by the central ring, the main NOON plane presents a torsion angle of 8.14 °, similar to that found in [Ni(^{iPr}Psalen)] (8.91 °) and intermediate between those of [Ni(Psalen^{OMe})] (11.96 °) and [Ni(Psalen^{tBu})] (6.15 °). Ni-N and Ni-O bond distances are similar to those of the alkyl phosphasalen derivatives. Ni-N bonds (1.891(3) and 1.903(3) Å) are equivalent to those of [Ni(^{iPr}Psalen)] (1.906(2) and 1.892(2) Å) but slightly larger compared to [Ni(Psalen^{OMe})] and [Ni(Psalen^{tBu})] (1.881 and 1.888 Å in average, respectively). Ni-O bond distances are not equivalent (1.880(2) and 1.851(2) Å)

and differ by 0.029 Å. This dissymmetry was not observed for the previously studied neutral nickel phosphasalen complexes which present similar Ni-O bond lengths ranging between 1.878 and 1.887 Å. N-P bond lengths measure 1.617(3) and 1.625(3) Å, and are very similar to those observed for [Ni(Psalen^{tBu})] (1.619(2) Å) and [Ni(^{iPr}Psalen)] (1.620(2) 1.633(2) Å). One of the N-P bonds (N2-P2) was found to be particularly out of the main NOON plane (Figure 71). Thus, P2 is placed at 1.439 Å from the calculated NOON plane, while P1 is placed at 0.244 Å. The geometry adopted by N2 is close to tetrahedral and the P2-Ni distance is 2.854 Å, while N1 is closer to the trigonal planar geometry and the P1-Ni distance is 3.081 Å. This distortion was not observed before for the neutral nickel phosphasalen complexes, and may be due to the rigidity of the phenylene linker.

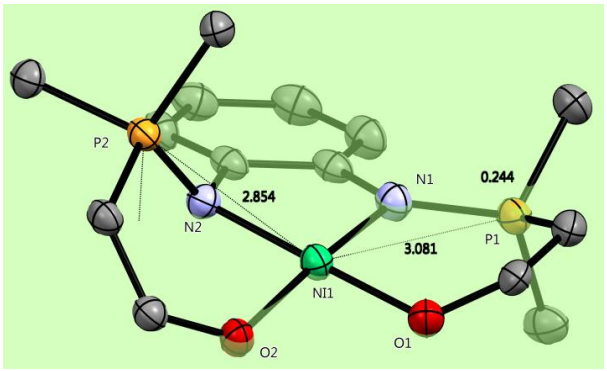

Figure 71. Zoom on the coordination sphere of nickel in [Ni(Psalophen)] and selected distances in Å. In green the plane defined by the two nitrogen and the two oxygen coordinating atoms (NOON plane).

	[Ni(Psalophen)]	[Cu(Psalophen)]
M-O1	1.880(2)	1.940(2)
M-O2	1.851(2)	1.966(2)
M-N1	1.891(3)	1.995(3)
M-N2	1.903(3)	1.951(3)
P1-N1	1.617(3)	1.612(3)
P2-N2	1.625(3)	1.612(3)
Torsion angle[a]	8.14	0.48

Table 17. Selected bond distances (Å) and angles (°) for [Ni(Psalophen)] and [Cu(Psalophen)]. [a] Torsion of the NOON plane.

Green crystals of [Cu(Psalophen)] suitable for X-ray diffraction were obtained *via* evaporation of a $CDCl_3$ solution.

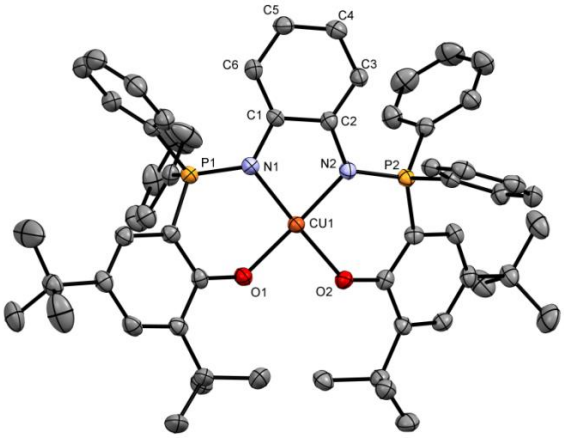

Figure 72. ORTEP of [Cu(Psalophen)] with thermal ellipsoids at 50 % probability. Hydrogen atoms have been omitted for clarity.

[Cu(Psalophen)] displays a nearly square planar geometry around the metal center with a torsion angle of the main plane of 0.48 °. This slight distortion contrasts with the ones found for other neutral copper phosphasalen complexes such as [Cu(^{iPr}Psalen)] (9.41 °) and [Cu(Psalen^{OMe})] (19.40 °). Here, the planarity imposed by the central ring leads to a planar coordination environment, contrary to what was observed for [Ni(Psalophen)]. However, the coordination sphere around the copper center turned out to be non-symmetrical: Cu-N bonds measure 1.995(3) and 1.951(3) Å (Δd = 0.044 Å), and Cu-O measure 1.940(2) and 1.966(2) Å (Δd = 0.026 Å). Thus, a long axis is present along the N1-Cu-O2 segment. These bond lengths are slightly longer than those observed in the alkyl phosphasalen derivatives, especially the Cu-N bonds which vary between 1.941(2) and 1.959(1) Å in these complexes. The longer Cu-N bonds may be due to the delocalization of the electron pairs of the nitrogen in the phenylene ring, so that less electron density is available for the metal center. P-N bonds (1.612(3) Å) were found to be slightly longer than those of the alkyl derivatives, which range between 1.953(2) and 1.603(2) Å, in agreement with less negative hyperconjugation. The distortion observed in one of the N-P bonds for [Ni(Psalophen)], is not observed for [Cu(Psalophen)], whose phosphorus atoms are found at 0.420 and 0.123 Å from the calculated NOON plane.

2.5 Electrochemical studies

The electrochemical properties of the neutral complexes were studied by cyclic voltammetry in dichloromethane solutions. All potentials are referred to Fc^+/Fc which was used as internal reference.

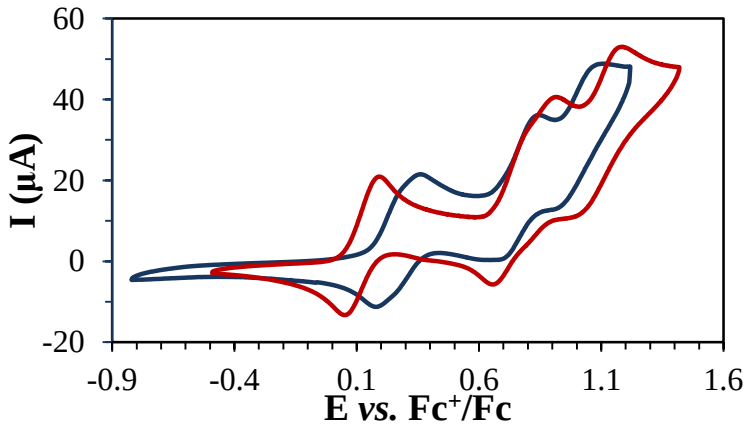

Figure 73. Cyclic voltammograms of [Cu(Psalophen)] (blue line) and [Ni(Psalophen)] (red line) recorded in dichloromethane. Conditions: 3 mM of complex in dichloromethane at 0.1 V/s.

The cyclic voltammogram of [Ni(Psalophen)] (Figure 73, red line) shows two reversible oxidations at $E^1_{1/2}$ = 0.15 V, $E^2_{1/2}$ = 0.78 V, and an irreversible oxidation at $E^3_{p,a}$ = 1.09 V. From its shape and intensity, the second wave may correspond to a two-electron redox process. Thus, these four redox processes may correspond to the oxidation of the four redox-active units present in the complex: the metal, the two phenoxide rings and the phenylene ring. The first oxidation occurs at higher potentials than for the alkyl-bridged phosphasalen analogues [Ni(Psalen^{tBu})] (0.01 V), [Ni(Psalen^{OMe})] (-0.06 V) and [Ni(^{iPr}Psalen)] (-0.02 V). The oxidation of [Ni(Psalophen)] is more difficult because of a lower electron-donation of the nitrogen atoms, explained by the delocalization of the electron pairs on the phenylene ring.

The second oxidation takes place at similar potentials than for [Ni(Psalen^{tBu})] (0.82 V) and [Ni(^{iPr}Psalen)] (0.83 V). The gap between the first and the second oxidation for [Ni(Psalophen)] is $\Delta E_{1\text{-}2}$ = 0.63 V; this value is intermediate between the Psalen^{tBu} ($\Delta E_{1\text{-}2}$ ~ 0.80 V) and Psalen^{OMe} ($\Delta E_{1\text{-}2}$ ~ 0.50 V) derivatives mentioned before, and indicates that the metal is getting partially oxidized in the first oxidation. However, the higher redox potential value obtained for [Ni(Psalophen)] compared to [Ni(Psalen^{tBu})] or [Ni(^{iPr}Psalen)], together with the presence of an electron rich phenylene linker, may indicate a shift of the oxidation locus from the metal to the phenyl bridge. However, it is premature to assign the different oxidations and further experiments will be needed to make a correct assignment.

The redox potentials obtained are lower than for the salen analogue, [Ni(salophen)], for which the oxidation occurs at 0.58 and 0.80 V.[1a] The better electron-donating ability of the iminophosphorane functions accounts for this difference.

Compound	$E^1_{1/2}$	$E^2_{1/2}/E^2_{p,a}$	$E^3_{p,a}$	ΔE_{1-2}
[Ni(Psalophen)]	0.15	0.78	1.09	0.63
[Cu(Psalophen)]	0.28	0.76	1.01	0.48

Table 18. Redox potentials for [Ni(Psalophen)] and [Cu(Psalophen)] expressed in V *vs*. Fc^+/Fc.

The cyclic voltammogram of [Cu(Psalophen)] (Figure 73, blue line) displays one reversible oxidation at $E^1_{1/2}$ = 0.28 V, a pseudo-reversible oxidation at $E^2_{p,a}$ = 0.76 V, and an irreversible one $E^3_{p,a}$ = 1.01 V. Contrarily to [Ni(Psalophen)], the first oxidation seems to correspond to a two-electron process. It occurs at higher potential than its nickel analogue, 0.15 versus 0.28 V, and at higher potentials compared to the alkyl phosphasalen analogues [Cu($Psalen^{tBu}$)] (0.10 V), [Cu($Psalen^{OMe}$)] (0.04 V) and [Cu(^{iPr}Psalen)] (0.03 V). The redox potential of copper complexes was found to be about 0.09 V higher than the nickel analogues (when featuring the same ligand) in the previous phosphasalen series. Here, this difference is slightly higher, 0.13 V, indicating than the introduction of the phenylene ring disfavors the oxidation of [Cu(Psalophen)] in a larger extent than for [Ni(Psalophen)].

Thus, a total of four redox processes are shown in the voltammogram, corresponding to the oxidation of the four redox-active units present in the complex, as for [Ni(Psalophen)], the assignment of the different oxidation processes is not feasible with this sole data.

For the sake of comparison, the redox potentials of the previously studied Psalen complexes are present in Table 19.

Compound	$E^1_{1/2}$	$E^2_{1/2}$	ΔE_{1-2}	$E^3_{p,a}$
[Ni(^{iPr}Psalen)]	-0.02	0.83	0.81	1.42
[Ni($Psalen^{tBu}$)]	0.01	0.82	0.81	1.24
[Ni($Psalen^{OMe}$)]	-0.06	0.47	0.53	1.00
[Cu(^{iPr}Psalen)]	0.03	0.84	0.81	1.42
[Cu($Psalen^{tBu}$)]	0.10	0.95	0.85	-
[Cu($Psalen^{OMe}$)]	0.04	0.54	0.50	-

Table 19. Redox potentials for copper and nickel phosphasalen complexes, expressed in V *vs* Fc^+/Fc

3. Oxidation of neutral complexes

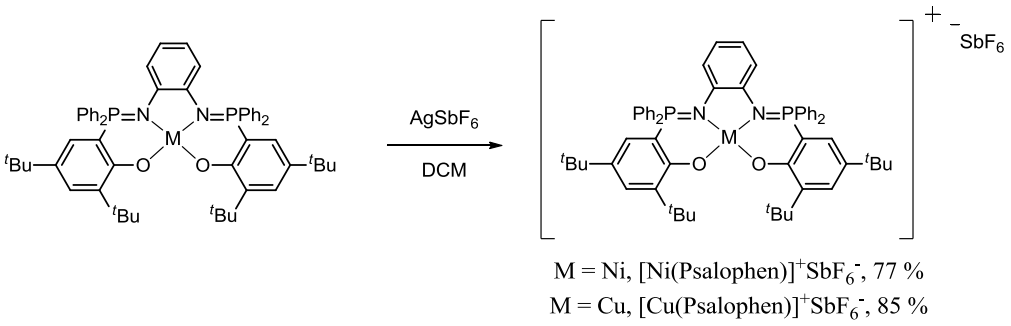

Scheme 61. Chemical oxidation of [Ni(Psalophen)] and [Cu(Psalophen)] complexes.

[Ni(Psalophen)] and [Cu(Psalophen)] complexes were oxidized using one equivalent of $AgSbF_6$ in a dichloromethane solution under inert conditions. Addition of the silver salt into a solution of [Ni(Psalophen)] induces an immediate color change from blue to dark brown, while the solution of [Cu(Psalophen)] changes from green to deep purple. The same color change was observed for the alkyl phosphasalen derivatives [M(Psalen^{OMe})], [M(Psalen^{tBu})] and [M(^{iPr}Psalen)]. Both solutions were concentrated and precipitation of the products was induced by addition of petroleum ether. The solids were washed with petroleum ether and dried under vacuum to yield [Ni(Psalophen)]$^+SbF_6^-$ as a dark brown solid in 77 % yield, and [Cu(Psalophen)]$^+SbF_6^-$ as a deep purple solid in 85 % yield.

4. Characterization of the oxidized complexes

4.1 NMR spectroscopy

[Ni(Psalophen)]$^+$ displays a paramagnetic ^{1}H NMR spectrum with signals between 0 and 12 ppm (Figure 74), and no signal in the ^{31}P NMR spectrum. The signals have a very broad shape and merge with the baseline albeit the high concentration of the NMR sample (18 mg in 0.5 mL of CD_2Cl_2). Only the signals present at 1.67 and 0.32 ppm could be assigned to the tert-butyl groups due their position and relative areas. The three broad signals at 11.29, 7.27 and 3.14 may correspond to the phenyl phosphine and phenoxide protons, since they present large integration areas, and the signals at 8.49, 8.21, 7.86 and 7.57 ppm may correspond to phenylene bridge protons.

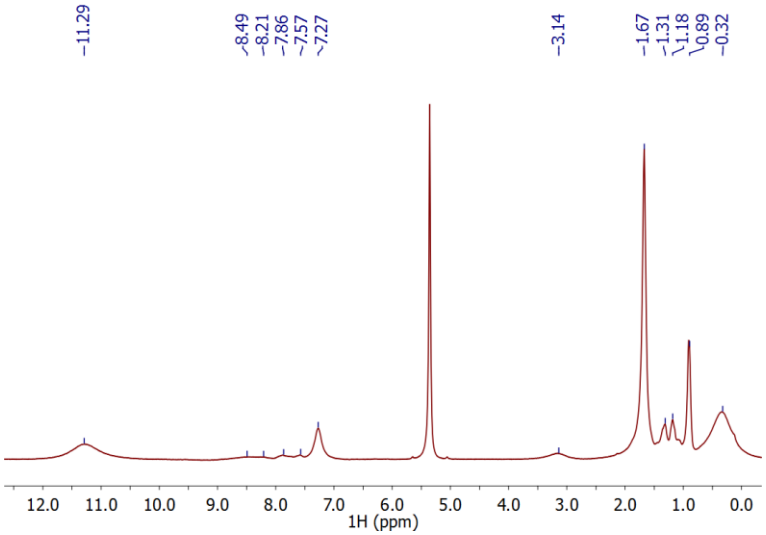

Figure 74. ^{1}H NMR spectrum of $[Ni(Psalophen)]^{+}$ in CD_2Cl_2. The signals present at 1.31, 1.18 and 0.89 ppm corresponds to pentane.

This spectrum contrasts with those obtained for the alkyl phosphasalen derivatives, which display signals at low (~ 20 ppm) and high fields (~ -3 ppm), out of the diamagnetic region, and differ also in the shape of the signals, which are broader for $[Ni(Psalophen)]^{+}$. This may suggest a predominantly ligand-based oxidation.

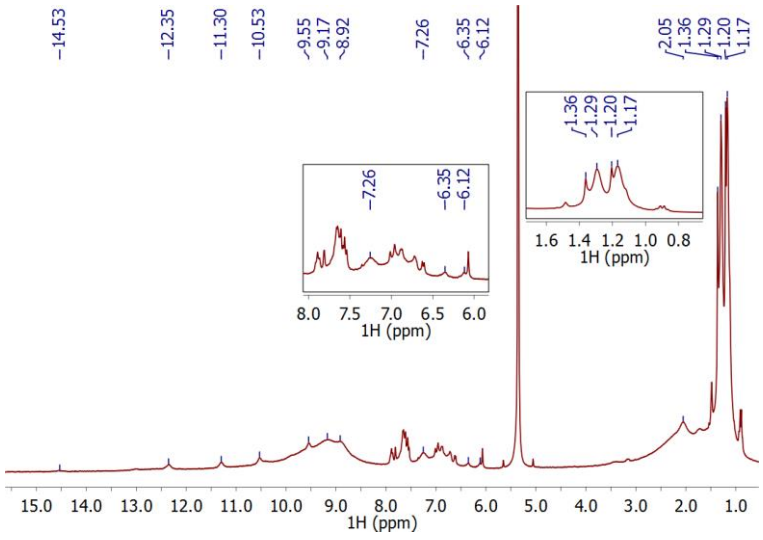

Figure 75. ^{1}H NMR spectrum of $[Cu(Psalophen)]^{+}$ in CD_2Cl_2. Insets shows a zoom of the aromatic region and the t-butyl signals.

$[Cu(Psalophen)]^{+}$ displays a ^{1}H NMR spectrum with signals between 1 and 15 ppm (Figure 75), and a narrow singlet at 42.5 ppm in the $^{31}P\{^{1}H\}$ NMR spectrum. Two set of signals seem to be present in the ^{1}H NMR spectrum. One set presents broad shape and chemical shifts shifted down-field; these are the signals between 14.53 and 8.92 ppm, and at 7.26, 6.35, 6.12, 1.29 and 1.17 ppm. Because of their high shift and their broad shape, these

signals may correspond to paramagnetic species. Another set of signals are sharp and presents coupling patterns; these are the signals between 6 and 8 ppm, and at 1.36 and 1.20 ppm (inset in Figure 75), that may correspond to diamagnetic species. One possible explanation for these diamagnetic signals is the presence of a degradation product. Indeed, a ^{31}P signal is observed around 42.5 ppm. Another possibility is the presence of a mixture of oxidized species in solution: a Cu^{III} complex, which would explain the presence of diamagnetic species, and a Cu(II)-ligand radical complex, which would explain the presence of paramagnetic species.

This spectrum is certainly different from those observed for $[Cu(Psalen^{tBu})]^+$ and $[Cu(Psalen^{iPr})]^+$ which are essentially diamagnetic. The formation of a ligand radical seems likely, so with the introduction of the phenylene linker has promoted a shift of the oxidation locus from the metal to the ligand.

4.2 EPR spectroscopy

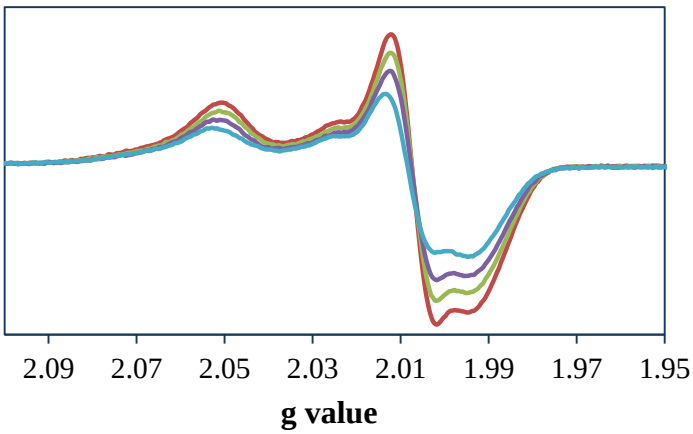

Figure 76. X-band EPR spectrum of $[Ni(Psalophen)]^+$ in dichloromethane at 80 K (red line), 100 K (green line), 120 K (purple line) and 140 K (blue line).

$[Ni(Psalophen)]^+$ displays a rhombic EPR signal below 160 K with $g_1 = 2.051$, $g_2 = 2.007$ and $g_3 = 1.993$. The intensity of the signal increases when decreasing the temperature. The EPR spectrum obtained contrasts with those recorded for $[Ni(Psalen^{OMe})]^+$, $[Ni(Psalen^{tBu})]^+$ and $[Ni(^{iPr}Psalen)]^+$. The first two also display rhombic signals with comparable g_1 and g_2 values, while the latter displays an axial signal where $g_1 = g_2$. The opposite situation is found in the EPR spectrum of $[Ni(Psalophen)]^+$ where $g_1 \gg g_2 \simeq g_3$, suggesting a significant change in the geometry and the anisotropy of the SOMO. In addition, the lower g_{av} obtained (2.017) compared to those of $[Ni(Psalen^{tBu})]^+$ and $[Ni(^{iPr}Psalen)]^+$ (both g_{av} = 2.19), may indicate a shift of the oxidation locus from the metal to the ligand in

[Ni(Psalophen)]$^{+}$. An additional feature was observed between g_1 and g_2, at g = 2.025 , which might correspond to a second minor. This feature, being very small, was not further investigated.

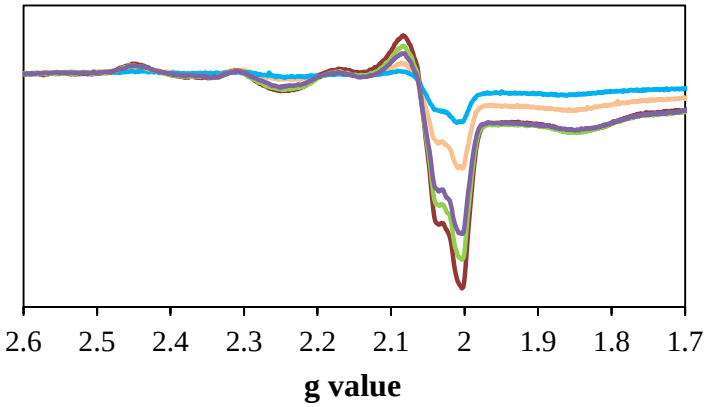

Figure 77. X-band EPR spectrum of [Cu(Psalophen)]$^{+}$ in dichloromethane at 80 K (red line), 100 K (green line), 120 K (purple line), 140 K (orange line) and 150 K (blue line).

[Cu(Psalophen)]$^{+}$ displays an apparent rhombic signal different from that obtained for the neutral complex (Figure 68). The presence of this signal rules out the possibility of a metal-centered oxidation. The g values deduced from the experimental spectrum are g_1 = 2.250, g_2 = 2.052 and g_3 = 2.013, and are up-field shifted compared to those obtained for the neutral complex. A coupling with the copper atom (I = 3/2) is observed in g_1 with an estimated value of A_{Cu} = 450 MHz. This is much higher compared to that calculated for the neutral complex, 250 MHz. Similar coupling constants have been observed for the neutral and oxidized species of the [Cu(Salophen^{NMe2})] derivative (A ≃ 550 MHz).[9] This signal was assigned to a Cu^{II} center (S = 1/2).

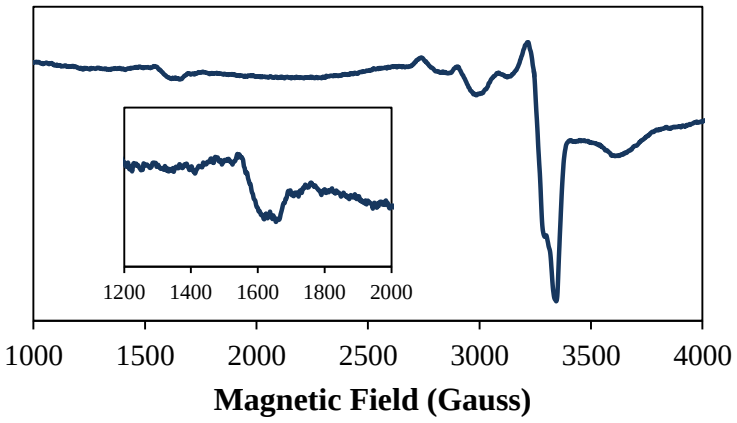

Figure 78. X-band EPR spectrum of [Cu(Psalophen)]$^{+}$ in dichloromethane at 100 K. Conditions: Frequency: 9.384 GHz; Power: 1.003 mW; modulation frequency: 100 kHz; amplitude: 1.0 mT.

Other features besides the Cu^{II} signal were observed in the EPR spectrum of $[Cu(Psalophen)]^+$. Figure 78 shows an extended spectrum where a feature centered at 1600 G (g ~ 4.2) is observed. This feature is typical of a triplet state (S = 1) configuration arising from a ferromagnetic coupling between the copper center and a radical spin, likely a diaminobenzene radical.[9-11] The low resolution of the spectrum (modulation amplitude of 10 G) does not allow observing the coupling pattern in the ferromagnetic feature, which should show a four line pattern signal, corresponding to the coupling with the copper center (I = 3/2). This contrasts with the EPR spectra obtained for the oxidized alkyl phosphasalen derivatives, which are silent at any temperature. The introduction of the phenylene ring in the ligand backbone resulted in a shift of the oxidation locus from the metal in $[Cu(Psalen^{tBu})]$ (the alkyl analogue), to the ligand (potentially the phenylene bridge) in $[Cu(Psalophen)]^+$.

4.3 UV-visible spectroscopy

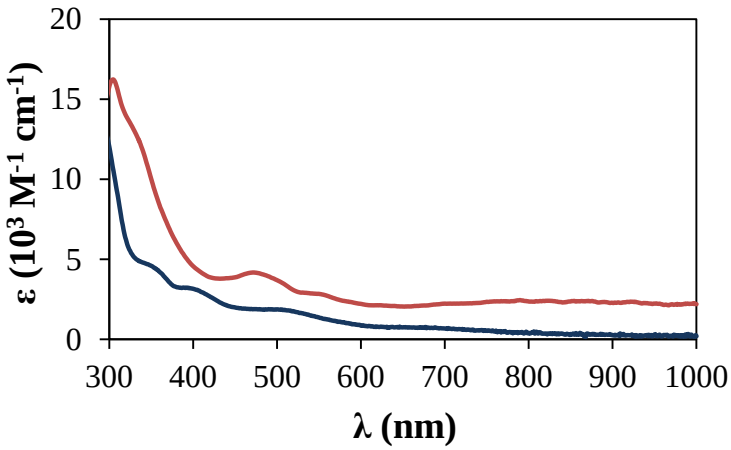

Figure 79. UV-vis spectra of [Ni(Psalophen)] (blue line) and $[Ni(Psalophen)]^+$ (red line) in dichloromethane.

The UV-visible spectrum of $[Ni(Psalophen)]^+$ shows a broad band at 830 nm (ε = 2300 M^{-1} cm^{-1}), and small bands at 560 nm (ε = 2700 M^{-1} cm^{-1}) and 420 nm (ε = 4200 M^{-1} cm^{-1}). This spectrum contrasts with those obtained for the alkyl bridged phosphasalen analogues which display intense bands around 1000 nm and 560 nm. An intense band starts to appear at 400 nm and reaches an absorption of ε = 16200 M^{-1} cm^{-1} at 300 nm. A shoulder is observed for this band at 330 nm (ε = 13000 M^{-1} cm^{-1}).

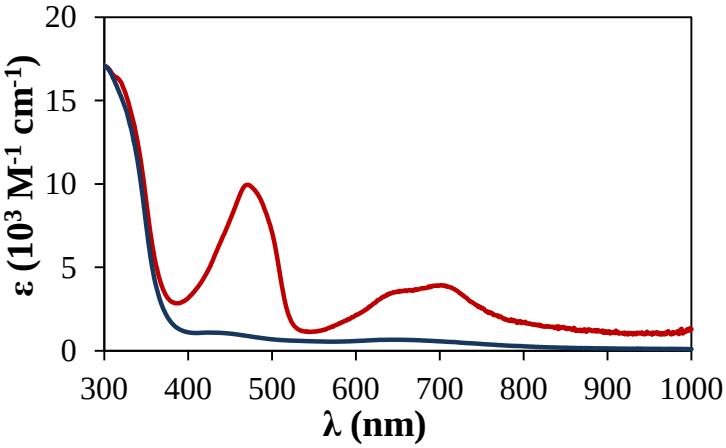

Figure 80. UV-vis spectra of [Cu(Psalophen)] (blue line) and $[Cu(Psalophen)]^+$ (red line) in dichloromethane.

The absorption spectrum of $[Cu(Psalophen)]^+$ displays intense bands at 640 nm (ε = 3400 M^{-1} cm^{-1}) and 475 nm (ε = 9800 M^{-1} cm^{-1}). This also contrasts with the spectra obtained for the alkyl bridged derivatives which displays intense absorptions around 1000, 550 and 450 nm. This indicates a difference on the electronic structure of the generated oxidized species. An intense absorption, also present in [Cu(Psalophen)], is seen at 300 nm (ε = 17000 M^{-1} cm^{-1}).

4.4 X-ray diffraction

Single crystals of $[Ni(Psalophen)]^+SbF_6^-$ were obtained from a toluene/dichloromethane solution stored at -40 °C.

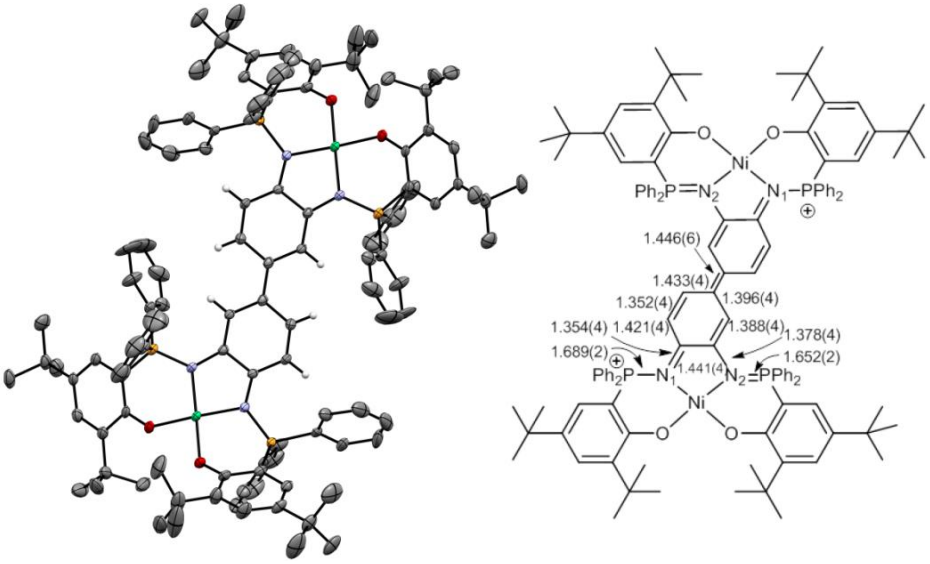

Figure 81. ORTEP of $[Ni(Psalophen)]^+SbF_6^-$ with thermal ellipsoids at 50 % probability. Hydrogen atoms and two molecules of SbF_6^- have been omitted for clarity.

The X-ray structure evidences a dimerization after oxidation through the phenylene bridge to lead a dicationic complex (Figure 81). Nevertheless, the formation of this dimer and the nature of the species in solution remain in question and will be discussed below.

The cell unit presents a C_2 symmetry axis, so that the asymmetric unit is constituted by one molecule of $[Ni(Psalophen)]^+$ and one SbF_6^- counter ion. A loss of two hydrogen atoms occurs during the dimerization resulting in a large conjugated system in the central part of the complex. The positive charges seem to be localized on one of the phosphorus atoms of each subunit, making the P-N bonds no longer equivalent: P1-N1 (where the positive charge is delocalized) measures 1.689(2) Å, while P2-N2 measures 1.652(2) Å; these bonds have lengthened upon oxidation by 0.072 and 0.027 Å, respectively. The phenylene ring displays a quinoid pattern alternating short and long C-C bonds (Figure 81, right). Both N-C bonds have significantly shortened upon oxidation, by 0.065 and 0.054 Å (especially N1-C1 which measures 1.354(4) Å), and display bond lengths intermediate between those typical of amine (1.465 Å) and imine (1.279 Å) units. No hydrogen atoms were found on the link between the two subunits, so that a double bond was established between them besides the long bond distance found (1.446(6) Å).

In the asymmetric unit, the nickel center presents a distorted square planar geometry with a torsion angle of the main plane of 12.21 °, larger than the one of the neutral complex [Ni(Psalophen)] (8.14 °). The coordination sphere does not experience important variations; Ni-O bonds shorten by 0.014 and 0.005 ppm, and Ni-N bonds by 0.008 and 0.007 Å. This, in addition to the fact that the positive charges are localized on the phosphorus atoms, suggests that the metal center has preserved its oxidation state upon oxidation. Table 20 gathers the bond distances of [Ni(Psalophen)] and the asymmetric unit of $([Ni(Psalophen)]^+SbF_6^-)_2$.

	[Ni(Psalophen)]	[Ni(Psalophen)]$^+$ [a]	Δ
Ni-O1	1.880(2)	1.866(2)	-0.014
Ni -O2	1.851(2)	1.846(2)	-0.005
Ni -N1	1.891(3)	1.883(2)	-0.008
Ni -N2	1.903(3)	1.896(2)	-0.007
P1-N1	1.617(3)	1.689(2)	0.072
P2-N2	1.625(3)	1.652(2)	0.027
Torsion angle[b]	8.14	12.21	4.07

Table 20. Selected bond lengths (Å) and angles (°) for [Ni(Psalophen)] and $([Ni(Psalophen)]^+SbF_6^-)_2$. [a] asymmetric unit. [b] Torsion of the NOON plane.

Single crystals of $[Cu(Psalophen)]^+SbF_6^-$ were obtained from saturated benzene and toluene solutions.

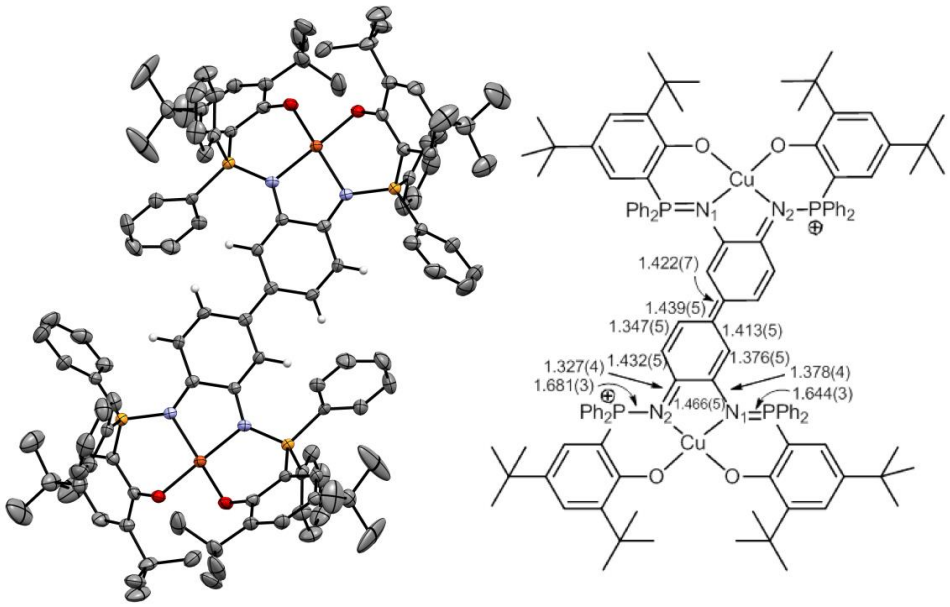

Figure 82. ORTEP of $([Cu(Psalophen)]^{+}SbF_6^{-})_2$ with thermal ellipsoids at 50 % probability. Hydrogen atoms, twelve molecules of benzene and two molecules of SbF_6^{-} have been omitted for clarity.

The copper analogue [Cu(Psalophen)] also dimerizes upon oxidation leading to a dicationic complex (Figure 82). The cell unit presents a C_2 symmetry axis so both subunits are equivalent. The loss of two hydrogen atoms also occurs upon dimerization resulting in a double bond binding the two subunits. The phenylene ring adopts a quinoid pattern with C-C bond distances similar to those observed for $([Ni(Psalophen)]^{+}SbF_6^{-})_2$ (Figure 82, right). The positive charges seem also to be placed in one of the phosphorus atoms of each subunit because of the difference in P-N bond lengths: P1-N1 bond measures 1.644(3) Å versus 1.681(3) Å for P2-N2, the latter being longer due to the presence of the positive charge in P2. A shift of the electronic density of the nitrogen occurs and consequently the N-C bonds shorten upon oxidation by 0.093 and 0.042 Å, the contraction being more important for N2-C2 which belongs to the quinoid moiety (1.327(4) Å).

Contrary to the nickel derivative, the coordination sphere around the copper center changes significantly upon oxidation. The metal presents an important tetrahedral distortion from the square planar geometry: the torsion angle of the main plane is 18.12 ° while is only 0.48 ° for the neutral complex. Cu-O bonds shorten by 0.053 and 0.063 Å upon oxidation. For Cu-N bonds, a contraction was observed for Cu-N1 by 0.040 Å while Cu-N2 lengthens by 0.042 Å. This difference is due to the shift of the electron density on the N2 towards the carbon atom of the phenylene cycle, resulting in the contraction of the N2-C2 bond and the elongation of the Cu-N2 bond. The Cu-N and Cu-O bonds as well as the torsion angle in the asymmetric unit of $([Cu(Psalophen)]^{+}SbF_6^{-})_2$ are similar to those

observed for the neutral complexes [Cu(Psalen^{tBu})] and [Cu(Psalen^{OMe})]. This indicates an oxidation state of +II for the metal center.

	[Cu(Psalophen)]	[Cu(Psalophen)]$^{+}$ [a]	Δ
Cu-O1	1.940(2)	1.887(2)	-0.053
Cu -O2	1.966(2)	1.903(2)	-0.063
Cu -N1	1.995(3)	1.955(3)	-0.040
Cu -N2	1.951(3)	1.993(3)	0.042
P1-N1	1.612(3)	1.644(3)	0.030
P2-N2	1.612(3)	1.681(3)	0.069
Torsion angle	0.48	18.12	17.64

Table 21. Selected bond lengths (Å) and angles (°) for [Cu(Psalophen)] and ([Cu(Psalophen)]$^{+}SbF_6^{-}$)$_2$. [a] asymmetric unit.

5. Study of the dimers ([Ni(Psalophen)]$^{+}SbF_6^{-}$)$_2$ and ([Cu(Psalophen)]$^{+}SbF_6^{-}$)$_2$

5.1 Dimerization process

Dimerization of complexes featuring redox-active ligands has been already observed.[2d,12] A recent example is the case of the pyrimidinenorcorrolato complex, [Ni(Corr)], reported by P. J. Chmielewski and co-workers (Scheme 62).[12a] The dimer [Ni(Corr)]$_2$, obtained in an attempt of amination of [Ni(Corr)], was found to be in a reversible equilibrium with the monomer [Ni(Corr)]·. This equilibrium was proved by VT-ESR, VT-NMR and VT-UV-vis-NIR spectroscopies, establishing the predominance of the radical species at high temperature and of the dimeric form at low temperature. [Ni(Corr)]$_2$ can undergo an irreversible loss of two hydrogen atoms leading to the generation of the dimer [Ni(Corr-S)]$_2$. This dimer displays a double bond between the two subunits of 1.437(5) Å in length, and was found to be in equilibrium with the triplet species [Ni(Corr-T)]$_2$.

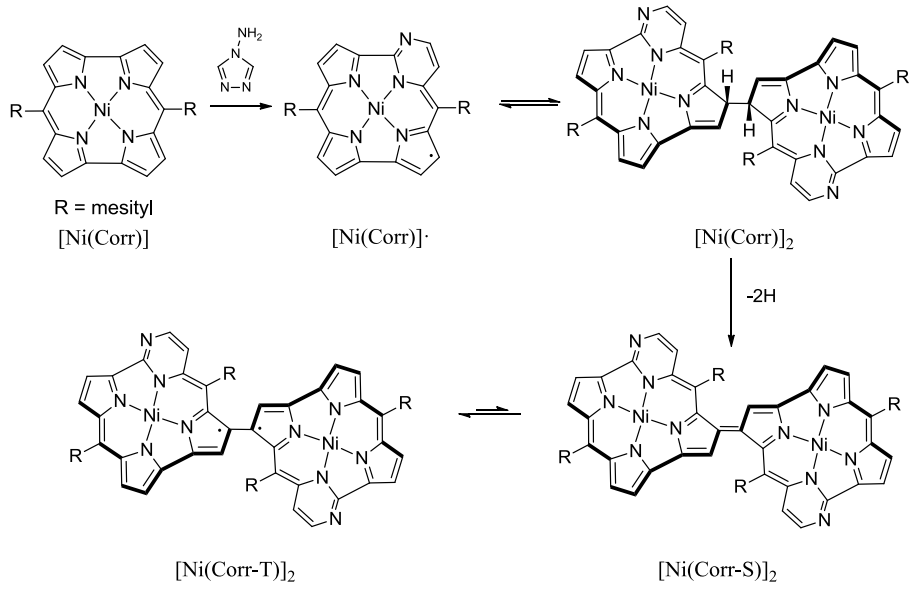

Scheme 62. Amination of the norcorrolato [Ni(Corr)] complex and corresponding dimerization and spin equilibria.[12a]

In the molecules presented here, since the dimerization has taken place through the phenylene ring we hypothesize the generation of a radical ligand which is localized on the central ring (Scheme 63, A). In presence of another radical complex, both unpaired electrons combine to form a C-C bond (Scheme 63, B). The loss of two hydrogen atoms leads to the formation of the structure isolated by X-ray diffraction (Scheme 63, E). Two questions remain unresolved: how these two hydrogen atoms leave the molecule (as hydrogen radicals or as a molecule of dihydrogen), and what is the rate of the dimerization.

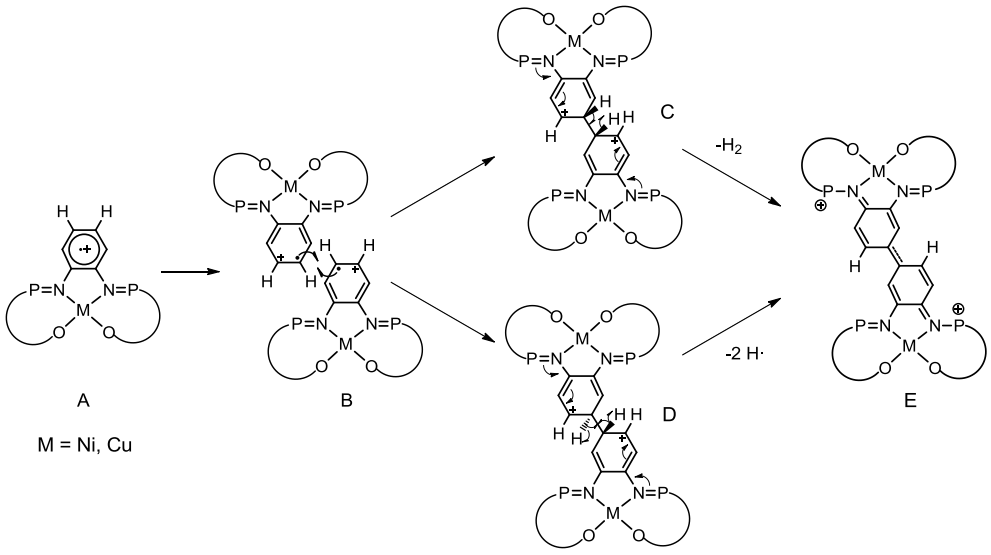

Scheme 63. Proposed dimerization mechanism for [Cu(Psalophen)]+ and [Ni(Psalophen)]+ complexes.

For the first question two possibilities exist: a homolytic cleavage of the C-H bonds and consequent H_2 and C-C double bond formation in a concerted process (Scheme 63, C), or a homolytic cleavage of the C-H bonds and consequent generation of two H· (Scheme 63, D) that go on to react with the molecules in the medium or form H_2.

In order to discern between these two situations two different experiments were carried out. The first one aims at detecting the formation of H_2 during the oxidation reaction by NMR spectroscopy. CD_2Cl_2 was condensed on a mixture of $AgSbF_6$ and the neutral complex placed in a young NMR tube under inert atmosphere. Once the tube is removed from the nitrogen bath and warmed up, the solvent melts and the oxidation reaction starts. This experiment was performed for both copper and nickel derivatives; unfortunately no signal corresponding to H_2 was detected in the ^1H NMR spectrum of any of the complexes. The second experiment was designed to detect the formation of hydrogen radicals (H·). The oxidation reaction was performed in presence of half equivalent of 9,10-dihydroanthracene. In presence of two H·, the dihydroanthracene reacts to give two molecules of H_2 and become aromatic (anthracene). If hydrogen radicals are released upon oxidation, formation of anthracene can be followed ^1H NMR since a new signal corresponding to the protons in positions 9 and 10 will appear at 8.40 ppm and simultaneously, the signal corresponding to the aliphatic protons of the 9,10-dihydroanthracene at 3.94 ppm will disappear. Different tests for which 9,10-dihydroanthracene was added to the oxidation reaction medium were performed but they remain unsuccessful.

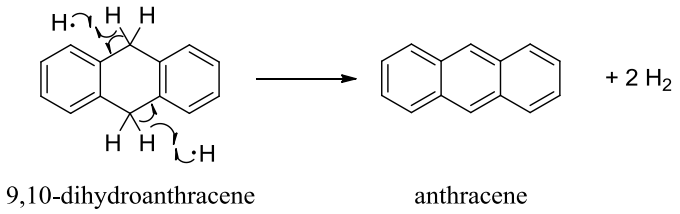

Scheme 64. Aromatization of 9,10-dihydroanthracene.

Therefore, the loss of the hydrogen atoms and consequent formation of the double bond is still needs further investigation. A deuterated derivative has been synthesized, for which hydrogen atoms have been substituted by deuterium in the phenyl ring. Since the detection of H_2 by NMR failed, we plan to perform new tests with the deuterated derivative in other to observe the formation of D_2 or HD by NMR spectroscopy. On the other hand, the formation hydrogen radicals that immediately react in the medium with other molecules of complex is also plausible.

The second question concerning the rate of dimerization remains also unresolved; so that, the composition of the solution obtained upon oxidation remain unknown. Both radical monomeric species ([M(Psalophen·)]) and dimeric species may be present in solution, as suggested by the ^{1}H NMR spectrum obtained for $[Cu(Psalophen)]^{+}$.

5.2 NMR spectroscopy

The NMR spectra of both nickel and copper dimers were recorded using single crystals, in order to ensure that the only species present in solution correspond to the dimeric species.

$([Ni(Psalophen)]^{+}SbF_6^{-})_2$ displays an apparent diamagnetic ^{1}H NMR spectrum with signals between 0 and 9 ppm (Figure 83), and the ^{31}P NMR spectrum exhibits two broad singlets at 14.5 and 10.0 ppm. This agrees perfectly with the crystal structure which points to the presence of two Ni^{II} centers in a square planar environment, *i.e.*, closed-shell diamagnetic species, and two non-equivalent phosphorus atoms, due to the presence of a positive charge on one of them. However, the difference in electron density of each phosphorus atom should lead to very different ^{31}P chemical, which is not the case. This may be explained by the presence of different resonance forms in solution due to the extended π-system along the central part of the molecule.

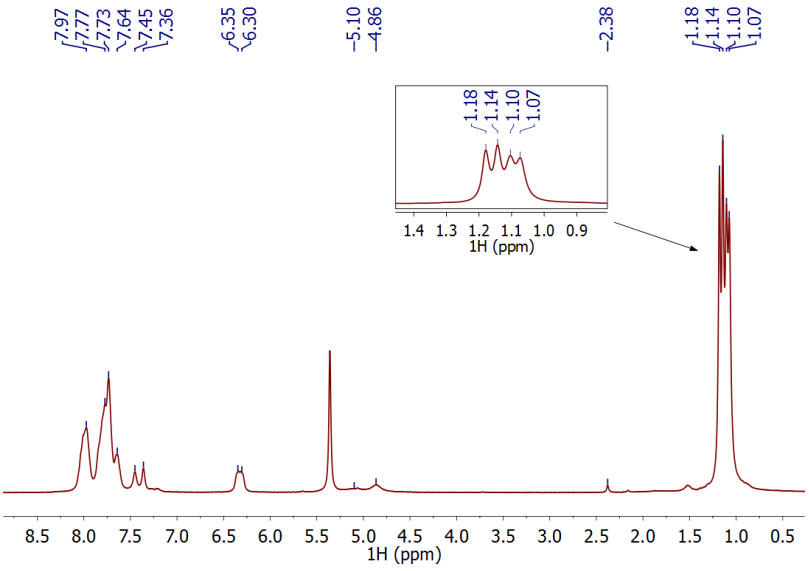

Figure 83. ^{1}H NMR spectrum of $([Ni(Psalophen)]^{+}SbF_6^{-})_2$ at 20 °C in CD_2Cl_2. Signal at 2.38 corresponds to toluene.

The signals observed in the ^{1}H NMR spectrum were assigned thanks to their integration and chemical shifts as follow: the protons of the phenyl phosphine substituents are seen

between 7.60 and 8.30 ppm, the phenoxide protons are observed at 7.46 and 7.36 ppm, the protons of the conjugated quinoid system resonate at 6.30 and 4.86 ppm, and the signal of the tert-butyl protons appear as four different singlets due to the non-symmetry of the molecule at 1.18, 1.14, 1.10 and 1.07 ppm. An additional broad signal was observed at 5.10 ppm that could not be assigned. These resonances were studied at temperatures between 34 and -90 °C.

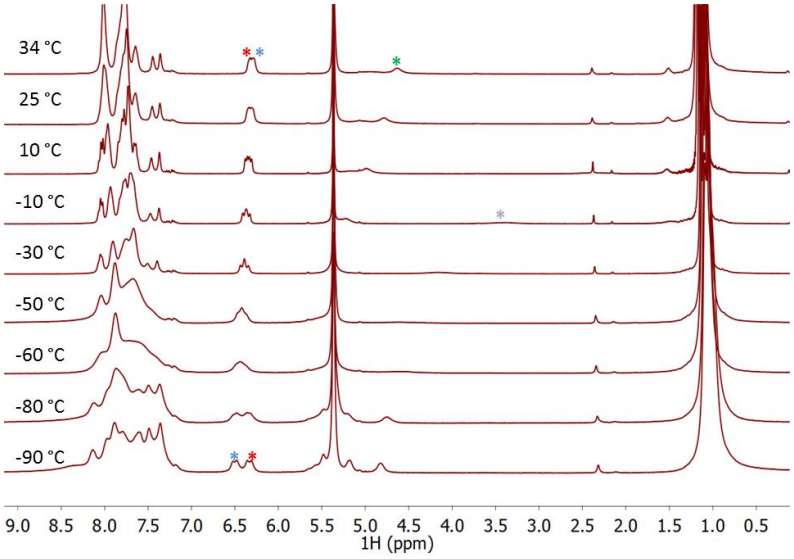

Figure 84. ^{1}H NMR spectrum of ([Ni(Psalophen)]$^{+}$SbF$_6^{-}$)$_2$ in CD_2Cl_2 at different temperatures.

Contrary to what expected for a diamagnetic compound, the signals of the ^{1}H NMR of ([Ni(Psalophen)]$^{+}$SbF$_6^{-}$)$_2$ experience significant variations with the temperature (Figure 84), suggesting a certain paramagnetic character of the complex. Some of the signals of the aromatic region shift when changing the temperature, but due to the presence of numerous signals on this region these changes could not be investigated. One of the signals assigned to the conjugated framework, marked with blue stars in Figure 84, experienced a shit from 6.29 ppm at 34 °C to 6.50 ppm at -90 °C ($\Delta\delta$ = 0.21 ppm), while the other one (red star) did not shift. Both signals are present as doublets with a coupling constant of 12.5 Hz (value obtained from the spectrum recorded at -90 °C). This constant is higher than that corresponding to an *ortho* coupling in benzene and closer to that typical of *cis* coupling in alkenes. Since the assignment of the signals was intuitive, the signals marked with red and blue stars could perfectly correspond to the protons in *ortho* position to the phosphorus in the phenoxide ring, and the coupling constant might correspond to a $^{4}J_{P,H}$ constant. Since more signals than expected are present in the VT-NMR spectra, the presence of different species in solution cannot be discarded.

The variation with the temperature of the signal assigned to a phenylene proton and marked with a green star in Figure 84 was investigated, as well as that of the signal marked with a purple star. The latter was not observed at room temperature and could not be consequently assigned. The plot of the chemical shifts versus the inverse of the temperature is shown in Figure 85. These variations are not linear with the temperature as expected for paramagnetic species following the Curie law.

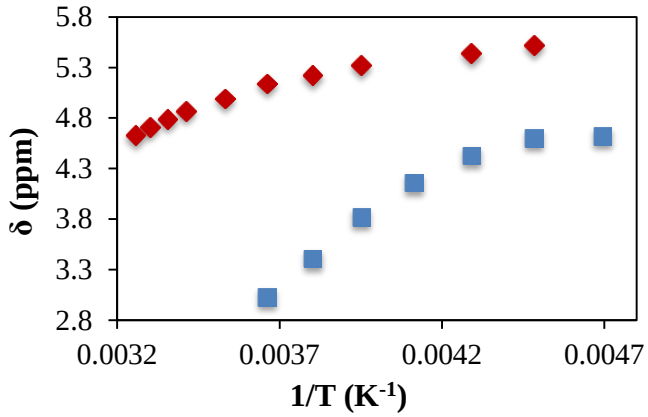

Figure 85. Plot of the chemical shifts of the protons marked with a green star (red diamonds) and the protons marked with a purple star (blue squares) with the inverse of the temperature (Figure 84).

This temperature dependence indicates a certain paramagnetism of the sample which diminishes when decreasing the temperature, since the variations are lower at low temperature. This may correspond to a spin equilibrium between the closed-shell form (Scheme 65, E), favored at low temperatures, and the diradical open-shell form (Scheme 65, F), present at rather high temperatures. Similar spin equilibrium was established for the norcorrolato species mentioned above (Scheme 62).[12a] Since $([Ni(Psalophen)]^{+}SbF_6^{-})_2$ displays a nearly diamagnetic ^1H NMR spectrum at room temperature, the amount of paramagnetic species in solution must be rather small. Qualitative information of the ratio of paramagnetic species in solution could be obtained by Evans' method measurements.[13]

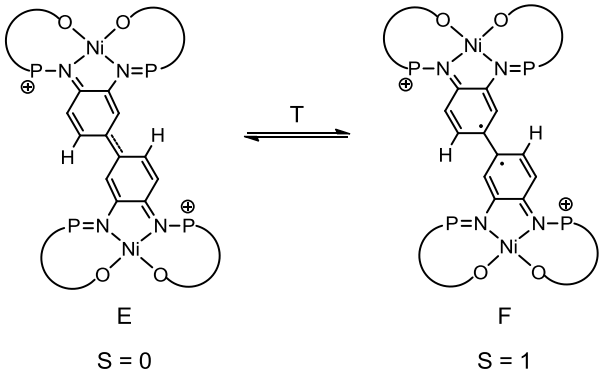

Scheme 65. Proposed singlet-triplet equilibrium for ([Ni(Psalophen)]$^{+}$SbF$_6^{-}$)$_2$.

This equilibrium might also explain the variations observed in the ^{31}P NMR spectrum throughout the temperature range studied (Figure 86). The phosphorus resonances shift from 7.1 and 3.6 ppm at 34 °C to 40.3 and 33.9 ppm at -90 °C, and become sharper when decreasing the temperature. Unexpectedly, two small signals were observed at -90 °C close to the main singlets. Since the possibility of impurities present in the sample is very unlikely, these signals could not be explained.

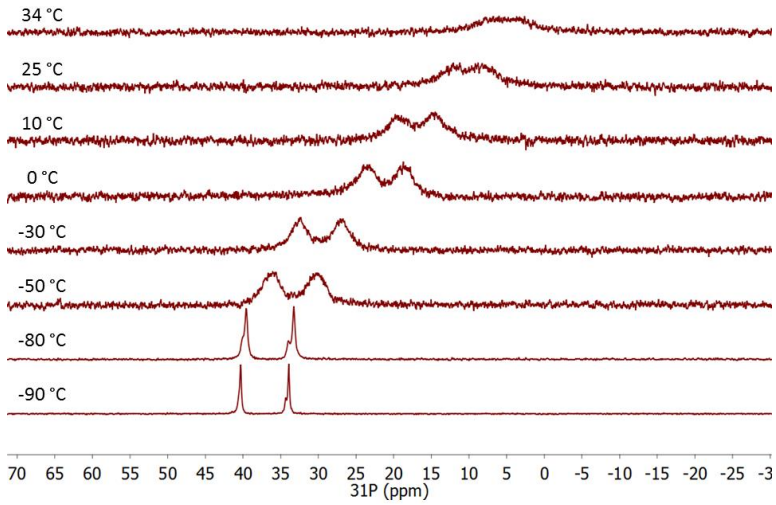

Figure 86. ^{31}P NMR spectrum of ([Ni(Psalophen)]$^{+}$SbF$_6^{-}$)$_2$ in CD_2Cl_2 at different temperatures.

([Cu(Psalophen)]$^{+}$SbF$_6^{-}$)$_2$ displays a ^{1}H NMR spectrum similar to those obtained for Cu^{II} phosphasalen complexes and a silent ^{31}P NMR spectrum, as expected for a complex containing two Cu^{II} centers. The ^{1}H NMR shows broad signals present between 0 and 14 ppm. Unlike the spectrum recorded for the neutral species [Cu(Psalophen)], two sets of signals seem to be present in the spectrum of ([Cu(Psalophen)]$^{+}$SbF$_6^{-}$)$_2$ in agreement with the dissymmetry of the molecule. Due to the broad shape of the signals, only those of the tert-butyl groups were assigned at 1.93 ppm, as a very broad signal, and at 1.30 ppm.

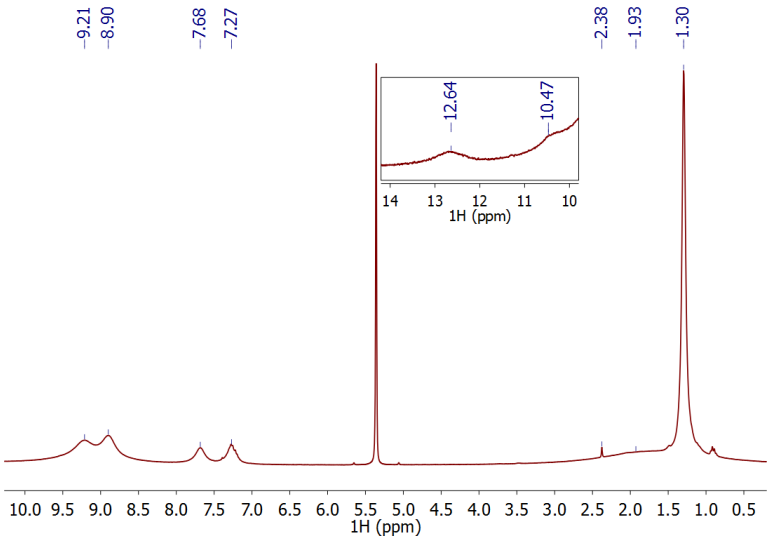

Figure 87. ^{1}H NMR spectrum of ([Cu(Psalophen)]$^{+}$SbF$_6^{-}$)$_2$ at 20 °C in CD_2Cl_2. Signal at 2.38 corresponds to toluene.

The ^{1}H NMR spectrum of ([Cu(Psalophen)]$^{+}$SbF$_6^{-}$)$_2$ was recorded between 34 and -90 °C (Figure 88). When decreasing the temperature the signals become broader and merge with the baseline.

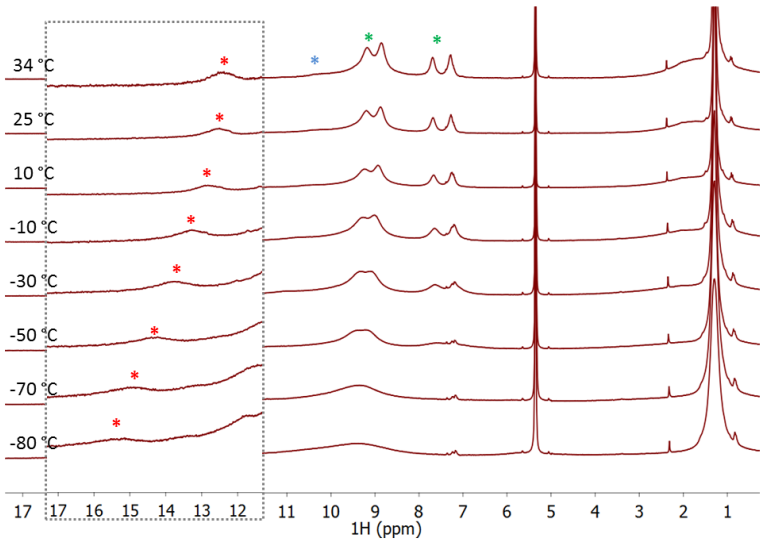

Figure 88. ^{1}H NMR spectrum of ([Cu(Psalophen)]$^{+}$SbF$_6^{-}$)$_2$ in CD_2Cl_2 at different temperatures. Inset shows a zoom of the signal marked with a red star.

The only variation with the temperature that could be investigated was that experienced by the signals marked with red stars. This signal shifts from 12.38 ppm at 34 °C to 15.34 ppm at -80 °C. Due to its small relative area this signal can correspond to one of the protons of the conjugated moiety. The plot of the chemical shifts with the inverse of the temperature is presented in Figure 89. The linear trend followed by with the temperature indicates a normal paramagnetic behavior.

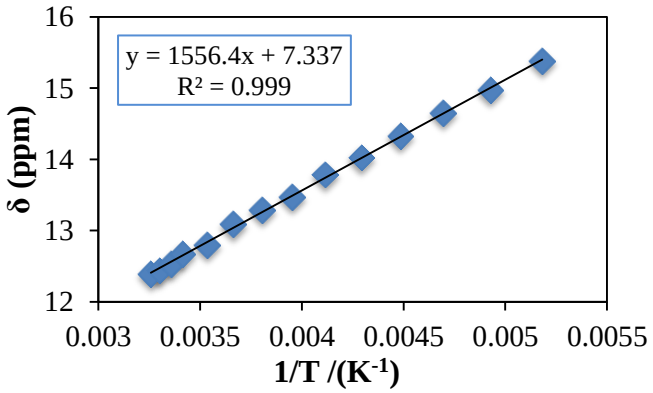

Figure 89. Plot of the chemical shifts (δ) in the 34 to -80 °C range of the signal present at 12.64 ppm at 20 °C *vs* 1/T for $([Cu(Psalophen)]^{+}SbF_6^{-})_2$.

No phosphorus signal was detected in the ^{31}P NMR spectrum throughout the temperature range studied.

5.3 EPR spectroscopy

$([Ni(Psalophen)]^{+}SbF_6^{-})_2$ and $([Cu(Psalophen)]^{+}SbF_6^{-})_2$ were studied by EPR spectroscopy in solution and in the solid state at low temperatures.

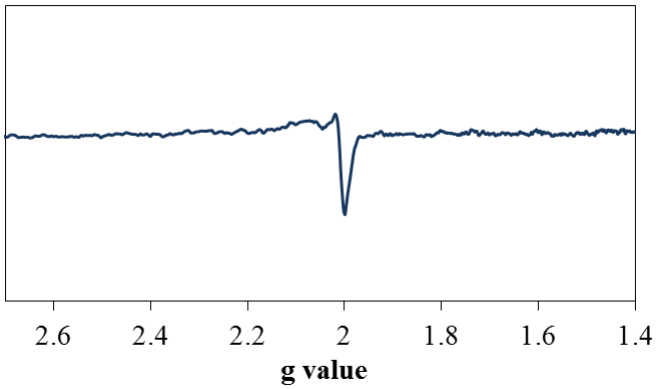

Figure 90. X-band EPR spectrum of $([Ni(Psalophen)]^{+}SbF_6^{-})_2$ in the solid state at 10 K. Conditions: Frequency: 9.640 GHz; Power: 0.5029 mW; modulation frequency: 100 kHz; amplitude: 0.8 mT.

The EPR spectrum of $([Ni(Psalophen)]^{+}SbF_6^{-})_2$ recorded for ground single crystals show a very small signal centered at g = 2.029 (Figure 90). This signal displays a pseudo-axial geometry with and $g_{\parallel}$ = 2.075 and $g_{\perp}$ = 2.007 (g_{av} = 2.029). The presence of this signal contrasts with the closed-shell structure determined by X-ray diffraction and can be explained by a weak paramagnetism of the dimer species in the solid state, or by the presence of paramagnetic impurities in the sample. A partial covalency of the double bond

formed upon dimerization, leaving some residual electronic density on each subunit would explain the weak paramagnetism observed.

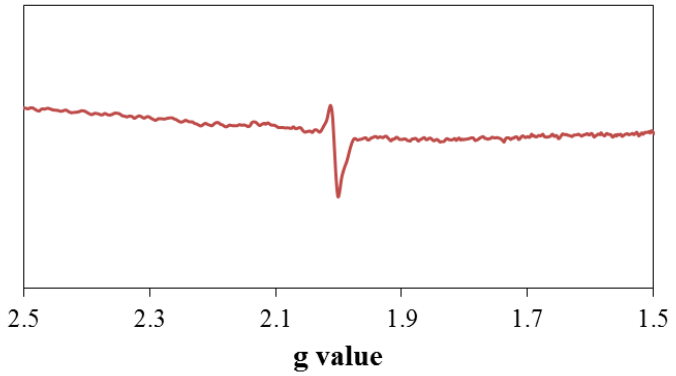

Figure 91. X-band EPR spectrum of $([Ni(Psalophen)]^{+}SbF_6^{-})_2$ in a dichloromethane at 60 K. Conditions: Frequency: 9.636 GHz; Power: 2.007 mW; modulation frequency: 100 kHz; amplitude: 0.8 mT.

The EPR spectrum was also recorded for a frozen dichloromethane solution at 60 K (Figure 91). A weak signal was also observed in solution at g = 2.007 with an isotropic symmetry indicating also a weak paramagnetism of the dimer in solution, or the presence of impurities in the sample. A small feature is present in the signal at g = 1.987 indicating a possible axial geometry where $g_x = g_y > g_z$, contrary to what observed in the solid state.

The EPR spectrum of $([Cu(Psalophen)]^{+}SbF_6^{-})_2$ recorded for ground crystals (Figure 92) at 40 K shows a complicated signal centered at g = 2.014, which corresponds to a Cu^{II} center.

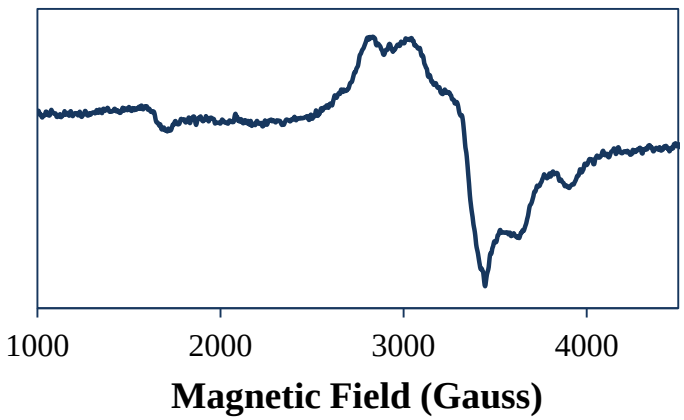

Figure 92. X-band EPR spectrum of $([Cu(Psalophen)]^{+}SbF_6^{-})_2$ in the solid state at 40 K. Conditions: Frequency: 9.637 GHz; Power: 2.002 mW; modulation frequency: 100 kHz; amplitude: 0.8 mT.

An additional feature typical of triplet states is observed at g ~ 4.1.[9-11] This indicates the presence of two electrons that are coupling ferromagnetically (S = 1), likely the unpaired electron of the copper center and an unpaired electron from a radical ligand.

The EPR spectrum of $([Cu(Psalophen)]^{+}SbF_6^{-})_2$ recorded for a frozen solution at 10 K (Figure 93) is similar to that observed for the non-crystalline species in solution (Figure 78). A signal corresponding to a Cu^{II} center is present at g = 2.060 and a triplet feature is also observed at g ~ 4.2. This signal is different to that recorded in the solid state probably due to different geometrical arrangements.

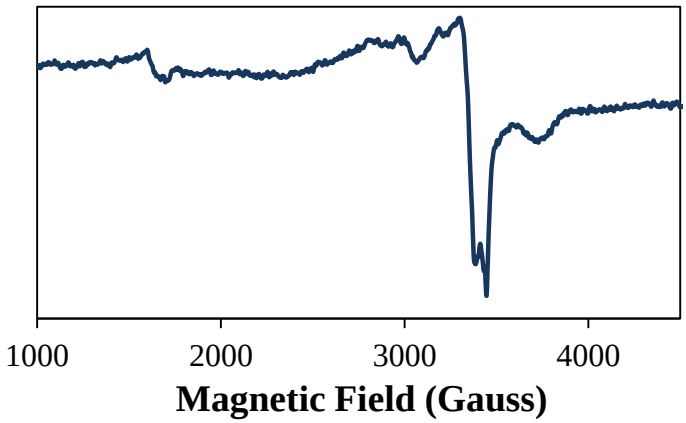

Figure 93. X-band EPR spectrum of $([Cu(Psalophen)]^{+}SbF_6^{-})_2$ in a dichloromethane solution at 10 K. Conditions: Frequency: 9.641 GHz; Power: 2.002 mW; modulation frequency: 100 kHz; amplitude: 0.8 mT. This spectrum was recorded under saturated conditions.

III. Psalophen^{Me} complexes

1. Synthesis of the ligand and neutral complexes

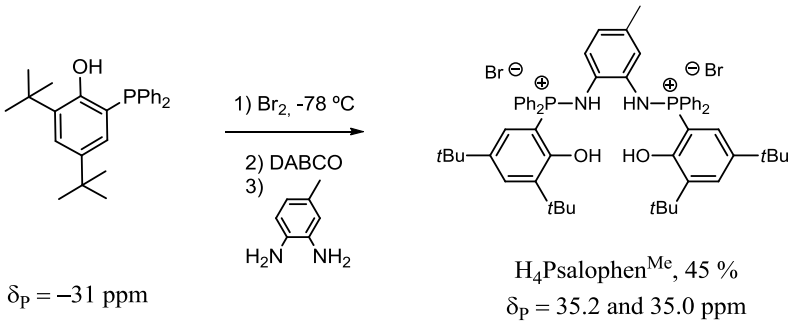

Scheme 66. Synthetic procedure for $(H_4Psalophen^{Me})Br_2$ and corresponding $^{31}P\{^1H\}$ chemical shifts in dichloromethane.

$(H_4Psalophen^{Me})Br_2$ was synthesized following the same procedure as the Psalophen ligand (Scheme 66). The formation of the bis-aminophosphonium $(H_4Psalophen^{Me})Br_2$ is evidenced by the presence of two signals at 35.2 and 35.0 ppm in the $^{31}P\{^1H\}$ NMR (the phosphorus atoms are not equivalent). Additional signals were observed at 37.7 and -33.3 ppm, corresponding to the phosphine. The DABCO salts were removed by centrifugation and the solvent was evaporated under reduced pressure. The residue was washed several times with diethyl ether and petroleum ether to remove side products, and dried under vacuum. The bis-aminophosphonium salt $(H_4Psalophen^{Me})Br_2$ was obtained as a pale pink solid in 45 % yield. The $^{31}P\{^1H\}$ NMR spectrum of $(H_4Psalophen^{Me})Br_2$ in $CDCl_3$ showed two singlets at 40.7 and 40.4 ppm. This modest yield was not optimized.

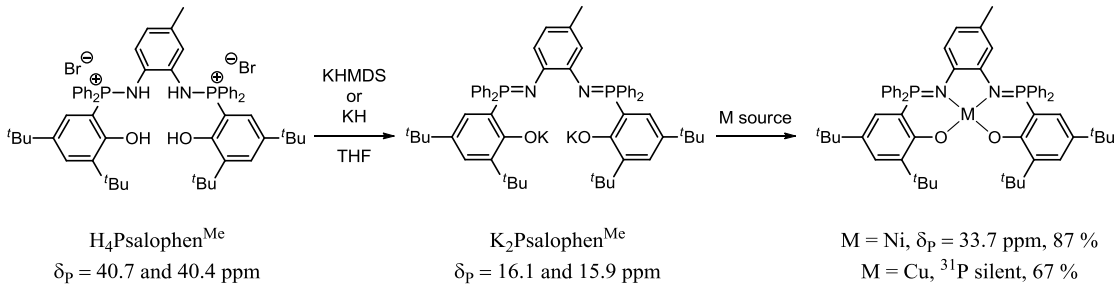

Scheme 67. Synthesis of [Ni(Psalophen^{Me})] and [Ni(Psalophen^{Me})] and their related $^{31}P\{^1H\}$ chemical shifts in THF.

The proligand was deprotonated using KHMDS in a THF solution. The disappearance of the signals of $H_4Psalophen^{Me}$ and the presence of two singlets at 16.1 and 15.9 ppm in the

$^{31}P\{^{1}H\}$ NMR evidences the completion of the deprotonation. The mixture was centrifuged to remove insoluble salts formed, and the metal precursors, either $[NiBr_2(DME)]$ or $CuBr_2$, were added. The formation of [Ni(Psalophen^{Me})] is indicated by a color change from green to blue and the apparition of a broad singlet at 33.7 ppm in the $^{31}P\{^{1}H\}$ NMR together with the disappearance of the signals from the ligand. The formation of [Cu(Psalophen^{Me})] is indicated by a silent $^{31}P\{^{1}H\}$ NMR spectrum, due to the paramagnetic nature of the complex (Cu^{II} $3d^9$ center). To obtain the complexes, the solutions were evaporated and the residues dissolved in dichloromethane and centrifuged. The solutions were concentrated and the solids were obtained by precipitation with pentane or petroleum ether. The precipitates were washed with petroleum ether and dried under reduced pressure to yield [Ni(Psalophen^{Me})] as a blue pale powder in 87 % yield, and [Cu(Psalophen^{Me})] as a pale green solid in 67 % yield. [Ni(Psalophen^{Me})], and specially [Cu(Psalophen^{Me})], are slightly soluble in petroleum ether explaining that some product was lost during the purification step.

1.1 NMR spectroscopy

[Ni(Psalophen^{Me})] displays a diamagnetic ^{1}H NMR spectrum (Figure 94) and two singlets at 30.2 and 30.0 ppm in the $^{31}P\{^{1}H\}$ NMR. The introduction of one methyl substituent in the phenylene bridge induces a dissymmetry in the molecule; as a consequence, the protons are present as two sets of signals with similar chemical shifts and coupling patterns. The ^{1}H signals were assigned to the different type of protons (PhO, PPh_2, tBu…) without being able to attribute them to a specific proton.

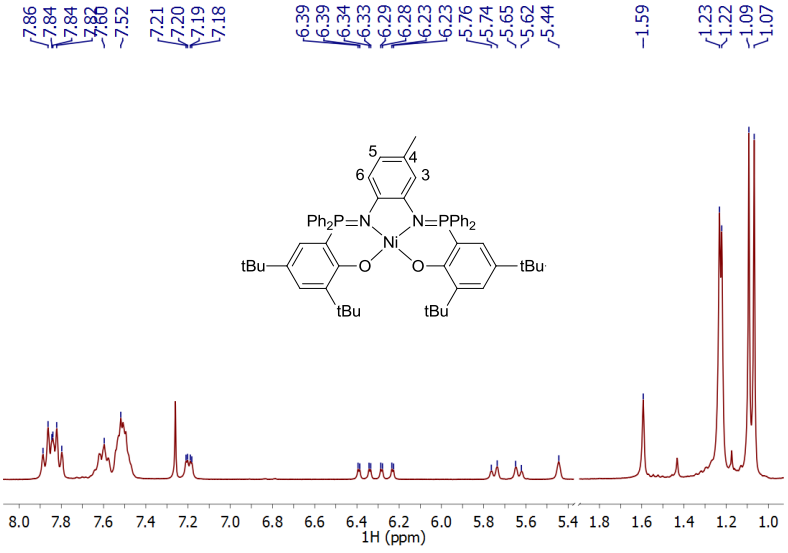

Figure 94. ^{1}H NMR spectrum of [Ni(Psalophen^{Me})] in $CDCl_3$.

The signals of the phenyl phosphine substituents are present as multiplets between 7.86 and 7.51 ppm; the protons of the phenolate ring in the *para* position of the phosphorus are present at 7.21 and 7.19 ppm as doublets ($^{4}J_{H,H}$ = 2.2 Hz); while the other phenolate protons are seen at 6.37 and 6.26 ppm as a doublet of doublets ($^{3}J_{P,H}$ = 15.8 Hz, $^{4}J_{H,H}$ = 2.2 Hz). The protons of the phenylenediamine ring are seen at 5.75 and 5.63 ppm (protons in positions 5 and 6) as doublets ($^{3}J_{H,H}$ = 8.2 Hz), and at 5.44 ppm as a singlet (proton in position 3). The protons of the methyl substituent are present at 1.59 ppm, the tert-butyl groups are present at 1.23 and 1.22 ppm, and at 1.09 and 1.07 ppm. The $^{31}P\{^{1}H\}$ NMR spectrum in $CDCl_3$ displayed two singlets at 30.22 and 30.05 ppm. A more detailed description of the ^{1}H and ^{13}C spectra is presented in the experimental part.

[Cu(Psalophen^{Me})], as a Cu^{II} $3d^9$ complex, displays a paramagnetic ^{1}H NMR spectrum (Figure 95) with broad signals that can only be tentatively assigned: the aromatic protons at 9.19 and 6.97 ppm, and the aliphatic protons, *i.e.*, the two t-butyl substituents and the methyl group at 1.71, 1.21 and 1.08 ppm, respectively. Nevertheless, the integration is not precise enough to determine if all the protons were included in these four signals. No ^{31}P signal was observed.

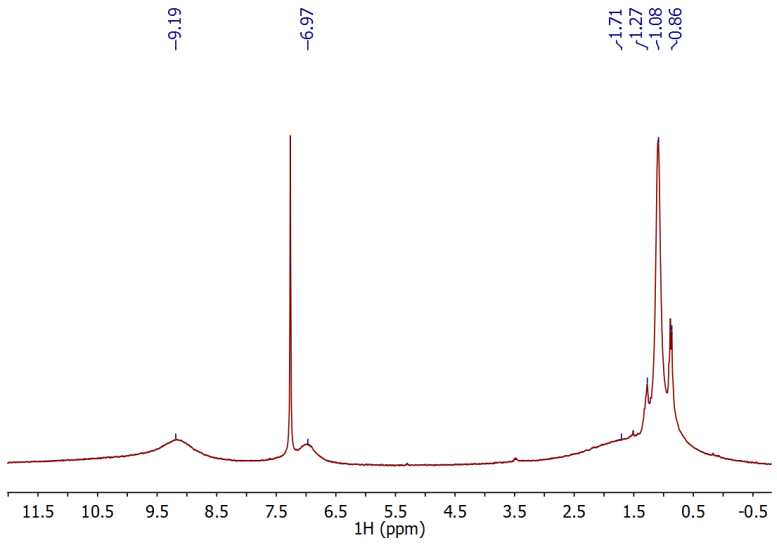

Figure 95. ^{1}H NMR spectrum of [Cu(Psalophen^{Me})] in $CDCl_3$. The signal at 1.27 and 0.86 ppm corresponds to pentane.

1.2 EPR spectroscopy

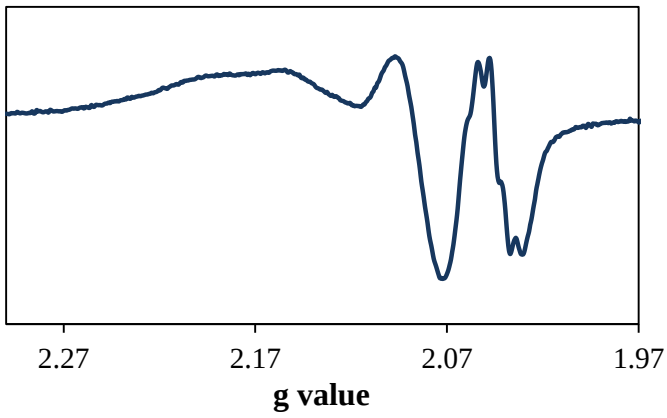

Figure 96. X-band EPR spectrum of [Cu(Psalophen^{Me})] in dichloromethane at 295 K. Conditions: Frequency: 9.810 GHz; Power: 4.004 mW; modulation frequency: 100 kHz; amplitude: 0.4 mT. Solid line: experimental spectrum; dotted lines: simulated spectrum.

The EPR spectrum of [Cu(Psalophen^{Me})] displays a rhombic signal centered at g = 2.11 different to that recorded for previous Cu^{II} phosphasalen complexes. A four-line pattern cannot be distinguished here since the two features around g = 2.17 are very close and appear as a broad transition. An superhyperfine coupling is seen in g_3, likely due to the coupling with the nitrogen atoms as reported for the other phosphasalen complexes. The introduction of the methyl group in the ligand backbone seems to induce a change in the electronics of the copper, since it displays a different EPR spectrum than the previously studied phosphasalen copper complexes.

1.3 UV-visible spectroscopy

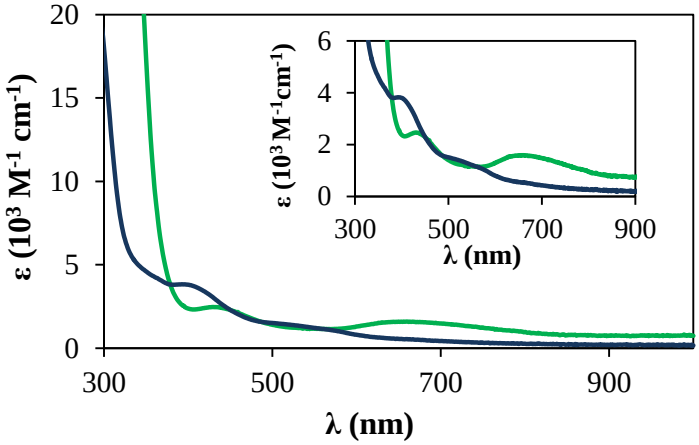

Figure 97. UV-vis spectra of [Cu(Psalophen^{Me})] (green line) and [Ni(Psalophen^{Me})] (blue line) in dichloromethane. Inset shows a zoom of the visible region.

The UV-vis spectrum of [Ni(Psalophen^{Me})] shows two weak bands at 550 nm (1300 M^{-1} cm^{-1}) and 408 nm (3800 M^{-1} cm^{-1}). The former can be assigned to a MLCT as in the previous complexes.[14] The later may be related to a transition involving the phenylene ring, since it was not observed for [Ni(Psalen^{tBu})] and [Ni(Psalen^{OMe})]. [Ni(Psalophen)] displays similar bands at 510 and 380 nm.

The UV-vis spectrum of [Cu(Psalophen^{Me})] shows also two weak bands at 660 nm (1600 M^{-1} cm^{-1}) and 430 nm (2500 M^{-1} cm^{-1}), and an intense transition above 350 nm (Figure 97, green line), similar to those observed for [Cu(Psalophen)] at 440, 640 and 390 nm. These bands were also observed for other phosphasalen complexes, such as [Cu(Psalen^{OMe})] or [Cu(Psalen^{tBu})]. The band at 660 nm was attributed to a d-d transition typical of Cu^{II} $3d^9$ complexes;[1b] the band at 440 nm, which is not present in the salen derivatives, may be related to a transition involving the iminophosphorane function. The band at 350 nm was assigned to a charge-transfer transition according to the literature.[1a]

1.4 X-ray diffraction

Crystals of [Ni(Psalophen^{Me})] and [Cu(Psalophen^{Me})] suitable for X-ray diffraction were obtained from saturated toluene solutions stored in the fridge.

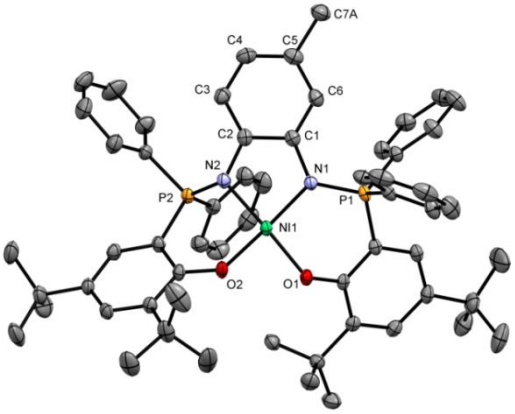

Figure 98. ORTEP of [Ni(Psalophen^{Me})] with thermal ellipsoids at 50 % probability. Hydrogen atoms and a molecule of toluene have been omitted for clarity.

[Ni(Psalophen^{Me})] presents a distorted square planar geometry around the metal center with a torsion angle of the main plane of 12.13 ° (Figure 98). This is the largest torsion observed for all the series of neutral Ni phosphasalen complexes; for the [Ni(Psalophen)] complex this torsion is 8.16 °. [Ni(Psalophen^{Me})] displays Ni-O and Ni-N bond distances similar to those observed for the unsubstituted phenylene derivative: Ni-N bonds measure 1.890(3) Å for [Ni(Psalophen^{Me})] versus 1.903(3) and 1.891(3) Å for [Ni(Psalophen)],

while the Ni-O bond distances are 1.865(2) and 1.875(2) Å for [Ni(Psalophen^{Me})] versus 1.851(2) and 1.880(2) Å for [Ni(Psalophen)]. The similar Ni-O and Ni-N bonds observed for [Ni(Psalophen^{Me})] suggest that the mono-substitution of the central ring does not influence much the coordination sphere of the metal center.

An unusual feature already observed in the structure of [Ni(Psalophen)], but not in those of the alkyl-bridged phosphasalen derivatives, was also observed for [Ni(Psalophen^{Me})]. One of the nitrogen atoms presents an almost tetrahedral geometry while the other nitrogen is close to a trigonal planar arrangement. Ni-N2-C2, C2-N2-P2, and P2-N2-Ni angles measure 112, 123 and 107 °, while these angles are at 113, 124 and 123 ° for Ni-N1-C1, C1-N1-P1 and P1-N1-Ni, respectively. So, while the N1-P1 bond stays in the NOON plane, the N2-P2 bond is placed above this plane. Albeit this different geometry, the N-P bond distances are very similar (1.620(2) and 1.625(2) Å).

	[Ni(Psalophen^{Me})]	**[Cu(Psalophen^{Me})]**
M-O1	1.875(2)	1.895(2)
M-O2	1.865(2)	1.895(2)
M-N1	1.890(3)	1.944(2)
M-N2	1.890(3)	1.944(2)
P1-N1	1.620(2)	1.610(2)
P2-N2	1.625(2)	1.610(2)
Torsion angle[a]	12.13	24.11

Table 22. Selected bond lengths (Å) and angles (°) for [Ni(Psalophen^{Me})] and [Cu(Psalophen^{Me}]. [a] Torsion of the NOON plane.

[Cu(Psalophen^{Me})] also displays a square planar geometry around the metal center with a significant tetrahedral distortion of the main plane, 24.11 °. This contrasts drastically with the planarity observed for the unsubstituted [Cu(Psalophen)] complex, whose torsion angle measures 0.48 ° (Figure 99). This distortion is even larger than those observed for the alkyl-bridged phosphasalen complexes [Cu(Psalen^{tBu})], [Cu(Psalen^{OMe})] and [Cu(^{iPr}Psalen)]. The angles of the N-Cu-O segments are 161.44 ° for both (the structure possesses a C2 symmetry axis), far from the 180 ° expected for ideal square planar structures.

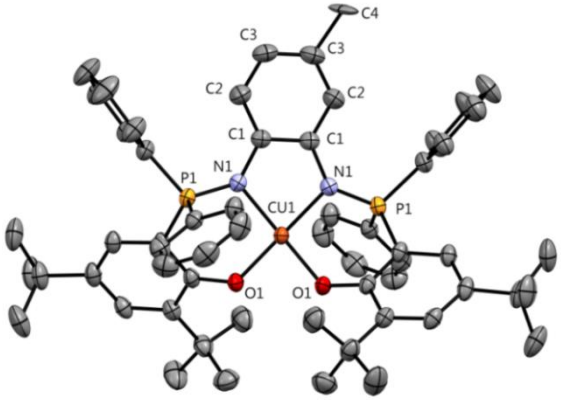

Figure 99. ORTEP of [Cu(Psalophen^{Me})] with thermal ellipsoids at 50 % probability. Hydrogen atoms and two molecules of toluene have been omitted for clarity.

The Cu-O bond distances measure 1.895(2) Å and the Cu-N 1.944(2) Å. These distances are significantly shorter compared to those in [Cu(Psalophen)], for which Cu-N bonds lengths measure 1.903(3) and 1.891(3) Å, and the Cu-O measure 1.966(2) and 1.940(2) Å. The differences in the metrical parameters of these two complexes are very large compared to the small modification introduced in the structure. The structure being symmetric, no difference in the geometry of the N atoms was observed, contrary to [Ni(Psalophen^{Me})], which suggests that this feature is typical for nickel phosphasalophen derivatives.

1.5 Electrochemical studies

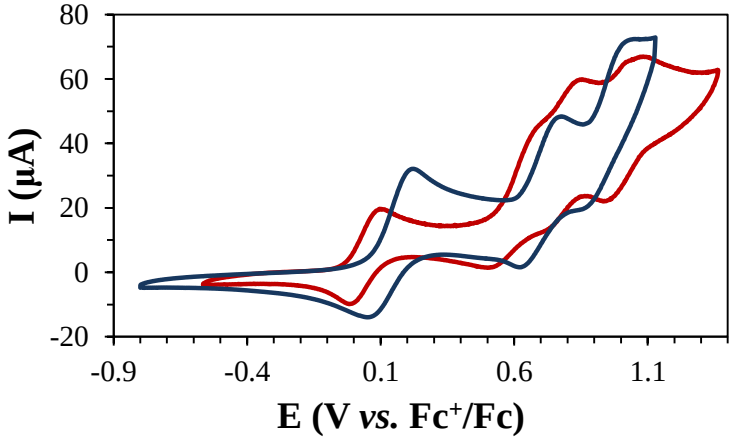

Figure 100. Cyclic voltammograms of [Cu(Psalophen^{Me})] (blue line) and [Ni(Psalophen^{Me})] (red line) recorded in dichloromethane. Conditions: 3 mM of complex in dichloromethane at 0.1 V/s.

The cyclic voltammogram of [Ni(Psalophen^{Me})] shows a reversible oxidation at $E^1_{1/2}$ = 0.04 V, two irreversible oxidations at $E^2_{p,a}$ = 0.70 V and $E^3_{p,a}$ = 0.85 V, and a third pseudo-reversible oxidation at $E^4_{1/2}$ = 1.03 V. As for [Ni(Psalophen)], the four redox processes may

correspond to the oxidation of the metal center, the phenyl bridge and the two phenoxide rings. The first oxidation occurs at lower potential compared to the unsubstituted [Ni(Psalophen)] (0.15 V). If the oxidation takes places also in the phenylene ring, the introduction of the methyl group seems to favor it. The second and third oxidations take place at potentials very similar to those observed for [Ni(Psalophen)]. The gap between the first and the second oxidation is $\Delta E_{1\text{-}2}$ = 0.66 V, very similar to that obtained for [Ni(Psalophen)] (0.63 V). This suggests that their oxidized species possess very similar electronic structure. The assignment of the different redox processes is not achievable with this sole data, for which spectro-eletrochemistry experiments will be necessary

Compound	$E^1_{1/2}$	$E^2_{p,a}/E^2_{1/2}$	$E^3_{p,a}$	$E^4_{p,a}$
[Ni(Psalophen)]	0.15	0.78	1.09	-
[Ni(Psalophen^{Me})]	0.04	0.70	0.85	1.03
[Cu(Psalophen)]	0.28	0.76	1.01	-
[Cu(Psalophen^{Me})]	0.14	0.70	0.95	-

Table 23. Redox potentials for [M(Psalophen)] and [M(Psalophen^{Me})] complexes, expressed in V *vs* Fc^+/Fc.

The cyclic voltammogram of [Cu(Psalophen^{Me})] displays a reversible oxidations at $E^1_{1/2}$ = 0.14 V, a pseudo-reversible at $E^2_{1/2}$ = 0.70 V and an irreversible oxidation at $E^3_{p,a}$ = 0.95 V. As for [Ni(Psalophen^{Me})], these values are lower than those observed for the unsubstituted analogue [Cu(Psalophen)] ($E^1_{1/2}$ = 0.28 V), suggesting that the methyl substitution facilitates the oxidation of the phenyl ring. Nevertheless, in this case the first oxidation corresponds to a two-electron oxidation process. This voltammogram differs from the nickel analogue. In the series of phosphasalen complexes studied, nickel and copper derivatives used to display similar electrochemical behaviors. It does not seem to be the case in phosphasalophen complexes. The methyl substitution influences differently on the structure of these complexes. Second and third oxidations present a gap of 0.25 V, similar to that observed in [Cu(Psalophen)]. The assignment of the oxidation processes must be completed with spectro-electrochemistry experiments.

2. Oxidation of neutral complexes

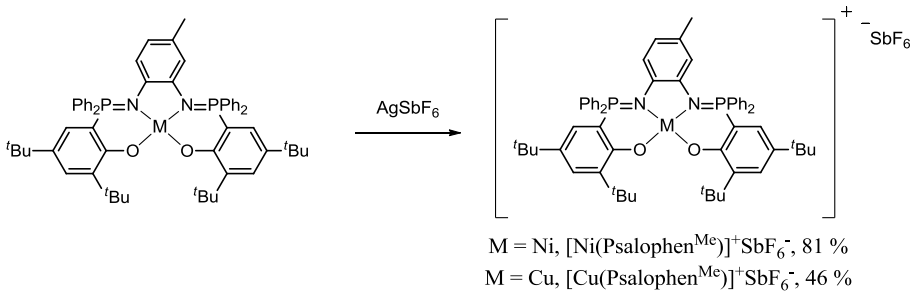

Scheme 68. Chemical oxidation of [Ni(Psalophen^{Me})] and [Cu(Psalophen^{Me})] complexes.

The oxidized products [Ni(Psalophen^{Me})]$^{+}$SbF$_6^{-}$ and [Cu(Psalophen^{Me})]$^{+}$SbF$_6^{-}$ were obtained by reaction of the neutral complexes with one equivalent of AgSbF$_6$ in dichloromethane under inert atmosphere (Scheme 68). For [Ni(Psalophen^{Me})]$^{+}$SbF$_6^{-}$, the addition of AgSbF$_6$ induced a color change from blue to dark blue and the disappearance of the ^{31}P signals. However, no significant color change was observed in the solution of [Cu(Psalophen^{Me})]$^{+}$SbF$_6^{-}$, which remained green, while no apparition of any ^{31}P signal was observed. The solutions were filtered, concentrated, and precipitation of the products was induced by addition of petroleum ether. The powders were washed with petroleum ether and dried under vacuum. [Ni(Psalophen^{Me})]$^{+}$SbF$_6^{-}$ was obtained as a dark powder in 81 % yield, and [Cu(Psalophen^{Me})]$^{+}$SbF$_6^{-}$ as green solid in 46 % yield. Different attempts of crystallization were made for these complexes, but none of them was yet successful. The typical crystallization mixtures used for other phosphasalen complexes, including dichloromethane/pentane or toluene/pentane, resulted in the formation of an oily product.

3. Characterization of the oxidized complexes [Ni(Psalophen^{Me})] and [Cu(Psalophen^{Me})]

3.1 NMR spectroscopy

Both [Ni(Psalophen^{Me})]$^{+}$SbF$_6^{-}$ and [Cu(Psalophen^{Me})]$^{+}$SbF$_6^{-}$ complexes displayed paramagnetic ^{1}H NMR spectra.

[Ni(Psalophen^{Me})]$^{+}$SbF$_6^{-}$ could not be obtained as a pure complex. Some diamagnetic signals from the neutral species [Ni(Psalophen^{Me})] remain present in the ^{1}H NMR

spectrum, due probably to the low stability of the generated oxidized species. The similar solubility of both neutral and oxidized complexes, and the impossibility to crystallize [Ni(Psalophen^{Me})]$^{+}$$SbF_6^-$, did not allow us to purify it. Figure 101 shows two superimposed spectra of [Ni(Psalophen^{Me})]$^{+}$ obtained from two independent oxidation reactions.

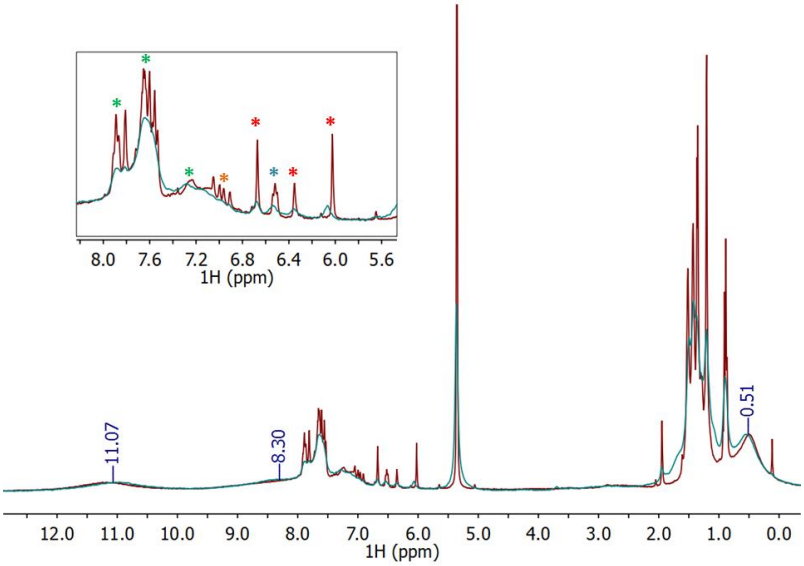

Figure 101. ^{1}H NMR spectra of [Ni(Psalophen^{Me})]$^{+}$ in CD_2Cl_2. Inset shows a zoom of the aromatic region.

The signals at 11.07, 8.30 and 0.51 ppm display a broad shape and were attributed to the paramagnetic species [Ni(Psalophen^{Me})]$^{+}$, while the narrow signals present in the aromatic and the aliphatic region must be related to the diamagnetic impurity. When comparing both spectra, the signals at 11.07, 8.30 and 0.51 ppm have the same intensity, whereas the intensity of the diamagnetic signals (notably those of the aliphatic region) is different. These intensity differences indicate that these two set of signals (paramagnetic and diamagnetic) are not related, confirming the presence of two species in solution: [Ni(Psalophen^{Me})]$^{+}$ and [Ni(Psalophen^{Me})]. As a consequence, two signals were present in the ^{31}P NMR spectrum at 42.6 and 42.2 ppm.

Apart from the signals at 11.07, 8.30 and 0.51 ppm, no other signals were observed in a 200 ppm spectral width range for [Ni(Psalophen^{Me})]$^{+}$ which may indicate a strong radical ligand character. When the metal is involved in the oxidation process, like for [Ni(Psalen^{tBu})], [Ni(Psalen^{OMe})] and [Ni(Psalen^{iPr})], the chemical shifts are observed in a larger spectral window (*e.g.* 20.65 ppm in [Ni(Psalen^{iPr})]$^{+}$).

The ^{1}H NMR spectrum was recorded at different temperatures in order to study the variation of the signals with the temperature and/or the apparition of new signals. When

decreasing the temperature, only the signals attributed to the paramagnetic species experienced variations. Despite high concentration of the NMR sample (14 mg in 0.4 mL), the spectrum displays very broad signals and their variation with the temperature could not be further investigated.

[Cu(Psalophen^{Me})]$^+$ also displays a paramagnetic ^{1}H NMR spectrum which was very similar to that of the neutral complex [Cu(Psalophen^{Me})] (Figure 95Figure 102).

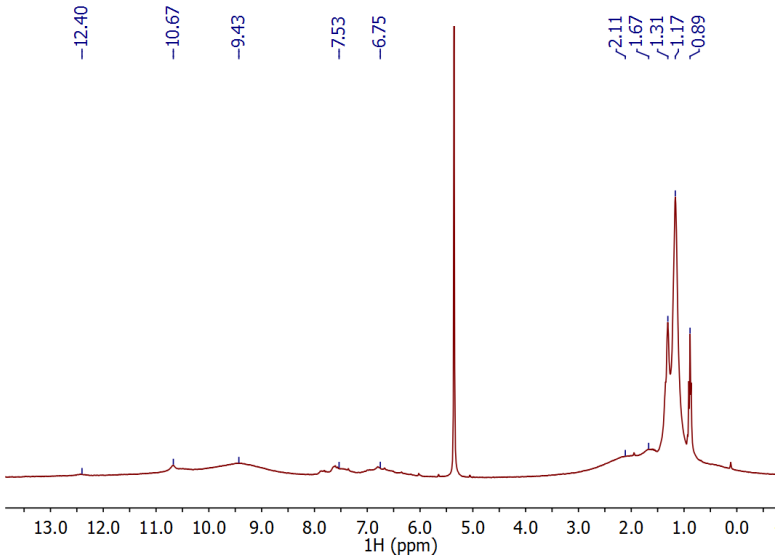

Figure 102. ^{1}H NMR spectrum of [Cu(Psalophen^{Me})]$^+$ in CD_2Cl_2. Signals at 1.31 and 0.89 ppm correspond to pentane.

For [Cu(Psalophen^{Me})]$^+$, large signals are present at 9.43, 2.11, 1.67 and 1.17 ppm, similar to those observed for [Cu(Psalophen^{Me})], which contrasts with the presence of other narrow signals at 12.40, 10.67, 7.53 and 6.75 ppm. These narrow signals may be due to a decomposition of the oxidized product leading to diamagnetic species. Actually, two small signals are observed at 42.6 and 42.2 ppm in the ^{31}P NMR spectrum after long acquisition duration. The few differences observed between the spectra of [Cu(Psalophen^{Me})] and [Cu(Psalophen^{Me})]$^+$, and the lack of color change upon oxidization preclude to conclude about the oxidation process. This spectrum contrasts with those of the alkyl-bridged [Cu(Psalen^{tBu})]$^+$, [Cu(Psalen^{OMe})]$^+$ and [Cu(Psalen^{iPr})]$^+$ phosphasalen complexes which displayed apparent diamagnetic spectra. This points towards a more radical ligand character in [Cu(Psalophen^{Me})]$^+$ since the spectrum does not show proper signals, in spite of the high concentration of the sample (15 mg in 0.4 mL of CD_2Cl_2).

The ^{1}H NMR spectrum was recorded at different temperatures but no large variations were observed. The signals broaden when decreasing the temperature and merge with the baseline so that the variation of the chemical shifts with the temperature could not be investigated. For $[Cu(Psalophen^{Me})]^{+}$, VT-NMR does also not provide useful information about the electronic structure of the complex.

3.2 EPR spectroscopy

EPR spectra were recorded at different temperatures for both oxidized $[Ni(Psalophen^{Me})]^{+}$ and $[Cu(Psalophen^{Me})]^{+}$ complexes.

The EPR spectrum of $[Ni(Psalophen^{Me})]^{+}$ at room temperature displays an isotropic signal centered at g_{iso} = 2.035 with a peak-to-peak line width of 50 G (Figure 103). This contrasts with the signal observed for $[Ni(Psalophen)]^{+}$, or $[Ni(Psalen^{OMe})]^{+}$.

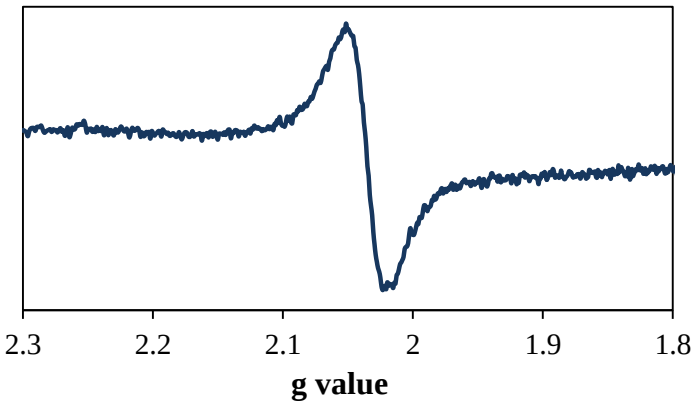

Figure 103. X-band EPR spectrum of $[Ni(Psalophen^{Me})]^{+}$ in dichloromethane at room temperature.

This spectrum is similar to those reported by the teams of J. Reedijk and J-L- Pierre for $[Ni(Salophen)]^{+}$ and $[Ni(Salophen^{Me})]^{+}$ complexes.[15] In the case of $[Ni(Salophen)]^{+}$, an isotropic signal centered at g_{iso} = 2.034 with a peak to peak line width of 31 G was observed at 260 K. In that case, the oxidized species $[Ni(Salophen)]^{+}$ was described as a ligand radical complex with a small contribution of the metal orbitals in the SOMO of the complex. For $[Ni(Salophen^{Me})]^{+}$ also an isotropic signal was observed centered at g_{iso} = 2.04 with a peak to peak line width of 100 G. [15]

When decreasing the temperature below the melting point of the solvent (dichloromethane, 176 K), the spectrum changes and displays a rhombic signal at g_{av} = 2.030. The g values obtained by simulation are: g_1 = 2.098, g_2 = 2.005 and g_3 = 1.987, and remain the same between 140 and 10 K. The intensity of the signal increases when

decreasing the temperature as can be noticed in Figure 104. At 160 K (temperature close to the liquid-solid phase transition), the spectrum displays an axial signal with $g_{\parallel}$ = 2.092 and $g_{\perp}$ = 2.005 (Figure 104, pink line); these g values are intermediate between those obtained at room and low temperatures.

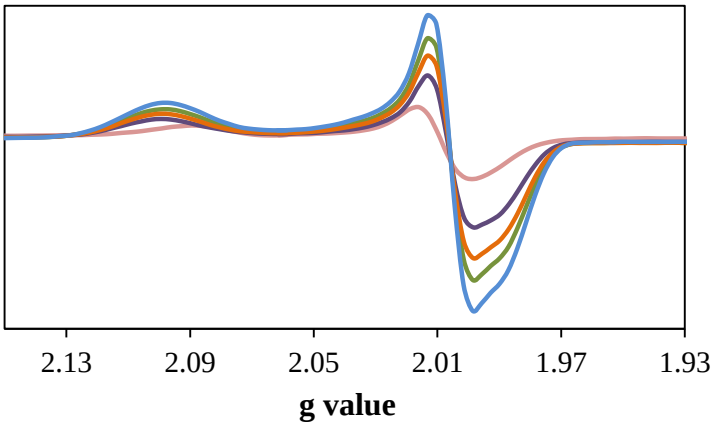

Figure 104. X-band EPR spectrum of [Ni(Psalophen^{Me})]$^{+}$ in dichloromethane at 80 K (blue line), 100 K (green line), 120 K (orange line), 140 K (purple line) and 160 K (pink line).

This change in the symmetry of the signal at low temperature was also observed for [Ni(Salophen)]$^{+}$ and [Ni(Salophen^{Me})]$^{+}$. [Ni(salophen)]$^{+}$ displays at low temperatures a rhombic signal characterized by g_1 = 2.270, g_2 = 2.220 and g_3 = 2.022 (g_{av} = 2.17),[1a,4b] which is typical of Ni^{III} complexes.[8] A temperature-dependent valence tautomerism, between the Ni^{III} and the ligand radical configuration, is one of the possible explanations for this change. Another one is the difference of the relaxation times for both the radical and the Ni^{III} center: the metal center relaxes faster than the radical, so that the signal of the metal is only observed at low temperature and at room temperature only the radical contribution is observed.[1a]

On the other hand, the spectrum of [Ni(Salophen^{Me})]$^{+}$ recorded below 170 K showed a rhombic signal with g_1 = 2.10, g_2 = 2.02 and g_3 = 2.00.[16] The g_{av} = 2.04 of this signal matches perfectly with the g_{av} obtained for the spectrum recorded at room temperature (g_{av} = 2.04). Both signals were attributed to Ni(II)-radical species which remained stable throughout the 10-240 K temperature range.

For [Ni(Psalophen^{Me})]$^{+}$ the g_{av} value obtained at room temperature (g_{av} = 2.035) is very similar to that obtained at low temperatures (g_{av} = 2.030) and indicates that the species present at room and low temperature possess similar SOMOs, and their anisotropy changes with the phase of the solvent. The g values obtained are intermediate between the typical g values of Ni^{III} centers (~ 2.13-2.17),[8] and the g values characteristic of

phenoxyl[7] (and diaminobenzene) radicals (2.005).[6,17] Thus, [Ni(Psalophen^{Me})]$^+$ can be formulated as a Ni(II)-radical ligand with a small metal contribution into the SOMO orbital. The nature of this radical species, either phenoxyl or diaminobenzene radical, as well as the extent of the delocalization remain yet unknown for [Ni(Psalophen^{Me})]$^+$ after EPR studies. However, the formation of a diaminobenzene radical is more likely since this was already the case for the unsubstituted [Ni(Psalophen)]$^+$ complex.

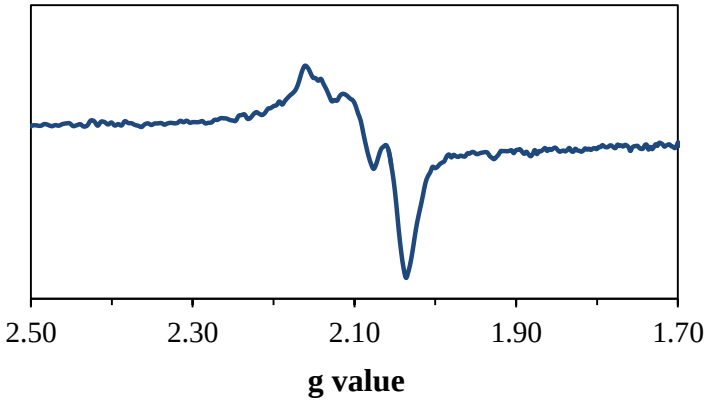

Figure 105. X-band EPR spectrum of [Cu(Psalophen^{Me})]$^+$ in dichloromethane at 293 K. Frequency: 9.360 GHz; Power: 1.003 mW; modulation frequency: 100 kHz; amplitude: 1 mT.

At room temperature, [Cu(Psalophen^{Me})]$^+$ displays a complicated spectrum centered at g = 2.077 which could not be interpreted (Figure 105). This spectrum differs from that of the neutral species [Cu(Psalophen^{Me})] (Figure 96) indicating that the oxidation of the complex was successful achieved despite the lack of color change during the oxidation reaction.

When decreasing the temperature, the spectrum of [Cu(Psalophen^{Me})]$^+$ is better defined and a four-line pattern corresponding to an hyperfine coupling with the Cu center (I = 3/2) appears.

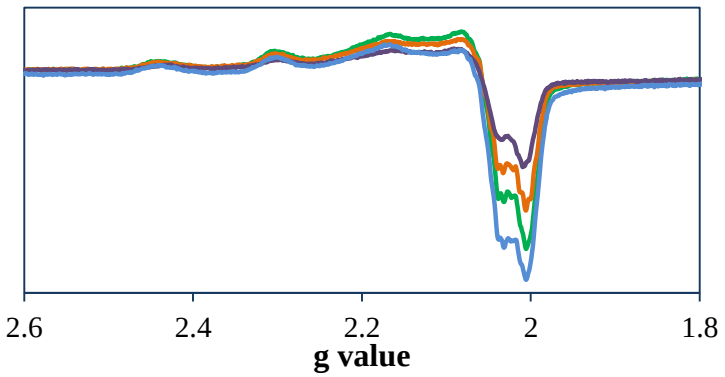

Figure 106. X-band EPR spectrum of [Cu(Psalophen^{Me})]$^+$ in dichloromethane at 80 K (blue line), 100 K (green line), 130 K (orange line), 150 K (purple line).

This spectrum displays a signal centered at g = 2.21. The g values drawn from the EPR spectrum are g_1= 2.32, g_2= 2.19, and g_1= 2.06. This spectrum is down-field shifted compared to that obtained for [Cu(Psalophen^{Me})] and seems to display larger A_{Cu} coupling constants. The differences between the spectra of the neutral and oxidized species indicate a change of the electronic density in the metal center upon oxidation. However, no ligand signal or triplet feature were observed in the spectrum, suggesting that no radical ligand species are present in solution. Since the cyclic voltammetry shows a first two-electron redox process, it is possible that a double oxidation of the ligand had occurred. The resulting dicationic species [Cu(Psalophen^{Me})]$^{2+}$ possesses a Cu^{II} center, and the ligand in a closed-shell configuration. This may explain the presence of the Cu^{II} signal and the absence of any radical feature.

As for [Ni(Psalophen^{Me})]$^{+}$, the oxidation of the phenylene ring is more likely than the oxidation of the phenolate due to the electron-donation of the nitrogen lone pairs and the methyl group.

3.3 UV-vis spectroscopy

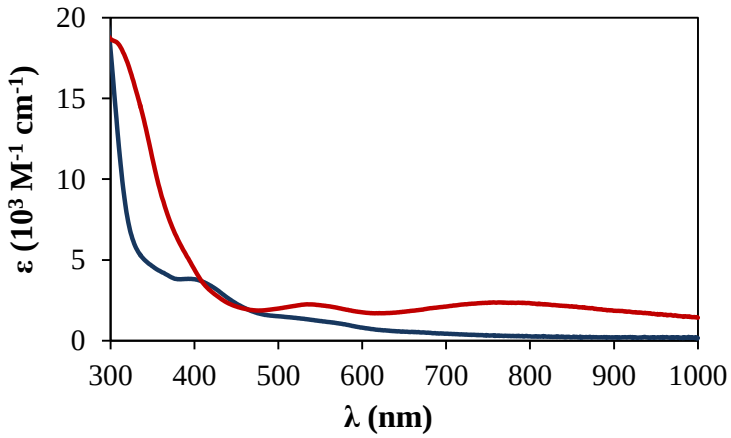

Figure 107. UV-vis spectra of [Ni(Psalophen^{Me})] (blue line) and oxidized [Ni(Psalophen^{Me})]$^{+}$ (red line) in dichloromethane.

The UV-vis spectrum of [Ni(Psalophen^{Me})]$^{+}$ showed two weak bands at 530 nm (2200 M^{-1} cm^{-1}) and 775 nm (2300 M^{-1} cm^{-1}), and an intense band above 330 nm (Figure 107, red line). From the intensity the band at 530 nm may correspond to a charge transfer transition. The band at 775 nm has also been observed for other nickel phosphasalen complexes and may be related to a transition involving the iminophosphorane function. This spectrum contrasts with those of the alkyl-bridged oxidized phosphasalen complexes [Ni(Psalen^{tBu})]$^{+}$, [Ni(Psalen^{OMe})]$^{+}$ and [Ni(^{iPr}Psalen)]$^{+}$ which were characterized by the

presence of two intense bands around 500 and 1000 nm, and confirms the shift of the oxidation locus to the phenyl bridge.

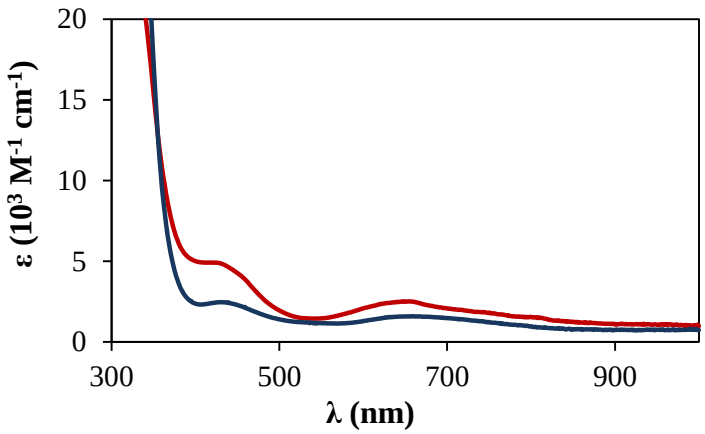

Figure 108. UV-vis spectra of [Cu(Psalophen^{Me})] (blue line) and oxidized [Cu(Psalophen^{Me})]$^{+}$ (red line) in dichloromethane.

The UV-vis spectrum of [Cu(Psalophen^{Me})]$^{+}$ differed only slightly from that of the neutral complex [Cu(Psalophen^{Me})]. Both weak bands observed in [Cu(Psalophen^{Me})] seem reinforced and slightly blue-shifted upon oxidation. The UV-vis spectrum of [Cu(Psalophen^{Me})]$^{+}$ displayed a weak band at 645 nm (2500 M^{-1} cm^{-1}) and a more intense band at 430 nm (4900 M^{-1} cm^{-1}). This spectrum is different from those obtained for the Psalen derivatives and confirms, as in the case of [Ni(Psalophen^{Me})]$^{+}$ the shift of the oxidation locus to the aromatic bridge.

3.4 Magnetic measurements

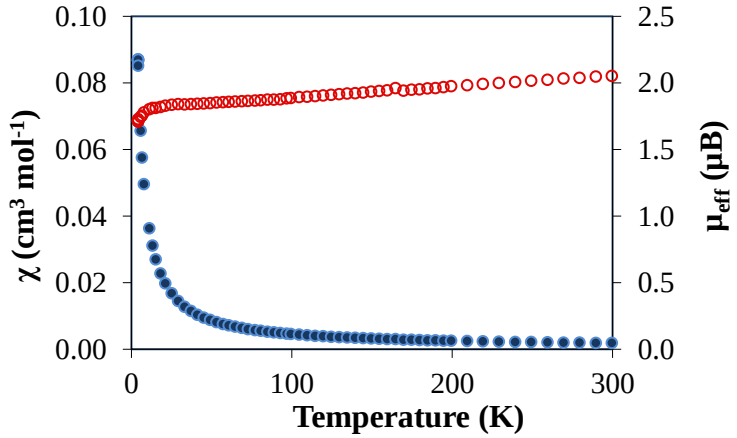

Figure 109. Plot of magnetic susceptibility (blue circles) and effective magnetic moment (red circles) *vs.* temperature for [Ni(Psalophen^{Me})]$^{+}SbF_6^{-}$.

The magnetic properties of [Ni(Psalophen^{Me})]$^{+}$SbF$_6^{-}$ were also studied in the solid state using a SQUID magnetometer. [Ni(Psalophen^{Me})]$^{+}$SbF$_6^{-}$ follows the Curie-Weiss law with a Curie constant of C = 0.436 cm^3 K mol^{-1}, a Weiss temperature of 10.82 K, and an average effective moment of 1.87 μ_B. The calculated g_{iso} value is 2.15, much higher than expected for a radical complex and points to an important contribution of the nickel orbitals into the SOMO. This value contrast with the g_{av} obtained from the EPR spectrum of the frozen solution, 2.035, which points to a lower contribution of the nickel orbitals due to a difference in the nature of the species in both solid state and in solution. This value is very similar to that obtained for [Ni(Psalen^{OMe})]$^{+}$SbF$_6^{-}$ (2.16), which is described as a predominantly ligand radical complex, suggesting the contribution of the metal center to the SOMO in [Ni(Psalophen^{Me})]$^{+}$SbF$_6^{-}$ must be similar.

The reason of the differences found between the solid state magnetic measurements and the EPR in solution could not be elucidated.

IV. Psalophen^{CF3} complexes

1. Synthesis of the ligand and neutral complexes

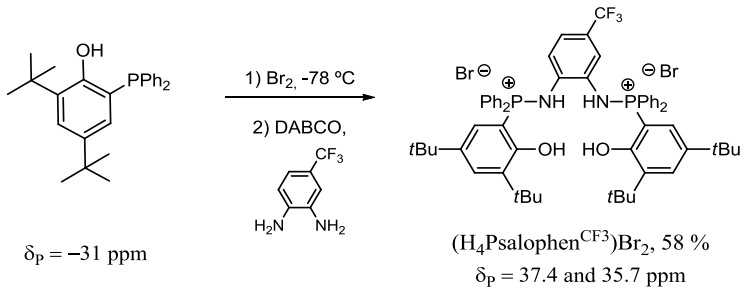

Scheme 69. Synthetic procedure for $(H_4Psalophen^{CF3})Br_2$ and related ^{31}P chemical shifts in dichloromethane.

$(H_4Psalophen^{CF3})Br_2$ was synthesized following the procedure previously described for phosphasalophen ligands (Scheme 69). The $^{31}P\{^1H\}$ NMR spectrum showed for aminophosphonium two main singlets at 37.4 and 35.7 ppm and smaller singlets at 37.9, 36.5 and 62.5 ppm corresponding to side products formed during the reaction. Ammonium salts were removed by centrifugation and the solvent was evaporated. The obtained residue was washed with diethyl ether and petroleum ether until the supernatant solution did not present the impurity signals. $(H_4Psalophen^{CF3})Br_2$ was obtained as a pale yellow solid in 58 % yield. The ^{31}P NMR spectrum in chloroform showed two singlets at 43.0 and 40.6 ppm corresponding to the desired product, and an additional singlet at 42.1 ppm corresponding to a side product. This modest yield was not optimized. No further purification of the ligand was performed since the impurity was removed after the coordination reaction.

The complexation of the ligand was performed in two steps, as for the other phosphasalen ligands (Scheme 70). The deprotonation of $(H_4Psalophen^{CF3})Br_2$ was achieved with KHMDS and was evidenced by the disappearance of the signals of the aminophosphonium salt and the appearance of two singlets in the ^{31}P NMR spectrum at 12.7 and 12.3 ppm corresponding to $K_2Psalophen^{CF3}$. The insoluble salts were removed by centrifugation, and the metal precursors, either $[NiBr_2(DME)]$ or $CuBr_2$, were added to the solution. The formation of $[Ni(Psalophen^{CF3})]$ is indicated by a color change from dark brown to dark blue, and the presence of a broad signal at 46.8 ppm, together with the disappearance of the signal corresponding to the ligand. For $[Cu(Psalophen^{CF3})]$ the solution changes to

green but the disappearance of the ligand signal leads to a silent spectrum, as expected for a paramagnetic complex (Cu^{II}, $3d^9$ center).

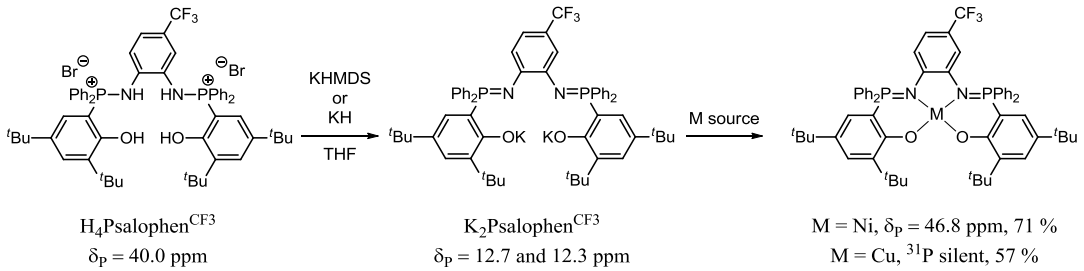

Scheme 70. Synthetic procedure for [Ni(Psalophen^{CF3})] and [Cu(Psalophen^{CF3})] and their related ^{31}P NMR signals in THF.

The solvent was evaporated and the residues dissolved in dichloromethane and centrifuged to remove the insoluble salts formed. The solutions were concentrated and addition of petroleum ether led to the precipitation of a solid. The obtained residues were washed with petroleum ether and dried under vacuum. [Ni(Psalophen^{CF3})] and [Cu(Psalophen^{CF3})] were then isolated as pale blue and green powders in 65 and 61 % yields, respectively.

2. Characterization of neutral complexes [Ni(Psalophen^{CF3})] and [Cu(Psalophen^{CF3})]

2.1 NMR spectroscopy

[Ni(Psalophen^{CF3})] was easily characterized by multinuclear NMR. It displays a diamagnetic ^{1}H NMR spectrum (Figure 110) and two signals at 31.2 and 31.1 ppm in the ^{31}P{^{1}H} NMR spectrum in $CDCl_3$.

As observed for [Ni(Psalophen^{Me})], the substitution of one position of the phenylene ring entails a dissymmetry of the ligand that is observed in the ^{1}H NMR spectrum. The ^{1}H signals were assigned to the different type of protons (PhO-, PPh_2, tBu…) without being able to attribute the to a specific proton.

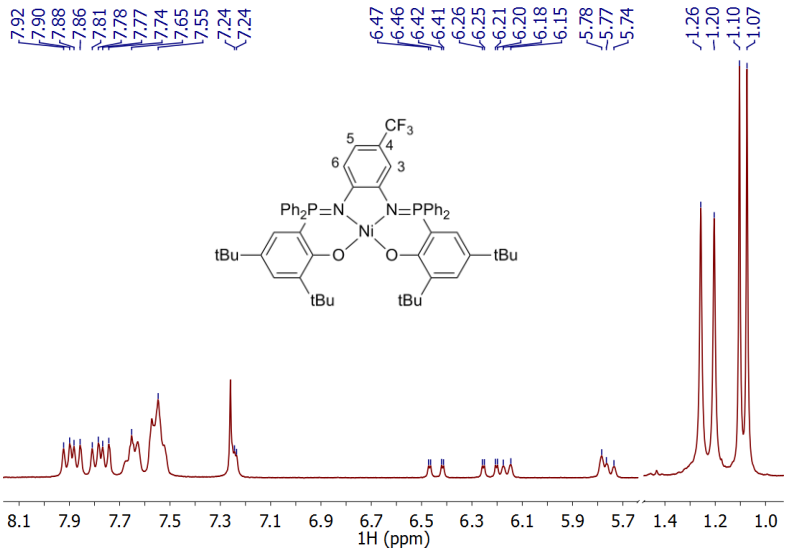

Figure 110. ^{1}H NMR spectrum of [Ni(Psalophen^{CF3})] in $CDCl_3$.

The phenyl phosphine protons are observed between 7.50 and 8.0 ppm as multiplets, the protons at *para* position to the phosphorus in the phenolate ring at 7.24 ppm, and the other phenolate protons as a doublet of doublets at 6.44 and 6.23 ppm ($^{3}J_{P,H}$ = 15.7 Hz, $^{4}J_{H,H}$ = 2.3 Hz). The protons of the phenylene bridge are observed as doublets at 6.16 and 5.75 ppm due to the coupling with the neighboring proton ($^{3}J_{H,H}$ = 8.5 Hz), and as a singlet at 5.78 ppm; these signals are down-field shifted with respect to those observed for [Ni(Psalophen^{Me})] due to the substitution of the methyl group by the electron-withdrawing trifluoromethane group. The t-butyl groups also appear as sets of different signals at 1.26 and 1.20 ppm, and at 1.10 and 1.07 ppm.

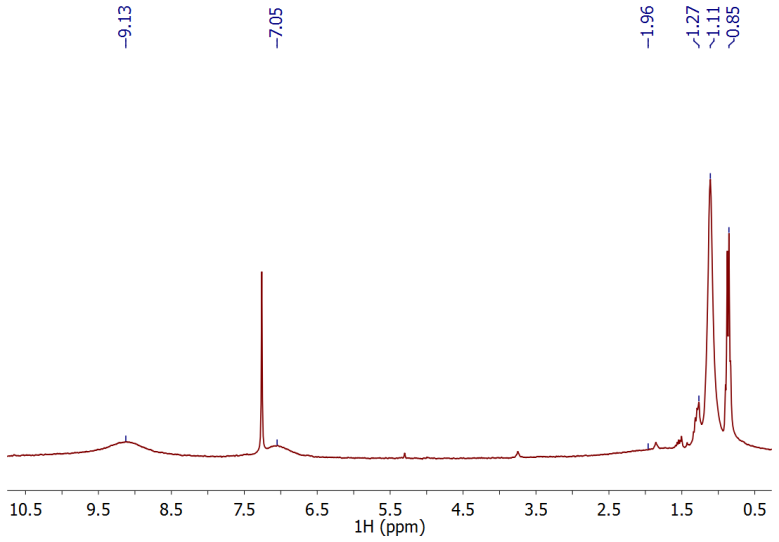

Figure 111. ^{1}H NMR spectrum of [Cu(Psalophen^{CF3})] in $CDCl_3$. Signals at 1.27 and 0.85 corresponds to pentane.

[Cu(Psalophen^{CF3})] displays a paramagnetic ^{1}H NMR spectrum and no ^{31}P resonance as expected for a Cu^{II} 3d^{9} complex. The ^{1}H NMR spectrum (Figure 111) is similar to those recorded for other copper phosphasalen neutral complexes. Only broad signals are observed at 9.13, 7.05, 1.96 and 1.11 ppm, which were tentatively assigned to the phenyl phosphine protons, the phenoxide and phenylene protons, and the t-butyl protons, respectively.

2.2 EPR spectroscopy

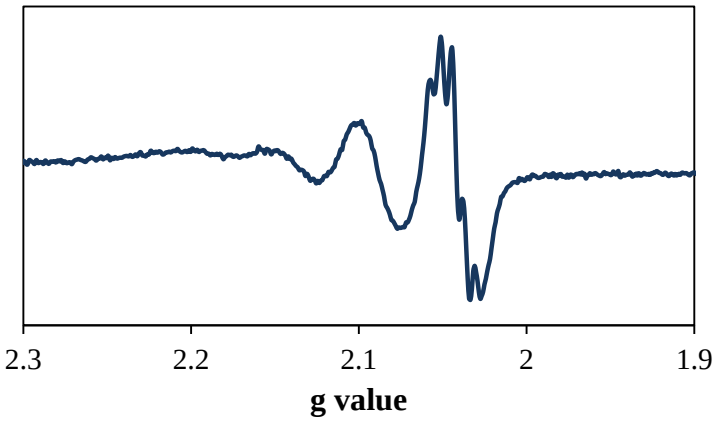

Figure 112. X-band EPR spectrum of [Cu(Psalophen^{CF3})] in dichloromethane at 295 K. Conditions: Frequency: 9.364 GHz; Power: 1.006 mW; modulation frequency: 100 kHz; amplitude: 0.2 mT.

[Cu(Psalophen^{CF3})] shows at room temperature an EPR spectrum very similar to those obtained for other Cu phosphasalen complexes indicating that the substitution of the phenylene ring by a CF_3 group does not induce large changes in the electronics of the copper center. It displays a rhombic signal characterized by a four line pattern due hyperfine coupling with the Cu center (I = 3/2), while a superhyperfine coupling is observed only in g_3. Since this spectrum and those obtained for the alkyl phosphasalen analogues are superimposable, we can assume that they possess the same g values and coupling constants. Thus, the EPR parameters are g_1 = 2.122, g_3 = 2.105 and g_3 = 2.051 and $|A|_{Cu}$ = 251, 210 and 75 MHz, and superhyperfine constants of $|A|_N$ = 28, 28 and 28 MHz for g_1, g_2 and g_3, respectively

2.3 UV-visible spectroscopy

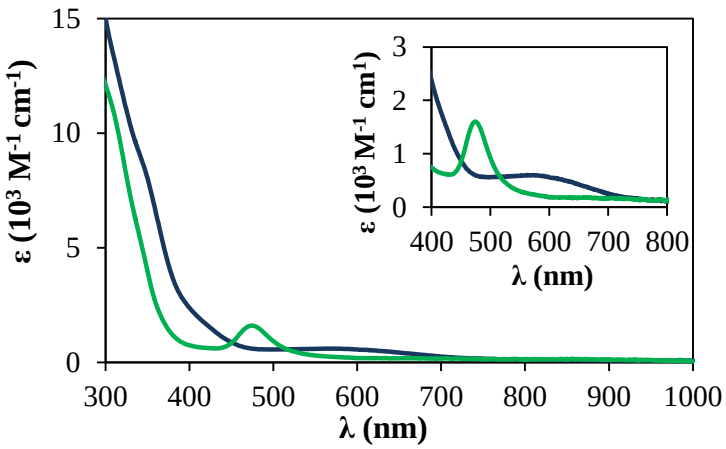

Figure 113. UV-vis spectra of [Cu(Psalophen^{CF3})] (green line) and [Ni(Psalophen^{CF3})] (blue line) in dichloromethane. Inset shows a zoom of the visible region.

Figure 113 (blue line) shows the absorption spectrum [Ni(Psalophen^{CF3})]. It is characterized by a broad weak band centered at 570 nm (ε = 600 M^{-1} cm^{-1}) and an intense band which starts from 450 nm and reaches an absorption with ε = 15000 M^{-1} cm^{-1} at 300 nm. It seems to be composed by different transitions since two "shoulders" are observed around 410 nm (ε ~ 1600 M^{-1} cm^{-1}) and 346 nm (ε ~ 8500 M^{-1} cm^{-1}).

The UV-visible spectrum of [Cu(Psalophen^{CF3})] (Figure 113, green line) is characterized by a sharp transition at 470 nm (ε = 1600 M^{-1} cm^{-1}) and an intense band which starts to appear at 400 nm. This spectrum contrasts to those observed for other phosphasalen complexes normally characterized by broad bands around 640 nm corresponding to d-d transitions. Unexpectedly, a color change occurred as the concentration of Cu(Psalophen^{CF3})] decreased. At high concentrations of [Cu(Psalophen^{CF3})] the dichloromethane solution in green, at 0.1 mM of concentration the solution became violet, and at 0.001 mM the solution was brownish. This may indicate that intermolecular interactions occur in solution and these diminish when decreasing the concentration giving a change of color of the sample.

2.4 X-Ray structures

Green/purple crystals of [Ni(Psalophen^{CF3})] suitable for X-ray diffraction were obtained *via* evaporation of a $CDCl_3$ solution.

[Ni(Psalophen^{CF3})] displays a slightly distorted square planar geometry around the metal center. The torsion angle on the main plane is 5.28 °, lower than those of [Ni(Psalophen)]

(8.16 °) and [Ni(Psalophen^{Me})] (12.13 °). However, as in the case of its phosphasalophen analogues, [Ni(Psalophen^{CF3})] presents differences in the geometrical arrangement of the nitrogen atoms. Here, the N2 adopts a nearly tetrahedral geometry and the P2-N2 bond is placed out of the NOON plane, while N1 displays a trigonal planar arrangement and the P1-N1 bond remains close to the coordination plane.

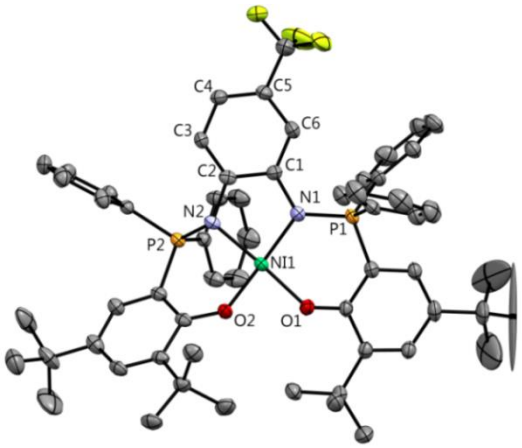

Figure 114. ORTEP of [Ni(Psalophen^{CF3})] with thermal ellipsoids at 50 % probability. Hydrogen atoms and one and a half molecules of toluene have been omitted for clarity.

Due to this distortion the P2 approaches the nickel center and they are separated by 2.850 Å. The coordination sphere around the nickel center is rather unsymmetrical. Ni-O bonds measure 1.876(2) and 1.855(2) Å, and Ni-N bonds measure 1.888(3) and 1.918(3) Å, similarly to those observed for [Ni(Psalophen)] and [Ni(Psalophen^{Me})]. This dissymmetry generates a long axis along the N2-Ni-O1 segment, and it is worth noting that the longer N-Ni bond corresponds to the nitrogen atom adopting a tetrahedral geometry.

	[Ni(Psalophen^{CF3})]	**[Cu(Psalophen^{CF3})]**
M-O1	1.876(2)	1.904(2)
M-O2	1.855(2)	1.878(2)
M-N1	1.888(3)	1.953(3)
M-N2	1.918(3)	1.951(3)
P1-N1	1.621 (3)	1.618(3)
P2-N2	1.631(3)	1.619(3)
Torsion angle[a]	5.28	24.91

Table 24. Selected bond distances (Å) and angles (°) for [Ni(Psalophen^{CF3})] and [Cu(Psalophen^{CF3}]. [a] Torsion of the NOON plane.

Dark crystals of [Cu(Psalophen^{CF3})] suitable for X-ray diffraction were obtained from a toluene/dichloromethane solution.

[Cu(Psalophen^{CF3})] displays a highly distorted square planar geometry around the metal center (Figure 115). The torsion angle of the main plane, 24.91 °, is very similar to that

observed in [Cu(Psalophen^{Me})] (24.11 °), but drastically different to that of [Cu(Psalophen)] (0.48 °).

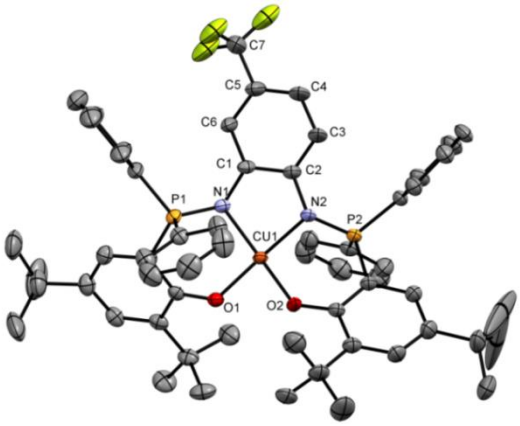

Figure 115. ORTEP of [Cu(Psalophen^{CF3})] with thermal ellipsoids at 50 % probability. Hydrogen atoms and one and a half molecules of toluene have been omitted for clarity.

Cu-N bond distances (1.953(3) and 1.951(3) Å) and Cu-O bond lengths (1.904(2) and 1.878(2) Å) are similar to those of [Cu(Psalophen^{Me})], 1.944(2) Å and 1.895(2), respectively. P-N bonds are equivalent (1.618(3) and 1.619(3) Å) and similar to those of [Cu(Psalophen)] (1.612(3) Å) and [Cu(Psalophen^{Me})] (1.610(2) Å). The geometry of both nitrogen atoms was found to be similar, and each P-N bonds are directed towards opposite directions with respect to the main NOON plane. Despite the different nature of the phenyl substituents, [Cu(Psalophen^{CF3})] and [Cu(Psalophen^{Me})] present similar X-ray structures. Figure 116 shows the coordination spheres of [Cu(Psalophen)] [Cu(Psalophen^{Me})] and [Cu(Psalophen^{CF3})] along the NOON plane.

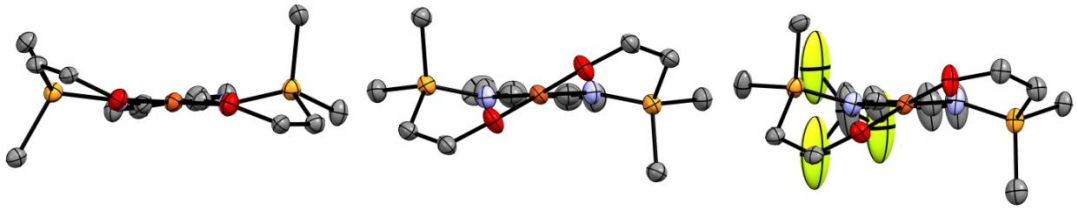

Figure 116. View of the coordination sphere through the NOON plane for [Cu(Psalophen)] (left), [Cu(Psalophen^{Me})] (middle) and [Cu(Psalophen^{CF3})] (right).

2.5 Electrochemical studies

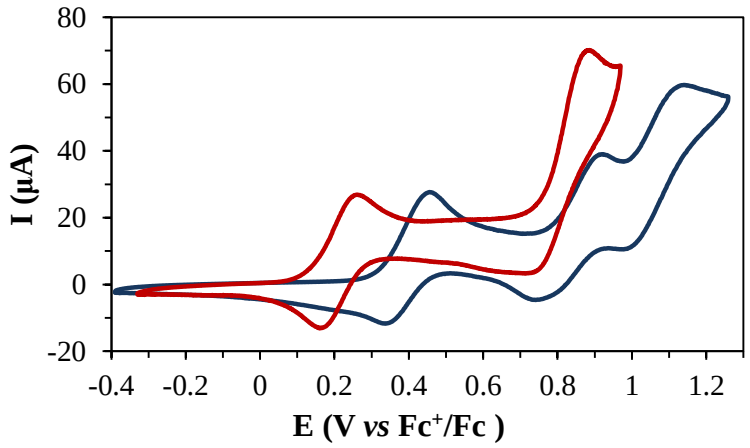

Figure 117. Cyclic voltammograms of [Cu(Psalophen^{CF3})] (blue line) and [Ni(Psalophen^{CF3})] (red line) recorded in dichloromethane. Conditions: 3 mM of complex at 0.1 V/s.

[Ni(Psalophen^{CF3})] displays a reversible one-electron oxidation at $E^1_{1/2}$ = 0.21 V (I_{pa}-I_{pc} = 22.7 µA), and a second nearly irreversible oxidation at $E^2_{p,a}$ = 0.81 V which accounts for two electrons. The first oxidation potential is higher than those obtained for [Ni(Psalophen)] ($E^1_{1/2}$ = 0.15 V), and for [Ni(Psalophen^{Me})] ($E^1_{1/2}$ = 0.04 V). We assume that the oxidation takes place in the aromatic bridge, as in the previous phosphasalen derivatives, and the CF_3 substitution renders more difficult the oxidation. The gap between the first and the second oxidation is $\Delta E_{1\text{-}2}$ = 0.60 V, similar to those found for [Ni(Psalophen^{Me})] (0.66 V) and [Ni(Psalophen)] (0.63 V). This is counterintuitive since the presence of the CF_3 group in the phenylene ring should destabilize the formation of a radical in the central ring, and thus increase the delocalization in the metal orbitals, making this gap larger than for [Ni(Psalophen^{Me})]. Assuming a first oxidation centered in the phenyl ring, the second oxidation may correspond to the oxidation of the two phenoxide rings, which occurs at the same potential (indicating that no electronic communication between the two redox units exists in [Ni(Psalophen^{CF3})]$^+$), or to the oxidation of the metal and ligand.

Compound	$E^1_{1/2}$	$E^2_{p,a}/E^2_{1/2}$	$E^3_{p,a}$	$E^4_{p,a}$
[Ni(Psalophen)]	0.15	0.78	1.09	-
[Ni(Psalophen^{Me})]	0.04	0.70	0.85	1.03
[Ni(Psalophen^{CF3})]	0.21	0.81	-	-
[Cu(Psalophen)]	0.28	0.76	1.01	-
[Cu(Psalophen^{Me})]	0.14	0.70	0.95	-
[Cu(Psalophen^{CF3})]	0.39	0.86	1.05	-

Table 25. Redox potentials for nickel and copper phosphasalophen complexes, expressed in V *vs* Fc$^+$/Fc.

[Cu(Psalophen^{CF3})] displays two reversible oxidations at $E^1_{1/2}$ = 0.39 V, $E^2_{1/2}$ = 0.86 V and an irreversible one at $E^3_{p,a}$ = 1.05 V. The first oxidation is anodically shifted compared to [Cu(Psalophen^{Me})] (0.14 V) and [Cu(Psalophen)] (0.28 V), as expected by the introduction of the CF_3 group. This oxidation is also anodically shifted compared to [Ni(Psalophen^{CF3})] by 0.18 V, suggesting that the introduction of the CF_3 group disfavors the oxidation of the complex in a greater extent than for [Ni(Psalophen^{CF3})]. Assuming the oxidation of the phenylene ring in first place, the second and third oxidation may correspond to a double oxidation of the ligand, or the oxidation of the ligand and the metal.

As occurred with the other Psalophen derivatives, the cyclic voltammograms of copper and nickel analogues differ markedly, while these were very similar when displaying Psalen ligands. However, contrarily to other Psalophen derivatives, a total of three redox processes were observed, instead of four.

3. Oxidation of neutral complexes

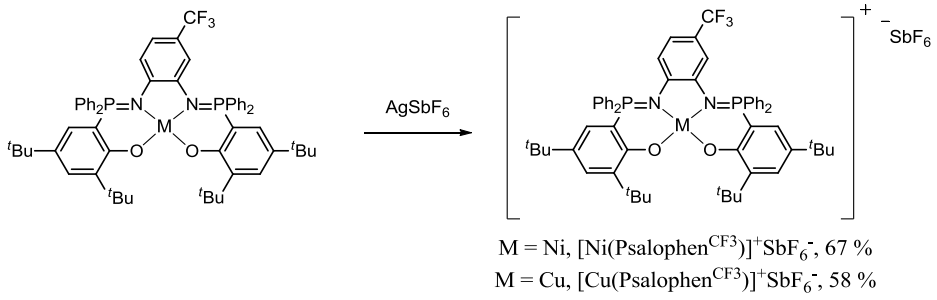

M = Ni, [Ni(Psalophen^{CF3})]$^+$SbF$_6^-$, 67 %
M = Cu, [Cu(Psalophen^{CF3})]$^+$SbF$_6^-$, 58 %

Scheme 71. Chemical oxidation of [Ni(Psalophen^{CF3})] and [Cu(Psalophen^{CF3})] complexes.

[Ni(Psalophen^{CF3})] and [Cu(Psalophen^{CF3})] were oxidized using one equivalent of $AgSbF_6$ in dichloromethane solutions under inert atmosphere (Scheme 71). Addition of the silver salt in a solution of [Ni(Psalophen^{CF3})] induced an immediate color change from blue to dark brown. However, the solution of [Cu(Psalophen^{CF3})] did not experience any change and remained green after the addition. The suspensions were stirred for one hour at room temperature, and then filtered and concentrated. Addition of petroleum ether led to formation of a dark-brown precipitate for [Ni(Psalophen^{CF3})]$^+$SbF$_6^-$ and a green precipitate for [Cu(Psalophen^{CF3})]$^+$SbF$_6^-$. The solids were washed with petroleum ether and dried under vacuum to yield [Ni(Psalophen^{CF3})]$^+$SbF$_6^-$ in 67 % yield, and [Cu(Psalophen^{CF3})]$^+$SbF$_6^-$ in 58 % yield. Both oxidized complexes are slightly soluble in petroleum ether entailing a loss of product during the purification.

4. Characterization of the oxidized species

4.1 NMR spectroscopy

Both oxidized [Ni(Psalophen^{CF3})]$^+$ and [Cu(Psalophen^{CF3})]$^+$ complexes display paramagnetic ^{1}H NMR spectra, while no ^{31}P resonance was observed.

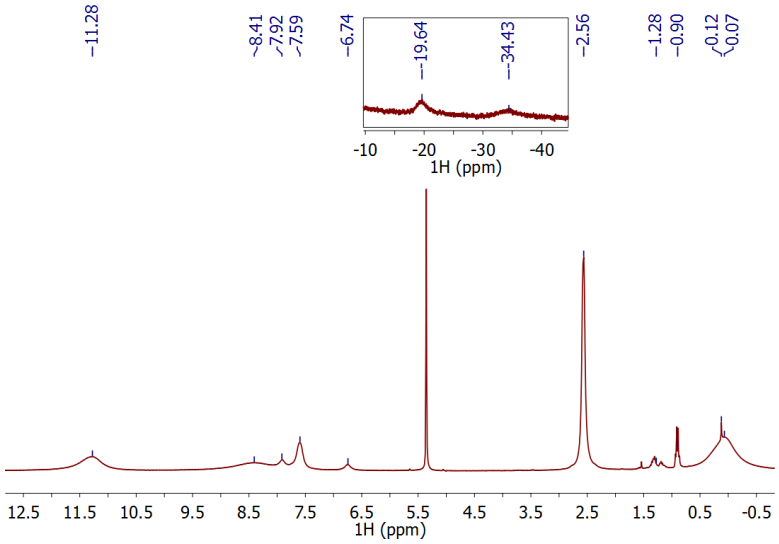

Figure 118. ^{1}H NMR spectrum of [Ni(Psalophen^{CF3})]$^+$ in CD_2Cl_2 at 20 °C. Inset shows a zoom of the high field region. Signals at 1.28, 0.90 and 0.12 correspond to pentane and silicon grease.

The ^{1}H NMR spectrum of [Ni(Psalophen^{CF3})]$^+$ in dichloromethane (Figure 118) presents broad signals between -40 and 12 ppm and resembles those recorded for [Ni(Psalophen^{Me})]$^+$ and the non-crystallized product of [Ni(Psalophen)]$^+$. A spectral width window of 300 ppm was investigated and no other signals were detected. The signals were tentatively assigned thanks to their integrated areas: at 11.28, 8.41 and 7.59 ppm to the phenyl phosphine protons; at 7.92, 6.74, -19.64 and -34.43 ppm to the protons of the phenoxide and phenylene rings; and at 2.56 and 0.07 ppm the tert-butyl protons. These chemical shifts are very similar to those observed in the ^{1}H NMR of [Ni(Psalophen)]$^+$, especially those of the aromatic region which were at 11.29, 8.49, 8.21, 7.86, 7.57 and 7.27 ppm. However, the paramagnetic shift of the tert-butyl groups is larger in [Ni(Psalophen^{CF3})]$^+$ (2.56 and 0.07 ppm) than in [Ni(Psalophen)]$^+$ (0.32 and 1.67 ppm).

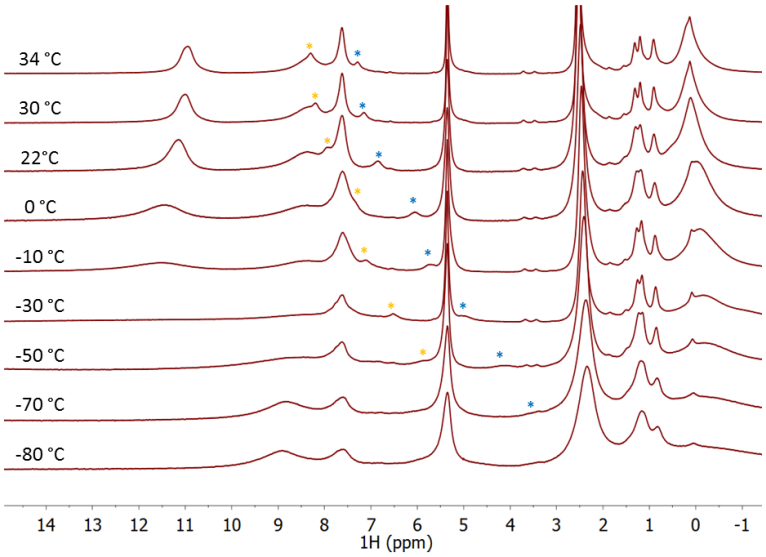

Figure 119. VT-NMR spectra of [Ni(Psalophen^{CF3})]$^+$ in CD_2Cl_2.

The ^{1}H NMR spectrum of [Ni(Psalophen^{CF3})]$^+$ was investigated between 34 and -90 °C (Figure 119), however not much information could be drawn from this experiments. Some of the signals, notably those present in the aromatic region, experienced a shift with the temperature. This shift was difficult to investigate since the signals broaden upon decreasing the temperature and merge with the baseline. Only the variation of two signals, marked with yellow and blue stars in Figure 119, was investigated. These signals, present at room temperature at 7.92 and 6.74 ppm, were assigned to phenoxide or phenylene protons and experienced a shift of 3.19 and 2.4 ppm, respectively, between 34 and -50 °C. This suggests that the phenoxide and/or phenylene rings have an important participation in the delocalization of the unpaired electron. The variation experienced by these signals is linear with the temperature, as expected for paramagnetic compounds following the Curie law (Figure 120). It is worth nothing that one of the tert-butyl signals broadens with the temperature while the other does not experience much change and shifts only by 0.19 ppm in the temperature range studied. The signals present at -19.64 and -34.43 ppm broaden when decreasing the temperature and merge with the baseline at -10 °C, making them undetectable. No ^{31}P resonance was detected at any temperature.

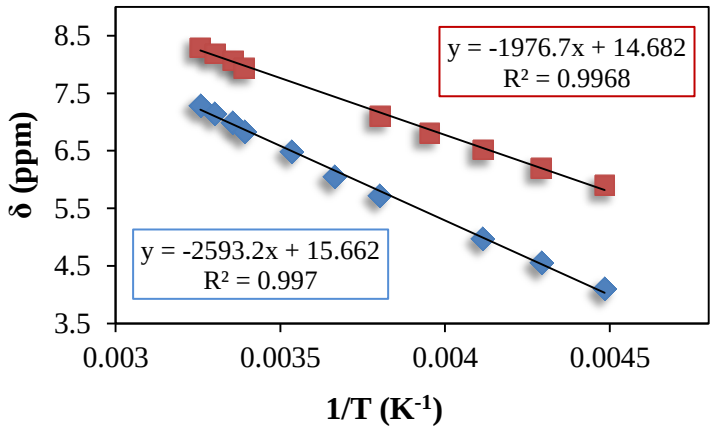

Figure 120. Plot of the chemical shifts (δ) in the 34 to -50 °C range of the signal present at 7.92 ppm at 20 °C (red squares) and the signal at 6.74 ppm at 20 °C (blue squares) *vs* 1/T for [Ni(Psalophen^{CF3})]$^{+}$.

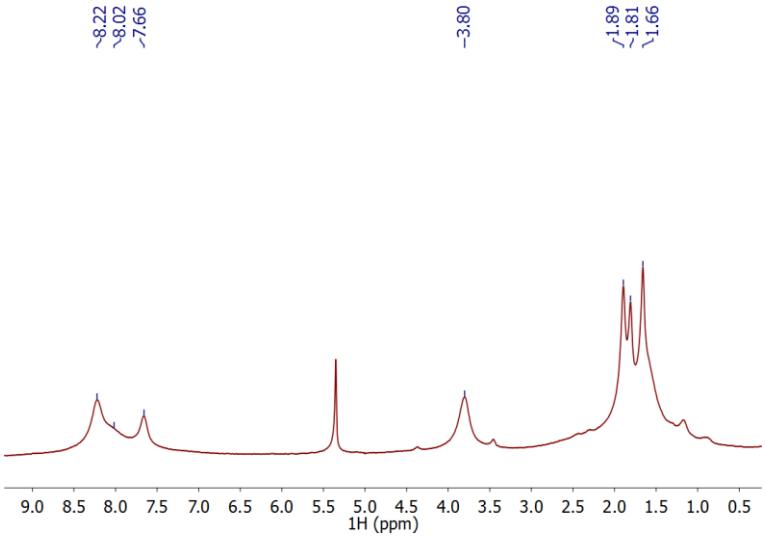

Figure 121. ^{1}H NMR spectrum of [Cu(Psalophen^{CF3})]$^{+}$ in CD_2Cl_2 at 20 °C.

[Cu(Psalophen^{CF3})]$^{+}$ displays a paramagnetic ^{1}H NMR spectrum and no ^{31}P resonance. The ^{1}H NMR spectrum (Figure 121) shows broad signals between 0 and 9 ppm, and it differs from that recorded for the neutral complex indicating that the oxidation reaction worked even if no color change had occurred. The signals observed could not be assigned since their integrated areas could not be properly determined. It is remarkable than in the aliphatic zone, where usually the tert-butyl protons are present as a sole singlet in the spectra of the Cu phosphasalen derivatives, three different signals were observed. Unfortunately, due to the paramagnetic nature of the sample, this could not be further investigated. The VT-NMR studies for [Cu(Psalophen^{CF3})]$^{+}$ were not performed.

4.2 EPR spectroscopy

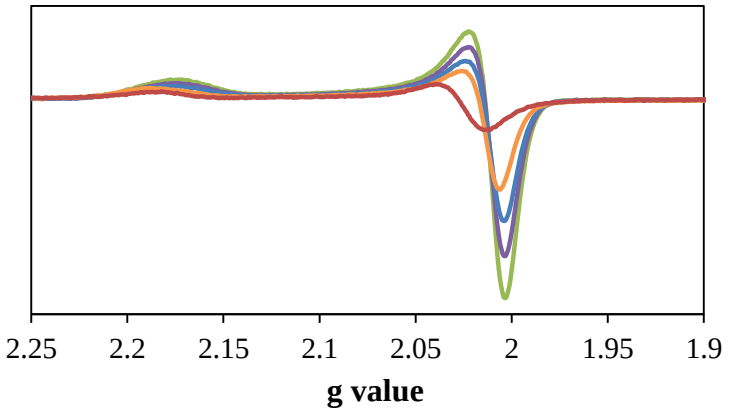

Figure 122. X-band EPR spectrum of [Ni(Psalophen^{CF3})]$^+$ in dichloromethane at 160 K (red), 140 K (orange), 120 K (blue), 100 K (purple), and 80 K (green). Conditions: Frequency: 9.380 - 9.381 GHz; Power: 0.2520-0.2526 mW; modulation frequency: 100 kHz; amplitude: 0.2 mT.

The EPR spectrum of [Ni(Psalophen^{CF3})]$^+$ turned out to be silent at room temperature, contrary to that of [Ni(Psalophen^{Me})]$^+$, and a signal was only observed below 160 K. This signal displays an axial symmetry and its intensity increases when decreasing the temperature (Figure 122). The shift of the signal recorded at 160 K is remarkable compared to the rest of the spectra taken at different temperatures (Figure 122, red line). At this temperature the phase transition of the solvent (dichloromethane) occurs from liquid to solid. This feature was already observed for [Ni(Psalophen^{Me})]$^+$ whose signal at 160 K displays an intermediate symmetry and anisotropy between those recorded at room temperature and at temperatures below 160 K.

The spectrum at 80 K was simulated and $g_{\parallel}$ = 2.178 and $g_{\perp}$ = 2.005 (g_{av} = 2.063) were obtained, therefore $g_x = g_y < g_z$. This contrast with the axial signal obtained for [Ni(^{iPr}Psalen)]$^+$ at $g_{\perp}$ = 2.249 and $g_{\parallel}$ = 2.061, so $g_x = g_y \gg g_z$, and point to significant differences of the nature of the SOMO between both oxidized complexes.

These values are higher than those obtained for the methylated analogue [Ni(Psalophen^{Me})]$^+$, which displayed a rhombic signal at low temperature at g_1 = 2.098, g_2 = 2.005 and g_3 = 1.987 (g_{av} = 2.030). This suggests a greater contribution of the metal orbitals to the SOMO of the oxidized complex, as expected by the introduction of the CF_3 group. Thus, this complex may also present a diaminobenzene radical configuration, but because of the lower electron density on the aromatic bridge, the delocalization towards the metal *via* the nitrogen atoms is larger. Besides, a phenoxyl radical configuration would also match with the g values obtained.

4.3 UV-vis spectroscopy

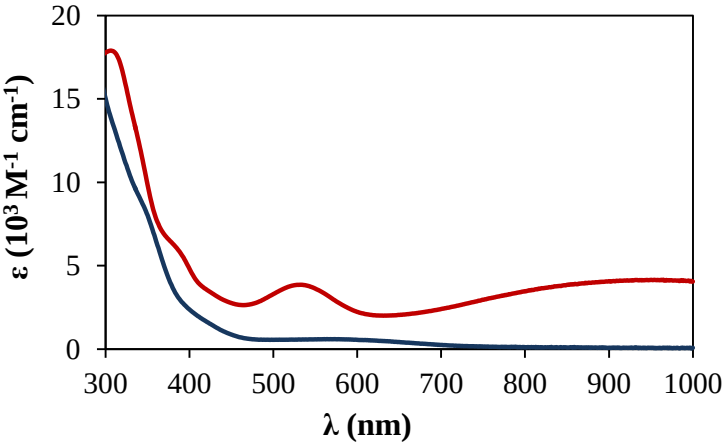

Figure 123. UV-vis spectra of [Ni(Psalophen^{CF3})] (blue line) and [Ni(Psalophen^{CF3})]$^{+}$ (red line) in dichloromethane.

The UV-visible spectrum of [Ni(Psalophen^{CF3})]$^{+}$ (Figure 123, red line) exhibits two broad bands at 530 nm (ε = 3900 M^{-1} cm^{-1}) and 950 nm (ε = 4100 M^{-1} cm^{-1}). An intense band starts to appear around 400 nm and reaches an absorption with ε = 17200 M^{-1} cm^{-1} at 300 nm. A "shoulder" is observed at 390 nm (ε = 5900 M^{-1} cm^{-1}).

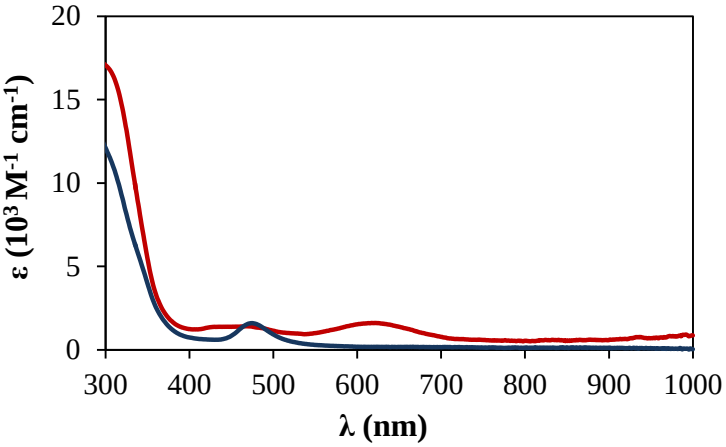

Figure 124. UV-vis spectra of [Cu(Psalophen^{CF3})] (blue line) and [Cu(Psalophen^{CF3})]$^{+}$ (red line) in dichloromethane.

[Cu(Psalophen^{CF3})]$^{+}$ (Figure 124, red line) presents two large bands at 620 nm (ε = 1600 M^{-1} cm^{-1}) and at 460 nm (ε = 1400 M^{-1} cm^{-1}) and at 465 nm (ε = 4500 M^{-1} cm^{-1}). An intense band starts to appear around 370 nm, as for [Cu(Psalophen^{CF3})], and reaches an absorption with ε = 17000 M^{-1} cm^{-1} at 300 nm.

4.4 X-ray structures

Dark brown crystals of [Ni(Psalophen^{CF3})]$^{+}$SbF$_6^-$ were obtained by slow diffusion of pentane in a dichloromethane solution.

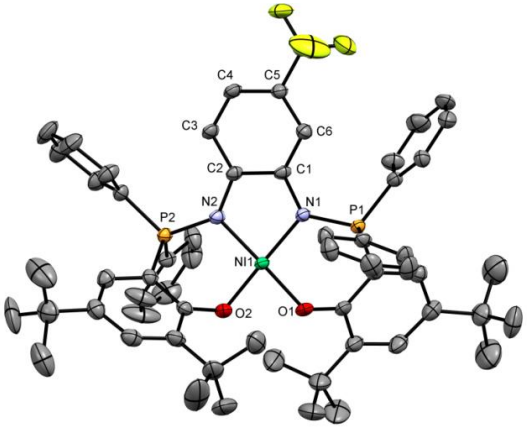

Figure 125. ORTEP of [Ni(Psalophen^{CF3})]$^{+}$SbF$_6^-$ with thermal ellipsoids at 50 % probability. Hydrogen atoms, a molecule of dichloromethane and the SbF$_6^-$ anion have been removed for clarity.

[Ni(Psalophen^{CF3})]$^{+}$SbF$_6^-$ displays a distorted square planar geometry around the nickel center (Figure 125). The torsion angle of the main plane increases upon oxidation from 5.28 to 15.74 °. This distortion is the largest observed in all the series of oxidized nickel phosphasalen complexes studied in this work. Contrary to [Ni(Psalophen^{CF3})], no difference between the geometry of the nitrogen atoms were found and both P-N bonds lay in in the coordination plane. [Ni(Psalophen^{CF3})]$^{+}$SbF$_6^-$ experiences a more pronounced contraction around the metal center than that observed for [Ni(Psalophen)]$^{+}$SbF$_6^-$. Ni-O bonds contract non-symmetrically and shorten by 0.038 and 0.013 Å, while for Ni-N bonds this contraction is comparable (Δd = 0.035 and 0.038 Å). Additionally, the P-N bonds are elongated by 0.052 and 0.031 Å. These variations are larger than those observed for the alkyl derivatives [Ni(Psalen^{tBu})]$^{+}$SbF$_6^-$, [Ni(Psalen^{OMe})]$^{+}$SbF$_6^-$, and [Ni(^{iPr}Psalen)]$^{+}$SbF$_6^-$ whose P-N bonds elongated from 0.012 to 0.031 Å upon oxidation, but closer to those observed for the asymmetric unit of the [Ni(Psalophen)]$^{+}$ dimer.

	[Ni(Psalophen^{CF3})]	[Ni(Psalophen^{CF3})]$^{+}$SbF$_6^-$	Δd
Ni-O1	1.876(2)	1.838(3)	-0.038
Ni-O2	1.855(2)	1.842(3)	-0.013
Ni -N1	1.888 (3)	1.853(3)	-0.035
Ni -N2	1.918(3)	1.880(3)	-0.038
P1-N1	1.621 (3)	1.673(4)	0.052
P2-N2	1.631(3)	1.662(4)	0.031
Torsion angle[a]	5.28	15.74	6.22

Table 26. Selected bond distances (Å) and angles (°) for [Ni(Psalophen^{CF3})] and [Ni(Psalophen^{CF3})]$^{+}$SbF$_6^-$. [a] Torsion of the NOON plane.

The bond lengths of the phenylene cycle also experienced variations upon oxidation: C2-C3 and C6-C1 elongate upon oxidation by 0.023 and 0.022 Å, as well as C1-C2 and C4-C5 by 0.013 and 0.033 Å, while C3-C4 and C5-C6 shorten by 0.009 and 0.013 Å. The N-C bonds contract by 0.042 and 0.045 Å, as a consequence of the shift of the nitrogen pairs from the phosphorus atoms to the central ring. This explains the elongation observed for the P-N bonds. A slight contraction occurs also for the C4-CF_3 bond, which shortens by 0.015 Å. These metrical variations were also observed by Wiedghart and co-workers in the study of diaminobenzene radical ligands,[10,18] and by Thomas and co-workers in the study of the salophen derivative [Cu(Salophen^{OMe})]$^+SbF_6^-$.[9] The central ring adopts an iminobenzosemiquinonate pattern, typical of diaminobenzene radicals, evidencing the oxidation of the bridging ring. The contraction of the coordination sphere indicates that the metal center is also getting partially oxidized. The phenoxide rings do not experience significant variations upon oxidation, nevertheless the C-O bonds of the phenolate rings were found to be non-equivalent, 1.341(6) and 1.324(6) Å, maybe due to the distortion adopted by the complex.

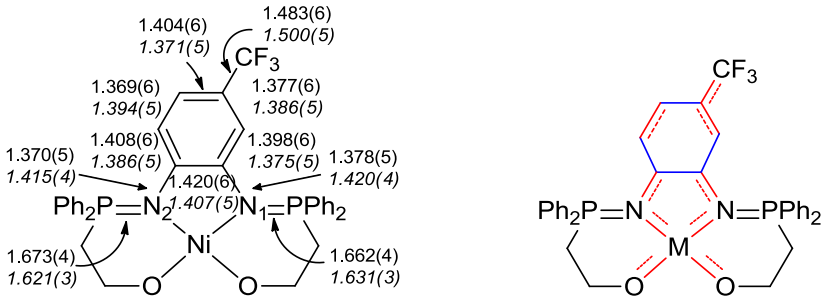

Figure 126. Left: experimental bond lengths of [Ni(Psalophen^{CF3})] (italic) and [Ni(Psalophen^{CF3})]$^+SbF_6^-$ (regular police) expressed in Å. Right: bond elongations (blue) and contractions (red) of the phenylene ring and coordination sphere for [Ni(Psalophen^{CF3})]$^+SbF_6^-$.

Unfortunately, suitable crystals for X-ray diffraction could not be obtained yet for [Cu(Psalophen^{CF3})]$^+SbF_6^-$.

4.5 Magnetic measurements

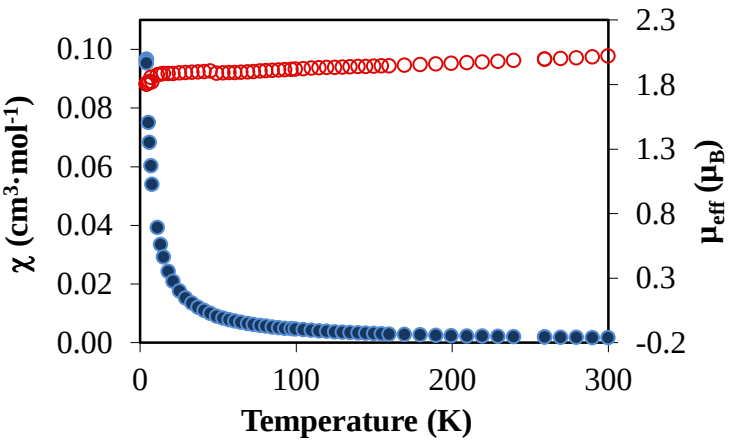

Figure 127. Plot of magnetic susceptibility (blue circles) and effective magnetic moment (red circles) *vs.* temperature for [Ni(Psalophen^{CF3})]$^{+}$SbF$_6^{-}$.

The magnetic properties of [Ni(Psalophen^{CF3})]$^{+}$SbF$_6^{-}$ were also studied in the solid state using a SQUID magnetometer. Ground crystals were used for this sample. [Ni(Psalophen^{CF3})]$^{+}$SbF$_6^{-}$ follows the Curie-Weiss law with a Curie constant of C = 0.460 cm^3 K mol^{-1}, a Weiss θ of 13.36 K, and an average effective moment of 1.92 μ_B. The calculated g_{iso} value is 2.21, much higher than expected for a radical complex and points to an important contribution of the nickel orbitals into the SOMO. This contrasts with the g_{av} value of 2.063 obtained from the EPR measurements in solution, suggesting that the nature of the species in both solid state and in solution is not the same. The reasons of such differences in the magnetic properties between solid state and solution have not been clarify yet. This also contrasts with the X-ray structure obtained for [Ni(Psalophen^{CF3})]$^{+}$SbF$_6^{-}$ which points to a partial oxidation of the ligand and the metal. This g value is very similar to that obtained for [Ni(Psalen^{tBu})]$^{+}$SbF$_6^{-}$ and indicates a predominantly Ni^{III} configuration of the ground state.

V. Psalophen^{OMe2} complexes

1. Synthesis of the ligand and neutral complexes

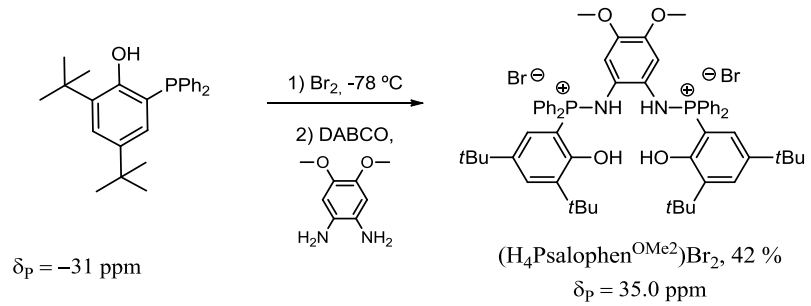

Scheme 72. Synthetic procedure for $(H_4Psalophen^{OMe2})Br_2$ and corresponding ^{31}P chemical shifts in dichloromethane.

$(H_4Psalophen^{OMe2})Br_2$ proligand was synthesized following the previously described procedure. The ^{31}P NMR spectrum showed a main singlet at 35.0 ppm as well as small singlets at 37.9 and 36.2 ppm corresponding to side products formed during the reaction. A signal around -35.0 ppm was also present and may correspond to some unreacted phosphine. Ammonium salts were removed by centrifugation and the solvent was evaporated. The obtained residue was washed with diethyl ether to remove impurities and dried under vacuum. The bis-aminophosphonium salt $(H_4Psalophen^{OMe2})Br_2$ was obtained as a pale pink solid in 42 % yield. The ^{31}P NMR spectrum of $(H_4Psalophen^{OMe2})Br_2$ in $CDCl_3$ showed a main singlet at 40.5 ppm, and an additional singlet at 43.3 ppm corresponding to a side product. This modest yield was not optimized. No further purification of the ligand was performed since the impurity was removed after the coordination reaction.

The complexation of the ligand was performed in two steps, as for the other phosphasalen ligands (Scheme 73). First, the ligand was deprotonated in THF using KHMDS or an excess of KH. The deprotonation is evidenced by the disappearance of the signal of the $H_4Psalophen^{OMe2}$ and the presence of a singlet in the ^{31}P NMR spectrum at 8.2 ppm corresponding to $K_2Psalophen^{OMe2}$. The solution was centrifuged to remove the insoluble salts, and the metal precursors, either $[NiBr_2(DME)]$ or $CuBr_2$, were added. The formation of $[Ni(Psalophen^{OMe2})]$ is indicated by a color change from dark orange to dark green and a signal at 33.4 ppm together with the disappearance of the signal corresponding to the ligand in the ^{31}P NMR. For $[Cu(Psalophen^{OMe2})]$ the solution also becomes green but the

disappearance of the ligand signal leads to a silent spectrum, as expected for a paramagnetic complex (Cu^{II} $3d^9$ center).

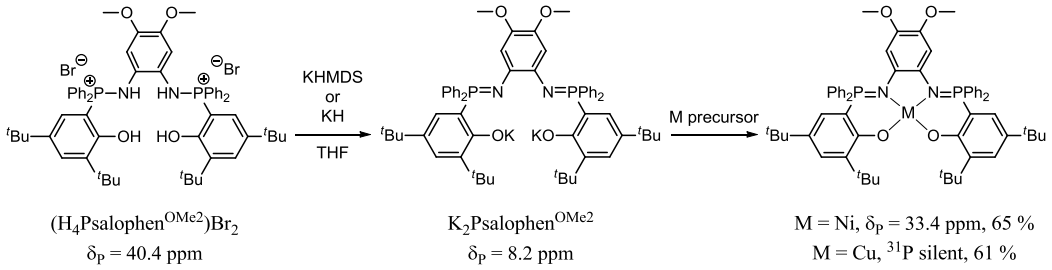

Scheme 73. Synthesis of [Ni(Psalophen^{OMe2})] and [Cu(Psalophen^{OMe2})] and their related ^{31}P NMR signals in THF.

To isolate the complexes, the solvent was evaporated and the residue dissolved in dichloromethane and centrifuged. The solutions were concentrated and addition of petroleum ether led to the precipitation of a solid. The obtained residues were washed with petroleum ether and dried under vacuum. [Ni(Psalophen^{OMe2})] and [Cu(Psalophen^{OMe2})] were then isolated as pale blue powders in 65 and 61 % yields, respectively.

2. Characterization of neutral complexes [Ni(Psalophen^{OMe2})] and [Cu(Psalophen^{OMe2})]

2.1 NMR spectroscopy

Both [Ni(Psalophen^{OMe2})] and [Cu(Psalophen^{OMe2})] were studied by NMR spectroscopy. [Ni(Psalophen^{OMe2})] showed a diamagnetic ^{1}H NMR spectrum typical of a Ni^{II} $3d^8$ square planar complex, and a ^{31}P resonance at 30.5 ppm in $CDCl_3$.

Figure 128 shows the ^{1}H NMR spectrum of [Ni(Psalophen^{OMe2})] which is very similar to that of [Ni(Psalophen)], where all the signals were assigned. The phenyl protons from the phosphorus substituents are oberved between 7.54 and 7.90 ppm as multiplets, and the phenolate protons appear at 7.20 and 6.29 ppm, the latter displays a doublet pattern due to the coupling with the phosphorus atom ($^3J_{P,H}$ = 15.6 Hz).

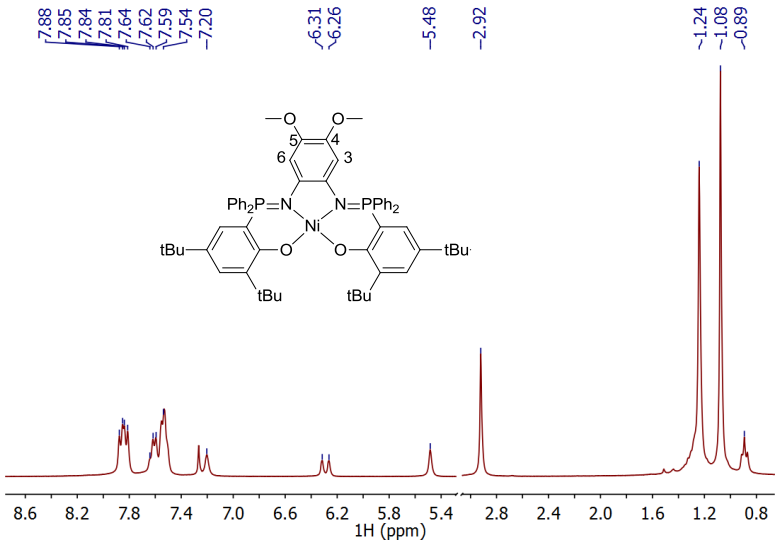

Figure 128. ^{1}H NMR spectrum of [Ni(Psalophen^{OMe2})] in $CDCl_3$. The signal at 0.89 ppm corresponds to pentane.

The sole aromatic protons of the phenylene bridge are observed at 5.48 ppm. This signal is shifted up-field compared to the signal obtained for [Ni(Psalophen)] due to the presence of the electron-donating methoxy groups on the phenylene ring of [Ni(Psalophen^{OMe2})]. The methoxy protons are observed at 2.92 ppm and the t-butyl groups at 1.24 and 1.08 ppm. The ^{13}C NMR spectrum is described in the experimental part.

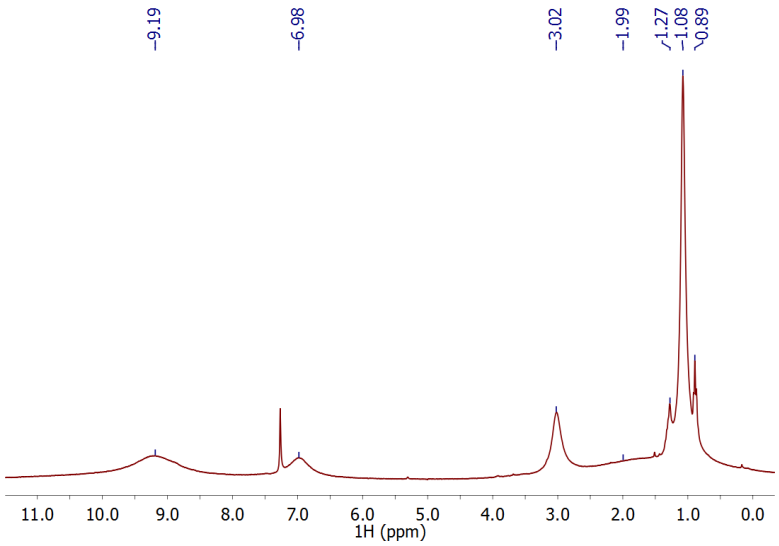

Figure 129. ^{1}H NMR spectrum of [Cu(Psalophen^{OMe2})] in $CDCl_3$ at 20 ° C. Signals present around 1.27 and 0.89 ppm correspond to pentane.

[Cu(Psalophen^{OMe2})] displays a paramagnetic ^{1}H NMR spectrum and no ^{31}P signal, as expected for a Cu^{II} $3d^9$ complex. Broad signals were observed in the ^{1}H NMR spectrum (Figure 129) which were tentatively assigned: at 9.19 ppm the protons from the phenyl phosphine substituents, at 6.98 ppm the protons of the phenolate and diaminobenzene

rings, at 3.02 ppm the methoxy protons, and at 1.80 ppm, as a very broad signal, and at 1.08 ppm the t-butyl groups.

2.2 EPR spectroscopy

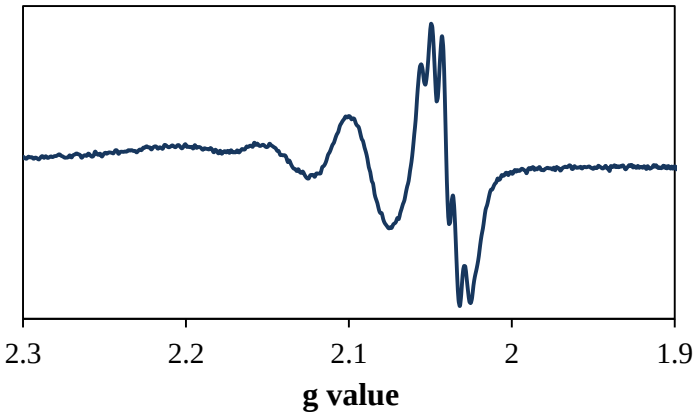

Figure 130. X-band EPR spectrum of [Cu(Psalophen^{OMe2})] in dichloromethane at 295 K. Conditions: Frequency: 9.361 GHz; Power: 0.25 mW; modulation frequency: 100 kHz; amplitude: 0.2 mT.

[Cu(Psalophen^{OMe2})] displays at room temperature an EPR spectrum very similar to those obtained for other copper phosphasalen complexes. It shows a rhombic signal with a four line pattern due to the hyperfine coupling with the Cu center (I = 3/2), and superhyperfine coupling with the ^{14}N atoms is only observed in g_3. Since this spectrum resembles those recorded for the alkyl-bridged derivatives, the g values and coupling constants were assumed to be the same as those obtained from the simulations made for [Cu(Psalen^{tBu})] and [Cu(Psalen^{OMe})]. Thus, g_1 = 2.127, g_3 = 2.108 and g_3 = 2.051; $|A|_{Cu}$ = 250, 210 and 80 MHz, and superhyperfine constants of $|A|_N$ = 28, 28 and 28 MHz for g_1, g_2 and g_3, respectively. This indicates that the bis-substitution of the phenylene ring does not have much influence on the electronic structure of the Cu^{II} complex, thus the anisotropy of the SOMO orbital remains almost the same.

2.3 UV-vis spectroscopy

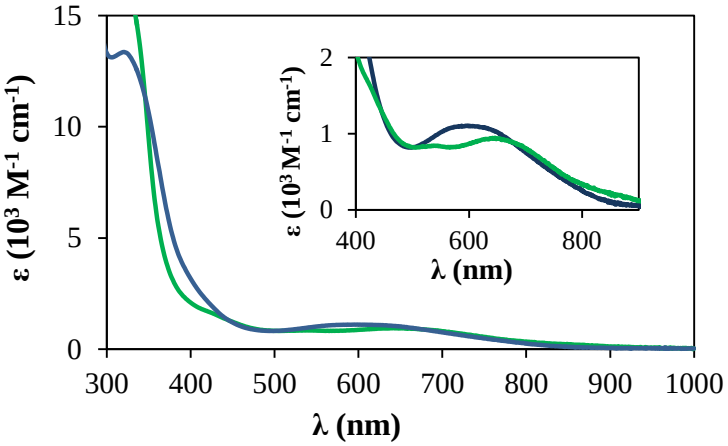

Figure 131. UV-vis spectra of [Cu(Psalophen^{OMe2})] (green line) and [Ni(Psalophen^{OMe2})] (blue line) in dichloromethane. Inset shows a zoom of the visible region.

The UV-vis spectrum of [Ni(Psalophen^{OMe})] presents a large band at 602 nm (ε = 1100 M^{-1} cm^{-1}), and an intense band at 330 nm (ε = 13500 M^{-1} cm^{-1}).

The UV-vis spectrum of [Cu(Psalophen^{OMe})] (Figure 131, green line) shows two weak bands at 650 nm (ε = 950 M^{-1} cm^{-1}) which can be attributed to a d-d transition,[1b] and at 530 nm (ε = 840 M^{-1} cm^{-1}). The latter was not observed in the absorption spectrum of the phosphasalen complexes [Cu(Psalen^{tBu})], [Cu(Psalen^{OMe})] and [Cu(^{iPr}Psalen)] featuring an ethylene linker between the nitrogen atoms, thus this may be related to a transition involving the phenylene ring. Another intense band was observed at 307 nm (ε = 840 M^{-1} cm^{-1}), which is also present in the UV-vis spectrum of other Cu phosphasalen complexes.

2.4 X-Ray diffraction

Dark crystals of [Ni(Psalophen^{OMe2})] suitable for X-ray diffraction were obtained from a concentrated dichloromethane solution with some drops of diethyl ether and petroleum ether stored in the fridge.

[Ni(Psalophen^{OMe2})] presents a distorted square planar geometry around the metal center. The torsion angle of the main plane is 9.50 °, larger than that observed for [Ni(Psalophen)] (8.16 °) and [Ni(Psalophen^{CF3})] (5.28 °), but lower than for [Ni(Psalophen^{Me})] (12.13 °).

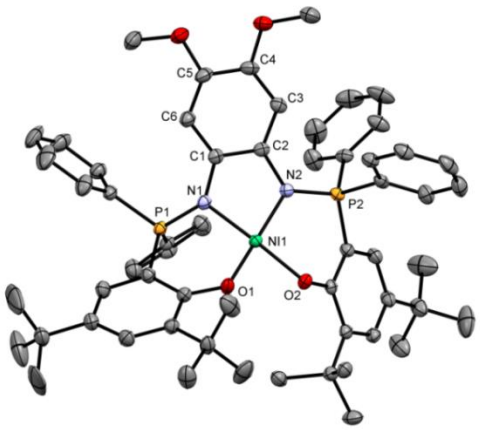

Figure 132. ORTEP of [Ni(Psalophen^{OMe2})] with thermal ellipsoids at 50 % probability. Hydrogen atoms and a molecule of diethyl ether have been omitted for clarity.

It is worth noting that one of the nitrogen atoms (N1) adopts a tetrahedral geometry in [Ni(Psalophen^{OMe2})], while the other presents a trigonal planar geometry. Ni-N1-C1, Ni-N1-P1, P1-N1-C1 angles measure 112, 110 and 125 ° respectively, *vs.* 112, 123 and 125 ° for Ni-N2-C1, Ni-N2-P1, P1-N2-C1, respectively. The main difference is found in the Ni-N-P angle, which varies by 12 °. Thus, the P1-N1 bond is placed above the main NOON plane, while the P2-N2 bond remains in the plane. Despite these differences the P-N bonds are equivalent with distances of 1.622(2) and 1.620(2) Å. This feature was already observed for [Ni(Psalophen)] complex. The difference in the geometry of the nitrogen atoms could be explained by protonation of N1, but neither a counter ion is present to balance the charge (HN-P^{+}), nor any electronic density was found close to this fragment, ruling out this possibility. Ni-N (1.893(2) and 1.895(2) Å) and Ni-O (1.861(3) and 1.886(2) Å) bond distances are very similar to those measured for [Ni(Psalophen^{Me})] (Ni-N bonds measure 1.890(3) Å and Ni-O 1.866(2) and 1.875(2) Å).

	[Ni(Psalophen^{OMe2})]	**[Cu(Psalophen^{OMe2})]**
M-O1	1.861(2)	1.882(2)
M -O2	1.886(2)	1.871(2)
M -N1	1.893(2)	1.900(2)
M -N2	1.895(2)	1.911(2)
P1-N1	1.622(2)	1.612(2)
P2-N2	1.620(2)	1.629(2)
Torsion angle[a]	9.50	5.38

Table 27. Selected bond distances (Å) and angles (°) for [Ni(Psalophen^{OMe2})] and [Cu(Psalophen^{OMe2})]. [a] Torsion of the NOON plane.

Brown crystals of [Cu(Psalophen^{OMe2})] suitable for X-ray diffraction were obtained from a concentrated dichloromethane solution with some drops of petroleum ether stored in the fridge.

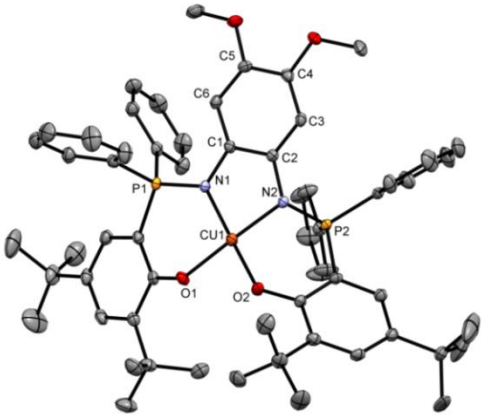

Figure 133. ORTEP of [Cu(Psalophen^{OMe2})] with thermal ellipsoids at 50 % probability. Hydrogen atoms and a molecule of dichloromethane have been omitted for clarity.

[Cu(Psalophen^{OMe2})] displays a square planar geometry around the metal center with a small distortion of the main plane of 5.38 °. This distortion is higher than in [Cu(Psalophen)] (0.48 °) but notably lower than that observed in the mono-substituted phenylene derivatives [Cu(Psalophen^{CF3})] and [Cu(Psalophen^{Me})], both exhibiting distortions of about 24 °. The planarity imposed by the central ring contrasts with the distortion observed for the phenolate rings. The angles between the main NOON plane and the plane described by each phenolate ring are 41.92 and 23.88 °. As for [Ni(Psalophen^{OMe2})], one of the nitrogen atoms, here N2, presents an almost tetrahedral geometry with angles of 119, 106 and 111 ° for the P2-N2-C2, P2-N2-Cu and C2-N2-Cu segments, respectively. As a consequence, N-P bonds are slightly different: the P2-N2 measures 1.629(2) Å, while P1-N1 measures 1.612(2) Å and N1 remains trigonal planar. Neither an electronic density nor a counter ion was found next to N2, ruling out the possibility of protonation of the iminophosphorane function. Due to this distortion a short contact has been established between P2 and the Cu which are separated by 2.847 Å. A similar interaction was observed for other Cu and Ni phosphasalophen derivatives. The Cu-O bonds were measured at 1.882(2) and 1.871(2) Å, these values are slightly lower compared to [Cu(Psalophen^{Me})] and [Cu(Psalophen^{CF3})] but much lower to those measured in [Cu(Psalophen)] (1.966(2) and 1.940(2) Å). Cu-N bond lengths are the shortest measured in the Cu phosphasalophen series with 1.900(2) and 1.911(2) Å, compared to 1.995(3) and 1.951(3) Å bond lengths obtained for [Cu(Psalophen)]. This can be explained by the better electron-donating ability of the nitrogen atoms due to lower delocalization of its electron pairs in the phenylene ring.

2.5 Electrochemical studies

The electrochemical properties of the neutral complexes were studied by cyclic voltammetry in dichloromethane solutions. All potentials are referred to Fc^+/Fc which was used as internal reference.

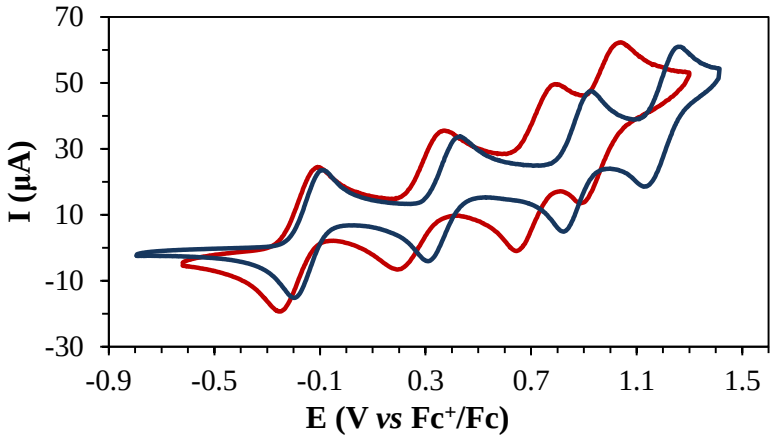

Figure 134. Cyclic voltammograms of [Cu(Psalophen^{OMe2})] (blue line) and [Ni(Psalophen^{OMe2})] (red line) recorded in dichloromethane. Conditions: 3 mM of complex in dichloromethane at 0.1 V/s.

[Ni(Psalophen^{OMe2})] complex displays four reversible one-electron oxidations corresponding to the oxidation of the four redox-active sites present in the molecule: the phenylene bridge, the metal center and both phenolate rings (Figure 134, red line). On the other hand, no reduction process was observed in the solvent range studied. The first oxidation occurs at $E^1_{1/2}$ = -0.17 V which is the lowest value obtained for all the nickel and copper phosphasalen complexes studied in this work. This first oxidation was assigned to the phenylene ring which was favored by the presence of the two methoxy substituents. The second oxidation takes place at $E^2_{1/2}$ = 0.31 V, still lower compared to other phosphasalen complexes. The gap between the two oxidations is ΔE_{1-2} = 0.48 V is lower than for [Ni(Psalophen^{Me})] (ΔE_{1-2} = 0.59 V) and for [Ni(Psalophen^{CF3})] (ΔE_{1-2} = 0.60 V), in agreement with a lower contribution of the metal orbitals in the SOMO, *i.e.*, a larger localization of the radical in the ligand. The assignment of the other oxidations would require spectro-electrochemistry experiments.

These oxidations take place at lower potentials than the salen analogue [Ni(Salophen^{OMe})] which occurred at $E^1_{1/2}$ = 0.45 V and $E^2_{1/2}$ = 0.69 V (ΔE_{1-2} = 0.24 V).[3a] Note that for this complex the first oxidation was attributed to the oxidation of a phenolate ring.

Compound	$E^1_{1/2}$	$E^2_{p,a}$	$E^3_{p,a}$	$E^4_{p,a}$
[Ni(Psalophen)]	0.15	0.78[a]	1.09	-
[Ni(Psalophen^{Me})]	0.04	0.70	0.85	1.03
[Ni(Psalophen^{CF3})]	0.21	0.81	-	-
[Ni(Psalophen^{OMe2})]	-0.17	0.31[a]	0.74[a]	0.96[a]
[Cu(Psalophen)]	0.28	0.76	1.01	-
[Cu(Psalophen^{Me})]	0.14	0.70[a]	0.95	-
[Cu(Psalophen^{CF3})]	0.39	0.86[a]	1.05	-
[Cu(Psalophen^{OMe2})]	-0.14	0.37[a]	0.88[a]	1.19[a]

Table 28. Redox potentials for nickel and copper phosphasalophen complexes, expressed in V *vs* Fc^+/Fc. [a] $E_{1/2}$ potentials.

The cyclic voltammogram of [Cu(Psalophen^{OMe2})] is very similar to that of the nickel analogue (Figure 134, blue line), suggesting a similar electronic structure. It displays four reversible oxidations at $E^1_{1/2}$ = -0.14 V, $E^2_{1/2}$ = 0.37 V, $E^3_{1/2}$ = 0.88 V and $E^4_{1/2}$ = 1.19 V. The redox potentials are slightly anodically shifted compared to [Ni(Psalophen^{OMe2})], as it has been observed for other phosphasalen complexes. The values obtained are also significantly lower than those observed for the salen analogue [Cu(Salophen^{OMe})], $E^1_{1/2}$ = 0.41 V and $E^2_{1/2}$ = 0.70 V,[4a] due to the presence of iminophosphorane functions.

Despite the similarity between the two voltammograms, some differences were found in the gaps between the different oxidations. The ΔE_{n-n+1} are larger for [Cu(Psalophen^{OMe2})] than for [Ni(Psalophen^{OMe2})] (Table 29), and points to a greater delocalization in [Cu(Psalophen^{OMe2})]$^{n+}$ upon the successive oxidation steps compared to [Ni(Psalophen^{OMe2})]$^{n+}$. The geometrical arrangements derived from the different oxidations may also influence the values of the oxidation potentials.

	ΔE_{1-2}	ΔE_{2-3}	ΔE_{3-4}
[Ni(Psalophen^{OMe2})]	0.48	0.43	0.22
[Cu(Psalophen^{OMe2})]	0.51	0.51	0.31

Table 29. Successive redox potential gaps for [Ni(Psalophen^{OMe2})] and [Cu(Psalophen^{OMe2})] in V.

3. Oxidation of neutral complexes

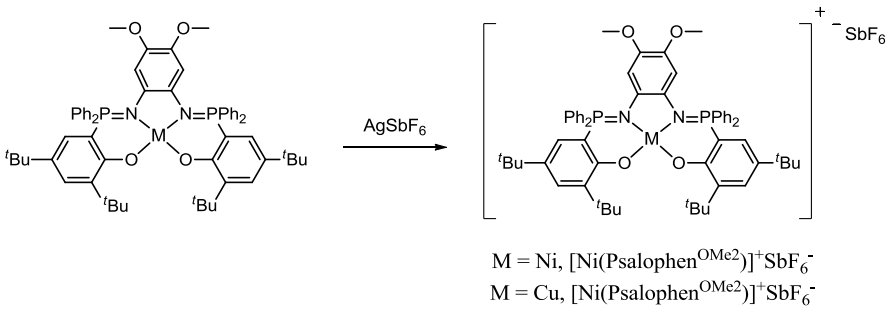

Scheme 74. Chemical oxidation of [Ni(Psalophen^{OMe2})] and [Cu(Psalophen^{OMe2})] complexes.

[Ni(Psalophen^{OMe2})] and [Cu(Psalophen^{OMe2})] were oxidized using one equivalent of $AgSbF_6$ in either dichloromethane or THF solutions under inert conditions (Scheme 74). Addition of $AgSbF_6$ into a solution of [Ni(Psalophen^{OMe2})] induces a color change from blue to dark brown, while the solution of [Cu(Psalophen^{OMe2})] remains green. The solution containing [Ni(Psalophen^{OMe2})]$^+$ was filtered, the solvent was evaporated and the residue dissolved in a small amount of diethyl ether followed by precipitation with petroleum ether. The solution containing [Cu(Psalophen^{OMe2})]$^+$ was filtered and then concentrated. Precipitation of the product was induced by addition of petroleum ether. The obtained solids were washed with petroleum ether and dried under vacuum, leading to [Ni(Psalophen^{OMe2})]$^+SbF_6^-$ as a dark blue solid in 77 % yield, and [Cu(Psalophen^{OMe2})]$^+SbF_6^-$ as a dark red solid in 65 % yield.

4. Characterization of the oxidized complexes

4.1 NMR spectroscopy

Both oxidized [Ni(Psalophen^{OMe2})]$^+$ and [Cu(Psalophen^{OMe2})]$^+$ complexes display paramagnetic ^{1}H NMR spectra, while no ^{31}P resonance was observed.

The ^{1}H NMR spectrum of [Ni(Psalophen^{OMe2})]$^+$ recorded in CD_2Cl_2 shows signals at 11.05, 8.11, 7.71, 6.96, 4.66, 1.22 and 0.97 ppm (Figure 135). The other signals correspond to residual THF and diethyl ether. The spectrum was recorded in a 300 ppm spectral width window and no other signals were detected.

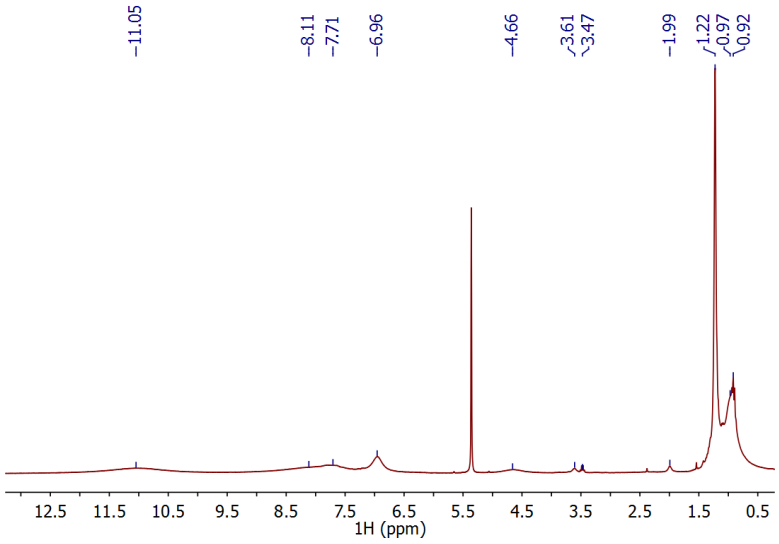

Figure 135. ^{1}H NMR spectrum of [Ni(Psalophen^{OMe2})]$^{+}$ in CD_2Cl_2 at 20 ° C.

From the intensity and the chemical shift of the signals, they were assigned as follow: t-butyl protons at 1.22 and 0.97 ppm, protons of the phenoxide or the phenylene ring at 4.66 ppm, the protons of the methoxy groups at 6.96 ppm, and the remaining aromatic protons (phenyl phosphine and phenoxide protons) at 7.71, 8.11 and 11.05 ppm. Despite the high concentration of the complex in the NMR sample (12 mg in 0.5 mL) the signals are very broad, except for the tert-butyl signals (especially the one at 1.22 ppm) which do not present significant paramagnetic shifts. This contrasts with the ^{1}H NMR spectra of the alkyl phosphasalen derivatives [Ni(^{iPr}Psalen)]$^{+}$, [Ni(Psalen^{OMe})]$^{+}$ and [Ni(Psalen^{tBu})]$^{+}$ whose signals were sharper and at down-field shifted (20-30 ppm).

In order to get further information about the electronic structure of [Ni(Psalophen^{OMe2})]$^{+}$, the ^{1}H NMR spectrum was recorded at different temperatures (Figure 136).

When decreasing the temperature most of the signals broaden making difficult the study of the chemical shift variations with the temperature. The signals of THF shift by 0.44 and 0.24 ppm between 30 and -30 °C; below this temperature they merge with the baseline. This evidences a paramagnetic behavior of the solvent that could be explained by binding to the nickel center.

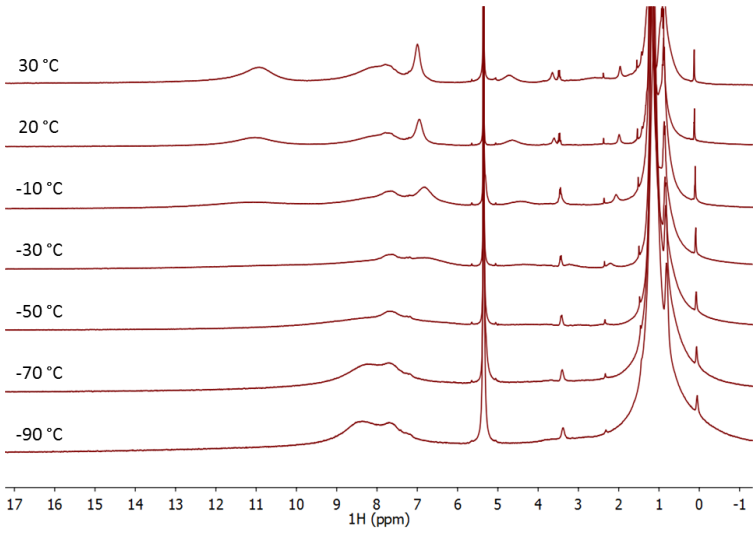

Figure 136. ^{1}H NMR spectrum of [Ni(Psalophen^{OMe2})]$^{+}$ in CD_2Cl_2 at different temperatures.

Coordination of solvent (H_2O, MeOH, py…) molecules to oxidized nickel salen complexes has been reported and was demonstrated to stabilize Ni^{III} centers.[15b] To get more information about the influence of the solvent in [Ni(Psalophen^{OMe2})]$^{+}$, its ^{1}H NMR spectrum was also recorded in THF-d^8 (Figure 137).

The spectrum of [Ni(Psalophen^{OMe2})]$^{+}$ in THF-d^8 dramatically changes from that recorded in CD_2Cl_2 (Figure 137).

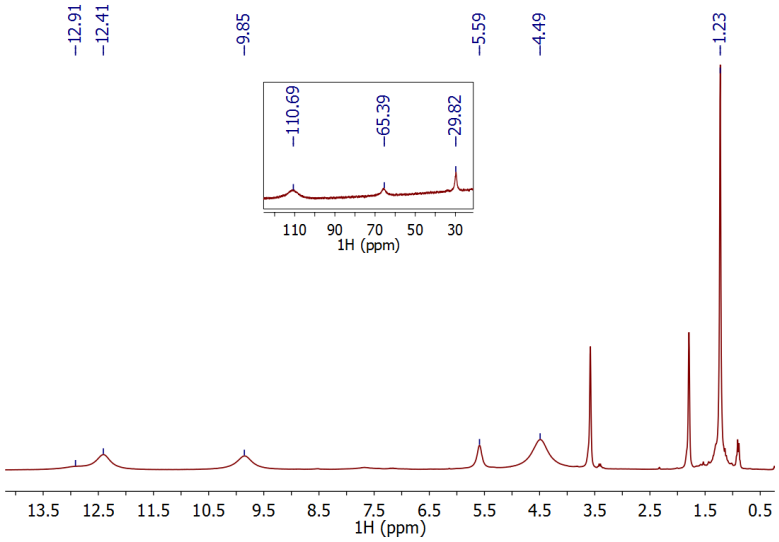

Figure 137. ^{1}H NMR spectrum of [Ni(Psalophen^{OMe2})]$^{+}$ in THF-d^8 at 20 ° C.

Some resonances are strongly shifted to 110.69, 65.39 and 29.82 ppm, while others as the t-butyl protons at 1.23 ppm are not affected. From their integrated areas these signals were tentatively assigned: the t-butyl protons at 1.23 and 4.49 ppm, the methoxy groups

at 5.59 ppm, the aromatic protons of the phenyl phosphine substituents at 9.85, 12.41 and 12.91 ppm, and the signals at 110.69, 65.39 and 29.82 may correspond to the protons of the phenoxide and the phenylene ring. Thus, the paramagnetic isotropic shift increases in presence of THF.

The behavior of these signals was investigated with respect to temperature, between 45 and -90 °C, and contrary to the spectra recorded in CD_2Cl_2, the signals experienced significant variations with the temperature. The only signal which does not experience any change is the signal corresponding to the t-butyl protons present at 1.23 ppm.

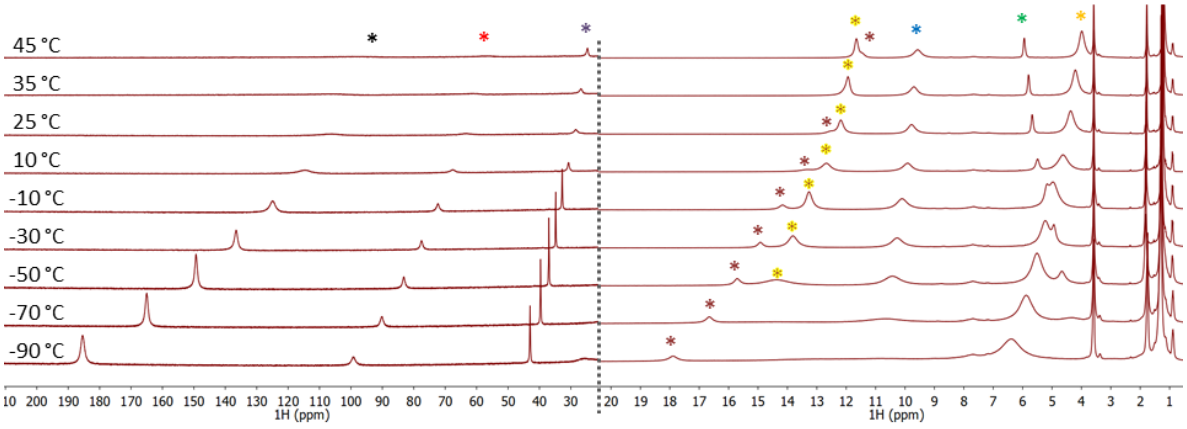

Figure 138. ^{1}H NMR spectra of [Ni(Psalophen^{OMe2})]$^+$ in THF-d8 at different temperatures. Both spectra (left and right) do not present the same intensity. The color code from left to right is: black, red, purple, yellow, brown, blue, green, and orange.

Figure 138 (right) presents a zoom of the 0-20 ppm region. When decreasing the temperature from 45 to -90 °C, the t-butyl protons signal at 1.23 ppm shifts only by 0.10 ppm, while the signal of the other t-butyl groups (orange star) shifts by 4.49 ppm. The signal assigned to the methoxy protons which is present at room temperature at 5.59 ppm (green star) shifts by 1.64 ppm between 45 and -80 °C. The signals assigned to the phenyl phosphine protons (blue and yellow stars) shift by 1.10 ppm and 2.72 ppm, respectively, while the signal at 12.91 ppm (phenyl phosphine protons, brown star) experiences a larger variation of 6.42 ppm between 45 and -90 °C.

The signals present at low field experienced the largest variations (Figure 138, left side). These signals become sharper when decreasing the temperature. The signals marked with the purple, red and black stars shift by 18.28, 42.65, and 90.90 ppm, respectively. Assuming that these signals correspond to the phenylene and phenoxide rings, this points to an important contribution of both aromatic rings in the SOMO of the complex

The plot of the chemical shifts *vs.* temperature shows that these variations are not linear with the temperature, as we could expect for a paramagnetic compound following the Curie law (Figure 139). The curve suggests the existence of two different linear regimes with an inflection point around -10 °C (0.0038 value in the abscissa axis).

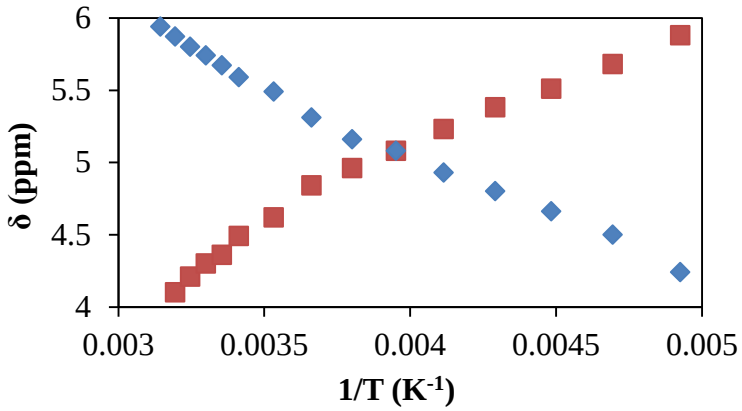

Figure 139. Plot of the chemical shifts (δ) of the signal present at 4.49 ppm at 20 °C marked with yellow stars (red squares) and signal at 5.59 ppm at 20 °C marked with green stars (blue squares) *vs* 1/T (in the 45 to -90 °C range) for [Ni(Psalophen^{OMe2})]$^{+}$.

Taking in account this inflection point, two different linear fits were done for each proton. Figure 140 and Figure 141 present two different plots corresponding to the variation with temperature of the signals present at 5.59 (green star) and 4.49 ppm (orange star) at room temperature, respectively.

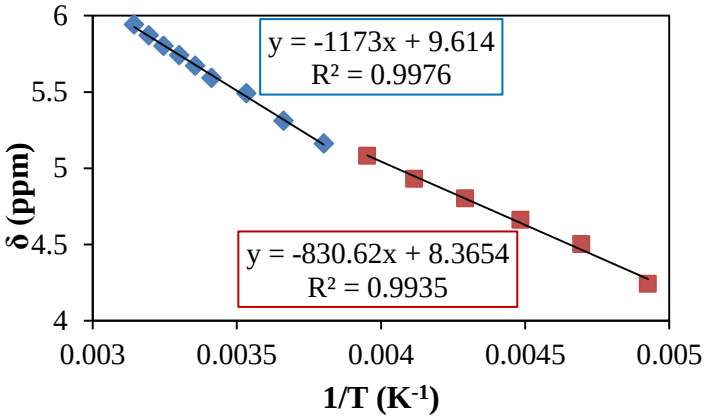

Figure 140. Plot of the chemical shifts (δ) of the signal present at 5.59 ppm at 20 °C (marked with a green star) *vs.* 1/T. Two different linear fits are done from 45 to -10 °C (blue squares), and from -20 to -70 °C (red squares).

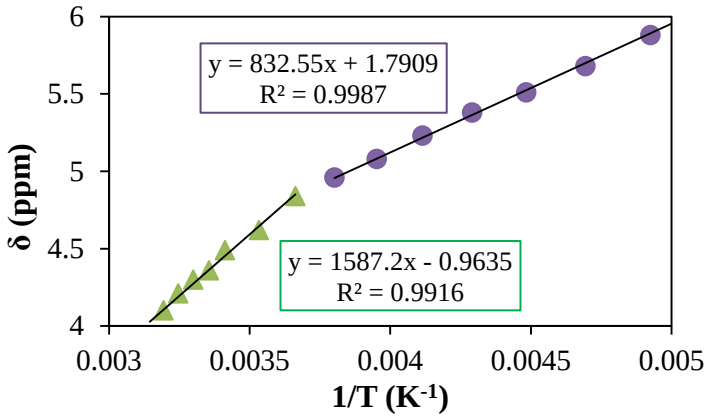

Figure 141. Plot of the chemical shifts (δ) of the signal present at 4.49 ppm at 20 °C (marked with a yellow star) *vs.* 1/T. Two different linear fits are done from 45 to -10 °C (blue squares), and from -20 to -90 °C (red squares).

This different behavior observed for the same proton should be related to the presence of two different species in solution, *i.e.*, two different environments for the same proton. From the differences observed between the ^{1}H NMR spectrum in both CD_2Cl_2 and THF-d^8 solutions, we hypothesize that coordination of THF plays a role, this coordination being favored at low temperatures.

Thus, at high temperatures only a weak interaction between $[Ni(Psalophen^{OMe2})]^+$ and the THF molecules may predominate, while $[Ni(Psalophen^{OMe2})(THF)_n]^+$ may predominate at low temperatures (below -10 °C). This would explain the presence of two different species.

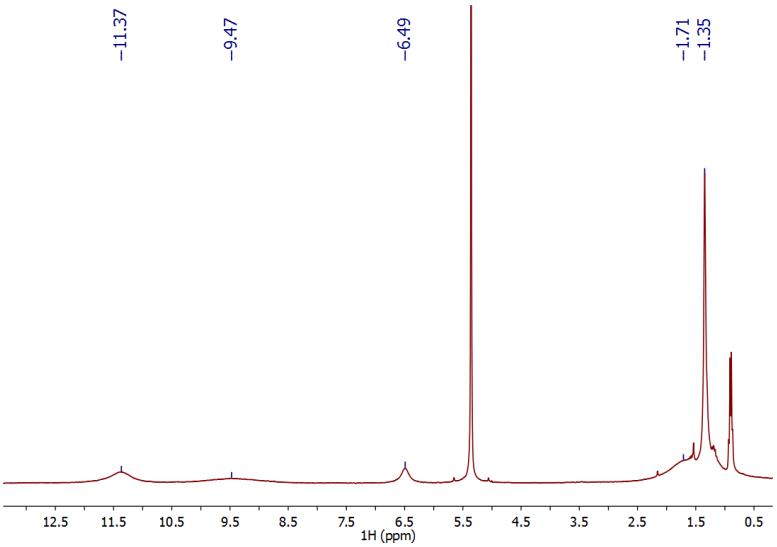

Figure 142. ^{1}H NMR spectrum of $[Cu(Psalophen^{OMe2})]^+$ in CD_2Cl_2 at 20 ° C. The signal at 0.9 ppm corresponds to pentane.

[Cu(Psalophen^{OMe2})]$^{+}$ exhibits also a paramagnetic ^{1}H NMR spectrum and no resonance in the ^{31}P NMR spectrum. The ^{1}H NMR spectrum recorded at room temperature resembles that obtained for the neutral complex [Cu(Psalophen^{OMe2})] (Figure 129 and Figure 142). Broad signals are present between 1 and 12 ppm; no other signal was detected in a spectral window of 300 ppm width. It is difficult to assign the signals observed since their broad shape does not allow proper integration. Only the signals at 6.49, 1.71 and 1.35 ppm were assigned thanks to their relative intensities and chemical shifts to the methoxy protons and the t-butyl protons, respectively.

The signals observed for [Cu(Psalophen^{OMe2})]$^{+}$ are only slightly shifted compared to those of [Cu(Psalophen^{OMe2})], the t-butyl signals shift by 0.29 and 0.09 ppm, and the methoxy signals shift by 3.42 ppm.

The ^{1}H NMR spectrum was recorded at different temperatures, between 30 and -90 °C in CD_2Cl_2 (Figure 143). An important shift is observed for all the signals except the one corresponding to the t-butyl protons at 1.35 ppm, which shifts only by 0.24 ppm in the temperature range studied. While some signals broaden when decreasing the temperature, others appear at 43.32 and 88.94 ppm at -40 °C (Figure 143, left).

The variation of the chemical shifts with the temperature was investigated for the signals present at 6.49 and 11.37 ppm at 20 °C, marked in Figure 143 with blue and orange stars, respectively. The plots of the chemical shifts *vs* the temperature are represented in Figure 144 and Figure 145.

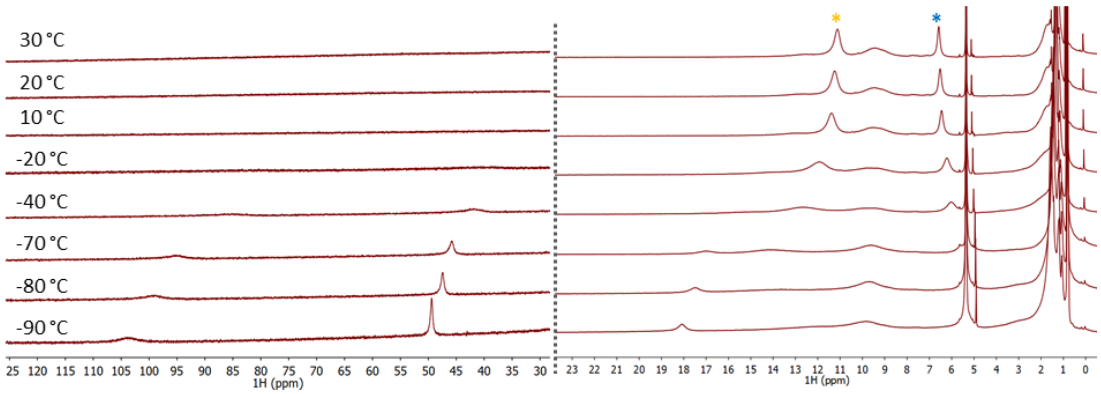

Figure 143. ^{1}H NMR spectra of [Cu(Psalophen^{OMe2})]$^{+}$ in CD_2Cl_2 at different temperatures.

The variations experienced by the signal with a blue stars (assigned to the methoxy protons) follow a linear response with the temperature, as expected for a paramagnetic compound following the Curie law (Figure 144).

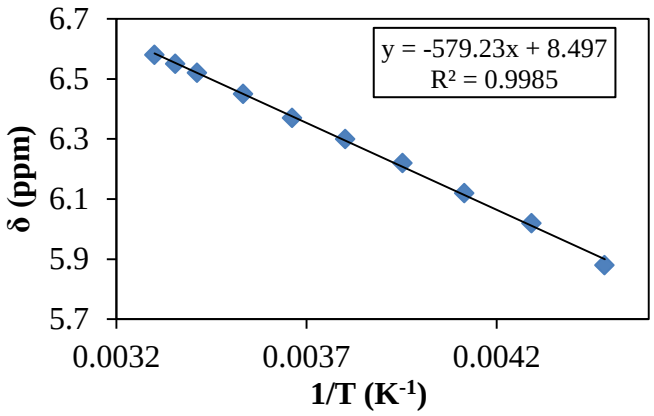

Figure 144. Plot of the chemical shifts (δ) of the signal at 6.49 ppm at 20 °C (blue star) in CD_2Cl_2 *vs.* 1/T (in the 30 to -50 °C temperature range) for $[Cu(Psalophen^{OMe2})]^+$.

However, the variations observed for the signal marked with an orange star are not linear with the temperature (Figure 145). In this case, a possible coordination of THF molecules cannot account for this behavior since no THF is detected in the NMR spectrum. This unusual behavior could not be explained.

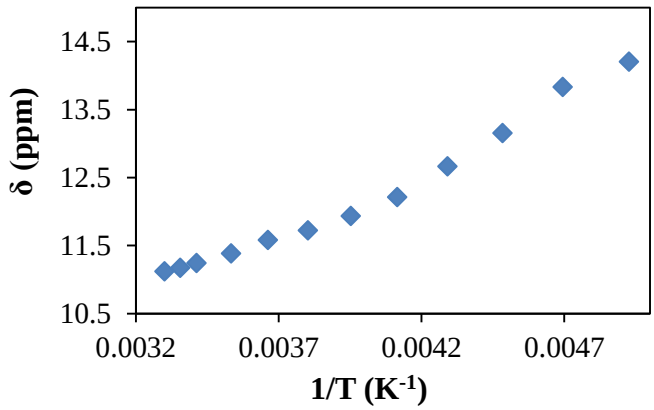

Figure 145. Plot of the chemical shifts (δ) of the signal at 11.37 ppm at 20 °C (yellow star) in CD_2Cl_2 *vs.* 1/T (in the 30 to -70 °C temperature range) in $[Cu(Psalophen^{OMe2})]^+$.

4.2 EPR spectroscopy

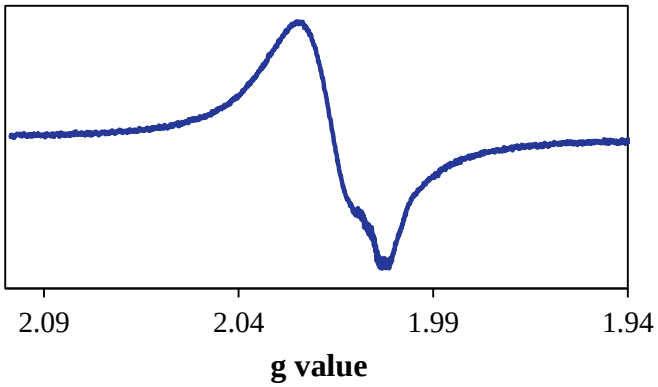

Figure 146. X-band EPR spectrum of [Ni(Psalophen^{OMe2})]$^+$ in dichloromethane at 290 K. Conditions: Frequency: 9.381 GHz; Power: 1.00 mW; modulation frequency: 100 kHz; amplitude: 1.0 mT.

[Ni(Psalophen^{OMe2})]$^+$ displays an isotropic signal centered at g_{iso} = 2.015 at room temperature with a peak-to-peak line width of 37 G, consistent with a Ni^{II} radical complex. This signal is similar to that observed for [Ni(Psalophen^{Me})]$^+$ at room temperature (g_{iso} = 2.035), and to those observed by J. Reedijk and J-L- Pierre for [Ni(salophen)] (g_{iso} = 2.035)[1a] and [Ni(Salophen^{Me})]$^+$ (g_{iso} = 2.040) complexes.[15a] The lower g_{iso} value obtained for [Ni(Psalophen^{OMe2})]$^+$ points to a small contribution of the metallic orbitals to the SOMO.

As discussed with [Ni(Psalophen^{Me})]$^+$, the symmetry of the signal obtained for [Ni(Psalophen^{OMe2})]$^+$ changes when decreasing the temperature.

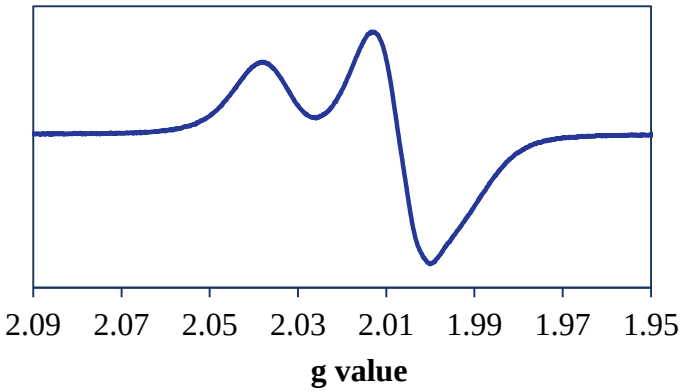

Figure 147. X-band EPR spectrum of [Ni(Psalophen^{OMe2})]$^+$ in dichloromethane at 160 K. Conditions: Frequency: 9.387 GHz; Power: 1.006 mW; modulation frequency: 100 kHz; amplitude: 0.1 mT.

At 160 K, once the solution is frozen, the signal displays an almost rhombic symmetry with g_1 = 2.038 and g_2 = 2.005, and a poorly defined g_3 around 1.994 (Figure 147). The intensity of the rhombic signal increases when decreasing the temperature and the g_3 value splits

from the g_2 line. At 80 K, the signal displays a clear rhombic pattern (Figure 148). The g values obtained by simulation are $g_1 = 2.042$, $g_2 = 2.007$ and $g_3 = 1.987$ ($g_{av} = 2.012$).

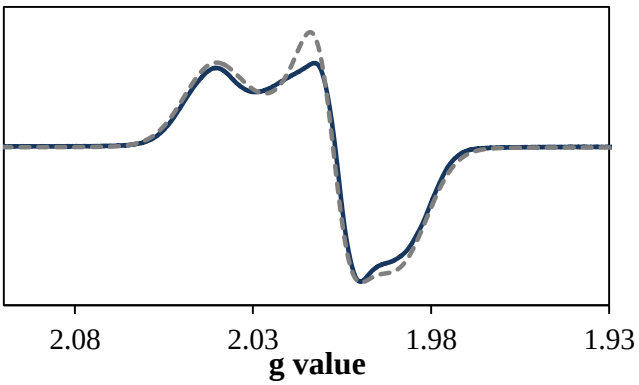

Figure 148. X-band EPR spectrum of [Ni(Psalophen^{OMe2})]$^+$ in dichloromethane at 80 K. Conditions: Frequency: 9.389 GHz; Power: 1.003 mW; modulation frequency: 100 kHz; amplitude: 0.1 mT. Solid line: experimental spectrum; dotted lines: simulated spectrum.

When compared to values obtained for [Ni(Psalophen^{Me})]$^+$ ($g_1 = 2.098$, $g_2 = 2.005$ and $g_3 = 1.987$, $g_{av} = 2.030$), only g_1 differs substantially being higher for the latter. This suggests the metal orbitals contribute more to g_1 in [Ni(Psalophen^{Me})]$^+$ than in [Ni(Psalophen^{OMe2})]$^+$. The similarity between the g_{iso} value obtained at room (2.015) temperature and the g_{av} value obtained at low temperature (2.012) for [Ni(Psalophen^{OMe2})]$^+$ indicates that a unique species is present throughout the temperature range studied. From the symmetry and the g_{av} value observed, intermediate between that of Ni^{III} species (2.15-2.22)[8c,19] and that of phenol and diaminobenzene radicals species (2.005)[6-7,20], it is difficult to conclude about the nature of the generated species. However, it presents a main organic radical nature.

The differences in the symmetry of the signals observed may be due to a difference in the mobility of the molecule between high and low temperatures, which leads to broad signals when the mobility is high (high temperature) and sharper signals when the mobility of the molecule is reduced (low temperatures).[11]

The analogous salen complex [Ni(Salophen^{OMe})]$^+$ exhibits also a rhombic signal at low temperatures characterized by $g_1 = 2.070$, $g_2 = 2.014$ and $g_3 = 2.000$ ($g_{av} = 2.028$), which was described as a phenoxyl Ni(II)-radical complex.[3a]

[Cu(Psalophen^{OMe2})]$^+$ displays a rhombic signal in dichloromethane with a four line-pattern typical for the coupling with a ^{63}Cu center (I = 3/2). This signal is well defined only at temperatures below 160 K.

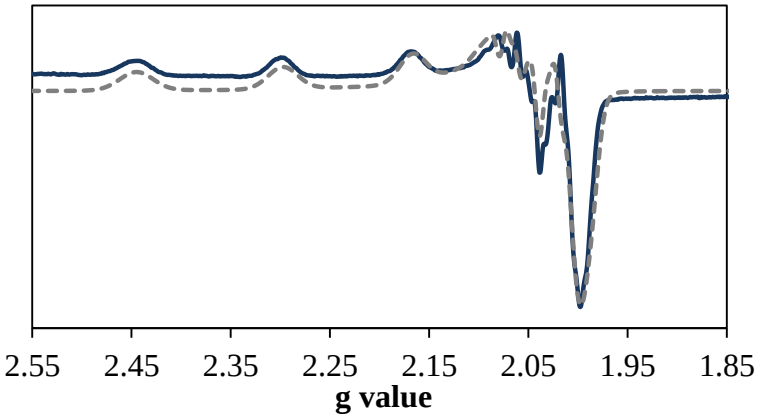

Figure 149. X-band EPR spectrum of [Cu(Psalophen^{OMe2})]$^{+}$ in dichloromethane at 80 K. Conditions: Frequency: 9.386 GHz; Power: 1.00 mW; modulation frequency: 100 kHz; amplitude: 1.0 mT. Solid line: experimental spectrum; dotted lines: simulated spectrum.

Such signal discards the possibility of a Cu^{III} $3d^8$ complex formed upon oxidation, in agreement with the paramagnetic ^1H NMR spectrum. The formation of a radical ligand results in three possible spin arrangements for [Cu(Psalophen^{OMe2})]$^{+}$ depending on the interaction between the unpaired electron on the copper and the one on the ligand. In agreement with the EPR spectrum observed, a weak antiferromagnetic coupling between the two unpaired electrons, a ferromagnetic coupling with a small zero-field splitting, or a diradical complex where the two unpaired electrons cannot interact may be proposed as electronic configurations.

The signal recorded for [Cu(Psalophen^{OMe2})]$^{+}$ is very different from the one observed for [Cu(Psalophen^{OMe2})] (Figure 130), evidencing a change in the anisotropy of the metal orbitals, so a change on the geometry of the copper center upon oxidation.

To simplify the simulation of the spectrum, we considered a Cu^{II} $3d^9$ center and only two nitrogen atoms responsible of the superhyperfine coupling. No feature typical of a triplet state was observed at high-field values (g ~ 4).[9-11] Therefore, the possibility of two superimposed signals, a main one corresponding to the Cu^{II} center and another to the phenylene radical, was the most likely situation. The g values obtained from simulation are g_1 = 2.230, g_2 = 2.044 and g_3 = 2.044, and the hyperfine coupling constants are A_{Cu} = 550, 80 and 55 MHz, respectively. The superhyperfine coupling observed with the two nitrogen atoms are A_N = 10, 48, 48 MHz for g_1, g_2 and g_3, respectively. An isotropic signal corresponding to the ligand radical could be superimposed with the Cu^{II} signal at g = 2.005, where a large feature is observed, making the possibility of a diradical complex likely. These values contrast with those obtained for the neutral complex

[Cu(Psalophen^{OMe2})], g_1 = 2.127, g_3 = 2.108 and g_3 = 2.051, and A_{Cu} = 250, 210 and 80 MHz, respectively. The superhyperfine coupling with the two nitrogen atoms are A_N = 10, 48 and 48 MHz

This spectrum resembles that obtained for the neutral salen complex [Cu(Salophen^{NMe2})] (Scheme 55).[9] For this, g_1 = 2.197, g_2 = 2.042 and g_3 = 2.042 and hyperfine coupling constants A_{Cu} = 568, 106 and 106 MHz were obtained.

4.3 UV-vis spectroscopy

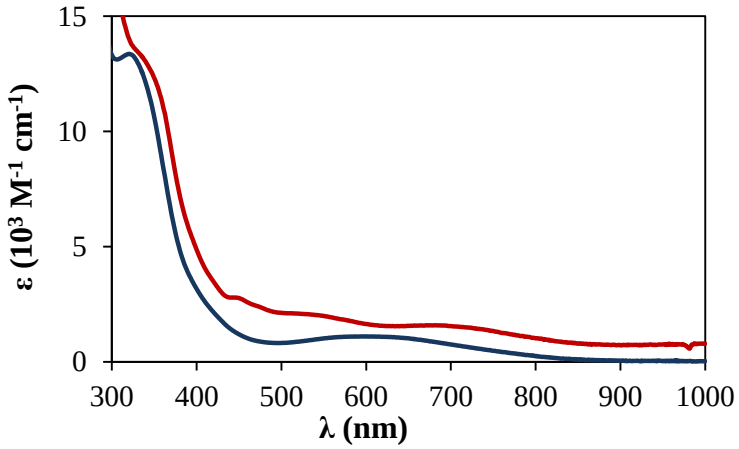

Figure 150. UV-vis spectra of [Ni(Psalophen^{OMe2})] (blue line) and [Ni(Psalophen^{OMe2})]$^+$ (red line) in dichloromethane.

The UV-vis spectrum of [Ni(Psalophen^{OMe2})]$^+$ changes slightly from that of the neutral complex. The band at 650 nm present in [Ni(Psalophen^{OMe2})] disappears upon oxidation and two new bands appear at 685 nm (ε = 1600 M^{-1} cm^{-1}) and at 505 nm (ε = 2100 M^{-1} cm^{-1}). The intense band present at 330 nm in [Ni(Psalophen^{OMe2})] seems to be slightly red-shifted to 340 nm and more intense (ε = 13400 M^{-1} cm^{-1}).

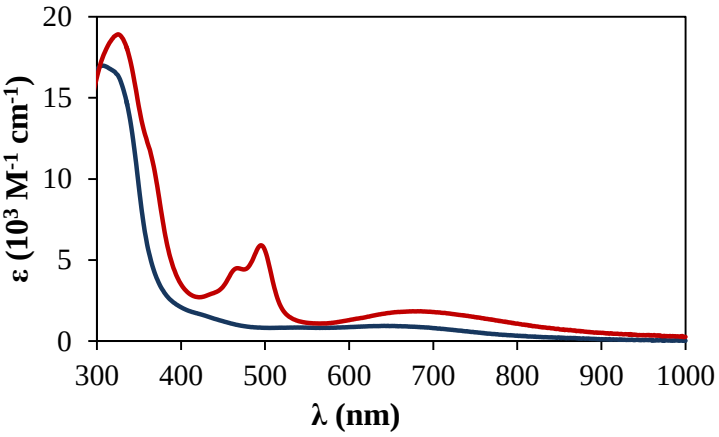

Figure 151. UV-vis spectra of [Cu(Psalophen^{OMe2})] (blue line) and [Cu(Psalophen^{OMe2})]$^{+}$ (red line) in dichloromethane.

[Cu(Psalophen^{OMe2})]$^{+}$ presents a large band at 680 nm (ε = 1800 M^{-1} cm^{-1}) and two sharp transitions at 495 nm (ε = 5900 M^{-1} cm^{-1}) and at 465 nm (ε = 4500 M^{-1} cm^{-1}). The intense band present at 307 nm in [Cu(Psalophen^{OMe2})] is slightly red-shifted to 324 nm and more intense (ε = 18900 M^{-1} cm^{-1}).

The UV-vis spectra of [Ni(Psalophen^{OMe2})]$^{+}$ and [Cu(Psalophen^{OMe2})]$^{+}$ are very different from those recorded for the oxidized phosphasalen featuring alkyl linker, namely [M(Psalen^{tBu})]$^{+}$, [M(Psalen^{OMe})]$^{+}$ and [M(^{iPr}Psalen)]$^{+}$, which were characterized by two intense transitions (ε ≤ 5000 M^{-1} cm^{-1}) ranging between 500-560 nm and at 1000 nm. However, these spectra are similar to those obtained for the mono-substituted phenylene derivatives [Cu(Psalophen^{Me})]$^{+}$ and [Cu(Psalophen^{CF3})]$^{+}$.

4.4 X-ray diffraction

Single crystals of [Ni(Psalophen^{OMe2})]$^{+}SbF_6^{-}$ were obtained from a toluene/dichloromethane solution stored at -40 °C.

The X-ray structure of [Ni(Psalophen^{OMe2})]$^{+}SbF_6^{-}$ shows a small contraction of the coordination sphere along the N1-Ni-O2 axis: Ni-N1 bond shorten by 0.013 Å, and Ni-O2 by 0.028 Å (Table 30). The distortion from the square planar geometry slightly decreases from 9.52 ° in [Ni(Psalophen^{OMe2})] to 7.52 ° in the oxidized complex.

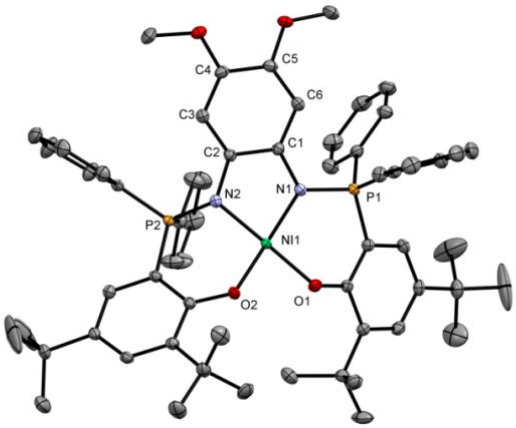

Figure 152. ORTEP of [Ni(Psalophen^{OMe2})]$^{+}$SbF$_6^{-}$ with thermal ellipsoids at 50 % probability. Hydrogen atoms and a molecule of SbF$_6^{-}$ have been omitted for clarity.

The bond lengths of the phenoxide rings do not experience significant variations but the bonds of the phenylene ring do. The N1-C1 and N2-C2 bonds shorten by 0.051 and 0.040 Å, and as a consequence, the N1-P1 and N2-P2 lengthen by 0.038 and 0.027 Å. The C1-C2 and C4-C5 bonds of the phenylene ring lengthen by 0.037 and 0.035 Å, respectively, while the C5-C6 and C3-C4 shorten by 0.013 and 0.016 Å. The C4-OMe and C5-OMe also shorten by 0.032 and 0.026 Å. The C1-C6 and C2-C3 bonds do not experience significant changes. These metrical variations correspond to an iminobenzosemiquinonate pattern of the phenyl ring as found for the [Cu(Salophen^{OMe})]$^{+}$SbF$_6^{-}$ salen derivative and other similar diaminobenzene radical ligands.[4a,10,18] Scheme 75 shows the bond distances of the phenylene ring for neutral and oxidized complexes.

The variations observed in the phenylene ring clearly indicate a ligand-based oxidation with a partial localization of the charge in the central ring. The small contractions observed for Ni-N and Ni-O bonds may indicate a small contribution of the metal in the stabilization of the charge.

	[Ni(Psalophen^{OMe2})]	**[Ni(Psalophen^{OMe2})]$^{+}$SbF$_6$**	**Δ**
Ni-O1	1.861(2)	1.861(1)	0.000
Ni -O2	1.886(2)	1.858(2)	-0.028
Ni -N1	1.893(2)	1.880(2)	-0.013
Ni -N2	1.895(2)	1.903(2)	0.008
P1-N1	1.622(2)	1.660(2)	0.038
P2-N2	1.620(2)	1.647(2)	0.027
Torsion angle[a]	9.50	7.52	-2.00

Table 30. Selected bond distances (Å) and angles (°) for [Ni(Psalophen^{OMe2})] and [Ni(Psalophen^{OMe2})]$^{+}$SbF$_6^{-}$. [a] Torsion of the NOON plane.

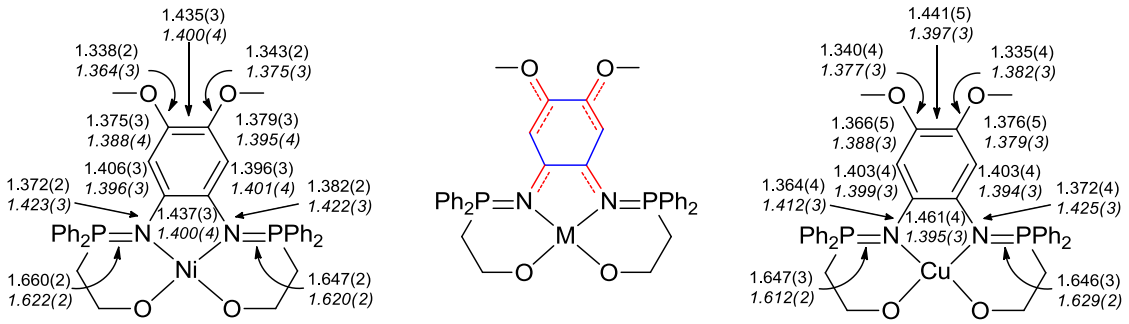

Scheme 75. Experimental bond lengths (italic) of [Ni(Psalophen^{OMe2})] (left) and [Cu(Psalophen^{OMe2})] (right) and their oxidized products (regular police), expressed in Å. Bond elongations (blue) and contractions (red) of the phenylene ring for [M(Psalophen^{OMe2})]$^{+}$SbF$_6^{-}$ are represented in the middle structure.

A structure of the nickel oxidized product showing two coordinated THF was also obtained, [Ni(Psalophen^{OMe2})](THF)$_2$]$^{+}$SbF$_6^{-}$. It is well known that octahedral coordination sphere stabilizes Ni^{III} centers.[20-21]

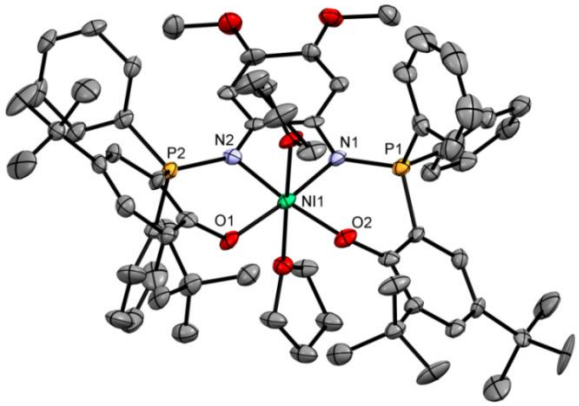

Figure 153. ORTEP of [Ni(Psalophen^{OMe2})](THF)$_2$]$^{+}$SbF$_6^{-}$ with thermal ellipsoids at 50 % probability. Hydrogen atoms, a molecule of THF and a molecule of SbF$_6^{-}$ have been omitted for clarity.

In [Ni(Psalophen^{OMe2})(THF)$_2$]$^{+}$SbF$_6^{-}$ the Ni center displays a octahedral geometry where the main plane contains the four coordinating atoms of the phosphasalophen ligand (NOON) and two molecules of THF occupy apical positions. Ni-O bonds measure 2.025(6) and 2.020(6) Å, while the Ni-N are 2.074(7) and 2.085(7) Å. These bonds are longer than the ones observed for the tetracoordinated [Ni(Psalophen^{OMe2})]$^{+}$SbF$_6^{-}$ complex. The Ni-O axial bond distances are 2.162(6) and 2.147(6) Å and the angle between these three atoms (O3-Ni-O4) is 177.04 °, presenting a slight distortion from the ideal geometry.

	[Ni(Psalophen^{OMe2})]	[Ni(Psalophen^{OMe2})(THF)$_2$]$^+$SbF$_6^-$	Δ
Ni-O1	1.862(2)	2.025(6)	-0.001
Ni-O2	1.886(2)	2.020(6)	-0.028
Ni -N1	1.895(2)	2.074(7)	-0.015
Ni -N2	1.896(2)	2.085(7)	0.007
P1-N1	1.622(2)	1.643(7)	0.038
P2-N2	1.620(2)	1.633(7)	0.027
Ni-O3	-	2.162(6)	-
Ni-O4	-	2.147(6)	-

Table 31. Selected bond distances (Å) for [Ni(Psalophen^{OMe2})] and [Ni(Psalophen^{OMe2})(THF)$_2$]$^+$SbF$_6^-$.

Single crystals of [Cu(Psalophen^{OMe2})]$^+$SbF$_6^-$ were obtained from a dichloromethane/pentane solution stored at -40 °C.

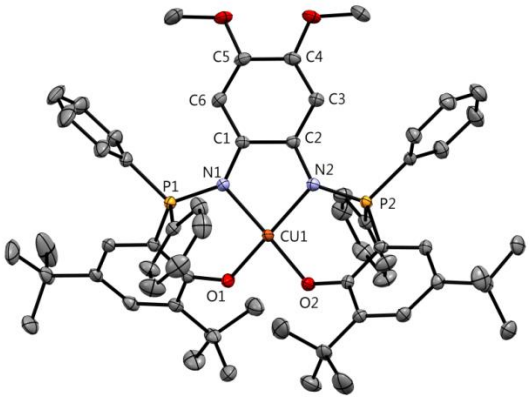

Figure 154. ORTEP of [Cu(Psalophen^{OMe2})]$^+$SbF$_6^-$ with thermal ellipsoids at 50 % probability. Hydrogen atoms, five molecules of toluene and a molecule of SbF$_6^-$ have been omitted for clarity.

Upon oxidation, the distortion from the square planar geometry increases significantly from 5.38 ° in [Cu(Psalophen^{OMe2})] to 24.07 ° in [Cu(Psalophen^{OMe2})]$^+$SbF$_6^-$ (Figure 154). The angles for the N1-Cu-O2 and N2-Cu-O1 axes are 164.08 and 158.49 °, respectively. The phenylene ring in [Cu(Psalophen^{OMe2})]$^+$SbF$_6^-$ displays a pattern similar to that observed for [Ni(Psalophen^{OMe2})]$^+$SbF$_6^-$, with larger variations (Figure 154). For [Cu(Psalophen^{OMe2})]$^+$SbF$_6^-$ no contraction of the coordination sphere is observed, contrary to [Ni(Psalophen^{OMe2})]$^+$SbF$_6^-$, ruling out the possibility of a metal-centered oxidation. Conversely, an elongation of the Cu-O and Cu-N bonds is observed, especially for the latter ones which lengthened by 0.062 and 0.060 Å. This can be explained by a shift of the electron density of the nitrogen toward the carbon atoms of the phenylene ring, as these bonds have shortened by 0.032 Å for N1-C1 and 0.027 Å for N2-C2. The C-O bonds of the methoxy substitution also shorten by 0.048 and 0.039 Å. In contrast, the C1-C2 and C4-C5 bonds are elongated by 0.069 and 0.049 Å respectively (Scheme 75). The phenylene rings

exhibits, as for [Ni(Psalophen^{OMe2})]$^{+}$SbF$_6^-$ and [Cu(Salophen^{OMe})]$^{+}$SbF$_6^-$ a *ortho*-iminobenzosemiquinonato pattern. The de-aromatization of the central ring in [Cu(Psalophen^{OMe2})]$^{+}$SbF$_6^-$ is more pronounced than for [Ni(Psalophen^{OMe2})]$^{+}$SbF$_6^-$: C1-C2 and C4-C5 bonds measure 1.461(4) and 1.441(5) Å, for [Cu(Psalophen^{OMe2})]$^{+}$SbF$_6^-$, while these are 1.437(3) and 1.435(3) Å for [Ni(Psalophen^{OMe2})]$^{+}$SbF$_6^-$. The C-N bonds are slightly shorter for [Cu(Psalophen^{OMe2})]$^{+}$SbF$_6^-$, they measure 1.364(4) and 1.372(4) Å, while for [Ni(Psalophen^{OMe2})]$^{+}$SbF$_6^-$ these measure 1.382(2) and 1.372(2) Å.

These features reveal that the oxidation occurs in the central ring. The more pronounced variations observed for [Cu(Psalophen^{OMe2})]$^{+}$SbF$_6^-$ in addition with the elongation of Cu-N bonds indicate that the generated radical is more localized in the phenylene ring in [Cu(Psalophen^{OMe2})]$^{+}$SbF$_6^-$ than in [Ni(Psalophen^{OMe2})]$^{+}$SbF$_6^-$.

	[Cu(Psalophen^{OMe2})]	**[Cu(Psalophen^{OMe2})]$^{+}$SbF$_6^-$**	**Δ**
Cu-O1	1.882(2)	1.888(2)	0.006
Cu -O2	1.871(2)	1.889(2)	0.018
Cu -N1	1.900(2)	1.962(3)	0.062
Cu -N2	1.911(2)	1.971(3)	0.060
P1-N1	1.612 (2)	1.647(3)	0.032
P2-N2	1.629(2)	1.646(3)	0.027
Torsion angle[a]	5.38	24.07	18.06

Table 32. Selected bond distances (Å) and angles (°) for [Cu(Psalophen^{OMe2})] and [Cu(Psalophen^{OMe2})]$^{+}$SbF$_6^-$. [a] Torsion of the NOON plane.

VI. Conclusion

A series of phosphasalophen complexes have been synthesized and characterized. The parent complexes [M(Psalophen)] (M = Ni, Cu) dimerize upon oxidation, evidencing the oxidation of the phenylene link in both cases. This dimerization was not observed in the case of the salen analogues and must be promoted by the partial delocalization of the lone pairs of the nitrogen in the phenylene ring. The dimerization process still needs to be studied in more detail, but EPR studies suggest the presence of an equilibrium between the open and closed-shell species in solution.

In an attempt to tune the electronic properties of the linker, some mono and disubstituted derivatives have also been synthesized. The oxidation of the aryl linker is suggested for the Psalophen^{Me}, the Psalophen^{CF3}, and the Psalophen^{OMe2} derivatives, even though no structural evidences were obtained for the Psalophen^{Me} complexes. EPR studies of the oxidized nickel complexes point to the formation of radical species for which the metal orbitals contribute differently in the stabilization of the electronic hole (Psalophen^{OMe2}<Psalophen^{Me}<Psalophen^{CF3}).

For the Psalophen^{CF3} derivatives, a lower stabilization of the *o*-diaminobenzene radical was aimed by the introduction of an electron-withdrawing group in the phenyl linker. This is evidenced by the oxidation potential values obtained for these complexes, which are the highest of the studied phosphasalophen series. Structural evidences obtained for the nickel derivative indicates that both the phenylene linker and metal center have been affected upon oxidation.

In the last place, the stabilization of the *o*-diaminobenzene radical was aimed by the introduction of two electron-donating groups on the phenyl linker. Both nickel and copper oxidized Psalophen^{OMe2} derivatives were characterized in solution and in the solid state and can be described as localized *o*-diaminobenzene radical complexes.

Phosphasalophen ligands are therefore redox-active ligands whose electronic properties can be easily modified by varying the phenyl substituents. Multiple oxidation processes can be achieved with these ligands when coordinated to nickel and copper centers; these are more accessible than in the case of salophen ligands. In a future, it will be interesting to investigate further oxidations of these complexes, as well as the electronic structure of phosphasalophen complexes when changing as well the phenolate substituents.

VII. References

[1] a) O. Rotthaus, O. Jarjayes, F. Thomas, C. Philouze, C. Perez Del Valle, E. Saint-Aman, J.-L. Pierre, *Chem. Eur. J.* **2006**, *12*, 2293-2302; b) F. Thomas, O. Jarjayes, C. Duboc, C. Philouze, E. Saint-Aman, J.-L. Pierre, *Dalton Trans.* **2004**, 2662-2669.

[2] a) K. Asami, A. Takashina, M. Kobayashi, S. Iwatsuki, T. Yajima, A. Kochem, M. v. Gastel, F. Tani, T. Kohzuma, F. Thomas, Y. Shimazaki, *Dalton Trans.* **2014**, *43*, 2283-2293; b) K. Asami, A. Takashina, M. Kobayashi, S. Iwatsuki, T. Yajima, A. Kochem, M. van Gastel, F. Tani, T. Kohzuma, F. Thomas, Y. Shimazaki, *Dalton Trans.* **2014**, *43*, 2283-2293; c) C. W. Anson, S. Gosh, S. Hammes-Schiffer, S. S. Stahl, *J. Am. Chem. Soc.* **2016**, *138*, 4186-4193; d) J. Andrez, V. Guidal, R. Scopelliti, J. Pécaut, S. Gambarelli, M. Mazzanti, *J. Am. Chem. Soc.* **2017**, *139*, 8628-8638.

[3] a) O. Rotthaus, O. Jarjayes, C. Philouze, C. P. Del Valle, F. Thomas, *Dalton Trans.* **2009**, 1792-1800; b) O. Rotthaus, O. Jarjayes, C. Perez Del Valle, C. Philouze, F. Thomas, *Chem. Comm.* **2007**, 4462-4464.

[4] a) A. Kochem, O. Jarjayes, B. Baptiste, C. Philouze, H. Vezin, K. Tsukidate, F. Tani, M. Orio, Y. Shimazaki, F. Thomas, *Chem. Eur. J.* **2012**, *18*, 1068-1072; b) L. Lecarme, L. Chiang, C. Philouze, O. Jarjayes, T. Storr, F. Thomas, *Eur. J. Inorg. Chem.* **2014**, *2014*, 3479-3487.

[5] M. B. Robin, P. Day, *Advances in Inorganic Chemistry and Radiochemistry* **1968**, *10*, 247-422.

[6] D. de Bellefeuille, M. S. Askari, B. Lassalle-Kaiser, Y. Journaux, A. Aukauloo, M. Orio, F. Thomas, X. Ottenwaelder, *Inorg. Chem.* **2012**, *51*, 12796-12804.

[7] Y. Shimazaki, T. Yajima, T. Shiraiwa, O. Yamauchi, *Inorg. Chim. Acta* **2009**, *362*, 2467-2474.

[8] a) R. S. Drago, E. I. Baucom, *Inorg. Chem.* **1972**, *11*, 2064-2069; b) H. J. Krueger, R. H. Holm, *Inorg. Chem.* **1987**, *26*, 3645-3647; c) N. D. J. Branscombe, A. J. Atkins, A. Marin-Becerra, E. J. L. McInnes, F. E. Mabbs, J. McMaster, M. Schroder, *Chem. Comm.* **2003**, 1098-1099.

[9] D. de Bellefeuille, M. Orio, A.-L. Barra, A. Aukauloo, Y. Journaux, C. Philouze, X. Ottenwaelder, F. Thomas, *Inorg. Chem.* **2015**, *54*, 9013-9026.

[10] P. Chaudhuri, C. N. Verani, E. Bill, E. Bothe, T. Weyhermüller, K. Wieghardt, *J. Am. Chem. Soc.* **2001**, *123*, 2213-2223.

[11] P. Bertrand, *La spectroscopie de résonance paramagnétique électronique : fondements*, EDP sciences, Les Ulis, **2014**.

[12] a) B. Liu, T. Yoshida, X. Li, M. Stępień, H. Shinokubo, P. J. Chmielewski, *Angew. Chem. Int. Ed.* **2016**, *55*, 13142-13146; b) T. R. Dugan, E. Bill, K. C. MacLeod, G. J. Christian, R. E. Cowley, W. W. Brennessel, S. Ye, F. Neese, P. L. Holland, *J. Am. Chem. Soc.* **2012**, *134*, 20352-20364.

[13] J. L. Deutsch, S. M. Poling, *J. Chem. Educ.***1969**, *46*, 167-168.

[14] T. P. A. Cao, G. Nocton, L. Ricard, X. F. Le Goff, A. Auffrant, *Angew. Chem. Int. Ed.* **2014**, *53*, 1368-1372.

[15] a) L. Benisvy, R. Kannappan, Y. F. Song, S. Milikisyants, M. Huber, I. Mutikainen, U. Turpeinen, P. Gamez, L. Bernasconi, E. J. Baerends, F. Hartl, J. Reedijk, *Eur. J. Inorg. Chem.* **2007**, 637-642; b) O. Rotthaus, F. Thomas, O. Jarjayes, C. Philouze, E. Saint-Aman, J. L. Pierre, *Chem. Eur. J.* **2006**, *12*, 6953-6962.

[16] L. Benisvy, R. Kannappan, Y.-F. Song, S. Milikisyants, M. Huber, I. Mutikainen, U. Turpeinen, P. Gamez, L. Bernasconi, E. J. Baerends, F. Hartl, J. Reedijk, *Eur. J. Inorg. Chem.* **2007**, *2007*, 637-642.

[17] X. Ottenwaelder, R. Ruiz-Garcia, G. Blondin, R. Carasco, J. Cano, D. Lexa, Y. Journaux, A. Aukauloo, *Chem. Comm.* **2004**, 504-505.

[18] D. Herebian, E. Bothe, F. Neese, T. Weyhermüller, K. Wieghardt, *J. Am. Chem. Soc.* **2003**, *125*, 9116-9128.

[19] Z. Xiao, B. O. Patrick, D. Dolphin, *Inorg. Chem.* **2003**, *42*, 8125-8127.

[20] L. Chiang, A. Kochem, O. Jarjayes, T. J. Dunn, H. Vézin, M. Sakaguchi, T. Ogura, M. Orio, Y. Shimazaki, F. Thomas, T. Storr, *Chem. Eur. J.* **2012**, *18*, 14117-14127.

[21] Y. Shimazaki, T. Yajima, F. Tani, S. Karasawa, K. Fukui, Y. Naruta, O. Yamauchi, *J. Am. Chem. Soc.* **2007**, *129*, 2559-2568.

Chapter 5: Mn phosphasalen complexes: coordination and reactivity

1. Introduction

The previous chapters were focused on the study of the electronic structure of oxidized copper and nickel complexes displaying various phosphasalen ligands. In this chapter we investigate the stabilization of high-valent manganese complexes and their application in catalysis. Chromium and manganese salen complexes are effective catalysts for the epoxidation of alkenes using sodium hypochlorite or iodosyl arenes as oxidants. The most famous one is the Jacobsen's catalyst (see Chapter 1, section 2.1).[1-2] The species proposed as key intermediates in these reactions are $O=M^{V}$ complexes (M = Mn, Cr). However, these species were only isolated in the case of chromium and used indeed as stoichiometric oxidants,[3] but not for manganese. Instead, a transient species was detected and identified as a μ-oxo-Mn^{IV} salen. The mechanism proposed by Kochi and co-workers is depicted in Scheme 76.[2] The detected dimeric species were hypothesized to be in equilibrium with the $O=Mn^{V}$ species.

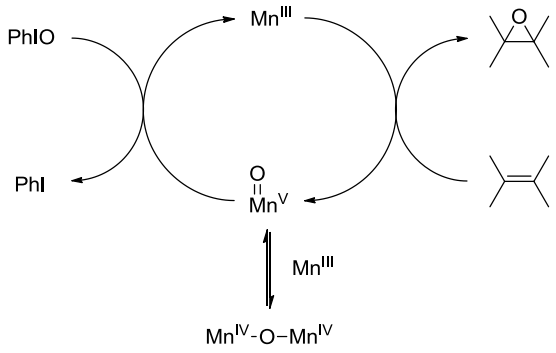

Scheme 76. Catalytic cycle for the epoxidation of alkenes using Mn salen complexes.[2]

Some years ago, Plattner and co-workers reported the first evidences of $[O=Mn^{V}(salen)]^{+}$ intermediates by MS and MS-MS experiments, corresponding to $[PhIO(salen)Mn\text{-}O\text{-}(salen)MnOIPh]^{2+}$ species.[4] Recently, spectroscopic evidences (UV-vis) of high-valent

manganese complexes have been reported.[5] However, until the day, no Mn(V)-salen oxo complex has been isolated.

The stabilization of high-valent manganese-oxo complexes is being highly persecuted since these complexes are proposed as intermediate species in the Photosystem II, or as a result of the oxygen activation and the concomitant O-O bond cleavage.[6]

Since phosphasalen are strong electron-donor ligands, the stabilization of manganese complexes in high oxidation states, such as manganese-oxo complexes should be favored. For this purpose, manganese complexes featuring different phosphasalen ligands have been synthesized and characterized in different oxidation states. The catalytic activity of these complexes towards alkene epoxidation has been studied as well.

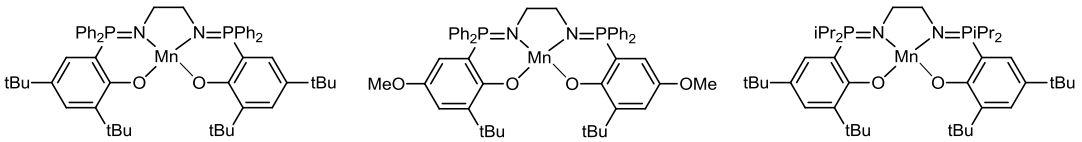

[Mn(Psalen^{tBu})] [Mn(Psalen^{OMe})] [Mn(^{iPr}Psalen)]

Scheme 77. Manganese(II) phosphasalen complexes studied in this chapter.

2. Synthesis of complexes

2.1 Mn^{II} complexes

Manganese neutral complexes (Mn^{II}) were obtained following the same procedure used for the nickel and copper derivatives. $Mn(OAc)_2$ precursor was used because of its commercial availability and its better solubility compared to $MnCl_2$.

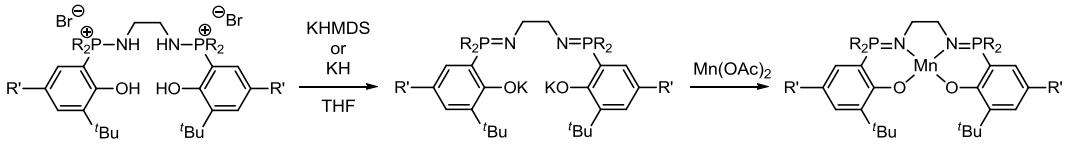

R = Ph, R' = tBu, [Mn(Psalen^{tBu})], 98 %
R = Ph, R' = OMe, [Mn(Psalen^{OMe})], 74 %
R = iPr, R' = tBu, [Mn(^{iPr}Psalen)], 84 %

Scheme 78. Synthetic procedure for [Mn(Psalen^{tBu})], [Mn(Psalen^{OMe})] and [Mn(^{iPr}Psalen)].

The ligands were deprotonated using KHMDS, and after elimination of the insoluble salts, $Mn(OAc)_2$ was added. To accelerate the complexation reaction, the mixture is heated at

reflux for 8 hours. The formation of the neutral complexes is indicated by the absence of ^{31}P resonances in the NMR spectrum due to the paramagnetic nature of the complexes ($3d^5$ ions). For [Mn(Psalen^{tBu})] and [Mn(Psalen^{OMe})] the solutions become light yellow, while for [Mn(^{iPr}Psalen)] is brown. The THF solutions were evaporated and the residue was washed with petroleum ether and dried under vacuum to lead [Mn(Psalen^{tBu})] and [Mn(Psalen^{OMe})] as pale yellow solids in 98 and 74 % yield, and [Mn(^{iPr}Psalen)] as a green solid in 84 % yield.

In some occasions, a small signal around 40 ppm was observed in the ^{31}P NMR. This accounts from a diamagnetic impurity that can be removed by washing the solid with toluene.

These complexes are very sensitive to air and water, thus all the synthesis and storage of the products were done under inert atmosphere or in the glove box. In presence of air, solutions or powders of these complexes became immediately dark due to their oxidation.

2.2 Mn^{III} complexes

Manganese(III) phosphasalen complexes were obtained by the oxidation of the neutral complexes using silver salts. The advantages of using this oxidant are the facile removal of the Ag^0 formed (by filtration) and the variety of commercially available salts with both coordinating and no-coordinating counterions.

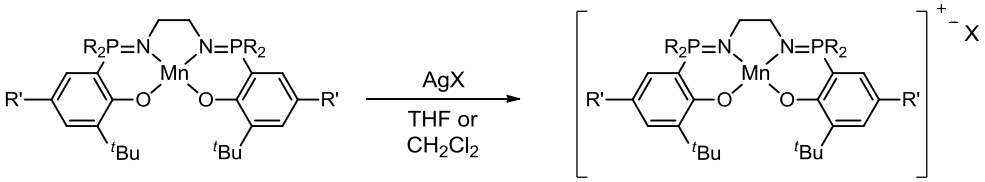

R = Ph, R' = tBu, X= Cl [Mn(Psalen^{tBu})Cl], 95 %
R = Ph, R' = tBu, X= PF_6 [Mn(Psalen^{tBu})]PF_6, 57 %

R = iPr, R' = tBu, X= Cl [Mn(^{iPr}Psalen)Cl], 49 %
R = Ph, R' = tBu, X= PF_6 [Mn(^{iPr}Psalen)]PF_6, 60 %

R = Ph, R' = OMe, X= PF_6 [Mn(Psalen^{tBu})]PF_6, 57 %

Scheme 79. Mn^{III} phosphasalen complexes synthesized.

The salts used in this work were $AgPF_6$ and AgCl. Addition of one equivalent of $AgPF_6$ into a THF solution of Mn^{II} phosphasalen complexes induces an immediate color change from yellow, or green in the case of [Mn(^{iPr}Psalen)], to dark red. The color change is not immediate when adding AgCl into dichloromethane solutions, but few minutes later the solutions become dark green. The suspensions were filtered and concentrated. Addition of

petroleum ether or pentane induces the precipitation of a solid. The precipitates were washed with petroleum ether and dried under reduced pressure. [Mn(Psalen^{tBu})Cl] and [Mn(^{iPr}Psalen)Cl] were obtained as dark green solids in 95, 49 % yield, respectively. [Mn(^{iPr}Psalen)Cl], being slightly soluble in diethyl ether and petroleum ether, was difficult to precipitate and some product was lost during the washing step. [Mn(Psalen^{tBu})]PF_6, [Mn(Psalen^{OMe})]PF_6 and [Mn(^{iPr}Psalen)]PF_6 were obtained as a dark red, pink and brown-red solids in 57, 57, 60 %, respectively.

We noticed that after air exposure of dichloromethane or chloroform solutions of Mn^{II} phosphasalen complexes, Mn^{III} chloride derivatives were isolated and characterized by X-ray diffraction. Thus, chloride abstraction from the solvent molecules occurs when the Mn^{II} complex is exposed to the air.

3. Characterization of Mn^{II} complexes

3.1 NMR spectroscopy

The formation of Mn^{II} complexes was evidenced by the absence of any ^{31}P NMR signal. These complexes are paramagnetic ($3d^5$ configuration) and display broad signals in their ^1H NMR spectra.

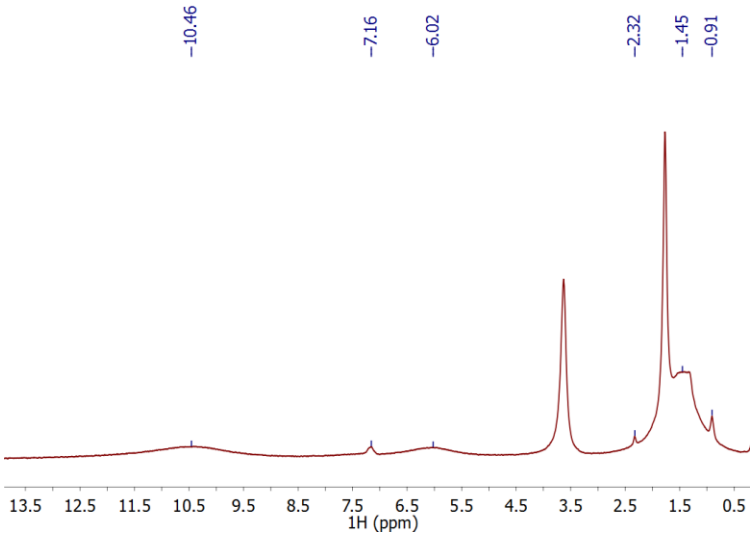

Figure 155. ^1H NMR spectrum of [Mn(Psalen^{tBu})] in THF-d^8. Signals at 7.16, 2.32 and 0.91 correspond to toluene and pentane, respectively.

Figure 155 shows the ^1H NMR spectrum of [Mn(Psalen^{tBu})]. Few information can be drawn from this spectrum since only broad signals were observed at 10.46, 7.16, 6.02 and

1.45 ppm. These signals may correspond to the phenyl phosphine protons, phenolate protons, and aliphatic protons, respectively. The absence of diamagnetic signals in the ^{1}H NMR, as well as the lack of any phosphorus signal, were used as an indication of the purity of the compound.

^{1}H NMR spectra of [Mn(Psalen^{OMe})] and [Mn(^{iPr}Psalen)] are very similar to that of [Mn(Psalen^{tBu})] and do not provide relevant information, so they were not included here.

The effective magnetic moment of [Mn(Psalen^{tBu})] and [Mn(^{iPr}Psalen)] were measured in chloroform solutions using the Evans' method. Values of 5.32 and 5.09 μ_B were obtained for [Mn(Psalen^{tBu})] and [Mn(^{iPr}Psalen)] respectively. Mn^{II} square planar complexes in a high-spin configuration possess 5 unpaired electrons and a spin-only value of 5.92 μ_B. This value is close to those obtained experimentally, indicating that these species mainly exist in a high-spin configuration. A small ratio of the species presenting a low-spin configuration may explain the difference between the experimental and the spin-only magnetic moments.

3.2 X-ray diffraction

Since the ^{1}H NMR spectra do not provide much information about the structure of the neutral complexes, X-ray diffraction was determinant for their characterization.

Yellow crystals of [Mn(Psalen^{tBu})(py)] suitable for X-ray diffraction were obtained from a dichloromethane/pyridine solution stored at -40 °C for one week under inert conditions.

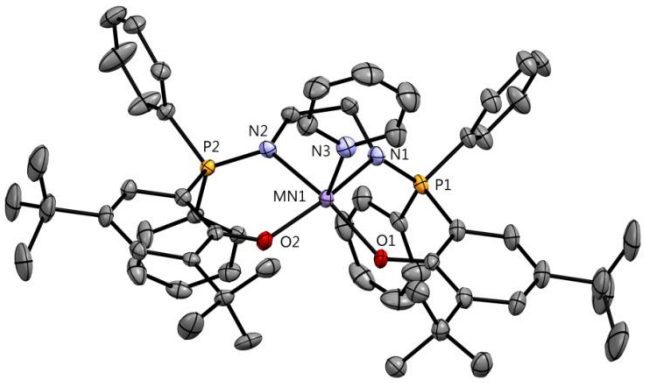

Figure 156. ORTEP of [Mn(Psalen^{tBu})(py)] with thermal ellipsoids at 50 % probability. Hydrogen atoms and two molecules of dichloromethane have been removed for clarity.

[Mn(Psalen^{tBu})(py)] displays a square pyramidal geometry around the metal center. Nitrogen and oxygen atoms of the ligand define the basal plane (NOON plane) and a pyridine molecule occupies in the apical position. The main NOON plane presents a

distortion of 8.6 °. The coordination sphere around the metal center is rather symmetric: Mn-O bond distances measure 2.051(2) and 2.054(2) Å, and the Mn-N bonds measure 2.161(3) and 2.170(3) Å. The pyridine molecule is bound at 2.231(3) Å from the metal center. The P-N bonds are slightly different, 1.579(3) and 1.592(3) Å, and are smaller than those observed for copper and nickel phosphasalen derivatives.

	[Mn(Psalen^{tBu})(py)]	[Mn(^{iPr}Psalen)(THF)]	[Mn(Psalen^{OMe})(py)]
Mn-O1	2.051(2)	2.060(1)	2.049(1)
Mn-O2	2.054(2)	2.024(1)	2.063(1)
Mn-N1	2.161(3)	2.124(2)	2.137(2)
Mn-N2	2.170(3)	2.200(2)	2.163(2)
Mn-N3/O3	2.231(3)	2.267(2)	2.193(2)
P1-N1	1.579(3)	1.590(2)	1.586(2)
P2-N2	1.592(3)	1.595(2)	1.596(2)
Torsion angle[a]	8.6	20.43	1.68

Table 33. Selected bond distances (Å) and angles (°) for [Mn(Psalen^{tBu})(py)], [Mn(^{iPr}Psalen)(THF)] and [Mn(Psalen^{OMe})(py)]. [a] Torsion of the NOON plane.

Crystals of [Mn(^{iPr}Psalen)(THF)] were obtained by evaporation of a mixture of tetrahydrofurane/petroleum ether under inert conditions

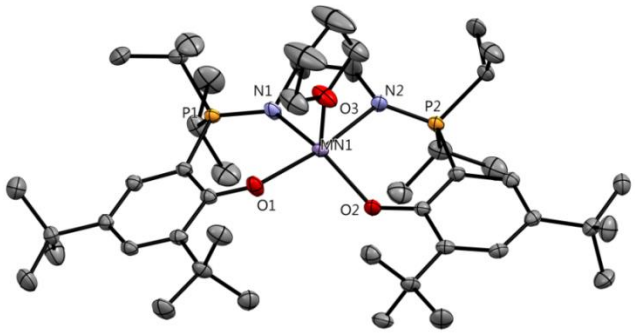

Figure 157. ORTEP of [Mn(^{iPr}Psalen)(THF)] with thermal ellipsoids at 50 % probability. Hydrogen atoms and two molecules have been removed for clarity.

The molecule presents a distorted square pyramidal geometry around the metal center. The distortion of the equatorial plane is 20.43 °, more pronounced than in [Mn(Psalen^{tBu})(py)]. Indeed, the coordination sphere is very dissymmetric: Mn-O bonds measure 2.060(1) and 2.024(1) Å (Δd = 0.036 Å), and Mn-N are at 2.124(2) and 2.200(2) Å (Δd = 0.076 Å). The molecule of THF is placed at 2.267(2) Å to the metal center. The molecule is distorted towards a trigonal bipyramidal geometry with N2 and O1 occupying the apical positions, and N1, O2 and O3 (from THF) in the equatorial plane. The angle between N2-Mn-O1 is 168.61 °, while the angle between N1-Mn-O2 is 143.73 °, much more

distorted. The P-N bonds measure 1.590(2) and 1.595(2) Å, similar values than those found in [Mn(Psalen^{tBu})(py)].

Single crystals of [Mn(Psalen^{OMe})(py)] were obtained from a diethyl ether/pyridine solution stored at -40 °C for one week under inert conditions.

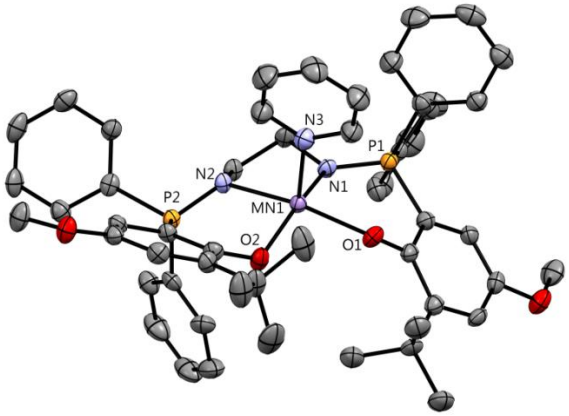

Figure 158. ORTEP of [Mn(Psalen^{OMe})(THF)] with thermal ellipsoids at 50 % probability. Hydrogen atoms have been removed for clarity.

[Mn(Psalen^{OMe})(py)] displays also a square pyramidal geometry. The distortion of the main plane is 1.68 °, lower than in the two previous cases. The bond distances are similar than those of [Mn(Psalen^{tBu})(py)], which displays the same apical ligand and only differs by the phenolate substituents. Mn-O bonds measures 2.049(2) and 2.063(1) Å, while Mn-N are at 2.137(2) and 2.163(2) Å. The pyridine molecule is found at 2.193(3) Å from the metal, closer than in [Mn(Psalen^{tBu})(py)] (2.231(3). N-P bonds lengths are very similar to those found in the other Mn^{II} analogues, 1.586(2) and 1.596(2) Å.

Figure 159 shows the coordination spheres of the three Mn^{II} phosphasalen complexes. In the three structures the manganese center is placed above the equatorial plane at distances ranging between 0.342-0.383 Å.

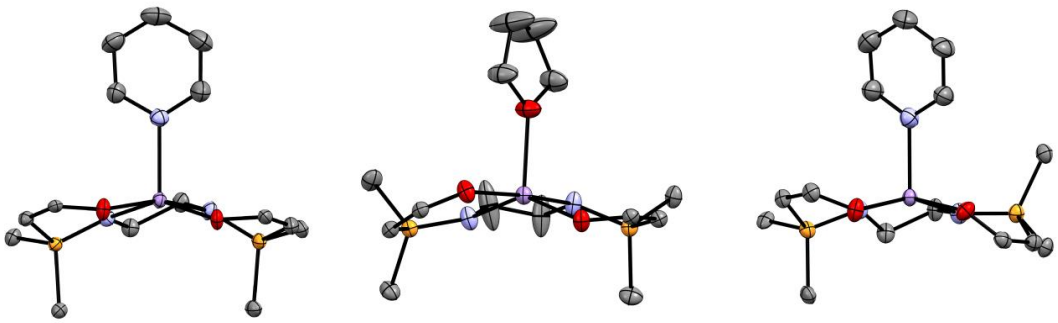

Figure 159. View of the coordination sphere through the NOON plane for [Mn(Psalen^{tBu})(py)] (left), [Mn(^{iPr}Psalen)(THF)] (middle) and [Mn(Psalen^{OMe})(py)] (right).

It is worth noting that while [Mn(Psalen^{tBu})(py)] and [Mn(^{iPr}Psalen)(THF)] display bowl (or umbrella) shapes, [Mn(Psalen^{OMe})(py)] presents a stepped conformation. This is easily noticeable by the position of the phosphorus atoms which are both above the main plane for [Mn(Psalen^{tBu})(py)] and [Mn(^{iPr}Psalen)(THF)], and alaternate above and below the plane in [Mn(Psalen^{OMe})(py)].

A X-ray structure of a Mn(II)-salen complex was found in the literature. It displays a propylene amine linker and naphthyl moieties instead of phenoxide rings. The Mn-O and Mn-N bond lengths for the tetracoordinated complex measure 1.842(3) and 1.867(4) Å, respectively. These distances are notably shorter compared to those observed in the Psalen complexes. This may be due to a chelating effect induced by the use of a three-carbon bridge in the case of the salen complex, or due to the presence of an additional ligand in the Psalen complexes.[7a]

X-ray structures of octahedral Mn^{II} complexes displaying various ligands were reported in the literature with coordination distances ranging between 2.1 and 2.4 Å.[7b,c]

3.3 UV-vis spectroscopy

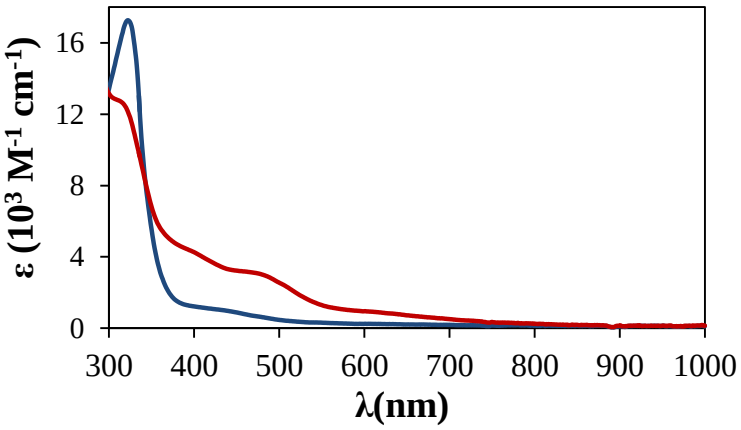

Figure 160. UV-vis spectrum of [Mn(Psalen^{tBu})] complex in THF solution (blue line), and after 1 hour air exposure (red line).

The absorption spectrum of [Mn(Psalen^{tBu})] in THF (Figure 160, blue line) exhibits a weak band at 440 nm (ε = 780 M^{-1} cm^{-1}) and an intense transition at 320 nm (ε = 17200 M^{-1} cm^{-1}). After air exposure (Figure 160, red line) new bands appear at 610 nm (ε = 930 M^{-1} cm^{-1}), 470 nm (ε = 3100 M^{-1} cm^{-1}), 400 nm (ε = 4300 M^{-1} cm^{-1}) accompanied by a decreasing of the intensity of the band at 320 nm (ε = 12600 M^{-1} cm^{-1}).

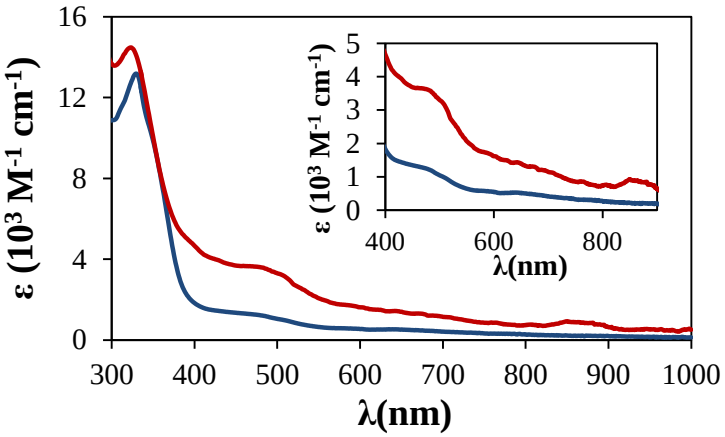

Figure 161. UV-vis spectrum of [Mn(Psalen^{OMe})] complex in THF solution (blue line), and after 1 hour air exposure (red line). Inset shows a zoom of the visible region.

The UV-visible spectrum of [Mn(Psalen^{OMe})] (Figure 161, blue line) presents two weak absorptions at 640 nm (ε = 530 M^{-1} cm^{-1}) and 460 nm (ε = 1300 M^{-1} cm^{-1}). An intense transition is also observed at 330 nm (ε = 13300 M^{-1} cm^{-1}). Once this solution is exposed to air (Figure 161, red line), the latter transition seems to shift to 320 nm and increase in intensity to ε = 14400 M^{-1} cm^{-1}. The band at 460 nm increases in intensity (ε = 3600 M^{-1} cm^{-1}) and slightly shifts to 470 nm, as well as the band at 640 nm which now presents an extinction coefficient of 1400 M^{-1} cm^{-1}. A new band appears at 860 nm (ε = 890 M^{-1} cm^{-1}).

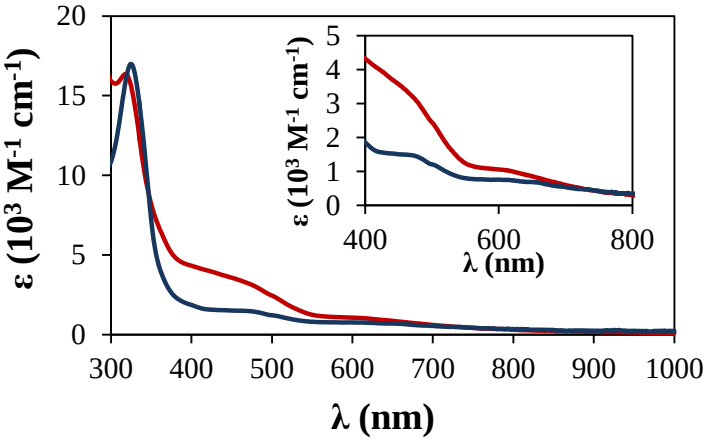

Figure 162. UV-vis spectrum of [Mn(^{iPr}Psalen)] complex in THF solution (blue line), and after one hour air exposure (red line). Inset shows a zoom of the visible region.

[Mn(^{iPr}Psalen)] exhibits two weak absorptions at 605 nm (ε = 750 M^{-1} cm^{-1}) and 450 nm (ε = 1500 M^{-1} cm^{-1}), and an intense transition at 325 nm (ε = 17000 M^{-1} cm^{-1}). After air exposure the band at 605 nm increases in intensity (ε = 1000 M^{-1} cm^{-1}), as well as the band at 450 nm, now present at 430 nm (ε = 3900 M^{-1} cm^{-1}). The band at 325 nm is slightly blue-shifted to 320 nm and less intense (ε = 16100 M^{-1} cm^{-1}).

Common bands are present in the spectra of Mn^{II} complexes. The three complexes display weak bands around 450 nm, which can be attributed to d-d transitions according to their intensity. Intense bands around 325 nm are also present in the three spectra and can be attributed to π-π* or charge transfer transitions. These bands increase in intensity once the solutions have been exposed to the air. Mn(II) complexes are not stable under aerobic condition and react with O_2, as clearly shown by the modifications observed on their UV-visible spectra.

4. Characterization of Mn^{III} complexes

4.1 NMR spectroscopy

Mn^{III} ions possesses a $3d^4$ configuration and in a square planar (or square pyramidal) environment can be paramagnetic (S = 2), if they display a high-spin configuration, or diamagnetic (S = 0), if they possess a low-spin configuration. In an octahedral environment, both low and high-spin configurations are paramagnetic. The ^1H NMR spectra of the different Mn^{III} species obtained turned out to be paramagnetic in both coordinating (THF-d^8) and non-coordinating (CD_2Cl_2) solvents, and no ^{31}P NMR was detected. Thus, Mn(III)-phosphasalen complexes can be formulated as high-spin square pyramidal, square planar or octahedral complexes, depending on the coordinated solvent molecules.

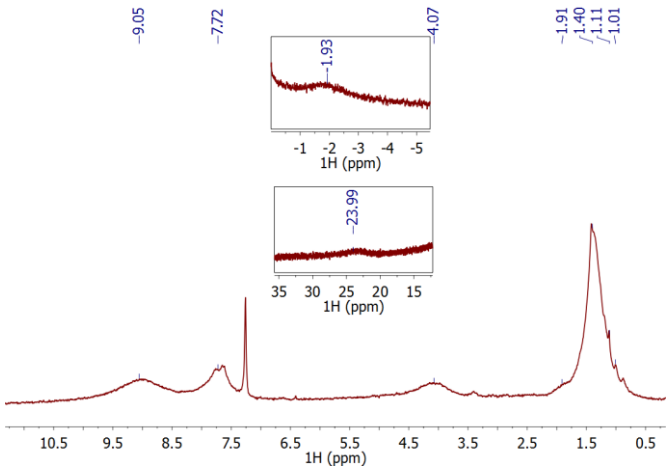

Figure 163. ^1H NMR spectrum of [Mn(Psalen^{tBu})]PF_6 in $CDCl_3$. The signal at 1.11 ppm corresponds to pentane.

Figure 163 shows the ^{1}H NMR spectrum of [Mn(Psalen^{tBu})]PF_6 in $CDCl_3$. This spectrum is characterized by broad signals present in the diamagnetic window, but also two small signals at 23.99 and -1.93 ppm. Because of their broad shape, these signals could not be attributed to their corresponding protons. Only the signal at 1.40 ppm could be assigned to the tert-butyl protons because of its intensity and chemical shift.

The other Mn^{III} complexes, [Mn(Psalen^{tBu})]X, [Mn(Psalen^{OMe})]X and [Mn(^{iPr}Psalen)]X (X = Cl or PF_6), display very similar ^{1}H NMR spectra. Because these spectra do not provide significant information about the structure and electronics of the Mn^{III} complexes, they were not included in this manuscript.

The effective magnetic moment of [Mn(Psalen^{tBu})Cl], [Mn(^{iPr}Psalen)Cl] and [Mn(Psalen^{OMe})]PF_6 were measured for chloroform solutions using the Evans' method. The values obtained for these complexes were 4.29, 4.52 and 4.76 μ_B, respectively. Mn^{III} square planar complexes in a high-spin configuration possess four unpaired electrons and a spin-only value of 4.90 μ_B. The effective magnetic moments measured for these complexes indicate that they exist mainly in the high-spin configuration.

4.2 X-ray diffraction

Because of their paramagnetism, X-ray diffraction was determinant to establish the structure of the Mn^{III} complexes. Unfortunately, not all the complexes could be crystallized.

Single crystals of [Mn(Psalen^{tBu})Cl] were obtained from a dichloromethane/pentane solution stored in the fridge for two days. Single crystals could be also obtained by evaporation of CD_2Cl_2 or $CDCl_3$ solutions of [Mn^{II}(Psalen^{tBu})] exposed to air.

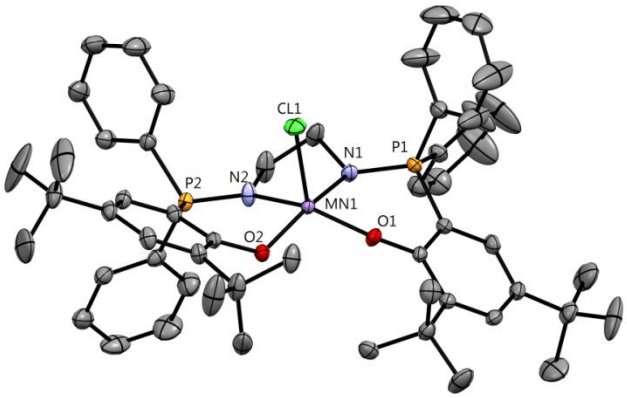

Figure 164. ORTEP of [Mn(Psalen^{tBu})Cl] with thermal ellipsoids at 50 % probability. Hydrogen atoms and a molecule of THF have been removed for clarity.

[Mn(Psalen^{tBu})Cl] presents a square pyramidal geometry around the metal center. The equatorial plane presents a slight distortion of 4.19 °. The coordination sphere around the metal center is rather symmetric: Mn-O bonds measure 1.927(1) and 1.909(1) Å, and Mn-N bonds measure 1.965(2) and 1.979(2) Å. These bonds are shorter than those observed for the Mn^{II} analogue, in agreement with the oxidation of the metal center. The P-N bonds elongate and are comparable to those observed for nickel and copper neutral complexes, 1.611(2) and 1.599(2) Å. The chloride anion is found at 2.4096(7) Å from the metal center; longer than the distances Mn-N(pyridine) and Mn-O(THF) found for the Mn^{II} analogue.

	[Mn(Psalen^{tBu})Cl]	[Mn(^{iPr}Psalen)Cl]
Mn-O1	1.927(1)	1.911(2)
Mn-O2	1.909(1)	1.898(2)
Mn-N1	1.965(2)	1.997(3)
Mn-N2	1.979(2)	1.951(3)
Mn-Cl	2.4096(7)	2.442(1)
P1-N1	1.611(2)	1.623(3)
P2-N2	1.599(2)	1.612(3)
Torsion angle[a]	4.19	16.47

Table 34. Selected bond distances (Å) and angles (°) for [Mn(Psalen^{tBu})Cl] and [Mn(^{iPr}Psalen)Cl]. [a] Torsion of the NOON plane.

Single crystals of [Mn(^{iPr}Psalen)Cl] were obtained by slow diffusion of pentane into a concentrated dichloromethane solution.

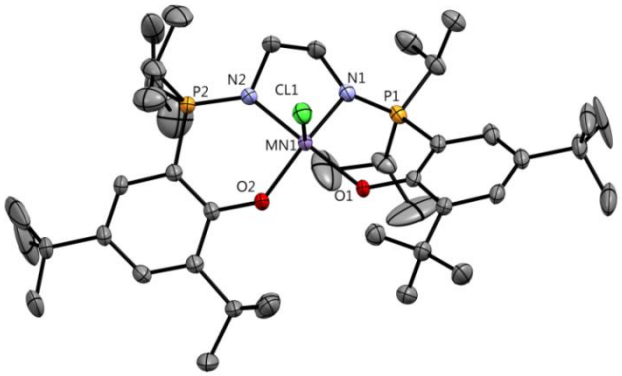

Figure 165. ORTEP of [Mn(^{iPr}Psalen)Cl] with thermal ellipsoids at 50 % probability. Hydrogen atoms have been removed for clarity.

[Mn(^{iPr}Psalen)Cl] displays a distorted square pyramidal geometry. The distortion of the equatorial plane is 16.47 °, larger than that obtained for [Mn(Psalen^{tBu})Cl] (4.19 °) but lower than in the Mn^{II} complex. The coordination sphere is slightly dissymmetric: Mn-O bonds measure 1.911(2) and 1.898(2) Å, and Mn-N are at 1.997(3) and 1.951(3) Å (Δd = 0.046 Å). These bonds are shorter compared to its reduced analogue, in agreement with the oxidation of the metal center.

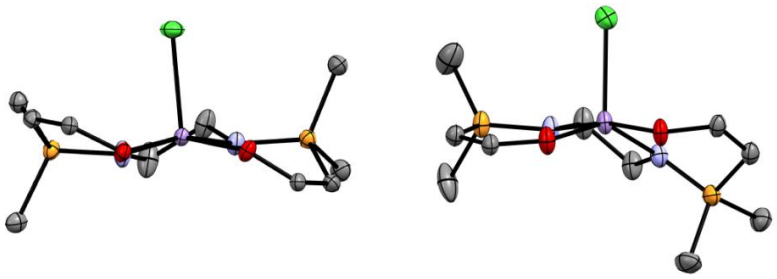

Figure 166. View of the coordination sphere through the NOON plane for [Mn(Psalen^{tBu})Cl] (left), and [Mn(iPrPsalen)Cl] (right).

Both [Mn(Psalen^{tBu})Cl] and [Mn(^{iPr}Psalen)Cl] complexes display stepped conformations. This is easily noticiable from the orientation of the phosphorus atoms with respect to the main plane (Figure 166). In both complexes the metal is placed slightly above the plane defined by the NOON plane. A strong distortion is observed for one of the P-N unities in [Mn(^{iPr}Psalen) Cl] which is significantly shifted above the main NOON plane.

Crystals of [Mn(^{iPr}Psalen)(THF)]PF_6 where obtained by slow diffusion of pentane into a saturated THF solution.

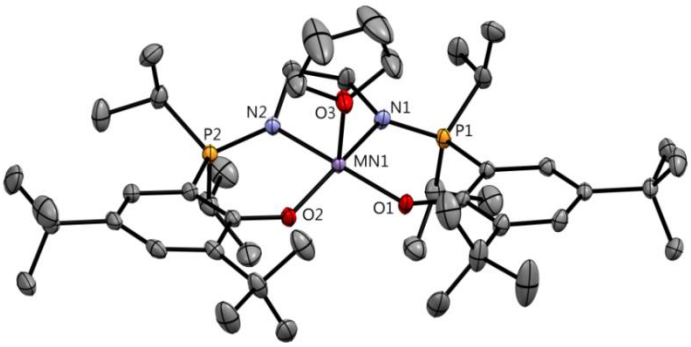

Figure 167. ORTEP of [Mn(^{iPr}Psalen)(THF)]PF_6 with thermal ellipsoids at 50 % probability. Hydrogen atoms and a molecule of PF_6 have been removed for clarity.

[Mn(^{iPr}Psalen)]PF_6 presents a molecule of THF coordinated to the metal center leading to a square pyramidal geometry. Contrary to [Mn(^{iPr}Psalen)(THF)] and [Mn(^{iPr}Psalen)Cl], the distortion measured for the NOON plane in [Mn(^{iPr}Psalen)(THF)]PF_6 is rather small (4.84 °). The coordination sphere distances are similar to those observed for [Mn(^{iPr}Psalen)Cl]: Mn-O bonds are at 1.896(1) and 1.902(1) Å, and Mn-N at 1.957(1) and 1.946(1) Å. However, the dissymmetry observed for the Mn-N bonds in [Mn(^{iPr}Psalen)Cl] is weaker here. These distances are also shorter than those found for [Mn(^{iPr}Psalen)(THF)] neutral species.

	[Mn(^{iPr}Psalen)(THF)]PF_6	[Mn(Psalen^{OMe})(THF)] PF_6
Mn-O1	1.896(1)	1.893(2)
Mn-O2	1.902(1)	1.869(2)
Mn-O(THF)	2.203(1)	2.210(2)
Mn-N1	1.957(1)	1.985(2)
Mn-N2	1.946(1)	1.949(2)
P1-N1	1.630(1)	1.620(2)
P2-N2	1.618(1)	1.617(2)
Torsion angle[a]	4.84	6.81

Table 35. Selected bond distances (Å) and angles (°) for [Mn(Psalen^{OMe})(THF)]PF_6 and [Mn(^{iPr}Psalen)(THF)]PF_6. [a] Torsion of the NOON plane.

Crystals of [Mn(Psalen^{OMe})(THF)]PF_6 where obtained by slow diffusion of diethyl ether and pentane into a concentrated THF solution.

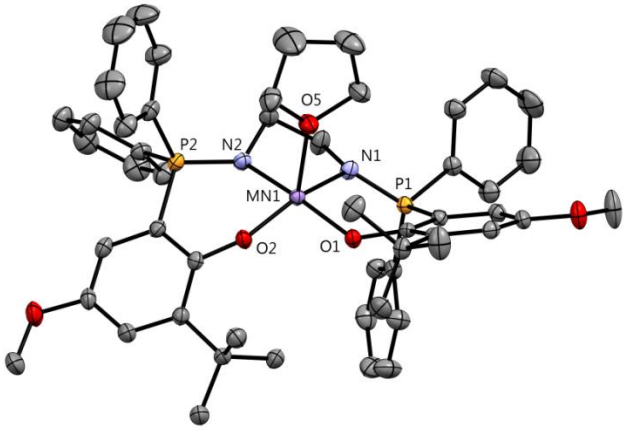

Figure 168. ORTEP of [Mn(Psalen^{OMe})(THF)]PF_6 with thermal ellipsoids at 50 % probability. Hydrogen atoms and a molecule of THF and a molecule of PF_6 have been removed for clarity

[Mn(Psalen^{OMe})]PF_6 also presents a THF molecule coordinated to the metal center, thus a square pyramidal geometry. The equatorial plane is distorted by 6.81 °, higher value than that calculated for [Mn(Psalen^{OMe})(py)]. The coordination sphere is slightly dissymmetric: Mn-O bonds measure 1.893(2) and 1.869(2) Å (Δd = 0.024 Å), and Mn-N measure 1.985(2) and 1.949(2) Å (Δd = 0.036 Å).

[Mn(^{iPr}Psalen)(THF)]PF_6 and [Mn(Psalen^{OMe})(THF)]PF_6 present similar distortions of the main plane but different conformation, since the phosphorus atoms are oriented differently with respect to the main plane (Figure 169).

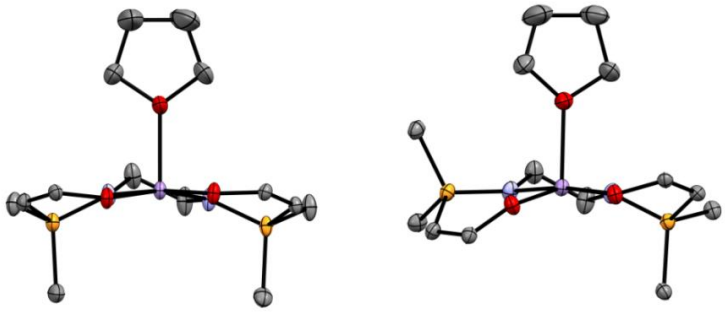

Figure 169. View of the coordination sphere through the NOON plane for [Mn(^{iPr}Psalen)(THF)]PF_6 (left), and [Mn(Psalen^{OMe})(THF)]PF_6 (right).

4.3 Electrochemical studies

Preliminary Cyclic voltammetry experiments were performed for [Mn(^{iPr}Psalen)]PF_6, [Mn(Psalen^{tBu})]PF_6, [Mn(^{iPr}Psalen)Cl] and [Mn(Psalen^{tBu})Cl]. Results shown here are only preliminary since the electrochemical properties of these complexes will be further investigated, and Psalen^{OMe} derivatives still need to be studied.

Figure 170 shows the cyclic voltammogram corresponding to the first oxidation. Redox potentials are here referred to SCE.

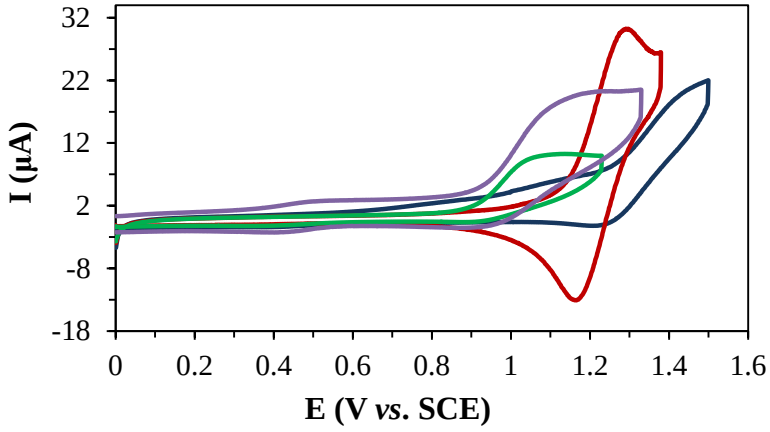

Figure 170. Cyclic voltammograms [Mn(^{iPr}Psalen)]PF_6 (red line), [Mn(Psalen^{tBu})]PF_6 (blue line), [Mn(^{iPr}Psalen)Cl] (green line)and [Mn(Psalen^{tBu})Cl] (purple line) recorded in dichloromethane. Conditions: 3 mM of complex in dichloromethane at 0.1 V/s.

[Mn(Psalen^{tBu})]PF_6, [Mn(Psalen^{tBu})Cl], and [Mn(^{iPr}Psalen)Cl] display irreversible oxidations, while [Mn(^{iPr}Psalen)]PF_6 is the only one presenting a reversible couple.

Compound	$E^1_{p,a}/E^1_{1/2}$	$E^1_{p,a}/E^1_{1/2}$[a]
[Mn(Psalen^{tBu})Cl]	1.12	0.67
[Mn(^{iPr}Psalen)Cl]	1.02	0.57
[Mn(Psalen^{tBu})]PF_6	1.41	0.96
[Mn(^{iPr}Psalen)]PF_6	1.23	0.78

Table 36. Redox potentials [Mn(^{iPr}Psalen)]PF_6, [Mn(Psalen^{tBu})]PF_6, [Mn(^{iPr}Psalen)Cl] and [Mn(Psalen^{tBu})Cl] expressed in [a] V *vs*. SCE, [b] expressed in V *vs.* Fc^+/Fc by considering that $E(Fc^+/Fc)$ = 0.45 V *vs.* SCE.

The estimated oxidation potentials for the irreversible couples are 1.12 V for [Mn(Psalen^{tBu})]PF_6, 1.02 V for [Mn(^{iPr}Psalen)Cl], and 1.41 V for [Mn(Psalen^{tBu})]PF_6. The half-wave potential calculated for [Mn(^{iPr}Psalen)]PF_6 is 1.23 V. The redox potential values of the complexes displaying a chloride counterion are slightly lower than their analogues displaying PF_6 counterions. The Psalen^{iPr} derivatives present lower potentials than the Psalen^{tBu} species. The presence of alkyl substituents in the phosphorus atoms favors the oxidation, as observed for the nickel and copper complexes. These values are as well similar to those of the Mn(salen) derivatives, while normally iminophosphorane functions make the oxidation of these complexes easier.

The unexpected high redox potentials values obtained for these complexes could not be explained. Further electrochemical studies must be carried out to elucidate the factors of this non-reversibility and the high values obtained.

5. Catalysis results

Since Mn(salen) complexes are good catalysts for the alkene epoxidation, the catalytic activity of the complexes synthesized here was tested. The better electron-donating iminophosphorane moieties should favor, to a larger extent than salen, the formation of high-valent intermediates.

Two different approaches were used to test the catalytic properties of the manganese phosphasalen complexes. The first one consists in the use of iodosylarenes and *m*-CPBA as oxidants, as reported by numerous groups.[3] In a second approach, the catalytic reactions were performed in presence of Lewis acids, such as $Ca(OTf)_2$ or $Al(OTf)_3$.[8]

5.1 Catalysis with *m*-CPBA and iodosylarenes

In a first instance, we followed the procedure described by Thomas and co-workers for the oxidation of styrene catalyzed by a manganese complex displaying a bis(phenolate)dipyrrin ligand.[9] The catalytic activity of [Mn(Psalen^{tBu})]X, [Mn(Psalen^{OMe})]X and [Mn(^{iPr}Psalen)]X (X = Cl or PF_6) were studied using PhIO as stoichiometric oxidant in presence of additives in some cases, such as pyridine or N-methyl imidazole. The reaction was performed in dichloromethane and followed by Gas Chromatography (GC). Unfortunately, these complexes did not display any catalytic activity since the conversion obtained was lower to that observed for the control.

We decided then to study the catalytic activity in presence of another substrate, cyclooctene (COE), using various oxidants apart PhIO, such as *m*-CPBA or $PhI(OAc)_2$. Oxidation of cyclooctene generates some side products, being cyclooctene oxide and cyclooctanone as the main oxidation products. The ketone is obtained by opening of the generated epoxide in presence of water traces (H^+), which is usual when using *m*-CPBA as oxidant.[10]

The tests were conducted in THF solutions using 5-10 mol % catalytic loadings and stoichiometric amounts of oxidant. A detailed explanation is included in the experimental section.

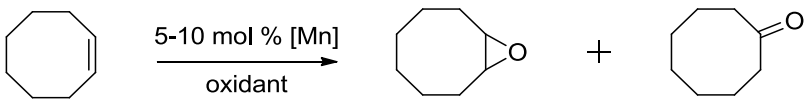

Scheme 80. Oxidation of COE.

Table 37 summarizes some of the results obtained for [Mn(^{iPr}Psalen)Cl], [Mn(Psalen^{tBu})]PF_6 and [Mn(^{iPr}Psalen)]PF_6. The activity of [Mn(Psalen^{OMe})]X (X = Cl or PF_6) was not tested in this study.

Entry	Complex	mol %	Additive	Oxidant	COE[c]	Epoxide[c]	Ketone[c]
1[a]	-	-	-	*m*-CPBA	85	1.5	13.5
2[a]	-	-	-	$PhI(OAC)_2$	85	2	13
3	[Mn(Psalen^{tBu})]PF_6	5	pyridine	*m*-CPBA	96	3	1
4	[Mn(Psalen^{tBu})]PF_6	10	NaOH	*m*-CPBA	97	-	3
5	[Mn(^{iPr}Psalen)Cl]	10	-	$PhI(OAc)_2$	93	2	5
6[b]	[Mn(^{iPr}Psalen)]PF_6	10	-	*m*-CPBA	92	2	6

Table 37. Results obtained for the oxidation of COE with Mn phosphasalen complexes after 2-6 h. [a] Control performed under the same conditions without addition of Mn complex. [b] MeOH used as solvent. [c] Rounded percent values are calculated only taking into account the amount of COE, Epoxide and Ketone.

The conversions are very low, and even lower than that obtained in the control reaction. These results indicate that manganese phosphasalen complexes are not catalysts for the oxidation of COE.

This is surprising since the structure of phosphasalen is very close to that of Mn(salen) complexes, and the presence of iminophosphorane functions should favor the formation of the oxo species, proposed as key intermediates species in these reactions. A reason for this low activity may be the presence of bulky substituents in the phosphorus atoms which induces a high steric hindrance blocking the approach of the substrate to the metal center. Another reason may be the difficulty to oxidize the metal center, as observed in the cyclic voltammetry experiments.

In order to isolate the manganese species generated upon oxidation with *m*-CPBA, the reactions of Mn^{III} complexes with one equivalent of oxidant were performed in THF. After evaporation of the solvent, the residue was dissolved in pentane and filtered. Brown crystals from the reaction with [Mn(Psalen^{tBu})]PF_6 were obtained by slow evaporation of the filtered solution (Figure 171).

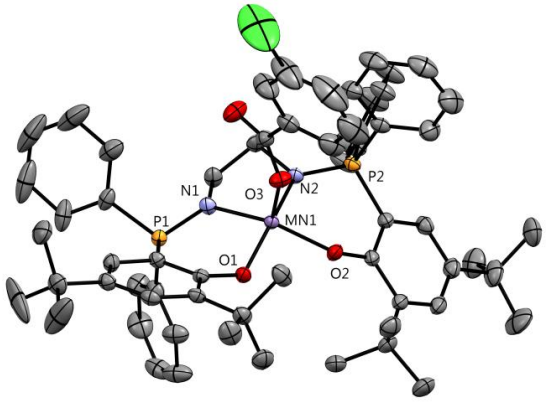

Figure 171. ORTEP of [Mn(Psalen^{tBu})(*m*-CB)] with thermal ellipsoids at 50 % probability. Hydrogen atoms and two molecules of dichloromethane have been removed for clarity. Selected bond lengths (Å): Mn-O1 1.910(1), Mn-O2 1.920(1), Mn-N1 1.984(2), Mn-N21 1.961(2), Mn-O3 2.039(3). Torsion of NOON plane: 8.77 °.

The product isolated from the reaction was the Mn^{III} complex with a molecule of *m*-chlorobenzoate coordinated in the apical position, [Mn(Psalen^{tBu})(*m*-CB)]. *m*-chlorobenzoate is generated after oxygen donation of the *m*-CPBA. Its coordination may cause the deactivation of the manganese complex. This may explain the low catalytic activity towards oxidation observed for these complexes.

Different attempts to isolate manganese-oxo intermediates were also performed by mixing one equivalent of PhIO with one equivalent of Mn^{II} or Mn^{III} complexes. In some cases, the

resulting products could not be characterized or the isolated products were the starting Mn^{III} complexes.

Further investigations of the reaction intermediates must be carry out in order to understand the low conversion observed.

5.2 Oxidation with Lewis acids

Non-redox metal ions can act as Lewis acids and increase the catalytic activity of high-valent metal complexes by formation of adducts or destabilization of reaction intermediates, making them more reactive. Lewis acids may also help in the dissociation of deactivated species.[8]

Catalytic reactions were performed in presence of $Ca(OTf)_2$ and $Al(OTf)_3$. Oxidant ($PhI(OAc)_2$) and manganese complexes were mixed together and stirred for 3 hours before the addition of the Lewis acid and the substrate. A small excess of oxidant was added with the substrate. The reactions were performed in THF using 5 mol % of catalyst. The results obtained after 48 hours of reaction are gathered in Table 38 and Table 39.

Entry	Complex	COE[b]	Epoxide[b]	Ketone[b]
1[a]	-	100	-	-
2	[Mn(Psalen^{tBu})Cl]	92.3	6.4	1.3
3	[Mn(Psalen^{tBu})]PF_6	92.4	2	5.6
4	[Mn(^{iPr}Psalen)Cl]	97	-	3
5	[Mn(^{iPr}Psalen)]PF_6	80	3	17

Table 38. Results obtained for the oxidation of COE with 5 mol % Mn phosphasalen complexes in presence of $Al(OTf)_3$ after 48 h. [a] Control performed under the same conditions without addition of Mn complex. [b] Rounded percent values are calculated only taking into account the amount of COE, epoxide and ketone.

Entry	Complex	COE[b]	Epoxide[b]	Ketone[b]
1[a]	-	100	-	-
2	[Mn(Psalen^{tBu})Cl]	85	-	15
3	[Mn(Psalen^{tBu})]PF_6	86	3	11
4	[Mn(^{iPr}Psalen)Cl]	57	-	43
5	[Mn(^{iPr}Psalen)]PF_6	86	3	11

Table 39. Results obtained for the oxidation of COE with 5 mol % Mn phosphasalen complexes in presence of $Ca(OTf)_2$ after 48 h. [a] Control performed under the same conditions without addition of Mn complex. [b] Rounded percent values are calculated only taking into account the amount of COE, epoxide and ketone

Addition of $Al(OTf)_3$ slightly increases the reactivity, especially for [Mn(^{iPr}Psalen)]PF_6 which achieves a 17 % formation of cycloctanone. The catalytic activity is significantly

enhanced in presence of $Ca(OTf)_2$ which favors the formation of the cyclooctanone with the four complexes. Complexes using PF_6 display the same activity, which is lower than that observed for chloride analogues, suggesting that the presence of a strong electron-donating axial ligand improves the activity. A conversion of the 43 % was observed for the [Mn(^{iPr}Psalen)Cl] complex.

The better catalytic activity detected in presence of Lewis acids may indicate a problem in the oxygen transfer from the complex to the substrate when the metal is not assisted. The formation of metal adducts in presence of Lewis acids may enhance the oxygen transfer reaction.

The intermediates species of this reaction, as well as a larger scope of substrates, will be further investigated.

6. Stabilization of high-valent complexes

6.1 Nitrido-complexes

Since our attempts to isolate manganese-oxo intermediates were unsuccessful, we focused on stabilizing the nitrogen analogue, a manganese-nitrido complex (Mn≡N). The interest on these complexes has increased since they are proposed as intermediates in nitrogen fixation processes.[11]

Manganese(V) salen nitrido complexes have been reported by Day and co-workers.[12] These complexes are rather stable to air and moisture and act as nitrogen transfer reagents.[12]

A first attempt to obtain nitrido complexes was done following the procedure described for salen complexes using bleach (as source of oxygen) and ammonium hydroxide as reagents.[12] Mn^{III} complexes displaying both Cl and PF_6 counterions were dissolved in methanol, and an excess of ammonium hydroxide, followed by an excess of bleach, were added to the solution. After treatment and extraction using dichloromethane, the products obtained by crystallization were [Mn(Psalen^{tBu})Cl] and [Mn(^{iPr}Psalen)Cl] complexes. The mixture may not be strong enough to oxidize the Mn^{III} phosphasalen complexes, or the products formed were not stable enough and degrade back to Mn^{III} complexes, which completes its coordination sphere with the chloride ions present in the reaction mixture.

A second approach was then used by employing azide reagents. This has been described by Sita and co-workers for the formation of Mo and W nitrido complexes.[13] The formation of the nitrido species was done in one step by reaction of the complexes with trimethylsilyl azide ($TMSN_3$) in toluene. K. Meyer and co-workers have described as well the formation of Mn≡N species using azides as nitrogen source. In this case, the generation of nitrido species occurs *via* the formation of the azide complex which loses a molecule of N_2 after exposure to ultraviolet radiation, leading to manganese nitrido species.[14]

Thus, Mn^{III} phosphasalen complexes displaying the PF_6 counterion were dissolved in toluene and treated with an excess of $TMSN_3$ in toluene. After stirring the solution at room temperature for 24 hours, pentane was added and the mixture kept in the fridge. After few days, crystals were obtained. This reaction was tested with [Mn(Psalen^{tBu})]PF_6 and [Mn(^{iPr}Psalen)]PF_6, in both cases Mn^{III} azide complexes were obtained. Figure 172 shows the X-ray structure of [Mn(Psalen^{tBu})(N_3)]. The structure of [Mn(^{iPr}Psalen)(N_3)] was not included here, but selected bond distances are present in Table 40.

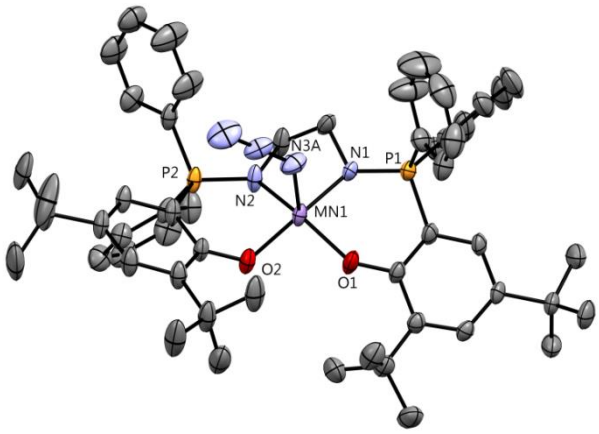

Figure 172. ORTEP of [Mn(Psalen^{tBu})(N_3)] with thermal ellipsoids at 50 % probability. Hydrogen atoms and a molecule of THF have been removed for clarity.

The coordination sphere distances are very similar to those observed for the other Mn^{III} phosphasalen complexes. [Mn(Psalen^{tBu})(N_3)] and [Mn(^{iPr}Psalen)(N_3)] display a square pyramidal geometry. Mn-N3 bond distances are shorter than the analogous Mn-Cl (~ 2.41 Å). The distortion of the plane described by the four NOON coordinating atoms is more significant for [Mn(^{iPr}Psalen)(N_3)] (20.97 °); similar distortions were observed in [Mn(^{iPr}Psalen)(THF)] and [Mn(^{iPr}Psalen)Cl].

	[Mn(Psalen^{tBu})(N$_3$)]	[Mn(^{iPr}Psalen)(N$_3$)]
Mn-O1	1.919 (2)	1.878(3)
Mn-O2	1.902(2)	1.887(3)
Mn-N1	1.967(2)	1.941(4)
Mn-N2	1.987(2)	1.996(4)
Mn-N3	2.29(2)	2.130(5)
P1-N1	1.615(2)	1.587(4)
P2-N2	1.602(2)	1.599(5)
Torsion angle	8.08	20.97

Table 40. Selected bond lengths (Å) and angles (°) for [Mn(Psalen^{tBu})(N$_3$)] and [Mn(^{iPr}Psalen)(N$_3$)].

To obtain the Mn≡N derivatives the azide complexes were heated under reduced pressure in order to facilitate the release of N_2. Unfortunately, no change on the nature of the species was detected by NMR. The formation of a Mn(V)-nitrido complex should by easily detected by ^{31}P and ^{1}H NMR since these species usually possess a closed-shell configuration (S = 0) and are diamagnetic.[12] The use of ultraviolet radiation and new synthetic pathways to obtain nitrido species are under current investigation.

6.2 Manganese-peroxo complex

Mn^{II} phosphasalen complexes were found to abstract a chlorine atom from chlorinated solvents upon air exposure. Oxidation of the metal occurs when the neutral complex is exposed to the air, activating the solvent.

This reactivity was further studied in presence of pyridine inspired by the iron(I)-pyridine complex [Fe^{I}L(py)] reported by Patrick L. Holland and co-workers (Scheme 81).[15] This complex is present in equilibrium with the radical form ([Fe^{II}L(py·)]), where an electron has been transferred from the metal to the pyridine, which is acting as a redox non-innocent ligand. The radical species dimerized through the pyridine moiety to yield the diiron(II) complex [Fe^{II}L(py)]$_2$.[15]

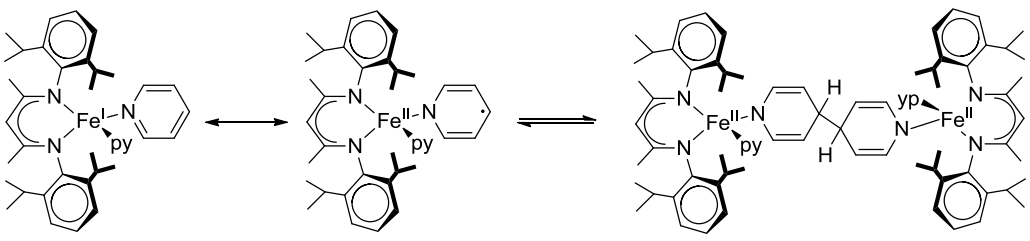

[Fe^{I}L(py)] [Fe^{II}L(py·)] [Fe^{II}L(py)]$_2$

Scheme 81. Resonance and dimerization equilibria for complex [Fe^{I}L(py)] reported by Holland and co-workers.[15]

A similar reactivity was expected for [Mn(Psalen^{tBu})] in presence of pyridine once the mixture was exposed to the air. An electron transfer may occur from the metal to the pyridine leading to Mn(III)-pyridine radical species.

Thus, [Mn(Psalen^{tBu})] complex was dissolved in THF inside the glove box, and one equivalent of pyridine was added. The mixture was taken out of the glove box and was stirred for 30 minutes, then opened to the air and stirred for 1 more hour. Once the mixture was exposed to the air, an immediate color change occurs from yellow to dark brown. In order to crystallize the product, some pentane was added to the solution and the mixture was kept in the fridge. The crystal structure obtained is shown in Figure 173.

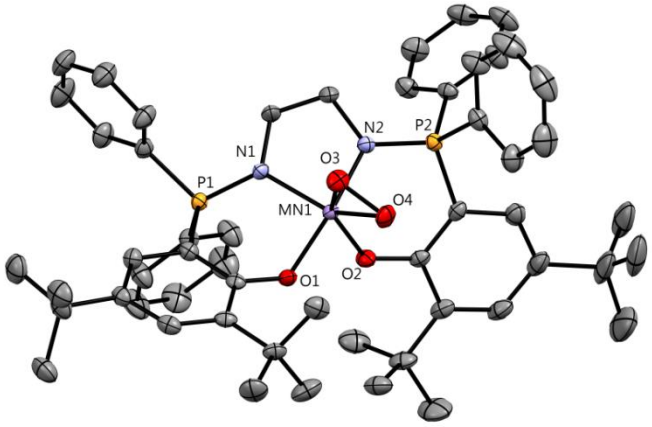

Figure 173. ORTEP of [Mn(Psalen^{tBu})(O_2)] with thermal ellipsoids at 50 % probability. Hydrogen atoms and have been removed for clarity.

The crystallized product was a manganese side-on peroxo or superoxo complex. No molecules of pyridine were found in the unit cell. A molecule of oxygen from the air has been activated and incorporated to the structure, oxidizing the manganese center. This structure can only correspond to a Mn^{IV} peroxo (O_2^{2-}) or a Mn^{III} superoxo ($O_2^{\cdot-}$) species, since no counter ion is present. The metal ion adopts a distorted octahedral geometry with N1, O2, O3 and O4 occupying the equatorial positions, and N2 and O1 in the apical positions (Figure 174). The manganese atom is placed at 0.622 Å from the NOON plane, which presents a torsion angle of 36.19 °. The Mn-N bonds are not symmetric, 1.990(2) and 1.951(2) Å (Δd = 0.039 Å), while for the Mn-O1 and Mn-O2 the difference is lower, 1.911(2) and 1.928(2) Å, respectively. The Mn-O bonds of the oxygen molecule are equivalent, 1.850(2) and 1.852(2) Å, and the O-O bond distance is 1.430(3) Å. The bite O3-Mn-O4 angle measures 45.46 °.

Few X-ray structure of side-on manganese-peroxo complexes have been reported in the literature, most of them being Mn^{III} or Mn^{IV} peroxide complexes.[16] Nam and co-workers

reported a Mn(IV)-peroxo complex which Mn-O average distance is 1.876 Å and O-O bond average distance is 1.415 Å, similar to those observed for the phosphasalen complex.[16a] Distances of 1.883(2) and 1.873(2) Å for Mn-O bonds and 1.379(2) Å for O-O bond have been reported recently by Lee and co-workers for a Mn(IV)-peroxo complex. [16b] Since the Mn-O bond distance can vary depending on the geometry, the metal and its oxidation state, the O-O bond distance is a better indicator of the oxidation state of the coordinated dioxygen. In our case, an O-O bond length of 1.430(3) Å points to the presence of Mn(IV)-peroxo species. Superoxo species possess shorter O-O bonds since its bond order is higher.[17] Values of 1.323(3) Å and 1.262(8) Å have been reported in the literature for iron and cobalt superoxo complexes, and are significantly shorter than those reported for peroxo-complexes.[16a,18] Thus, the obtained crystallographic data suggest that this species can be formulated as a Mn(IV)-peroxo complex, belonging to the few examples of manganese peroxide species existing in the literature, and the first displaying an NOON coordination environment or a salen-type ligand. The most interesting feature of this structure is that it has been generated using atmospheric oxygen, while in the literature these species need of an oxygen-containing oxidant or oxygen atmosphere to be formed.

	[MnOO)]
Mn-O1	1.911(2)
Mn-O2	1.928(2)
Mn-O3	1.850(2)
Mn-O4	1.852(2)
Mn-N1	1.990(2)
Mn-N2	1.951(2)
P1-N1	1.602(2)
P2-N2	1.603(2)
Torsion angle	8.91

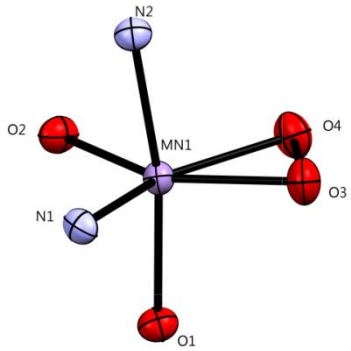

Table 41 (left). Selected bond lengths (Å) and angles (°) for [Mn(Psalen^{tBu})(py)]. Figure 174 (right). Coordination sphere of [Mn(Psalen^{tBu})(O_2)].

This reaction was also performed with the [Mn(^{iPr}Psalen)] derivative which seems to display the same reactivity. Crystals were obtained after air exposure but their quality was not enough to launch an acquisition.

The effective magnetic moment of [Mn(Psalen^{tBu})(O_2)] was measured in a chloroform solution using the Evans' method. The value obtained is 3.95 μ_B that corresponds to 3 unpaired electrons (spin-only value is 3.87 μ_B). Considering an octahedral geometry, this points to a Mn^{IV} $3d^3$ complex, in agreement with the assignment done from the crystallographic data. [Mn(Psalen^{tBu})(O_2)] displays a paramagnetic ^{1}H NMR and no ^{31}P signal, also in agreement with this assignment.

The stability of this complex was monitored by UV-vis spectroscopy (Figure 175). The absorption spectrum of [Mn(Psalen^{tBu})(O_2)] in THF shows a weak band at 600 nm (ε = 900 M^{-1} cm^{-1}), and a more intense band at 460 nm (ε = 2400 M^{-1} cm^{-1}). This band possesses a shoulder at 500 nm (ε = 1900 M^{-1} cm^{-1}). An intense band starts to appear at 400 nm and reaches an absorption of 10000 M^{-1} cm^{-1} at 300 nm. Two bands seem to be superimposed to this transition at 400 nm (ε = 2500 M^{-1} cm^{-1}) and 370 nm (ε = 3600 M^{-1} cm^{-1}). 20 minutes later the band at 400 nm has disappeared and the transition at 600 nm presents a higher intensity (ε = 1200 M^{-1} cm^{-1}). The spectrum was recorded after 1, 24, 48, and 72 hours and no significant change was observed suggesting that the complex is stable in THF solution for days. The disappearance of the band at 400 nm after 20 minutes could not be explained.

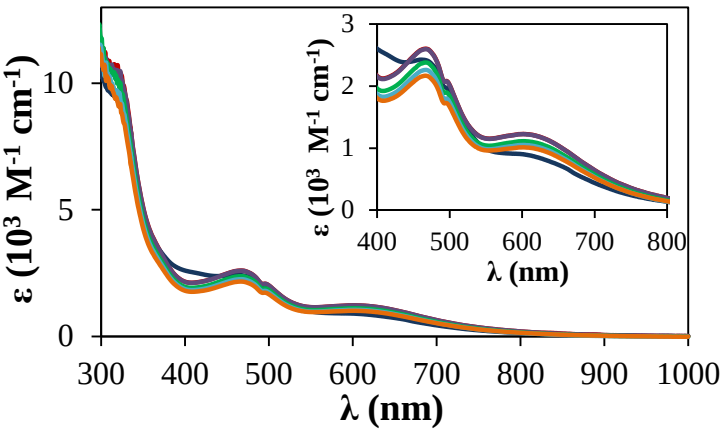

Figure 175. UV-vis spectrum of [Mn(Psalen^{tBu})(O_2)] complex in THF solution at t = 0 (dark blue line), t = 20 min (red line), t = 1 h (purple line), t = 24 h (green line), t = 48 h (light blue) and t = 72 h (orange line). Inset shows a zoom of the visible region.

It is worth noting that this spectrum is very similar to that obtained for the [Mn(Psalen^{tBu})] complex once it is exposed to the air (Figure 160). This suggests that peroxo species has also been formed in that case.

The infrared spectrum of a solid sample of [Mn(Psalen^{tBu})(O_2)] measured at room temperature shows different features at 799, 833, 878 and 901 cm^{-1}. This corresponds to the frequency range of the O-O stretching reported for peroxometallic complexes (800-930 cm^{-1}).[16] This spectrum was compared to those recorded for [Mn(Psalen^{tBu})Cl] and [Mn(Psalen^{tBu})]PF_6 and the feature at 901 cm^{-1} was the only not present in those spectra, then assigned to the O-O stretching. This value is very similar to those reported by Nam and Lee for M(IV)-peroxo complexes, 905 and 903 cm^{-1}, respectively.[16a,16b] IR spectra of the three mentioned complexes are present in Annex 1.

This reaction could be reproduced with a yield of 38 % corresponding to the crystallized product. The stability, reactivity and electronic structure of this species are being currently investigated.

7. Conclusion

A series of Mn^{II} and Mn^{III} phosphasalen complexes have been synthesized and characterized. These complexes have been characterized by NMR, X-ray diffraction and UV-visible spectroscopy. Both Mn^{II} and Mn^{III} series possess a high spin configuration. Mn^{III} complexes were tested in epoxidation catalysis of alkenes, but the results obtained were disappointing. This may be explained by the high oxidation potentials obtained for these complexes. Their catalytic activity can be enhanced by addition of non-redox metal ions, such as $Ca(OTf)_2$ in the reaction mixture. Since these are only preliminary results, it is too early to determine the influence of the ligand substituents or coordination sphere of the metal in the catalytic activity of the complexes.

Reaction intermediates could not be trapped and characterized; the isolated products were the Mn^{III} starting materials. A further characterization of the intermediates is aimed using EPR spectroscopy.

A side-on manganese-peroxo complex was isolated and characterized. The data obtained by X-ray diffraction, IR and magnetic measurements performed in solution point to manganese(IV)-peroxo species. The obtaining of this complex is relevant since it was formed by atmospheric oxygen activation and only few manganese peroxo species have been characterized. This is also the first manganese peroxo species displaying an NNOO coordinating environment.

A full characterization of this species is in progress. Its reactivity will be tested towards different substrates. The formation of analogous complexes displaying different phosphasalen ligands is aimed as well.

8. References

[1] W. Zhang, J. L. Loebach, S. R. Wilson, E. N. Jacobsen, *J. Am. Chem. Soc.* **1990**, *112*, 2801-2803.

[2] K. Srinivasan, P. Michaud, J. K. Kochi, *J. Am. Chem. Soc.* **1986**, *108*, 2309-2320.

[3] E. M. McGarrigle, D. G. Gilheany, *Chem. Rev.* **2005**, *105*, 1563-1602.

[4] a) D. Feichtinger, D. A. Plattner, *Chem. Eur. J.* **2001**, *7*, 591-599; b) D. A. Plattner, D. Feichtinger, J. El-Bahraoui, O. Wiest, *Int. J. Mass* **2000**, *195*, 351-362; c) D. Feichtinger, D. A. Plattner, *J. Chem. Soc., Perkin Trans. 2* **2000**, 1023-1028; d) D. Feichtinger, D. A. Plattner, *Angew. Chem. Int. Ed.* **1997**, *36*, 1718-1719.

[5] M. Guo, H. Dong, J. Li, B. Cheng, Y.-Q. Huang, Y.-Q. Feng, A. Lei, *Nat. Comm.* **2012**, *3*, 1190.

[6] C. S. Mullins, V. L. Pecoraro, *Coord. Chem. Rev.* **2008**, *252*, 416-443.

[7] Y-L. Zhang, *Acta Cryst.* **2006**, E62, m900–m901; b) M. Yu, R. J. Beyers, J. D. Gorden, J. N. Cross, C. R. Goldsmith, *Inorg. Chem.* **2012**, *51*, 9153-9155; c) C. Hureau, S. Groni, R. Guillot, G. Blondin, C. Duboc, E. Anxolabéhère-Mallart, *Inorg. Chem.* **2008**, *47*, 9238-9247.

[8] a) Z. Lv, W. Zheng, Z. Chen, Z. Tang, W. Mo, G. Yin, *Dalton Trans.* **2016**, *45*, 11369-11383; b) Z. Chen, L. Yang, C. Choe, Z. Lv, G. Yin, *Chem. Comm.* **2015**, *51*, 1874-1877.

[9] L. Lecarme, L. Chiang, J. Moutet, N. Leconte, C. Philouze, O. Jarjayes, T. Storr, F. Thomas, *Dalton Trans.* **2016**, *45*, 16325-16334.

[10] U. Neuenschwander, I. Hermans, *J. Org. Chem.* **2011**, *76*, 10236-10240.

[11] a) K. M. Lancaster, M. Roemelt, P. Ettenhuber, Y. Hu, M. W. Ribbe, F. Neese, U. Bergmann, S. DeBeer, *Science* **2011**, *334*, 974; b) G. Ertl, *Angew. Chem. Int. Ed.* **1990**, *29*, 1219-1227.

[12] J. Du Bois, J. Hong, E. M. Carreira, M. W. Day, *J. Am. Chem. Soc.* **1996**, *118*, 915-916.

[13] A. J. Keane, W. S. Farrell, B. L. Yonke, P. Y. Zavalij, L. R. Sita, *Angew. Chem. Int. Ed.* **2015**, *54*, 10220-10224.

[14] H. Kropp, A. E. King, M. M. Khusniyarov, F. W. Heinemann, K. M. Lancaster, S. DeBeer, E. Bill, K. Meyer, *J. Am. Chem. Soc.* **2012**, *134*, 15538-15544.

[15] T. R. Dugan, E. Bill, K. C. MacLeod, G. J. Christian, R. E. Cowley, W. W. Brennessel, S. Ye, F. Neese, P. L. Holland, *J. Am. Chem. Soc.* **2012**, *134*, 20352-20364.

[16] a) S. Hong, K. D. Sutherlin, J. Park, E. Kwon, M. A. Siegler, E. I. Solomon, W. Nam, *Nat. Commun.* **2014**, *5*, 5440; b) C.-M. Lee, C.-H. Chuo, C.-H. Chen, C.-C. Hu, M.-H. Chiang, Y.-J. Tseng, C.-H. Hu, G.-H. Lee, *Angew. Chem. Int. Ed.* **2012**, *51*, 5427-5430; c) M. S. Seo, J. Y. Kim, J. Annaraj, Y. Kim, Y.-M. Lee, S.-J. Kim, J. Kim, W. Nam, *Angew. Chem. Int. Ed.* **2007**, *46*, 377-380; d) J. Annaraj, J. Cho, Y.-M. Lee, S. Y. Kim, R. Latifi, S. P. de Visser, W. Nam, *Angew. Chem. Int. Ed.* **2009**, *48*, 4150-4153.

[17] C. J. Cramer, W. B. Tolman, K. H. Theopold, A. L. Rheingold, *Proc. Natl. Acad. Sci. U.S.A* **2003**, *100*, 3635-3640.

[18] J. W. Egan, B. S. Haggerty, A. L. Rheingold, S. C. Sendlinger, K. H. Theopold, *J. Am. Chem. Soc.* **1990**, *112*, 2445-2446.

Conclusions and perspectives

In this PhD thesis the electronic structure of phosphasalen oxidized complexes was studied. A variety of phosphasalen ligands differing by the phenoxide and the phosphorus substituents, as well as the amine linker were synthesized and coordinated to copper and nickel centers. Various characterization techniques such as cyclic voltammetry, NMR, EPR, UV-vis, SQUID measurements and theoretical calculations were employed to characterize the neutral and oxidized complexes. The stabilization of manganese centers in different oxidation states and their potential catalytic applications were also studied with these ligands.

The nitrogen atom of the iminophosphorane function possesses two lone pairs that are partially delocalized in the phosphorus orbitals, thus phosphasalen are better electron-donors than salen ligands. This allows an easier oxidation of the complexes and favors the involvement of the metal in the oxidation process. The characterization of the one-electron oxidized complexes shows a greater involvement of the metal in the oxidation process. Thus, [Cu(Psalen^{tBu})], [Cu(^{iPr}Psalen)] and [Ni(^{iPr}Psalen)] were characterized as Cu^{III} and Ni^{III} species and belong to the few examples of stable Cu^{III} and Ni^{III} salen-type complexes present in the literature. [Cu(Psalen^{OMe})] and [Ni(Psalen^{OMe})] were better described as ligand radical complexes with a significant contribution of the metallic orbitals in the stabilization of the electronic hole, while their salen analogues were characterized as localized phenoxyl complexes.

The study of the phosphasalophen series allowed us to determine the influence of the amine linker substitution. The electron pairs of the nitrogen are partially delocalized in the aryl linker, making it electron-richer and promoting its oxidation. Thus, unsubstituted nickel and copper phosphasalen complexes dimerize upon oxidation. This dimerization was not observed in the case of salen, and is due to the better donation of the iminophosphorane functions, compared to the imines. The dimerization process can be avoided with the introduction of substituents in the central ring. The nature of these groups, more or less electron-donating, influences the electronic structure of the oxidized species which possess more or less ligand radical character, respectively. A localized radical ligand in the central ring is obtained when the phenylene ring displays two methoxy groups.

Mn^{II}, Mn^{III} and Mn^{IV} phosphasalen complexes have been synthesized and characterized using various substituted Psalen ligands. Most of the complexes could be characterized by X-ray diffraction. This is relevant since very few structures of Mn^{II} and Mn^{IV} salen-type complexes have

been reported in the literature. Despite their similarity with the Jacobsen catalyst, the Mn^{III} complexes have not shown any catalytic activity. The stabilization of a high-valent metal complex was achieved with the isolation of a side-on peroxo Mn^{IV} complex formed *via* O_2 activation by the Mn^{II} complex. These species are rare in the literature and are usually intermediates in catalytic reactions. The isolated complex is very stable and demonstrates again the ability of phosphasalen ligands to stabilize metal in high oxidation states.

In a future work, it will be interesting to study the reactivity of the obtained oxidized complexes (Ni, Cu and Mn). For nickel and copper complexes only the first oxidation was investigated. To get more information about the influence of the different substituents and the phosphorus atom, the second, and third oxidation in some cases, must be studied. Especially the complexes presenting low redox potentials whose oxidized species may be easily stabilized by the presence of the iminophosphoranes.

The isolation of the manganese peroxo complex is a very promising result. This kind of complexes are very interesting because the involvement of these species in the Photosystem II. The reactivity of this complex must be investigated, as well as the stabilization of other peroxo complexes by using different phosphasalen ligands. The stabilization of oxo and nitrido complexes is under current investigation. Iron is, as manganese, an interesting metal from the biologically point of view; the isolation and characterization of iron O_2-containing species is largely persecuted. Thus, the next step of this work might be the coordination of this metal with phosphasalen ligands and the potential generation of stable peroxo, or oxo, species.

Experimental part

I. General considerations

All the experiments were carried out under inert conditions, either under a pure nitrogen atmosphere using Schlenk technics or in a drybox (O2 < 1 ppm, H2O < 0.1 ppm). Tetrahydrofurane, toluene, dichloromethane, diethyl ether and petroleum ether were used directly from the MBraun MB-SPS 800 Solvent Purification Machine. When necessary, solvents were distilled from sodium/benzophenone under dry conditions. All other reagents and chemicals were obtained commercially and used without further purification.

NMR spectra were recorded on a Bruker Avance 300 spectrometer operating at 300 MHz for ^{1}H, 75.5 MHz for ^{13}C and 121.5 MHz for ^{31}P. Solvent peaks were used as internal references for ^{1}H and ^{13}C chemical shifts (ppm). $^{31}P\{1H\}$ is relative to a 85% H_3PO_4 as external reference. The following abbreviations are used: br, broad; s, singlet; d, doublet; dd, doublet of doublets; t, triplet; m, multiplet.

Visible spectra were recorded in 200-1000 nm range at room temperature on an Agilent Cary 60 Spectrometer in 10 mm quartz cuvettes with solvent background correction.

Elemental analyses were performed by the Elemental Analysis Service of the London Metropolitan University (United Kingdom).

Magnetic measurements were performed using a Cryogenic SX600 SQUID magnetometer. Solid samples were placed in quartz tubes under inert atmosphere. Magnetic susceptibility measurements were recorded at 5 T for $[Cu(Psalen^{OMe})]^{+}SbF_6^{-}$ and $[Cu(Psalen^{tBu})]^{+}SbF_6^{-}$, and 0.5 and 2 T for the others, in the 4-300 K temperature range.

X-band EPR spectra were recorded on a Bruker ELEXSYS 500 spectrometer equipped with a Bruker ER4119HS X band resonator, an Oxford Instrument continuous flow ESR 900 cryostat, and a temperature control system.

X-ray diffraction data was collected on a Nonius Kappa CCD APEXII diffractometer using Mo Kα (λ= 0.71073 Å) as X-ray source and a graphite monochromator. The crystal structures were solved in SIR97, SHELXL-97 and SHELXL-2014; and refined in SHELXL-97 and SHELXL-2014 by full-matrix least-squares using anisotropic thermal displacement parameters for all non-hydrogen atoms. Hydrogen atoms were placed either at geometrically calculated positions or

according to the localization of electronic densities around the carbon atoms. Single crystals were mounted on a kapton loop using Paratone® oil and cooled at 150 K in a nitrogen stream for X-ray structure determination.

Electrochemical experiments were performed using a VERSASTAT potentiostat. An Pt wire was used as counter electrode, glassy carbon electrode as working electrode and SCE as reference electrode. All the experiments were carried out under inert atmosphere in 10 or 12 mL of CH_2Cl_2 solution with tetrabutylammonium hexafluorophosphate (0.12 M) as supporting electrolyte and 3 mM of complex.

Gas chromatography was performed in a Perichrom PR 2100 2317 Series gas chromatograph equipped with a split-mode, capillary injection system and flame ionization detectors using a SGE apolar ID-BP1 (25 m × 0.32 mm) column.

Mass spectrometry experiments were carried out in the positive mode with a QTOF Premier mass spectrometer (Waters Technologies). The ion source parameters were: cone voltage, 20 to 80 V; capillary voltage, 2.6 kV. Typical values for the other source parameters were: extraction cone voltage, 2 V; ion guide voltage, 2.4 V. The source and desolvation temperatures were set to 80°C and 450°C, respectively. Nitrogen was used as both the nebulizing and the desolvation gas, with gas flow rates ranging from 70 $L \cdot h^{-1}$to 700 $L \cdot h^{-1}$. Argon was used as the collision gas at a flow rate of 0.28 $mL \cdot min^{-1}$, corresponding to a pressure of *c*a $4 \cdot 10^{-3}$ mBar.

II. Experimental Part

Chapter 2

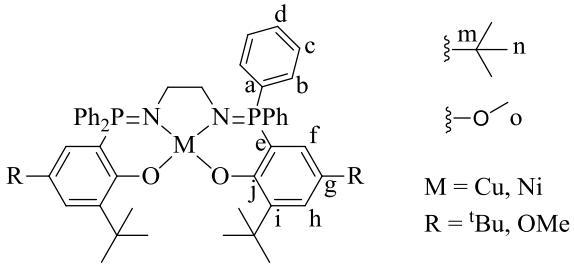

The synthesis of Psalen^{OMe} and Psalen^{tBu} ligands have been already described in the literature and are not included here.

Synthesis of [Ni(Psalen^{OMe})]

KHMDS (380 mg, 1.9 mmol) was added to a suspension of bis-aminophosphonium (H_4Psalen^{OMe})Br_2 proligand (450 mg, 0.47 mmol) in THF (30 mL) under inert conditions. After stirring at room temperature for 1 h, $^{31}P\{^1H\}$ NMR showed a sole singlet at 18 ppm confirming that the deprotonation was completed. Salts formed were removed by centrifugation and [$NiBr_2$(DME)] (146 mg, 0.47 mmol) was added. The mixture was stirred for 2 h until the disappearance of the ligand signal and the appearance of a new singlet at 34 ppm. The solvent was removed and the residue dissolved in CH_2Cl_2 (15 mL). The insoluble salts were removed by centrifugation, the solution was concentrated and a purple precipitate was obtained by addition of petroleum ether. The solid was washed with petroleum ether (5 × 10 mL) and dried under reduced pressure to afford [Ni(Psalen^{OMe})] (340 mg, 85 %). Crystals were obtained *via* petroleum ether diffusion into a saturated CH_2Cl_2 solution. $^{31}P\{^1H\}$ NMR (CD_2Cl_2): δ 35.2 ppm; ^1H NMR (CD_2Cl_2) δ 7.95 (dd, $^3J_{P,H}$ = 11.8 Hz, $^3J_{H,H}$ = 7.8 Hz, 8H, H_b), 7.66 (m, 12H, H_c, H_d), 6.87 (d, $^4J_{H,H}$ = 3.0 Hz, 2H, H_h), 5.71 (dd, $^3J_{P,H}$ = 15.5 Hz, $^4J_{H,H}$ = 3.0 Hz, 2H, H_f), 3.42 (s, 6H, H_o), 2.06 (t, $^3J_{H,H}$ = 3.8 Hz, 4H, H_p), 1.36 (s, 18H, H_l). $^{13}C\{^1H\}$ NMR (CD_2Cl_2): 165.5 (s, C_j), 148.0 (d, $^3J_{P,C}$ = 20.5 Hz, C_g), 144.9 (d, $^3J_{P,C}$ = 8.8 Hz, C_i), 133.9 (d, $^3J_{P,C}$ = 9.5 Hz, C_c), 132.4 (d, $^4J_{P,C}$ = 2.4 Hz, C_d), 129.1 (d, $^2J_{P,C}$ = 11.8 Hz, C_b), 128.3 (d, $^1J_{P,C}$ = 88.4 Hz, C_a), 120.0 (s, C_h), 116.7 (d, $^1J_{P,C}$ = 90.1 Hz, C_e), 111.6 (d, $^2J_{P,C}$ = 18.9 Hz, C_f), 56.4 (s, C_o), 50.6 (dd, $^2J_{P,C}$ = 19.5 Hz, $^3J_{P,C}$ = 4.6 Hz, C_p), 35.9 (s, C_k), 29.6 (s, C_l). Anal. Calcd. for $C_{48}H_{52}N_2NiO_4P_2$: C, 68.50; H, 6.23; N, 3.33. Found: C, 68.48; H, 6.36; N, 3.46.

Synthesis of [Cu(Psalen^{tBu})]

KHMDS (358 mg, 1.8 mmol) was added to a suspension of bis-aminophosphonium (H_4Psalen^{tBu})Br_2 proligand (450 mg, 0.45 mmol) in THF (30 mL) under inert conditions. After stirring 2 h at room temperature, the $^{31}P\{^1H\}$ NMR spectrum showed a sole singlet at 15.4 ppm indicating that the deprotonation was completed. Insoluble salts were removed by centrifugation and $CuBr_2$ (100 mg, 0.45 mmol) was added into solution. After 2 h of stirring, the solution turned green and no $^{31}P\{^1H\}$ NMR signal was observed. The solvent was removed under reduced pressure and the residue dissolved in CH_2Cl_2 and centrifuged. The solution was concentrated and a green precipitate was obtained by addition of petroleum ether. The green solid was washed with petroleum ether and dried under reduced pressure to yield [Cu(Psalen^{tBu})] (270 mg, 66 %). Crystals were obtained via evaporation of a $CDCl_3$ solution. $^{31}P\{^1H\}$ NMR ($CDCl_3$): no signal; ^1H NMR ($CDCl_3$) δ 9.38 (br s, H_b,H_c,H_d), 6.98 (br s, H_f,H_h), 3.34 (br s, H_p), 1.56 (br s, H_l or H_n), 0.99 (br s, H_l or H_n). Anal. Calcd. for $C_{54}H_{64}Cu\ N_2O_2P_2$: C, 72.18; H, 7.18; N, 3.12; Found: C, 72.29; H, 7.30; N, 2.98.

Synthesis of [Cu(Psalen^{OMe})]:

An excess of KH (102 mg, 2.5 mmol) was added to a suspension of bis-aminophosphonium (H_4Psalen^{OMe})Br_2 proligand (400 mg, 0.42 mmol) in THF (30 mL) under inert conditions. The mixture was stirred at 50 °C for 2 h. The presence of a sole singlet at 18 ppm in the $^{31}P\{^1H\}$ NMR spectrum was indicative that the deprotonation was completed. The solution was filtered and $CuBr_2$ (95 mg, 0.42 mmol) was added. After stirring for 2 h at room temperature, the complexation was completed and no signal in the $^{31}P\{^1H\}$ NMR spectra was observed. The solvent was removed under reduced pressure and the residue dissolved in CH_2Cl_2 (15 mL). KBr salts were removed by centrifugation and the solution was concentrated. A green precipitate was obtained by addition of petroleum ether. The solid was washed with petroleum ether (5 × 10 mL) and dried under reduced pressure to afford [Cu(Psalen^{OMe})] (291 mg, 82 %). Crystals were obtained *via* pentane diffusion into a saturated CH_2Cl_2 solution. $^{31}P\{^1H\}$ NMR ($CDCl_3$): no signal; ^1H NMR ($CDCl_3$) δ 9.37 (br s, H_b, H_c, H_d), 6.87 (br s, H_f, H_h), 3.69 (br s, H_o), 1.57 (br s, H_l). Anal. Calcd. for $C_{48}H_{52}CuN_2O_4P_2$: C, 68.11; H, 6.19; N, 3.31. Found: C, 67.94; H, 6.27; N, 3.26.

Synthesis of [Cu(Psalen^{tBu})]$^+SbF_6^-$

[Cu(Psalen^{tBu})] (250 mg, 0.28 mmol) was dissolved in CH_2Cl_2 (4 mL). Addition of $AgSbF_6$ (96 mg, 0.28 mmol) to the solution under Ar atmosphere immediately resulted in a color change from green to deep purple together with the formation of a suspension of Ag. This suspension was

stirred for 1 h and then filtered. The solvent was removed under reduced pressure and the residue dissolved in a minimum amount of diethyl ether. A purple precipitate was obtained by addition of petroleum ether. The solid was washed with petroleum ether (3 × 10 mL) and dried under reduced pressure to obtain [Cu(Psalen^{tBu})]$^{+}$SbF$_6^-$ as a purple powder (269 mg, 85 %). Dark purple crystals were obtained after one week of storage of a saturated solution of toluene/CH_2Cl_2 at -40 °C. $^{31}P\{^1H\}$ NMR (CD_2Cl_2): no signal; ^1H NMR (CD_2Cl_2) δ 7.50-8.09 (m, 22H, H_b, H_c, H_d, H_h), 6.56 (br s, 2H, H_f), 2.95 (br s, 4H, H_p), 1.40 (br s, 18H, H_l or H_n), 1.14 (br s, 18H, H_l or H_n). Anal. Calcd. for $C_{54}H_{64}F_6N_2NiO_2P_2Sb$: C, 57.18; H, 5.69; N, 2.47. Found: C, 57.12; H, 5.84; N, 2.57.

Synthesis of [Cu(Psalen^{OMe})]$^{+}$SbF$_6^-$

[Cu(Psalen^{OMe})] (200 mg, 0.23 mmol) was dissolved in CH_2Cl_2 (4 mL). Addition of $AgSbF_6$ (81 mg, 0.23 mmol) to the solution under Ar atmosphere immediately resulted in a color change from green to deep purple, and the formation of a suspension of Ag. This suspension was stirred for 1 h and then filtered. The solution was concentrated and a purple solid was obtained by addition of petroleum ether into the solution. The solid was washed with petroleum ether (3 × 10 mL) and dried under reduced pressure to yield [Cu(Psalen^{OMe})]$^{+}$SbF$_6^-$ (215 mg, 84 %). Dark purple crystals were obtained after one week of storage of a saturated solution of toluene/CH_2Cl_2 at -40 °C. $^{31}P\{^1H\}$ NMR (CD_2Cl_2): no signal; ^1H NMR (CD_2Cl_2) δ 7.77 (m, 22H, H_b, H_c, H_d, H_f or H_h), 5.65 (br s, 2H, H_f or H_h), 4.55 (bs, 8H, H_o), 1.42 (br s, 18H, H_l). Anal. Calcd. for $C_{48}H_{52}CuF_6N_2O_4P_2Sb$: C, 53.27; H, 4.84; N, 2.59. Found: C, 53.13; H, 4.89; N, 2.75.

Synthesis of [Ni(Psalen^{OMe})]$^{+}$ SbF$_6^-$

[Ni(Psalen^{OMe})] (110 mg, 0.13 mmol) was dissolved in CH_2Cl_2 (4 mL). Addition of $AgSbF_6$ (45 mg, 0.13 mmol) to the solution under Ar atmosphere immediately resulted in a color change from purple to dark brown and to the formation of a suspension of Ag. This suspension was stirred for 1 h and then filtered. The solution was concentrated and a dark brown-reddish solid was obtained by addition of petroleum ether into the solution. The solid was washed with petroleum ether (3 × 10 mL) and dried under reduced pressure to yield [Ni(Psalen^{OMe})]$^{+}$SbF$_6^-$ (115 mg, 82 %). Brown crystals were obtained via petroleum ether diffusion into a saturated CH_2Cl_2 solution. $^{31}P\{^1H\}$ NMR (CD_2Cl_2): no signal; ^1H NMR (CD_2Cl_2) δ 33.98 (bs, 6H, H_o), 25.99 (bs, 2H, H_f or H_h), 8.46 (d, J = 5.8 Hz, 8H, H_b or H_c), 7.87 (br s, 8H, H_c or H_b) 7.74 (t, $^3J_{H,H}$ = 6.8 Hz, 4H, H_d), 2.88 (br s, 18H, H_l), -2.84 (br s, 2H, H_b or H_c). Anal. Calcd for $C_{48}H_{52}F_6N_2NiO_4P_2Sb$: C, 53.51; H, 4.87; N, 2.60. Found: C, 53.28; H, 5.02; N, 2.57.

Chapter 3

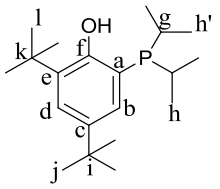

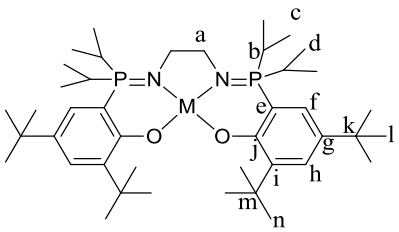

Synthesis of isopropyl phosphine

n-BuLi (33 mL, 52.8mmol) was added dropwise to a solution of 2-bromo-1,3-di-*tert*-butylphenol (7 g, 24.56 mmol) in diethyl ether (50 mL) at -78 °C under inert conditions. The resulting pale yellow solution was stirred for 1 hour at room temperature. Chlorodiisopropyl phosphine (4.07 mL, 24.56 mmol) was added to the solution at -78 °C and a white precipitate appeared. The suspension was stirred overnight. The mixture was extracted with a solution of NaH_2PO_4 (50 mL, 0.16 M) and the organic layer was dried over $MgSO_4$. The solid was filtered and the solution concentrated to 20 mL. Addition of methanol induces the precipitation of the desired product as a white solid, which was filtered and dried under reduced pressure to yield 3.5 g (44 %). $^{31}P\{^1H\}$ NMR ($CDCl_3$): δ -21.4 ppm; ^1H NMR ($CDCl_3$) δ 7.29 (d, $^3J_{P,H}$ = 2.8 Hz, 1H, OH), 7.27 (m, 1H, H_d), 7.10 (t, $^3J_{P,H}$ = 2.7 Hz, $^4J_{H,H}$ = 2.5 Hz, H_b), 2.14 (m, 1H, H_g), 1.41 (s, 9H, H_l or H_j), 1.30 (s, 9H, H_l or H_j), 1.12 (dd, $^3J_{P,H}$ = 16.5 Hz, $^3J_{H,H}$ = 7.0 Hz, H_h or $H_{h'}$), 0.94 (dd, $^3J_{P,H}$ = 16.5 Hz, $^3J_{H,H}$ = 7.0 Hz, H_h or $H_{h'}$). $^{13}C\{^1H\}$ NMR ($CDCl_3$): δ 157.2 (d, $^2J_{P,H}$ = 18.4 Hz, C_a), 140.7 (d, $^3J_{P,H}$ = 1 Hz, C_c), 134.5 (d, $^3J_{P,H}$ = 1.5 Hz, C_e), 126.6 (d, $^3J_{P,H}$ = 2.3 Hz, C_f), 125.1 (s, Cd), 117.1 (d, $^3J_{P,H}$ = 5.0 Hz, C_b), 34.9 (d, $^3J_{P,H}$ = 2.0 Hz, C_i or C_k), 34.3 (s, C_i or C_k), 31.6 (s, C_j or C_l), 29.5 (s, C_j or C_l), 22.8 (d, $^3J_{P,H}$ = 6.4 Hz, C_h or $C_{h'}$), 19.9 (d, $^3J_{P,H}$ = 17.7 Hz, C_g), 18.6 (d, $^3J_{P,H}$ = 7.0 Hz, C_h or $C_{h'}$).

Synthesis of (H_4^{iPr}Psalen)Br_2

The isopropyl phosphine (1.869 g, 5.8 mmol) was oxidized with bromine (0.3 mL, 5.8 mmol) at -78 °C in CH_2Cl_2 (20 mL) under inert conditions. After stirring for 2 hours the solution was placed again in a cold bath at -78 C and tributylamine (1.38 mL, 5.8 mmol) followed by ethylenediamine (0.193 mL, 2.9 mmol) were added. The cold bath was removed and the reaction was stirred overnight at room temperature. The formation of the ligand is indicated by the presence of a signal at 66.7 ppm in the $^{31}P\{^1H\}$ NMR spectrum. The tributylammonium salts were removed by centrifugation. THF (15 mL) was added to the slurry solution making the proligand precipitate. After filtration, the solid was washed with THF (3 x 10 mL) and dried under vacuum to lead (H_4^{iPr}Psalen)Br_2 as a white powder (1.997 g, 80%). $^{31}P\{^1H\}$ NMR ($CDCl_3$): δ 65.91 ppm; ^1H NMR

($CDCl_3$) δ 7.64 (s, 2H, H_h), 7.23 (dd, $^3J_{P,H}$ = 12.3 Hz, $^4J_{H,H}$ = 2.0, 2H, H_f), 6.49 (br s, 2H, OH), 3.57 (br s, 4H, H_a), 3.25 (m, 4H, H_b), 1.47 (s, 18H, H_n), 1.42 (dd, $^3J_{P,H}$ = 16.7 Hz, $^3J_{H,H}$ = 6.8 Hz, 12H, H_c or H_d), 1.36 (dd, $^3J_{P,H}$ = 16.7 Hz, $^3J_{H,H}$ = 6.8 Hz, 12H, H_c or H_d), 1.32 (s, 18H, H_l). ^{13}C {^1H} NMR ($CDCl_3$): δ 145.0 (s, C_g), 141.0 (s, C_i), 131.0 (s, C_h), 127.02 (s, C_f), 46.2 (s, C_l or C_n), 31.4 (s, C_c or C_d), 31.3 (s, C_m or C_k), 30.1 (s, C_c or C_d), 29.9 (s, C_m or C_k), 16.5 (d, $^3J_{P,H}$ = 16.5 Hz, C_b), 8.7 (s, C_l or C_n).

Synthesis of [Ni(Psalen^{iPr})]

KH (42mg, 1.04 mmol) was added to a suspension of bis-aminophosphonium (H_4Psalen^{iPr})Br_2 proligand (150 mg, 0.17 mmol) in THF (12 mL) under inert conditions. The reaction was stirred 2 h at 50 °C and completion of the deprotonation was indicated by the presence of a sole singlet in the $^{31}P\{^1H\}$ NMR spectrum at 31.0 ppm corresponding to the ligand. [$NiBr_2$(DME)] (53.2 mg, 0.17 mmol) was added and the solution became immediately purple. After stirring 1 h the reaction was completed, the $^{31}P\{^1H\}$ NMR spectrum shows a unique singlet at 49.7 ppm. The solvent was then removed and the residue dissolved in CH_2Cl_2 (10 mL) and centrifuged. The resulting solution was evaporated and a deep purple precipitate was obtained by addition of diethyl ether. The solid was washed with diethyl ether (3 x 10 mL) and dried under vacuum to yield [Ni(Psalen^{iPr})] (104.7 mg, 81%). $^{31}P\{^1H\}$ NMR ($CDCl_3$): δ 49.3 ppm; ^1H NMR ($CDCl_3$) δ 7.20 (d, $^4J_{H,H}$ = 2.5 Hz, 2H, H_h), 6.65 (dd, $^3J_{P,H}$ = 12.4 Hz, $^4J_{H,H}$ = 2.5, 2H, H_f), 2.65 (m, $^3J_{P,H}$ = 10.9 Hz, $^3J_{H,H}$ = 7.3 Hz, 4H, H_b), 2.29 (t, $^3J_{H,H}$ = 3.3 Hz, 4H, H_a), 1.84 (dd, $^3J_{P,H}$ = 14.6 Hz, $^3J_{H,H}$ = 7.3 Hz, 6H, H_c or H_d), 1.39 (s, 18H, H_l or H_n), 1.38 ($^3J_{P,H}$ = 14.6 Hz, $^3J_{H,H}$ = 7.2 Hz, 6H, H_c or H_d), 1.21 (s, 18H, H_l or H_n). ^{13}C {^1H} NMR ($CDCl_3$): δ 167.9 (s, C_j), 142.4 (d, $^3J_{P,C}$ = 7.8 Hz , C_i), 132.7 (d, $^3J_{P,C}$ = 12.8 Hz ,C_g), 126.6 (s, C_h), 122.5 (d, $^3J_{P,C}$ = 11.5 Hz, C_f), 105.9 (d, $^1J_{P,C}$ = 106.5 Hz, C_e), 50.6 (dd, $^3J_{P,C}$ = 16.3 Hz, $^4J_{P,C}$ = 5.0 Hz, C_a), 35.6 (s, C_m or C_k), 33.9 (s, C_m or C_k), 31.9 (s, C_l or C_n), 29.8 (s, C_n or C_l), 24.6 (d, $^1J_{P,C}$ = 53.2 Hz H_b), 17.9 (s, C_c or C_d), 17.0 (s, C_c or C_d). Anal. Calcd. for $C_{42}H_{72}N_2NiO_2P_2$: C, 66.58; H, 9.58; N, 3.70. Found: C, 66.51; H, 9.67; N, 3.82.

Synthesis of [Cu(Psalen^{iPr})]

KHMDS (369 mg, 1.85 mmol) was added to a suspension of bis-aminophosphonium (H_4Psalen^{iPr})Br_2 proligand (400 mg, 0.46 mmol) in THF (20 mL) under inert conditions. After stirring for 1 h at room temperature the deprotonation was completed and a sole singlet at 31.0 ppm corresponding to the ligand was observed in the $^{31}P\{^1H\}$ NMR. The insoluble salts formed were removed by centrifugation and $CuBr_2$ (103 mg, 0.46 mmol) was added to the solution. After stirring for 1 h the reaction was completed and the $^{31}P\{^1H\}$ NMR showed a silent spectrum. The

solvent was evaporated under vacuum and the residue dissolved in CH_2Cl_2 (10 mL) and centrifuged. The solution was then concentrated and addition of methanol allowed the precipitation of the complex as a green powder. The solid was washed with methanol (2 x 10 mL) and dried under reduced pressure to give [Cu(Psalen^{iPr})] (231 mg, 66 %). Purple crystals were obtained by evaporation of a chloroform solution. $^{31}P\{^1H\}$ NMR ($CDCl_3$): no signal; ^1H NMR ($CDCl_3$) δ 10.81 (br s), 3.89 (br s), 1.88 (br s), 1.63 (br s), 1.15 (br s). Anal. Calcd. for $C_{42}H_{72}CuN_2O_2P_2$: C, 66.15; H, 9.52; N, 3.67. Found: C, 66.02; H, 9.39; N, 3.81.

Synthesis of [Ni(Psalen^{iPr})]$^+SbF_6^-$

$AgSbF_6$ (36 mg, 0.10 mmol) was added to a solution of [Ni(Psalen^{iPr})] (90 mg, 0.10 mmol) in CH_2Cl_2 (4 mL) under Ar atmosphere. The solution changed immediately from purple to dark brown and a suspension of Ag was formed. After stirring for 1 h, the suspension was filtered and the solvent removed under vacuum. The residue was dissolved in a small amount of THF and precipitated with petroleum ether. The obtained dark brown solid was filtered, washed with petroleum ether (2 x 10 mL) and dried under reduced pressure to afford [Ni(Psalen^{iPr})]$^+SbF_6^-$ (90 mg, 86 %). Dark crystals were obtained by slow diffusion of petroleum ether to a CH_2Cl_2 solution. $^{31}P\{^1H\}$ NMR (CD_2Cl_2): no signal; ^1H NMR (CD_2Cl_2) δ 21.24 (s, 2H, H_f or H_h), 14.83 (s, 2H, H_f or H_h), 5.00 (br s, 12H, H_c or H_d), 4.57 (br s, 12H, H_c or H_d), 4.09 (s, 18H, H_l or H_n), 2.24 (br s, 18H, H_l or H_n). Anal. Calcd. for $C_{42}H_{72}F_6N_2NiO_2P_2Sb$: C, 50.78; H, 7.31; N, 2.82. Found: C, 50.65; H, 7.39; N, 2.80.

Synthesis of [Cu(Psalen^{iPr})]$^+SbF_6^-$

$AgSbF_6$ (54 mg, 0.16 mmol) was added to a solution of [Cu(Psalen^{iPr})] (150 mg, 0.19 mmol) in CH_2Cl_2 (4 mL) under Ar atmosphere. The solution changed immediately from green to deep purple and a suspension of Ag was formed. After stirring for 1 h, the suspension was filtered and the solution concentrated under vacuum. A deep purple solid was obtained by addition of petroleum ether. The solid was filtered, washed with petroleum ether (2 x 10 mL) and dried under reduced pressure to yield [Cu(Psalen^{iPr})]$^+SbF_6^-$ (130 mg, 83 %). Deep purple crystals were obtained from evaporation of a concentrated benzene solution. $^{31}P\{^1H\}$ NMR ($CDCl_3$): δ 65.38; ^1H NMR (CD_2Cl_2) δ 7.60 (s, 2H, H_h), 7.13 (dd, , $^3J_{P,H}$ = 12.0 Hz, $^4J_{H,H}$ = 2.0 Hz, 2H, H_f), 3.06 (bs, 4H, H_a), 2.94 (m, 4H, H_b), 1.65 (dd, , $^3J_{P,H}$ = 16.4 Hz, $^3J_{H,H}$ = 7.2 Hz, 12H, H_c or H_d), 1.53 (s, 18H, H_l or H_n), 1.36 (dd, $^3J_{P,H}$ = 16.4 Hz, $^3J_{H,H}$ = 7.2 Hz, 12H, H_c or H_d). Anal. Calcd. for $C_{42}H_{72}CuF_6N_2O_2P_2Sb$: C, 50.53; H, 7.27; N, 2.81. Found: C, 50.66; H, 7.18; N, 2.96.

Chapter 4

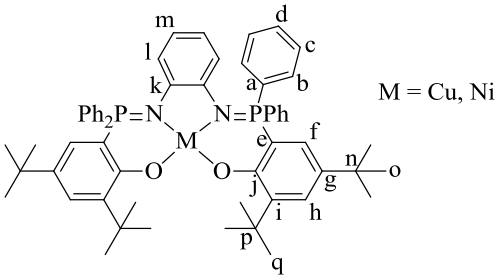

The synthesis of $(H_4Psalophen)Br_2$ ligand has been already described in the literature and is not included here.

Synthesis of [Ni(Psalophen)]

KHMDS (380 mg, 1.91 mmol) was added to a solution of bis-aminophosphonium $(H_4Psalophen)Br_2$ proligand (500mg, 0.47 mmol) in THF (20 mL) under inert conditions. After stirring during 2 h at room temperature the deprotonation is completed, the $^{31}P\{^1H\}$ NMR spectrum shows a singlet at 11 ppm. The solution was centrifuged to remove the insoluble salts and $[NiBr_2(DME)]$ (147 mg, 0.47 mmol) was added. After stirring at room temperature for 2 h complexation is completed, the $^{31}P\{^1H\}$ NMR spectrum shows a broad singlet at 34.7 ppm. After centrifugation, the solution was concentrated and a pale blue solid was obtained by precipitation with petroleum ether. The solid was washed with petroleum ether (3 x 10 mL) and dried under vacuum to yield [Ni(Psalophen)] (385 mg, 87%). Blue crystals were obtained by slow diffusion of pentane in a concentrated CH_2Cl_2 solution. $^{31}P\{^1H\}$ NMR ($CDCl_3$): δ 27 ppm; ^1H NMR ($CDCl_3$) δ 7.76 (dd, $^3J_{P,H}$ = 12.5 Hz, $^3J_{H,H}$ = 7.4 Hz, 8H, C_bH), 7.53 (t, $^3J_{H,H}$ = 6.9 Hz, 4H, C_dH), 7.43 (dt, $^3J_{H,H}$ = 7.0 Hz, $^4J_{H,H}$ = 2.3 Hz, 8H, C_cH), 7.12 (d, $^4J_{H,H}$ = 2.0 Hz, 2H, C_hH), 6.20 (dd, $^3J_{P,H}$ = 15.6 Hz, $^4J_{H,H}$ = 2.0 Hz, 2H, C_fH), 5.86 (dd, $^3J_{H,H}$ = 5.9 Hz, $^4J_{H,H}$ = 3.6 Hz, 2H, C_mH), 5.70 (m, 2H, C_lH), 1.16 (s, 18H, H_o or H_q), 1.00 (s, 18H, H_o or H_q). $^{13}C\{^1H\}$ NMR ($CDCl_3$): δ 168.4 (s, C_j), 144.8 (dd, $^2J_{P,C}$ = 13.6 Hz, $^3J_{P,C}$ = 3.7 Hz, C_k),142.5 (d, $^3J_{P,C}$ = 8.3 Hz,C_i), 133.5 (d, $^2J_{P,C}$ = 10.3 Hz, C_b), 133.4 (s, C_g), 132.3 (d, $^4J_{P,C}$ =2.8 Hz, C_d), 130.2 (d, $^1J_{P,C}$ = 90.4 Hz, C_e), 128.7 (d, $^3J_{P,C}$ = 12.3 Hz, C_c), 127.8 (s, C_h), 125.8 (d, $^2J_{P,C}$ = 12.3 Hz, C_f), 118.5 (d, $^3J_{P,C}$ = 5.4 Hz, C_l), 118.0 (s, C_m), 108.9 (d, $^1J_{P,C}$ = 121.0 Hz, C_a), 35.5 (d, $^4J_{P,C}$ = 1.7 Hz, C_p), 33.7 (s, C_n), 31.4 (s, C_o), 29.8 (s, C_q). Anal. Calcd. for $C_{58}H_{64}N_2NiO_2P_2$: C, 73.97; H, 6.85; N, 2.97. Found: C, 73.89; H, 6.76; N, 3.12.

Synthesis of [Cu(Psalophen)]

KHMDS (312 mg, 1.56 mmol) was added to a solution of bis-aminophosphonium $(H_4Psalophen)Br_2$ proligand (400mg, 0.38 mmol) in THF (20 mL) under inert conditions. After

stirring during 2 h at room temperature the deprotonation is completed, the $^{31}P\{^{1}H\}$ NMR spectrum shows a singlet at 11 ppm. The solution was centrifuged to remove the insoluble salts and $CuBr_2$ (84 mg, 0.38 mmol) was added. The solution was stirred at room temperature for 2 h. The total disappearance of the $^{31}P\{^{1}H\}$ NMR signal indicates that the complexation is completed. The solvent was removed under reduced pressure and the residue dissolved in CH_2Cl_2 (10mL). After centrifugation, the solution was concentrated and a green solid was obtained by precipitation with petroleum ether. The solid was washed with petroleum ether (3 x 10 mL) to yield [Cu(Psalophen)] (312 mg, 86%). Green crystals were obtained by evaporation of a chloroform solution. $^{31}P\{^{1}H\}$ NMR ($CDCl_3$): no signal; ^{1}H NMR ($CDCl_3$) δ 9.15 (br, aromatic H), 7.01 (br, phenolate protons), 1.09 (br, -$C(CH_3)_3$). Anal. Calcd. for $C_{58}H_{64}CuN_2O_2P_2$: C, 73.59; H, 6.81; N, 2.96. Found: C, 73.59; H, 7.15; N, 2.96. MS (ESI): m/z (%): 946.37 (100) $([Cu(Psalophen)] + H)^+$.

Synthesis of $[Ni(Psalophen)]^+SbF_6^-$

$AgSbF_6$ (73 mg, 0.21 mmol) was added to a solution of [Ni(Psalophen)] (200 mg, 0.21 mmol) in CH_2Cl_2 (4 mL) under Ar atmosphere. The solution changed immediately from green to dark brown and a suspension of Ag was formed. The mixture was stirred for 1 h at room temperature and filtered. A dark brown solid was obtained after precipitation of the concentrated solution with petroleum ether (10 mL). The solid was washed with petroleum ether (3 × 10 mL) and dried under reduced pressure to yield $[Ni(Psalophen)]^+SbF_6^-$ (191 mg, 77 %). Dark brown crystals were obtained after one week of storage of a saturated solution of toluene/CH_2Cl_2 at -40 °C. $^{31}P\{^{1}H\}$ NMR (CD_2Cl_2): no signal; ^{1}H NMR (CD_2Cl_2) δ 11.29 (br s, H_a, H_b or H_c), 8.49 (br s, H_l or H_m), 8.21 (br s, H_l or H_m),7.86(br s, H_l or H_m), 7.57 (br s, H_l or H_m), 7.27 (br s, H_a, H_b or H_c), 3.14 (br s, H_a, H_b or H_c), 1.67 (br s, H_f or H_h), 0.32 (br s, H_f or H_h).

Synthesis of $[Cu(Psalophen)]^+SbF_6^-$

$AgSbF_6$ (92 mg, 0.24 mmol) was added to a solution of [Cu(Psalophen)] (230 mg, 0.24 mmol) in CH_2Cl_2 (4 mL) under Ar atmosphere. The solution changed immediately from green to deep purple and a suspension of Ag was formed. The mixture was stirred for 1 h at room temperature and then filtered. A purple solid was obtained after precipitation of the concentrated solution with petroleum ether (10 mL). The solid was washed with petroleum ether (3 × 10 mL) and dried under reduced pressure to yield $[Cu(Psalophen)]^+SbF_6^-$ (243 mg, 85 %). Purple crystals were obtained after one week of storage of a saturated solution of toluene/CH_2Cl_2 at -40 °C, or from a saturated benzene solution.

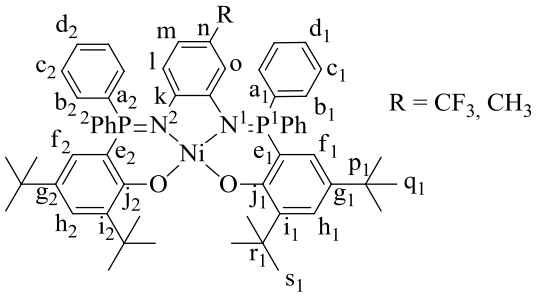

Synthesis of (H_4Psalophen^{Me})Br_2 Ligand

Br_2 (150 µL, 2.91 mmol)) was added to a solution of tert-butyl phosphine (1.136 g, 2.91 mmol) in CH_2Cl_2 (25 mL) at -78 °C under inert conditions. After stirring for 1 hour at room temperature, the solution was placed again in a cold bath at -78 C and DABCO (163 mg, 1.45 mmol) followed by 4-methyl-*o*-phenylenediamine (177 mg, 1.45 mmol) were added to the mixture. The cold bath was removed and the reaction was stirred overnight at room temperature. The formation of the ligand is indicated by the presence of two signals at 35.2 and 35.0 ppm in the $^{31}P\{^1H\}$ NMR spectrum. The solution was filtered and the solvent removed under reduced pressure. The residue was washed with diethyl ether and petroleum ether until none impurities were detected in the supernatant solution and was dried vacuum to yield H_4Psalophen^{Me} as a pale pink solid (696 mg, 45 %).$^{31}P\{^1H\}$ NMR ($CDCl_3$): δ 40.7 and 40.4 ppm; ^1H NMR ($CDCl_3$) δ 8.78 (d, $^2J_{P,H}$ = 3.5 Hz, 1H, NH), 8.75 ($^2J_{P,H}$ = 3.5 Hz, 1H, NH), 7.72 (m, 16H, H_b+H_c), 7.57 (m, 4H, H_d), 7.42 (m, 1H, H_{h1} or H_{h2}), 7.36 (s, 1H, H_{h1} or H_{h2}), 6.96 (dd, $^3J_{P,H}$ = 15.4 Hz, $^4J_{H,H}$ = 1.5 Hz, 1H, H_{f1} or H_{f2}), 6.85 (dd, $^3J_{P,H}$ = 15.4 Hz, $^4J_{H,H}$ = 1.5 Hz, 1H, H_{f1} or H_{f2}) 6.45 (s, H_m + H_l), 6.22 (s, 1H, H_o), 1.83 (s, 3H, -CH_3), 1.33 (s, 9H, H_q or H_r), 1.32 (s, 9H, H_q or H_r), 1.16 (s, 9H, H_q or H_r), 1.15 (s, 9H, H_q or H_r).

Synthesis of [Ni(Psalophen^{Me})]

KHMDS (374 mg, 1.88 mmol) was added to a solution of bis-aminophosphonium H_4Psalophen^{Me} proligand (500 mg, 0.47 mmol) in THF (20 mL) under inert conditions. The deprotonation is completed once two signals at 16.1 and 15.9 ppm are present in the $^{31}P\{^1H\}$ NMR. The solution was centrifuged to remove the insoluble salts and then [$NiBr_2$(DME)] (145 mg, 0.47 mmol) was added to the solution. After stirring 2 h at room temperature the solvent was removed under reduced pressure and the residue dissolved in CH_2Cl_2 (10 mL) and centrifuged. The solution was concentrated and a blue powder was obtained by addition of petroleum ether. The solid was washed with petroleum ether (3 x 10 mL) and dried under vacuum to lead [Ni(Psalophen^{Me})] (390 mg, 87 %). Purple crystals were obtained from a saturated toluene stored in fridge for one week. $^{31}P\{^1H\}$ NMR ($CDCl_3$): δ 30.22 (s, 1 P, P_1 or P_2), 30.04(s, 1 P, P_1 or P_2); ^1H NMR ($CDCl_3$) δ 7.84 (td, $^4J_{P,H}$ = 12.1 Hz, $^3J_{H,H}$ = 7.3 Hz, 8H, H_c), 7.60 (t, $^3J_{H,H}$ = 6.0 Hz, 4H, H_d), 7.51 (m, 8H, H_b), 7.21

(d, $^{4}J_{H,H}$ = 2.1 Hz, 1H, H_{h1} or H_{h2}), 7.19 (d, $^{4}J_{H,H}$ = 2.1 Hz, 1H, H_{h1} or H_{h2}) 6.37 (dd, $^{3}J_{P,H}$ = 15.4 Hz, $^{4}J_{H,H}$ = 2.3 Hz, 1H, H_{f1}), 6.26 (dd, $^{3}J_{P,H}$ = 15.6 Hz, $^{4}J_{H,H}$ = 2.1 Hz, 1H, H_{f2}) 5.77 (dd, $^{3}J_{H,H}$ = 8.1 Hz, 1H, H_m or H_l), 5.66 (d, $^{3}J_{H,H}$ = 8.1 Hz, 1H, H_m or H_l), 5.54 (s, 1H, H_o), 1.60 (s, 3H, -CH_3), 1.23 (s, 9H, H_q or H_r), 1.22 (s, 9H, H_q or H_r), 1.09 (s, 9H, H_q or H_r), 1.07 (s, 9H, H_q or H_r). Anal. Calcd. for $C_{59}H_{66}N_2NiO_2P_2$: C 74.14; H, 6.96; N, 2.93. Found: C 74.06; H, 7.03; N, 2.99.

Synthesis of [Cu(Psalophen^{Me})]

KHMDS (315 mg, 1.58 mmol) was added to a solution of bis-aminophosphonium (H_4Psalophen^{Me})Br_2 proligand (410mg, 0.38 mmol) in THF (25 mL) under inert conditions. After stirring during 2 h at room temperature the deprotonation is completed, the $^{31}P\{^{1}H\}$ NMR spectrum shows two signals at 16.1 and 15.9 ppm. The solution was centrifuged to remove the insoluble salts and $CuBr_2$ (84 mg, 0.38 mmol) was added. The solution was stirred at room temperature for 1 h. The total disappearance of the $^{31}P\{^{1}H\}$ NMR signal indicates that the complexation is completed. The solvent was removed under reduced pressure and the residue dissolved in CH_2Cl_2 (10mL). After centrifugation, the solution was concentrated and a green solid was obtained by precipitation with pentane. The solid was washed with pentane (3 x 10 mL) to yield [Cu(Psalophen)] (247 mg, 67%). Crystals were obtained from toluene saturated solutions stored in the fridge. $^{31}P\{^{1}H\}$ NMR ($CDCl_3$): no signal; ^{1}H NMR ($CDCl_3$) δ 9.19 (br s), 6.97 (br s), 1.71 (br s), 1.08 (br s). Anal. Calcd. for $C_{59}H_{66}CuN_2O_2P_2$: C 73.76; H, 6.92; N, 2.92. Found: C 73.63; H, 6.98; N, 2.93.

Synthesis of [Ni(Psalophen^{Me})]$^{+}SF_6^{-}$

$AgSbF_6$ (36 mg, 0.1 mmol) was added to a solution of [Ni(Psalophen^{Me})] (100 mg, 0.1 mmol) in CH_2Cl_2 (3 mL) under Ar atmosphere. The solution changed immediately from blue to dark brown a suspension of Ag was formed. After stirring at room temperature for 1 h, the suspension was filtered and concentrated. A dark solid was obtained by addition of petroleum ether (10 mL). The solid was washed with petroleum ether (2 x 10 mL) and dried under vacuum to lead [Ni(Psalophen^{Me})]$^{+}SF_6^{-}$ (90 mg, 72 %). NMR cannot be described since the product was not obtained in pure conditions.

Synthesis of [Cu(Psalophen^{Me})]$^{+}SF_6^{-}$

$AgSbF_6$ (32 mg, 0.09 mmol) was added to a solution of [Cu(Psalophen^{Me})] (90 mg, 0.09 mmol) in CH_2Cl_2 (3 mL) under Ar atmosphere. A suspension of Ag was formed but no color change was observed. After stirring at room temperature for 1 h, the suspension was filtered and

concentrated. A green was obtained by addition of petroleum ether (10 mL). The solid was washed with petroleum ether (2 x 10 mL) and dried under vacuum to lead [Cu(Psalophen^{Me})]$^{+}SF_6^{-}$ (50 mg. 46 %). NMR cannot be described since the product was not obtained in pure conditions.

Synthesis of Psalophen^{CF3} Ligand

Br_2 (200 µL, 3.89 mmol) was added to a solution of tert-butyl phosphine (1.520 g, 3.89 mmol) in CH_2Cl_2 (30 mL) at -78 °C under inert atmosphere. The cold bath was removed and the solution was stirred for 2 h at room temperature. At -78 °C, DABCO (218 mg, 1.94 mmol) was added to the solution followed by 3,4-diaminobenzotrifluoride (342 mg, 1.94 mmol). The cold bath was removed and the reaction was stirred overnight at room temperature. The formation of the ligand is indicated by the presence two main singlets at 37.4 and 35.7 ppm in the $^{31}P\{^{1}H\}$ NMR spectrum. The solution was filtered and the solvent removed under reduced pressure. The residue was washed with diethyl ether and petroleum ether until the supernatant solution did not present the impurity signals. The solid was dried vacuum to yield H_4Psalophen^{CF3} as a pale yellow solid (1.306 g, 58 %). $^{31}P\{^{1}H\}$ NMR ($CDCl_3$): δ 43.0 ppm (s, 1P, P_2), 40.5 (s, 1P, P_1); ^{1}H NMR ($CDCl_3$) δ 9.61 (d, $^{2}J_{P,H}$ = 9.4 Hz, 1H, N_2), 8.80 (d, $^{2}J_{P,H}$ = 7.8 Hz, 1H, N_1), 7.92 (dd, $^{3}J_{P,H}$ = 13.7 Hz, $^{3}J_{H,H}$ = 7.3 Hz, 8H, H_{b1} + H_{b2}), 7.76-7.65 (m, 6H, H_{d1}+ H_{d2} + H_h), 7.61 (m, 4H, H_{c1}), 7.55 (m, 4H, H_{c2}), 6.95 (dd, $^{3}J_{P,H}$ = 16.3 Hz, $^{4}J_{H,H}$ = 2.0 Hz, 1H, H_{f1}), 6.86 (dd, $^{3}J_{P,H}$ = 15.2 Hz, $^{4}J_{H,H}$ = 2.3 Hz, 1H, H_{f2}), 6.85 (d, 1H, $^{3}J_{H,H}$= 8.5 Hz, H_m), 6.58 (s, 1H, H_o), 6.52 (d, $^{3}J_{H,H}$ = 8.5 Hz, 1H, H_l), 1.33 (s, 9H, H_{s1} or H_{s2}), 1.28 (s, 9H, H_{s2} or H_{s1}), 1.17 (s, 9H, H_{q1} or H_{q2}), 1.14 (s, 9H, H_{q2} or H_{q1}). $^{13}C\{^{1}H\}$ NMR ($CDCl_3$): δ 167.92 (s, C_j), 145.8 (d, $^{3}J_{P,C}$= 2.13 Hz, C_{g1} or C_{g2}), 145.4 (d, $^{3}J_{P,C}$= 13.8 Hz, C_{g1} or C_{g2}), 141.7 (d, $^{3}J_{P,C}$= 3.75 Hz, C_{i1} or C_{i2}), 141.6 (d, $^{3}J_{P,C}$= 4.50 Hz, C_{i1} or C_{i2}), 137.4 (d, $^{3}J_{P,C}$= 6.81 Hz, C_m + C_l), 134.7 (d, $^{4}J_{P,C}$= 3.0 Hz, Cd), 133.4 (d, $^{4}J_{P,C}$= 2.8 Hz, Cd), 133.8 (d, $^{2}J_{P,C}$= 11.65 Hz, C_{b1} or C_{b2}), 133.4 (d, $^{2}J_{P,C}$= 11.65 Hz, C_{b1} or C_{b2}), 130.0 (d, $^{3}J_{P,C}$= 13.8 Hz, C_{c1} or C_{c2}), 129.9 (d, $^{3}J_{P,C}$= 13.8 Hz, C_{c1} or C_{c2}), 129.0 (d, $^{2}J_{P,C}$= 12.03 Hz, C_{f2}), 128.7 (d, $^{2}J_{P,C}$= 12.03 Hz, C_{f1}), 122.9 (m, C_o), 122.5 (d, $^{1}J_{P,C}$= 105.21 Hz, Ce), 122.4 (m, C_l or C_m), 121.9 (m, C_l or C_m), 120.7 (d, $^{2}J_{P,C}$= 104.0 Hz, C_e), 110.6 (d, $^{1}J_{P,C}$= 103.5 Hz, C_a), 109.3 (d, $^{1}J_{P,C}$= 103.5 Hz, C_a), 35.0 (m, C_{r1} + C_{r2}), 34.7 (s, C_{p1} or C_{p2}), 34.6 (m, C_{p1} or C_{p2}), 31.2 (s, C_{q1} or C_{q2}), 31.0 (s, C_{q2} or C_{q1}), 30.6 (s, C_{s1} + C_{s2}).

Synthesis of [Ni(Psalophen^{CF3})]

KHMDS (286 mg, 1.44 mmol) was added to a solution of bis-aminophosphonium (H_4Psalophen^{CF3})Br_2 proligand (400 mg, 0.36 mmol) in THF (20 mL) under inert conditions. After stirring the solution for 30 min at room temperature the deprotonation was completed and

two singlets are present in the $^{31}P\{^{1}H\}$ NMR spectrum at 12.7 and 12.3 ppm. [$NiBr_2$(DME)] (110 mg, 0.36 mmol) was added and the mixture was stirred overnight. A broad singlet at 46.7 ppm in the $^{31}P\{^{1}H\}$ NMR spectrum indicates the formation of the complex. The solvent was removed under reduced pressure and the residue dissolved in CH_2Cl_2 and centrifuged. The solution was concentrated and a purple precipitate was obtained by addition of petroleum ether. The solid was washed with petroleum ether (3 x 10 mL) and dried under vacuum to yield [Ni(Psalophen^{CF3})] (258 mg, 71 %). Green-purple crystals were obtained by evaporation of a $CDCl_3$ solution. $^{31}P\{^{1}H\}$ NMR ($CDCl_3$): δ 31.2 (s, 1 P, P_1 or P_2), 31.1 (s, 1 P, P_1 or P_2); ^{1}H NMR ($CDCl_3$) δ 7.89 (dd, $^{3}J_{P,H}$ = 12.3 Hz, $^{3}J_{H,H}$ = 7.5 Hz, 4H, H_{b1}), 7.77 (dd, $^{3}J_{P,H}$ = 12.3 Hz, $^{3}J_{H,H}$ = 7.3 Hz, 4H, H_{b2}), 7.65 (m, 4H, H_{c1}), 7.60-7.50 (m, 8H, H_{c2}, H_{d1}, H_{d2}), 7.24 (d, $^{4}J_{H,H}$ = 2.3 Hz, 2H, H_{h1}, H_{h2}), 6.44 (dd, $^{3}J_{P,H}$ = 15.7 Hz, $^{4}J_{H,H}$ = 2.3 Hz, 1H, H_{f1}), 6.23 (dd, $^{3}J_{P,H}$ = 15.7 Hz, $^{4}J_{H,H}$ = 2.3 Hz, 1H, H_{f2}), 6.16 (d, $^{3}J_{H,H}$ = 8.5 Hz, 1H, H_m), 5.78 (s, 1H, H_o), 5.75 (d, $^{3}J_{H,H}$ = 8.5 Hz, 1H, H_l), 1.26 (s, 9H, H_q or H_s), 1.21 (s, 9H, H_q or H_s), 1.11 (s, 9H, H_q or H_s), 1.08 (s, 9H, H_q or H_s). Anal. Calcd. for $C_{59}H_{63}CuF_3N_2O_2P_2$: C, 69.84; H, 6.26; N, 2.76. Found: C, 70.00; H, 6.21; N, 2.86.

Synthesis of [Cu(Psalophen^{CF3})]

KHMDS (192 mg, 0.96 mmol) was added to a solution of bis-aminophosphonium (H_4Psalophen^{CF3})Br_2 proligand (370 mg, 0.24 mmol) in THF (20 mL) under inert conditions. After stirring for 2 h the solution was centrifuged to remove the insoluble salts and $CuBr_2$ (54 mg, 0.24 mmol) was added. The mixture was stirred for 1 h at room temperature and the solvent was evaporated. The residue was dissolved in CH_2Cl_2 (10 mL), centrifuged and the solution concentrated. Addition of petroleum ether leads the formation of a green precipitate that was washed with petroleum ether and dried under vacuum to yield [Cu(Psalophen^{CF3})] (138 mg, 57 %). Dark brown crystals were obtained from a CH_2Cl_2/pentane solution stored in the fridge. $^{31}P\{^{1}H\}$ NMR ($CDCl_3$): no signal; ^{1}H NMR ($CDCl_3$) 9.15 (br s, aromatic protons), 7.05 (br s, aromatic protons), 1.69 (br s, aliphatic protons), 1.11 (br s, aliphatic protons). Anal. Calcd. for $C_{59}H_{63}F_3NiN_2O_2P_2$: C, 70.18; H, 6.29; N, 2.77. Found: C, 69.92; H, 6.37; N, 2.87.

Synthesis of [Ni(Psalophen^{CF3})]$^{+}SbF_6^{-}$

$AgSbF_6$ (44 mg, 0.12 mmol) was added to a solution of [Ni(Psalophen^{CF3})] (130 mg, 0.12 mmol) in CH_2Cl_2 (3 mL) under Ar atmosphere. The solution changed immediately from purple to dark brown and a suspension of Ag was formed. After stirring for 1 h at room temperature the dark solution was filtered and concentrated. A dark red-brown precipitate was obtained by addition of petroleum ether (10 mL). The solid was washed with petroleum ether (2 x 10 mL) and dried under vacuum to yield [Ni(Psalophen^{CF3})]$^{+}SbF_6^{-}$ (100 mg, 67 %). Dark brown crystals were

obtained by slow diffusion of pentane in a CH_2Cl_2 solution. $^{31}P\{^1H\}$ NMR (CD_2Cl_2): no signal; ^1H NMR (CD_2Cl_2) δ 11.26 (br s), 8.39 (br s), 7.93 (br s), 7.59 (br s), 6.74 (br s), 2.56 (br s), 0.07 (br s), -19.47 (br s), -34.43 (br s). Anal. Calcd. for $C_{59}H_{63}F_9N_2NiO_2P_2Sb$: C 56.89; H, 5.10; N, 2.25. Found: C 56.75; H, 5.11; N, 2.35.

Synthesis of [Cu(Psalophen^{CF3})]$^+SbF_6^-$

$AgSbF_6$ (24 mg, 0.06 mmol) was added to a solution of [Cu(Psalophen^{CF3})] (78 mg, 0.06 mmol) in CH_2Cl_2 (4 mL) under Ar atmosphere. A suspension of Ag was formed but no color change was observed. The mixture was stirred for 1 h at room temperature and then filtered. A green solid was obtained after precipitation of the concentrated solution with petroleum ether (10 mL). The solid was washed with petroleum ether (3 × 10 mL) and dried under reduced pressure to yield [Cu(Psalophen^{CF3})]$^+SbF_6^-$ (51 mg, 58 %). $^{31}P\{^1H\}$ NMR (CD2Cl_2): no signal; ^1H NMR (CD2Cl_2) δ 8.22 (br s), 8.02 (br s), 7.66 (br s), 3.80 (br s), 1.89 (br s), 1.81 (br s), 1.66(br s).

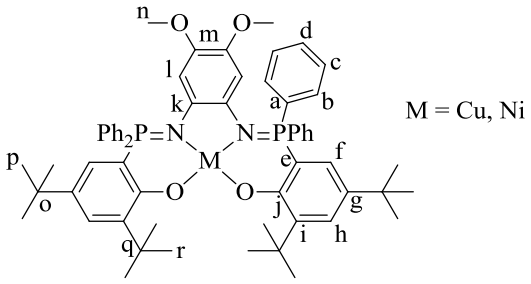

Synthesis of Psalophen^{OMe2} Ligand

Br_2 (192 µL, mmol) was added to a tert-butyl phosphine solution (1.457 g, 3.73 mmol) in CH_2Cl_2 (30 mL) at -78 °C under inert atmosphere. The cold bath was removed and the reaction was stirred for 2 h at room temperature. DABCO (209 mg, 1.86 mmol) and 1,2-diamino-4,5-dimethoxybenzene (313 mg, 1.86 mmol) were mixed together in 7 mL of CH_2Cl_2 and added to the reaction mixture at -78 °C. The solution changes from light yellow to dark pink. The mixture was stirred overnight at room temperature and then centrifuged to remove the DABCO salts. The formation of the ligand is indicated by the presence a sole singlet at 35.0 ppm in the $^{31}P\{^1H\}$ NMR spectrum. The solution was evaporated and the residue washed with diethyl ether several times until a pale pink solid was obtained which was dried under vacuum to yield (H_4Psalophen^{OMe2})Br_2 (861 mg, 42%). $^{31}P\{^1H\}$ NMR ($CDCl_3$): δ 40.35 ppm; ^1H NMR ($CDCl_3$) δ 8.72 (d, $^2J_{P,H}$ = 9.6 Hz, 2H, NH), 7.62-7.77 (m, 14H, H_b+H_d+H_h), 7.54 (m, 8H, H_c), 6.89 (dd, $^3J_{P,H}$ = 15.9 Hz, $^4J_{H,H}$ = 2.0 Hz, 2H, H_f), 5.97 (s, 2H, H_l), 3.16 (s, 6H, H_n), 1.31 (s, 18H, H_r), 1.13 (s, 18H, H_p). $^{13}C\{^1H\}$ NMR ($CDCl_3$): 155.7 (d, $^3J_{P,C}$ = 2.6 Hz, C_j), 145.8 (d, $^3J_{P,C}$ = 12.5 Hz, C_g or C_i), 145.8 (s, C_m), 141.6 (d, $^3J_{P,C}$ = 7.1 Hz, C_g or C_i), 134.8 (d, $^4J_{P,C}$ = 2.8 Hz, C_h), 133.6 (d, $^2J_{P,C}$ = 11.4 Hz, C_b), 133.0 (d, $^4J_{P,C}$ = 1.6

Hz, C_d), 129.9 (d, $^3J_{P,C}$ = 13.6 Hz, C_c), 129.0 (d, $^2J_{P,C}$ = 11.6 Hz, C_f), 124.8 (dd, $^2J_{P,C}$ = 7.5 Hz, $^3J_{P,C}$ = 1.5 Hz, C_k), 121.6 (d, $^1J_{P,C}$ = 104.6 Hz, C_a), 111.1 (d, $^1J_{P,C}$ = 104.9 Hz, C_e), 55.7 (s, C_n), 35.0 (d, $^3J_{P,C}$ = 1.6 Hz, C_o or C_q), 34.7 (s, C_o or C_q), 31.2 (s, C_p or C_r), 30.5 (s, C_p or C_r).

Synthesis of [Ni(Psalophen^{OMe2})]

KHMDS (316 mg, 1.59 mmol) was added to a solution of bis-aminophosphonium H_4Psalophen^{OMe2} proligand (400 mg, 0.39 mmol) in THF (25 mL) under inert conditions. After stirring for 1 h the deprotonation is completed and a sole singlet is present in the $^{31}P\{^1H\}$ NMR spectrum at 8.2 ppm. The solution was centrifuged to remove the insoluble salts and [$NiBr_2$(DME)] (122 mg, 0.39 mmol) was added. The mixture was stirred for 4 h at room temperature. A singlet at 33.4 ppm in the $^{31}P\{^1H\}$ NMR spectrum indicates the formation of the complex. The solvent was removed and the residue dissolved in CH_2Cl_2 (10 mL) and centrifuged. The resulting dark green solution was concentrated and a pale blue solid was obtained by addition of petroleum ether (15 mL). The solid was washed with petroleum ether (3 x 10 mL) and dried under vacuum to yield [Ni(Psalophen^{OMe2})] (258 mg, 65 %). Dark crystals were obtained from a concentrated dichloromethane solution with some drops of diethyl ether and petroleum ether stored in the fridge. $^{31}P\{^1H\}$ NMR ($CDCl_3$): δ 30.54 ppm; ^1H NMR ($CDCl_3$) δ 7.84 (dd, $^3J_{P,H}$ = 12.5 Hz, $^3J_{H,H}$ = 7.6 Hz, 8H, H_b), 7.62 (t, $^3J_{H,H}$ = 7.0 Hz, 4H, H_d), 7.53 (m, 8H, H_c), 7.20 (s, 2H, H_h), 6.29 (d, $^3J_{P,H}$ = 15.6 Hz, 2H, H_f), 5.48 (s, 2H, H_l), 2.92 (s, 6H, -OCH_3), 1.24 (s, 18H, H_p or H_r), 1.08 (s, 18H, H_p or H_r). $^{13}C\{^1H\}$ NMR ($CDCl_3$): δ 142.2 (s, C_i), 140.6 (s, C_m), 137.1 (s, C_k), 133.6 (d, $^2J_{P,C}$ = 10 Hz, C_b), 133.5 (s, C_g), 132.2 (s, C_d), 128.8 (d, $^3J_{P,C}$ = 11.7 Hz, C_c), 127.9 (s, C_h), 125.7 (s, C_f), 108.1 (d, $^2J_{P,C}$ = 119.5 Hz, C_a), 103.7 (s, C_d), 55.1 (s, C_n), 35.5 (s, C_o o C_q), 33.7 (s, C_o o C_q), 31.4 (s, C_p or C_r), 29.8 (s, C_p or C_r). MS (ESI): m/z (%): 1001.40 (100) ([Ni(Psalophen^{OMe2})]+H)$^+$.

Synthesis of [Cu(Psalophen^{OMe2})]

KHMDS (316 mg, 1.59 mmol) was added to a solution of bis-aminophosphonium H_4Psalophen^{OMe2} proligand (400 mg, 0.39 mmol) in THF (25 mL) under inert conditions. The deprotonation is completed when only a singlet at 8.15 ppm is present in the $^{31}P\{^1H\}$ NMR. The solution was centrifuged to remove the insoluble salts and $CuBr_2$ was added (88 mg, 0.39 mmol). The mixture was stirred at room temperature until the disappearance of the $^{31}P\{^1H\}$ NMR signal. The solvent was then removed and the residue dissolved in CH_2Cl_2 (10 mL) and centrifuged. The resulting dark green solution was concentrated and a pale blue powder was obtained by addition of petroleum ether. The solid was washed with petroleum ether (3 x 10 mL) and dried

under vacuum to yield [Cu(Psalophen^{OMe2})] (222 mg, 61 %). Dark crystals were obtained from a concentrated dichloromethane solution with some drops of petroleum ether stored in the fridge. $^{31}P\{^{1}H\}$ NMR ($CDCl_3$): δ no signal; ^{1}H NMR ($CDCl_3$) δ 9.21 (br s), 6.97 (br s), 3.02 (br s), 1.06 (br s), 1.08 (br s). MS (ESI): m/z (%): 1006.40 (100) [([Cu(Psalophen^{OMe2})]+H)]$^{+}$.

Synthesis of [Ni(Psalophen^{OMe2})]$^{+}$SbF$_6^{-}$

$AgSbF_6$ (34 mg, 0.09 mmol) was added to a solution of [Ni(Psalophen^{OMe2})] (100 mg, 0.09 mmol) in THF (4 mL) under Ar atmosphere. The solution changed immediately from blue to dark brown and a suspension of Ag was formed. The resulting dark solution was stirred for 1 h at room temperature and then filtered. The solvent was removed and the residue dissolved in a minimum amount of diethyl ether. A dark blue precipitate was obtained by addition of petroleum ether (10 mL). The solid was washed with petroleum ether (2 x 10 mL) and dried under vacuum to yield [Ni(Psalophen^{OMe2})]$^{+}$SbF$_6^{-}$ (95 mg, 77 %). Single crystals of [Ni(Psalophen^{OMe2})]$^{+}$SbF$_6^{-}$ were obtained from a toluene/dichloromethane solution stored at -40 °C. $^{31}P\{^{1}H\}$ NMR (CD_2Cl_2): δ no signal; ^{1}H NMR (CD_2Cl_2) δ 11.05 (br s), 8.11 (br s), 7.71 (m), 6.96 (br s), 6.66 (br s), 1.22 (br s), 0.97 (br s). $^{31}P\{^{1}H\}$ NMR (THF-d^8): δ no signal; ^{1}H NMR (THF-d^8) δ 111.22 (br s), 65.73 (br s), 29.79 (br s), 12.91 (br s), 12.41 (br s), 9.85 (br s), 5.59 (br s), 4.49 (br s), 1.23 (br s), 9.85 (br s), 5.59 (br s). MS (ESI): m/z (%): 1000.40 (100) [Ni(Psalophen^{OMe2})]$^{+}$.

Synthesis of [Cu(Psalophen^{OMe2})]$^{+}$SbF$_6^{-}$

$AgSbF_6$ (34 mg, 0.09 mmol) was added to a solution of [Cu(Psalophen^{OMe2})] (100 mg, 0.09 mmol) in THF (4 mL) under Ar atmosphere. A suspension of Ag was formed but no color change was observed. The dark green solution was stirred for 1 h and then filtered and concentrated. A dark red solid was obtained by addition of petroleum ether (10 mL). The solid was washed with petroleum ether (2 x 10 mL) and dried under vacuum to yield [Cu(Psalophen^{OMe2})]$^{+}$SbF$_6^{-}$ (80 mg, 65 %). Green-brown crystals were obtained from a solution of CH_2Cl_2/pentane stored at 3 °. $^{31}P\{^{1}H\}$ NMR (CD_2Cl_2): δ no signal; ^{1}H NMR (CD_2Cl_2) δ 12.85 (br s), 11.28 (br s), 9.48 (br s), 6.51 (br s), 1.72 (br s), 1.33 (br s).

Chapter 5

Synthesis of [Mn(Psalen^{tBu})]

KHMDS (400 mg, 2 mmol) was added into a suspension of bis-aminophosphonium (H_4Psalen^{tBu})Br_2 proligand (500 mg, 0.5 mmol) in THF (20 mL) under inert conditions. After stirring at room temperature for 1 h the $^{31}P\{^1H\}$ NMR showed a sole singlet at 15.4 ppm, confirming that the deprotonation was completed. Insoluble salts formed were removed by centrifugation and $Mn(OAc)_2$ (130 mg, 0.75 mmol) was added. The mixture was heated at 90°C until the disappearance of the ligand signal. The insoluble salts were removed by centrifugation and the solvent was removed to afford [Mn(Psalen^{tBu})] (436 mg, 98 %). Single crystals of [Mn(Psalen^{tBu})] were obtained from a dichloromethane/pyridine solution stored at -40 °C for one week.

Synthesis of [Mn(Psalen^{OMe})]

KHMDS (168 mg, 0.84 mmol) was added into a suspension of bis-aminophosphonium (H_4Psalen^{OMe})Br_2 proligand (200 mg, 0.21 mmol) in THF (20 mL) under inert conditions. After stirring at room temperature for 1 h the $^{31}P\{^1H\}$ NMR showed a sole singlet at 18 ppm, confirming that the deprotonation was completed. Insoluble salts formed were removed by centrifugation and $Mn(OAc)_2$ (37 mg, 0.21 mmol) was added. The mixture was heated at 90°C until the disappearance of the ligand signal. The insoluble salts were removed by centrifugation and the solvent was removed to afford [Mn(Psalen^{OMe})] (130 mg, 74 %). Single crystals of were obtained from a dichloromethane/pyridine solution stored at -40 °C for one week.

Synthesis of [Mn(Psalen^{iPr})]

KHMDS (461.68 mg, 2.32 mmol) was added into a suspension of bis-aminophosphonium (H_4Psalen^{iPr})Br_2 proligand (500 mg, 0.58 mmol) in THF (20 mL) under inert conditions. After stirring at room temperature for 1 h the $^{31}P\{^1H\}$ NMR showed a sole singlet at 31 ppm, confirming that the deprotonation was completed. Salts formed were removed by centrifugation and $Mn(OAc)_2$ (100 mg, 0.58 mmol) was added. The mixture was heated at 90°C until the disappearance of the ligand signal. The insoluble salts were removed by centrifugation and the solvent was evaporated to afford [Mn(Psalen^{iPr})] (367 mg, 84 %). Pale brown crystals were obtained by slow evaporation in a mixture of THF and Petroleum ether under nitrogen atmosphere.

Synthesis of [Mn(Psalen^{tBu})]$^{+}$PF$_6^{-}$:

[Mn(Psalen^{tBu})] (120 mg, 0.13 mmol) was dissolved in THF (5 mL) under inert conditions. Addition of $AgPF_6$ (34 mg, 0.13 mmol) to the solution immediately resulted in a color change from yellow to dark red and to the formation of a suspension of Ag. This suspension was stirred for 1 h and then filtered. The solvent was removed, the solid was dissolved in a small amount of CH_2Cl_2 and dark red precipitated was obtained by the addition of pentane. The solid was washed with pentane (2 x 5 mL) and dried under reduced pressure to yield [Mn(Psalen^{tBu})]$^{+}$PF$_6^{-}$ (80 mg, 57 %). Brown crystals were obtained via pentane diffusion into a saturated THF/diethyl ether solution. MS (ESI): m/z (%): 889.40 (100) [Mn(Psalen^{tBu})]$^{+}$.

Synthesis of [Mn(Psalen^{tBu})Cl]:

[Mn(Psalen^{tBu})] (150 mg, 0.17 mmol) was dissolved in CH_2Cl_2 (5 mL) under inert conditions. Addition of AgCl (34 mg, 0.13 mmol) to the solution resulted in a color change from yellow to dark green and to the formation of a suspension of Ag. This suspension was stirred overnight and then filtered. The solution was concentrated and a dark green solid was obtained by addition of pentane into the solution. The solid was washed with pentane (2 × 5 mL) and dried under reduced pressure to yield [Mn(Psalen^{tBu})Cl] (150 mg, 95 %). Single crystals of [Mn(Psalen^{tBu})Cl] were obtained from a dichloromethane/pentane solution stored in the fridge for two days. MS (ESI): m/z (%): 889.40 (100) [Mn(Psalen^{tBu})]$^{+}$.

Synthesis of [Mn(Psalen^{OMe})]$^{+}$PF$_6^{-}$:

[Mn(Psalen^{OMe})] (50 mg, 0.06 mmol) was dissolved in THF (3 mL) under inert conditions. Addition of $AgPF_6$ (13 mg, 0.06 mmol) to the solution immediately resulted in a color change from yellow to dark red and to the formation of a suspension of Ag. This suspension was stirred for 1 h and then filtered. The solvent was removed and the solid was dissolved in a small amount of CH_2Cl_2. A dark red precipitated was obtained by the addition of pentane. The solid was washed with pentane (2 x 5 mL) and dried under reduced pressure to yield [Mn(Psalen^{OMe})]$^{+}$PF$_6^{-}$ (33 mg, 57 %). Brown crystals were obtained by slow diffusion of diethyl ether and pentane into a concentrated THF solution. MS (ESI): m/z (%): 837.28 (100) [Mn(Psalen^{OMe})]$^{+}$.

Synthesis of [Mn(Psalen^{iPr})Cl]

[Mn(Psalen^{iPr})] (100 mg, 0.133 mmol) was dissolved in CH_2Cl_2 (5 mL) under inert conditions. Addition of AgCl (19 mg, 0.133 mmol) to the solution immediately resulted in a color change

from green to dark green and to the formation of a suspension of Ag. This suspension was stirred overnight and then filtered. The solution was concentrated and dark green solid was obtained by addition of pentane into the solution. The solid was washed with pentane (2 × 5 mL) and dried under reduced pressure to yield [Mn(Psalen^{iPr})Cl] (52 mg, 49 %). Dark green crystals were obtained by slow diffusion of CH_2Cl_2 and pentane. MS (ESI): m/z (%): 753.43 (100) [Mn(^{iPr}Psalen)]$^+$.

Synthesis of [Mn(Psalen^{iPr})]$^+$PF$_6^-$

[Mn(^{iPr}Psalen)] (190 mg, 0.25 mmol) was dissolved in THF (5 mL) under inert conditions. Addition of $AgPF_6$ (55.5 mg, 0.25 mmol) to the solution immediately resulted in a color change from green to dark red and to the formation of a suspension of Ag. This suspension was stirred for 1 h and then filtered. The solvent was removed, the solid was dissolved in a small amount of THF and pale pink precipitated was obtained by the addition of pentane. The solid was washed with pentane (2 x 5 mL) and dried under reduced pressure to yield [Mn(Psalen^{iPr})]$^+$PF$_6^-$ (136 mg, 60 %). Brown crystals were obtained by slow diffusion of pentane into a saturated THF solution. MS (ESI): m/z (%): 753.44 (100) [Mn(^{iPr}Psalen)]$^+$.

Synthesis of [Mn(Psalen^{tBu})(N$_3$)]

An excess of trimethylsilyl azide (0.5 mL, 3.8 mmol) was added to a solution of [Mn(Psalen^{tBu})]PF_6 (50 mg, 0.05 mmol) in toluene (6 mL) and stirred at room temperature for 24 h under inert conditions. The reaction mixture was transferred to a vial and pentane was added. The vial was stored in the fridge. Green crystals of [Mn(Psalen^{tBu})(N_3)] were obtained after 3 days.

Synthesis of [Mn(^{iPr}Psalen)(N$_3$)]

An excess of trimethylsilyl azide (0.5 mL, 3.8 mmol) was added to a solution of [Mn(^{iPr}Psalen)]PF_6 (40 mg, 0.04 mmol) in toluene (6 mL) and stirred at room temperature for 24 h under inert conditions. The reaction mixture was transferred to a vial and pentane was added. The vial was stored in the fridge. Green crystals of [Mn(^{iPr}Psalen)(N_3)] were obtained after 3 days.

Synthesis of [Mn(Psalen^{tBu})(O_2)]

[Mn(Psalen^{tBu})] (100 mg, 0.11 mmol) was dissolved in THF (3 mL) and pyridine (9.0 μL, 0.11 mmol) was added under Ar atmosphere. The mixture was stirred for 30 minutes and was opened to air and stirred for 20 more minutes. Pentane (around 2 mL) was added to the solution and it was stored in the fridge. Next day dark crystals were obtained corresponding to [Mn(Psalen^{tBu})(O_2)], which were washed with pentane and dried under reduced pressure (39 mg, 38 %).

Procedure for epoxidation catalysis tests

General catalysis test

Catalytic experiments were performed adding 1-2 equivalents of oxidant (m-CPBA, PhIO or $PhI(OAc)_2$) to a mixture of 5-10% of Mn catalyst, COE (solution 0.1 M in THF or MeOH, 1 mL, 0.1 mmol) and 1 mL of THF or MeOH. Aliquots of 0.2 mL were taken after different intervals and filtered on a Pasteur pipette charged with cotton, silica gel and anhydrous Na_2SO_4, using diethyl ether or THF as eluent for ^{iPr}Psalen and Psalen^{tBu} derivatives, respectively. The conversion of COE was calculated taking into account the integrated areas of the starting materials and the products.

Control experiments were performed with the same methodology without the addition of the manganese Psalen complex.

Catalysis test with Lewis acids

Catalytic experiments using triflates were performed in two steps: first a mixture of complex (0.005 mmol, 5 mol %) and $PhI(OAc)_2$ (0.025 mmol, 25 mol % equivalent) in 1 mL of MeOH was stirred vigorously for 3 hours. Then, another amount of $PhI(OAc)_2$ (0.2 mmol, 2 eq.) was added to the reaction mixture followed by the solution of COE (0.1 M in MeOH, 1 mL) and $Ca(OTf)_2$ or $Al(OTf)_3$ (0.01 mmol, 10 % equivalent) stirring was pursued. The time of the last addition was set as time 0. Aliquots of 0.2 mL were taken after different intervals and filtered on a Pasteur pipette charged with cotton, silica gel and anhydrous Na_2SO_4, and diethyl ether as eluent. The conversion of COE was monitored by GC using dodecane (100 μL) as internal standard.

Control experiments were performed with the same methodology without the addition of the manganese Psalen complex.

Résumé de thèse

Les ligands phosphasalen (Psalen) développés au sein du laboratoire peuvent être considérés comme les analogues phosphorés des ligands salen dont ils diffèrent par la présence de groupements iminophosphorane à la place des imines. L'introduction de ces fonctions a d'importantes conséquences sur les propriétés stériques et électroniques de ces ligands. Malgré l'écriture de la liaison P-N comme une double liaison, il n'existe pas de système π entre ces deux atomes. Cette fonction se caractérise par la présence de deux paires libres sur l'atome d'azote qui sont stabilisées par délocalisation dans les orbitales du phosphore (hyperconjugation négative). Cela a d'importantes répercussions sur l'électronique, faisant des ligands phosphasalen de meilleurs donneurs. Ils sont σ- et π-donneurs sans capacité acceptrice due par l'absence de système π. Les propriétés électroniques de la fonction iminophosphorane peuvent être contrôlées par les substituants de l'atome de phosphore ainsi que le lien entre les deux amines. La substitution par de groupements alkyles rend dans le deux cas l'iminophosphorane plus électrodonneur. L'introduction des atomes de phosphore a aussi une répercussion au niveau stérique car le phosphore porte deux substituants (du lieu d'un pour le carbone plan des imines) et peut induire de l'encombrement stérique.

Ces ligands ont également un caractère redox non-innocent, une propriété très étudiée de nos jours tant en chimie de coordination qu'en catalyse. En effet, l'oxydation peut se faire soit sur le ligand, soit sur le métal. Grace à cette propriété les complexes à ligands non-innocents peuvent servir de modèles pour certaines metalloenzymes, et sont donc très étudiés en chimie bioinorganique.

Cette thèse a comme objectif de comprendre les effets du phosphore et des différents substituants du ligand sur la structure électronique des complexes oxydés. Pour cela, nous avons synthétisé différents ligands en faisant varier les différents paramètres au sein du ligand et étudié la première oxydation des complexes de nickel et de cuivre. Pour déterminer précisément la structure électronique de ces complexes, différentes techniques ont été utilisées : des spectroscopies UV-visible, RMN et RPE, la voltammetrie cyclique, la diffraction de rayons X, des mesures magnétiques à l'état solide (SQUID), ainsi que des calculs DFT.

Le premier chapitre de cette thèse analyse l'effet des modifications induites sur le cycle phenolate. Les propriétés de deux ligands sont étudiées : Psalen^{tBu} qui porte de groups tert-butyle en les positions *para* du phenolate, et Psalen^{OMe} qui présente de propriétés plus électrodonneuses de par l'introduction de groupements methoxy à la place du tert-butyle. Un changement du lieu de l'oxydation peut être attendu avec cette modification.

Dans le deuxième chapitre, nous avons étudié l'influence des groupements sur le phosphore. Les substituants aryle phosphore du ligand Psalen^{tBu} ont été remplacés par des groupements alkyle. Les propriétés électroniques du nouveau ligand comportant des substituants isopropyle, ^{iPr}Psalen, sont discutées dans ce chapitre. Avec cette modification, une meilleure stabilisation du métal à haut degré d'oxydation est observée.

Dans le troisième chapitre, la modification est introduite dans le lien entre les deux azotes. Les complexes comportant un lien phénylènediamine, les complexes Psalophen, ainsi que certains dérivés mono- et disubstitués sont étudiés au chapitre 3. Le lien aryle peut agir comme une unité redox active et peut être oxydé lors de l'oxydation. L'influence des substituants du lien phénylènediamine sur la structure électronique a été étudiée avec les ligands Psalophen^{OMe2}, Psalophen^{Me} and Psalophen^{CF3}.

Dans le dernier chapitre, nous avons étudié la stabilisation de complexes de manganèse à différents degrés d'oxydation avec différents ligands phosphasalen. Les propriétés catalytiques des composés de Mn^{III} ont été ainsi évaluées.

Les ligands phosphasalen ont montré, en générale, une meilleure capacité pour à stabiliser des métaux a haut degré d'oxydation par rapport aux ligands salen. Des complexes de Cu^{III} et Ni^{III}, rares dans la littérature, ont pu être obtenus et ont été caractérisés. L'obtention d'un complexe de Mn^{IV} peroxo avec un ligand phosphasalen est aussi un résultat prometteur qui dénote l'intérêt de ces ligands en chimie de coordination.

université PARIS-SACLAY
ÉCOLE DOCTORALE
Sciences chimiques : molécules, matériaux, instrumentation et biosystèmes

Titre: Etude de l'oxydation de complexes à ligand phosphasalen

Mots clés: phosphasalen, iminophosphorane, ligands redox non-innocents

Résumé: Les ligands phosphasalen développés au sein du laboratoire peuvent être considérés comme les analogues phosphorés des ligands salen dont ils diffèrent par la présence de groupements iminophosphorane à la place des imines. L'introduction de ces fonctions a d'importantes conséquences sur les propriétés de ces ligands, qui sont plus électrodonneurs et plus flexibles que les dérivés salen correspondants, capables de stabiliser des métaux à haut degré d'oxydation. Ces ligands ont également un caractère redox non-innocent, une propriété très étudiée de nos jours tant en chimie de coordination qu'en catalyse.
Dans la cadre de cette thèse, différents ligands ont été synthétisés en modifiant les différents paramètres au sein du ligand : les substituants du cycle phenolate, MeO vs. tBu ($Psalen^{tBu}$ et $Psalen^{OMe}$); les substituants du phosphore, alkyl vs. aryl (^{iPr}Psalen); et le lien entre les deux azotes, avec l'introduction de différentes o-phenylenediamines à la place d'ethylenediamine, qui donne les ligands Psalophen, $Psalophen^{OMe2}$, $Psalophen^{Me}$ and $Psalophen^{CF3}$.
Les complexes neutres de cuivre et nickel, ainsi que les produits de mono-oxydation ont été synthétisés et caractérisés. Pour déterminer précisément la structure électronique des complexes différentes techniques ont été utilisés : des spectroscopies UV-visible, RMN et RPE, voltampérométrie cyclique, diffraction de rayons X, mesures magnétiques à l'état solide (SQUID), ainsi que des calculs DFT.
De manière générale ces travaux montrent que les phosphasalen sont mieux à même de stabiliser la densité de spin sur le métal, donnant en certains cas des complexes à haute valence (Ni^{III}, Cu^{III}) encore rares dans la littérature. Dans certains cas les observations expérimentales et les calculs pointent vers un état fondamental multiconfigurationel. Contrairement aux ligands salen, les complexes portant un lien aromatique entre les deux azotes dimerisent lors de l'oxydation. Afin de contrôler la densité électronique sur ce cycle, une série des complexes à ligands phosphasalophen ont été également étudies.
Une synthèse de complexes phosphasalen de Mn^{II} and Mn^{III} a été également réalisée. La stabilisation des complexes oxo ou nitrido, ainsi que la catalyse d'oxydation ont été envisagés avec ces complexes et des résultats prometteurs ont été obtenus.

Title: Study of the oxidation of phosphasalen complexes

Keywords: phosphasalen, iminophosphorane, redox non-innocent ligands

Abstract: Phosphasalen ligands developed in our laboratory can be considered as the phosphorous analogues of salen ligands where the imines are substituted by iminophosphorane functions. The presence of the P-N bond makes these ligands more electro-donating and more flexible than salen analogues. They are able to stabilize high-valent metal complexes, as in the case of a Ni phosphasalen complex, which was characterized as a Ni^{III} complex in solution and in solid state. This was never obtained before with salen-type ligands. Phosphasalen ligands, as the salen ones, can act as redox non-innocent ligands. Therefore, upon oxidation either the ligand or the metal center can be oxidized depending on the relative energy of metal and ligand orbitals. This behavior has been deeply investigated in coordination chemistry and in catalysis.
In order to elucidate the factors that influence the oxidation locus different ligands have been synthetized modifiying the phenolate subtituents, MeO vs. ^{t}Bu ($Psalen^{tBu}$ and $Psalen^{OMe}$); the phosphorous substituents, alkyl vs. aryl (^{iPr}Psalen); and the linker between the two nitrogen atoms, ethylenediamine vs. phenylenediamine (Psalophen, $Psalophen^{OMe2}$, $Psalophen^{Me}$ and $Psalophen^{CF3}$). The neutral and one-electron oxidized copper and nickel complexes were synthetized and characterized. In order to determine the electronic structure of the complexes, different characterization techniques were used: UV-vis, EPR and NMR spectroscopies, cyclic voltammetry, X-ray diffraction, magnetic measurements (SQUID), as well as theoretical calculations. In a general manner, phosphasalen ligands favor a metal center oxidation in a higher extent than salen derivatives, leading in some cases to high-valent metal complexes (Ni^{III}, Cu^{III}), remaining rare cases in the literature. For some complexes, experimental observations and theoretical calculations point to the presence of multiconfigurational ground states. Contrary to salen, complexes bearing an aromatic N,N linker dimerize upon oxidation. In order to tune the electronic density in the central ring, a series of phosphasalophen complexes displaying different substituents in the aromatic bridge, have been studied.
Mn^{II} and Mn^{III} phosphasalen complexes have been also studied. The stabilization of oxo and nitride complexes as well as catalytic applications have been targeted for these complexes and encouraging results have been obtained.

Université Paris-Saclay
Espace Technologique / Immeuble Discovery
Route de l'Orme aux Merisiers RD 128 / 91190 Saint-Aubin, France